THEORETICAL AND EXPERIMENTAL STUDIES OF THE TRANSONIC FLOW FIELD AND ASSOCIATED BOUNDARY CONDITIONS NEAR A LONGITUDINALLY-SLOTTED WIND-TUNNEL WALL

By

Joel Lee Everhart

B.S. Aerospace Engineering, December 1973

M.S. Mechanical Engineering, December 1975

North Carolina State University

A Dissertation submitted to

The Faculty of

The Graduate School of Engineering and Applied Science

of The George Washington University in partial satisfaction

of the requirements for the degree of

Doctor of Science in Fluid Mechanics

February 14, 1988

Dissertation directed by

Dr. John L. Whitesides

Professor of Engineering and Applied Science

THEORETICAL AND EXPERIMENTAL STUDIES OF THE TRANSONIC FLOW FIELD AND ASSOCIATED BOUNDARY CONDITIONS NEAR A LONGITUDINALLY-SLOTTED WIND-TUNNEL WALL

By

Joel L. Everhart

ABSTRACT

A theoretical examination of the slotted-wall flow field is conducted to determine the appropriate wall pressure-drop (or boundary condition) equation. This analysis improves the understanding of the fluid physics of these types of flow fields and helps to evaluate the uncertainties and limitations existing in previous mathematical developments. It is shown that the resulting slotted-wall boundary condition contains contributions from the airfoil-induced streamline curvature and the non-linear, quadratic, slot crossflow in addition to an often neglected linear term which results from viscous shearing in the slot. Existing and newly acquired experimental data are examined in the light of this formulation and previous theoretical developments.

A detailed, previously unpublished, set of slot-flow measurements which were obtained in the Langley Research Center's Diffuser Flow Apparatus are analyzed and the resulting conclusions on the character of slot flows are discussed. A description is also given of a series of wind tunnel experiments conducted in the Langley Research Center's 6- by 19-inch Transonic Tunnel expressly for this investigation. These experiments contain systematic variations in many of the pertinent wall-geometry variables such as the wall openness and the number of slots in concert with a systematic variation of the

free-stream Mach number and model angle of attack. Data from these experiments are discussed in the context of an alternate form of the boundary condition which focuses on the incremental effect of the model on tunnel-wall flow. A determination of the unknown coefficients in this form of the boundary condition, and in more conventional forms as well, is made using the available experimental data and the procedures outlined in the text. Values of the coefficients are presented in the paper and show good, systematic variations with free-stream conditions and wall parameters. These results also indicate that the alternate form of the boundary condition is valid over a wide range of flow and wall-geometry variables and, in addition, is in much better agreement with experiment than that yielded by previous treatments of the slot-flow boundary condition.

ACKNOWLEDGMENTS

The author expresses a sincere note of gratitude to Mr. Percy J. Bobbitt for the many hours of helpful guidance and fruitful discussions while serving as technical advisor for his dissertation. The author wishes to thank Dr. Richard W. Barnwell for originally suggesting this research topic, his guidance in the early stages of the study, the continued discussions, and for serving on his committee. A special thank you is also given to Dr. John L. Whitesides for serving as his committee chairman, faculty advisor, and for reviewing the preliminary versions of this dissertation.

The author also wishes to recognize and thank the following individuals and groups for their contributions to the experiment: Mr. Boyce E. Lavender, Jr. and his technicians for their careful and attentive work, particularly, that of Mr. Benjamin R. Freeman for his model preparation, meticulous setting of the flow-angle probes, and facility operation; and, Mr. Kurt Hitke and Mr. Dan Riddenhour of the System Development Corporation for the data acquisition software development.

Additionally, the author wishes to thank Mr. William B. Igoe and Mr. Stuart G. Flechner for making their unpublished, slot-flow data available for his analysis; to Dr. Suresh Goradia for helpful discussions concerning the dynamic similarity of fluids; and, also, to Mr. Stanley H. Husch, Jr. for his helpful suggestions and preparation of the final figures contained in this dissertation.

The author wishes to express his gratitude to his parents, Joe and Ruth Everhart, for their support and encouragement through all the years of study. The positive environment which they provided in early, developmental years set the course which motivated him to strive for higher goals.

Finally, and most importantly, the author can only say thank you to his wife, Kathy, and express his love and gratitude for her continued patience and support through the duration of these studies.

CONTENTS

APPENDICES

FIGURES

SYMBOLS

A	slotted-wall coefficient, see eqn. 7.37, also Model cross-sectional area, see eqn. B14, in^2
ALS	Tunnel Mach number calibration coefficient
a	slot spacing, in
B	slotted-wall viscous coefficient
B'	slotted-wall viscous coefficient
BLS	Tunnel Mach number calibration coefficient
BP	flow-angle-probe total-pressure correction factor, see eqn. A7
B_1	boundary condition variable, see eqn. 7.39b
B_2	boundary condition variable, see eqn. 7.39c
b	tunnel width, in
CLS	Tunnel Mach number calibration coefficient
C_D	airfoil drag coefficient
C_L	airfoil lift coefficient
C_m	airfoil pitching-moment coefficient
$\bar{\bar{C}}_m$	sidewall-corrected pitching-moment coefficient
C_n	airfoil normal force coefficient
$\bar{\bar{C}}_n$	sidewall-corrected normal-force coefficient

C_P	pressure coefficient, $\frac{p - p_\infty}{q_\infty}$
$C_{P,plenum}$	plenum pressure coefficient
C_{Ps}	slot pressure coefficient
C_{Pw}	pressure coefficient near the wall
C_{p32}	probe pressure coefficient, see eqn. A5
c	airfoil chord, in.
$\bar{c}$	mean aerodynamic chord, in.
D	measured slotted-wall variable, see eqn. 7.39a
D_F	fitted slotted-wall variable, see eqn. 7.41
d	slot width, in
dp_i	differential probe pressure measurements, i=1, 2, 3, psi
E	sum of the residual errors, see eqn. C4
e	residual error, see eqn. 7.41
f	similarity function, see equations 7.43, 7.45, and 7.47
K	slotted-wall streamline curvature coefficient
H	boundary layer shape factor
h	tunnel semi-height, in
M	local Mach number

M_∞	free-stream Mach number
$\bar{\bar{M}}$	sidewall-corrected free-stream Mach number
n	number of measurement stations
$\frac{Pbar}{P1}$	probe Mach-number parameter
p	local pressure, psi
p_t	total pressure, psi
p_i	probe pressure measurements, i=1, 2, 3, psi
Q_p	probe quasi-dynamic pressure, see eqn. A4, psi
q	dynamic pressure, psi
R_x	Reynolds number based on x
R^2	squared multiple correlation coefficient, see eqn. C11
t	wall thickness, in
U	longitudinal (axial) velocity component, ft/sec
V	transverse (crossflow) velocity component, ft/sec
V_R	total velocity, ft/sec
W	lateral velocity component, ft/sec
u, v, w	perturbation velocity components in the x, y, and z directions, respectively, ft/sec
XBC1	upstream evaluation limit for least-squares fitting

XBC2	downstream evaluation limit for least-squares fitting
X_{11}, X_{12}, X_{21}, X_{22}	least-squares matrix coefficients, see eqn. C7
Y_1, Y_2	least-squares matrix coefficients, see eqn. C7
x	longitudinal distance along tunnel, positive in downstream direction, in
x_{ac}	location of the airfoil aerodynamic center
x_0	upstream evaluation point for computed flow-angle
x_1	downstream evaluation point for computed flow-angle
y	normal distance to tunnel wall from centerline, in
y'	normalized distance from wall in 6X19, (y-9.5)/d
z	lateral distance normal to x-y plane, in
α	angle of attack, degrees
β	Prandtl compressibility factor, $\sqrt{1 - M_\infty^2}$
$\bar{\beta}$	sidewall-boundary-layer-modified Prandtl compressibility factor, see eqn. B3a
γ	gas constant
Δ	"the change in"
ΔK	incremental slotted-wall coefficient, see eqn. 8.7
ΔM	sidewall boundary-layer induced Mach number correction

Δu	perturbation velocity, see eqn. 3.9
$\Delta\alpha_{sc}$	angle of attack correction due to streamline curvature, deg
$\Delta\bar{\beta}$	sidewall correction to Prandtl compressibility factor, see eqn. B5b
δ^*	boundary layer displacement thickness
δ_0	lift-interference correction parameter
δ_1	streamline-curvature interference correction parameter
ϵ	orifice coefficient
ϵ_B	total-blockage correction coefficient
ϵ_{SB}	solid-blockage correction coefficient
ϵ_{WB}	wake-blockage correction coefficient
η	similarity variable, see eqn. 7.42
θ	flow angle, deg
λ_0, λ_1	coefficients of eqn. 7.21
ξ	similarity variable, see equations 7.44 and 7.46
ρ	density
σ	standard deviation
Φ	non-dimensional potential evaluated in slot
ϕ	potential

Subscripts

A	"at the point" A
B	Berndt theory
c	corrected
cal	calibrated
DM	Davis and Moore theory
ff	"far-field"
h	average
i	inviscid
l	local quantity
ref	reference
s	"in the slot"
t	total
te	tunnel empty
u	associated with the u velocity component
v	associated with the v velocity component, also, viscous component
vc	"at the vena contracta"
w	"at the wall"

∞	"in the free-stream"
0	"at the point 0"
1	in region 1, see equation 7.44
2	in region 2, see equation 7.46

Abbreviations

CM	Chen and Mears
DAS	data acquisition system
DFA	Langley Research Center Diffuser Flow Apparatus
DM	Davis and Moore
LRC	Langley Research Center
6X19	Langley Research Center 6- by 19-inch Transonic Tunnel

CHAPTER I

INTRODUCTION

Wind tunnels have long been used as tools for aerodynamic research, development, and testing and, as a result, their use is relatively well understood. However, the uncertainties in the data acquired from these facilities may be large due to the interactions between the fluid and the unnatural geometric constraints provided by the tunnel circuit. The most important and variable portion of the circuit is the test-section segment which may or may not have walls depending on the type of testing to be done and the speed range of interest. For low-speed testing, either closed-throat or open-jet test sections are typically used; transonic tunnels use either slotted- or porous-wall test sections. Supersonic and hypersonic tunnels have solid (closed-throat) test sections, which are a necessity for uniform flow.

For a solid-wall test section, the approximate boundary condition is zero normal flow at the wall. Solid walls constrain the flow about the model such that (for positive angles of attack) the velocities on the upper surface are higher than normal while the lower-surface velocities are lower. Thus, a relatively larger value of lift is measured as compared to the flow about the same model in free air.

For an open-jet test section the condition of zero longitudinal velocity perturbation or zero pressure drop across the interface between the jet and the "undisturbed" plenum is imposed. Open-jet tunnels force the local pressure at the interface to be equal to the free-stream (plenum) pressure which is larger than the pressure at an equivalent location in free air. Thus, for positive angles of attack, the measured value of lift is less than the free air value.

From the previous discussion, it is clear that closed-wall and open-jet test sections provide flow conditions that are different from those which exist about a body in free air. The resulting error in the model data acquired in these types of wind tunnels was analyzed for incompressible, two-dimensional flows as early as 1919 by Prandtl (ref. 1). His analytical methods used known solutions of Laplace's equation in conjunction with the method of images and lifting-line theory to predict tunnel-to-free-air corrections of the test conditions. Over a period of about 30 years extending into the late forties, Prandtl's analysis methods were extended to include effects such as those occuring in three-dimensional flows in wind tunnels with various cross-sectional geometries (for example, see ref. 2) and the influence of compressibility (ref. 3). Verification experiments were also conducted during this period. Several concise surveys of the resulting corrections are given in references 4, 5, 6, and 7.

The first thirty years of wind-tunnel wall-interference research yielded an important fact for modern wind tunnels; that is, theoretically and experimentally, solid-wall corrections are opposite in sign to those for open-jet test sections. Thus, if one has a slotted or perforated wall, which in terms of openness is somewhere between an open jet and a solid wall, it should be possible to adjust the geometric openness (porosity) to obtain a near zero wall-interference correction and thereby allow a more realistic simulation of free-air conditions. For reference, a schematic of a typical two-dimensional slotted-wall wind tunnel is shown in figure 1a along with a cross-sectional view of a slotted wall in figure 1b. Wright and Ward (ref. 8) were the first to determine theoretically the wall-induced interference of the slotted-wall tunnel. To do this, they solved Laplace's equation for a circular cross-section wind tunnel with different numbers of slots. The

tunnel disturbance was assumed to be caused by a doublet singularity whose strength is matched to the blockage of the model. They alternately applied the solid-wall and open-jet conditions at the slats and slots, respectively, at the wall boundary. Their analysis showed the "possibility of obtaining zero blockage interference" in a slotted-wall test section. Based on these theoretical calculations, a slotted test section was constructed for the NACA Langley Research Center's 8-Foot High Speed Tunnel (8-Foot HST) and placed in operation in early 1950 (ref. 9). Research conducted in this facility showed that by increasing the drive-system power slotted wind tunnels can be operated at supersonic speeds and that "the phenomena of choking, characteristic of closed tunnels, did not occur in the slotted tunnel" (ref. 8).

As with most advances in the "state-of-the-art", slotted walls introduced a new set of problems. Slotted walls have a mixed boundary composed of solid and open regions which, as a result, are very difficult to model mathematically. Estimates of the wall induced interference are, therefore, difficult to determine with any degree of certainty, particularly at transonic speeds and with large model-span-to-tunnel-height ratios. Davis and Moore (ref. 10, 1953) and Chen and Mears (ref. 11, 1957) each attempted to simplify the mathematical description of the wall and in the process derived what is now known as the classic or "ideal" form of the slotted-wall boundary condition. In their theoretical analyses, they assumed that all of the perturbations from the free-stream velocity at the wall were small. This allowed them to derive a relationship between the far-field average (homogeneous) pressure drop across the wall and the streamline curvature in the tunnel. Their formulation is given as

$$C_{Pw} - C_{Ps} = 2aK\frac{\partial \theta_w}{\partial x} \tag{1.1}$$

where the subscript w denotes the spanwise average of the flow property "at the wall". This average is in reality taken as that far from the slot in the tunnel where the rapidly varying changes due to the presence of the slot are negligible. The subscript s denotes "at the slot" and represents the local far-field pressure on the plenum side of the slotted wall. The slotted-wall, geometry-dependent coefficient K must be determined either through theoretical analysis or appropriate experiment. The major difference between the Chen and Mears and the Davis and Moore theories is an attempt by the former to model the influence of slat thickness whereas the Davis and Moore form considered zero-thickness slats.

Baldwin, et. al. (ref. 12, 1954) proposed an empirical extension to (1.1) which accounts for viscous effects in the slots. Likewise, Goethert (ref. 13, 1957) extended (1.1) by proposing a modification for slot configurations with porous cover plates. The resulting form of the boundary condition was the same in each case and is given by

$$C_{Pw} - C_{Ps} = 2aK\frac{\partial \theta_w}{\partial x} + B\theta_w \tag{1.2}$$

where a linear cross-flow term, $B\theta_w$, is the contribution due to viscosity. The assumption of small-velocity perturbations at the wall was again made. An estimate of the magnitude of the crossflow velocity for which (1.2) would apply was given in reference 12 and, using the present notation, is

$$\left(\frac{v}{U_\infty}\right)^2 \ll 2\sin^2\left(\frac{\pi d}{2a}\right)\frac{u}{U_\infty} \tag{1.3}$$

Thus, if a typical openness, d/a, is taken as 0.05, for the linear theory to apply the square of the crossflow velocity perturbation must be much smaller than 0.01 times the longitudinal perturbation. This places an unrealistic restriction on the validity of equations 1.1 and 1.2 for practical applications.

To remove the small crossflow restriction, Wood (ref. 14, 1964) reasoned that crossflow in the slot would be larger than that typically allowed in the previous theoretical developments and that it would dominate the effect of the streamline curvature for slots of small width. His perturbation analysis yielded a non-linear boundary condition of the form

$$C_{Pw} - C_{Ps} = \left(\frac{\pi + 2}{\pi}\,\frac{a}{d}\right)^2 \theta_w^2 \tag{1.4}$$

for both inflow and outflow through the slots. No published application of the boundary condition is known other than that of reference 14 where only "qualitatively similar" comparisons with experiment are demonstrated.

Finally, Berndt (ref. 15, 1975) derived, using the present notation,

$$C_{Pw} - C_{Ps} = 2\left(\frac{\rho U}{\rho_\infty U_\infty}\right) aK \frac{\partial \theta_s}{\partial x} + \left(\frac{\rho}{\rho_\infty}\right)\theta_s^2 \tag{1.5}$$

by integrating the pressure drop along a path from the center of the slat through the slot and into the plenum. His analysis neglected shear stress contributions and estimated the value of the wall coefficient K from an inviscid analysis in much the same way as the Davis and Moore theory only this time allowing for the effect of slot depth (wall thickness). This equation essentially combines the functional forms of equations 1.1 and 1.4 as the

applicable wall pressure-drop condition. In this and each of the previously cited forms of the boundary condition the equations have been derived after assuming an inviscid flow. A minor qualification of this statement is made for the development of equation 1.2 where the viscous effects were empirically added after the fact.

Comparisons between experimentally determined values of the slotted-wall coefficient K and the theoretically developed variations of K with openness ratio are in very poor agreement. Figure 2 shows the experimental variation of the coefficient K with wall openness ratio (ref. 11, 15, and 16) compared with the theories of Davis and Moore (ref. 10) and Chen and Mears as corrected by Barnwell (ref. 11 and ref. 17). The three experimentally determined values of K are parametrically inconsistent in that they were obtained over a speed range of 93 ft/sec to $M_\infty = 0.95$ and have a variation of the number of slots from 3 to 15. These comparisons show considerable disagreement not only between the experiment and the theory but also reveal large discrepancies which result from two different theoretical models of the wall geometry.

In order to resolve some of the uncertainties exhibited by past theoretical developments and to establish a definitive parametrically-varied data base from which estimates of wall boundary-condition coefficients could be obtained, a combined theoretical and experimental effort was initiated and is presented in this dissertation. Specific goals of the research were:

1. to gain an increased understanding of the physics of the flow in the vicinity of the slotted wall by examination of existing data,

2. to conduct an experiment where wall-geometry parameters were varied in a systematic manner and appropriate flow measurements were made,

3. to analyze the existing theoretical treatments of the slotted-wall boundary condition and determine the formulation which is the most consistent with the experimental measurements,

4. to estimate the value of the unknown coefficients in the resulting boundary condition from the existing (where possible) and newly established data bases.

With this increased understanding of the slotted-wall boundary condition, it is possible to design better wall configurations for existing and new wind tunnels which will reduce the interference in measured aerodynamic data. The results also point the way to additional slot-flow studies which focus on slot-boundary-layer interaction and the effects of changes in the slot cross-sectional geometry. Finally, this study should contribute to the development of adaptive slotted walls which can be modified "online" for increased data quality.

CHAPTER II

APPROACH

Because of the large number of experimental and analytical components of the present investigation, a "road map" of its layout is given as a guide. The study begins with the derivation of the slotted-wall boundary condition in Chapter III in order to determine its structure and understand the assumptions which go into it. This derivation will provide some insight into what to look for when examining data which were obtained by others in previous experiments (discussed in Chapter IV). These data will be analyzed for fluid-dynamic phenomena which are important to the discussion in subsequent chapters.

At this point, a discussion will be given (Chapter V) of the experimental study which was conducted expressly for this investigation in the Langley Research Center's 6- by 19-Inch Transonic Tunnel (6X19). Included in this discussion is a description of the wind tunnel facility, models (both airfoil and wall), the location of the pressure measurements, instrumentation, and test conditions. This section is then followed in Chapter VI by an analysis of the 6X19 data. Here, an examination of the data is made in the light of information presented in previous chapters relative to the consistency of fluid-dynamic phenomena between different data sets.

The next two chapters, VII and VIII, describe the methods by which the 6X19 data are theoretically analyzed to obtain the coefficients which are present in different formulations (including the present one) of the slotted-wall boundary condition as well as a presentation of the coefficients themselves. Included in chapter VIII is an almost "stand-alone" section which demonstrates the application of the principles of dynamic similarity to the flow in the vicinity of a slotted wall. These chapters represent the most

significant findings of the present research effort and are, primarily, the basis for the conclusions contained in Chapter IX and the recommendations which are contained in Chapter X.

CHAPTER III

DERIVATION OF THE SLOTTED-WALL BOUNDARY CONDITION

As discussed in the Introduction, a large measure of uncertainty exists in the form of the slotted-wall boundary condition and its unknown coefficients. This uncertainty has prompted many frustrated researchers to apply no wall corrections whatsoever because of often conflicting results. Clearly it is desirable to reduce or remove this uncertainty. In order to do do this, however, the boundary condition must be determined (as nearly as possible) such that an experiment can be designed which has the appropriate geometric variations and free-stream conditions. This chapter contains a general description of the slotted-wall tunnel, its geometry, and defines by theoretical derivation the boundary condition to be studied.

The purpose of tunnel walls is simply to confine the flow and to permit a prescribed velocity distribution around the tunnel circuit or, in the case of a blowdown tunnel, to the point where the flow is exhausted to the atmosphere. The test-section segment of the wind tunnel circuit is the most complex due to the presence of the model support system and, for transonic wind tunnels, the utilization of slots or holes to relieve the unnatural inhibiting effects of the walls on the flow. A slotted-wall tunnel, which is the type of facility of concern in this study, is composed of alternating open and solid members which marry the attributes of both the open-jet and closed-wall tunnels (as discussed in the Introduction).

In order to establish the boundary condition existing at the slotted wall, which represents in some sense the flow at the test section wall, it is necessary to understand the physics of the flow about and through the slots. With this understanding a physically meaningful boundary condition can be

developed and the open area of the slots can be prescribed to give the pressure drop (as closely as possible) which would exist in the undisturbed flow about the model. In subsequent sections the mathematical and flow considerations leading to the determination of the slotted-wall boundary condition are given.

A. Slotted-Wall Geometry

A view of a slotted-wall wind tunnel and its coordinate system is shown in figure 1a. The longitudinal coordinate, x, is taken along the centerline of the tunnel, y normal to the centerline and z perpendicular to the x-y plane. The velocities are denoted by U, V, and W corresponding the the coordinates x, y, and z, respectively. The tunnel typically has a settling chamber upstream of the test section to allow the dampening of disturbances in the flow. This is followed by a length of solid, converging walls through which the flow is accelerated to the desired test conditions. The test section has slotted walls extending both upstream and downstream of the model with the walls being separated by a distance 2h. Upstream, the slots allow the flow to expand around the model into the plenum chamber which surrounds the test section. Downstream, the slots allow the flow to re-enter the test section. The slotted-wall portion of different wind tunnel test sections may have different numbers of slots, different openness ratios and different cross-sectional geometries. At the downstream end of the test section there is a re-entry region which may or may not have re-entry flaps (depending on the construction of the tunnel) to allow the smooth transition of the flow into the diffuser section.

Figure 1b shows a cross-sectional view of a typical slotted wind-tunnel wall, defines its geometric parameters, and gives a portion of the flow field

as projected onto the cross-flow plane. The slotted-wall configuration shown is composed of rectangular members called slats which are periodically spaced a distance a apart. The geometric slot width is denoted by d and the thickness or depth of the slot is denoted by t. Other geometric parameters such as variations in cross-sectional shape and slot-lip radius-of-curvature have not been illustrated for the sake of clarity. The local flow angles, θ, as shown in figure 1a are measured with respect to the centerline of the tunnel and are taken positive for outflow. The approach velocity to the slotted wall, v_w, is taken as the spanwise average of the velocity in the cross-flow plane at some distance which is sufficiently far from the slot to avoid the large, rapidly varying flow into the slot. After entering the slot the flow may separate from the wall and narrow to form a vena contracta. This narrowing forms the effective "fluid" slot width and is typically treated through the use of an orifice coefficient. Though not noted, the subscript s will be used to denote "at the slot".

B. Development of the Slot Pressure Coefficient

Along the slotted wind-tunnel walls, viscosity manifests itself in at least two different ways. On the solid portion of the wall, along the slats, a boundary layer develops. Over and through the slot region, a shear layer exists. On the slot centerplane for outflow to the plenum, the total pressure in the slot should be near the total pressure of the tunnel free stream. Then, the pressure in the slot can be represented by

$$\frac{p_s}{p_\infty} = \left\{ 1 + \frac{(\gamma - 1)M_\infty^2}{2} \left[\left(\frac{V_R}{U_\infty} \right)^2 - 1 \right] \right\}_s^{\frac{\gamma}{\gamma - 1}} \tag{3.1}$$

which is derived in reference 18. The variables p_s and V_{Rs} are the static pressure and total velocity in the slot. The variables p_∞, U_∞, and M_∞ are the free-stream static pressure, velocity, and Mach number, respectively. Using the binomial expansion of equation (3.1), $\frac{p_s}{p_\infty}$ can be written as

$$\frac{p_s}{p_\infty} = 1 - \frac{\gamma M_\infty^2}{2}\left[\left(\frac{V_R}{U_\infty}\right)^2 - 1\right]_s + \frac{\gamma M_\infty^4}{8}\left[\left(\frac{V_R}{U_\infty}\right)^2 - 1\right]_s^2 - \ldots \tag{3.2}$$

By assuming that the flow in the slot may be written as a deviation from the undisturbed free stream, U_∞, we can write

$$\left(\frac{V_R}{U_\infty}\right)_s^2 = \left[\frac{\left(U_\infty + u\right)^2 + v^2 + w^2}{U_\infty^2}\right]_s \tag{3.3}$$

since

$$U_s = U_\infty + u_s, \quad V_s = v_s, \text{ and } \quad W_s = w_s$$

In the vicinity of the slot u and w and their squares are much less than U_∞ and U_∞^2. Note that, because of symmetry considerations, w approaches zero along both the slat and slot centerplanes; however, there is no requirement for v to be small. While v is much smaller than U_∞, it may still be much larger than u and must be retained. With these assumptions

$$\left(\frac{V_R}{U_\infty}\right)_s^2 - 1 \approx \left(\frac{2u}{U_\infty}\right)_s + \left(\frac{v}{U_\infty}\right)_s^2 \tag{3.4}$$

Likewise, to the same order

$$\frac{\gamma M_\infty^4}{8}\left[\left(\frac{V_R}{U_\infty}\right)_s^2 - 1\right]^2 \ll \frac{\gamma M_\infty^2}{2}\left[\left(\frac{V_R}{U_\infty}\right)_s^2 - 1\right] \tag{3.5}$$

with $M_\infty < 1$ allowing $\frac{p_s}{p_\infty}$ (eqn. 3.2) to be written as

$$\frac{p_s}{p_\infty} = 1 - \frac{\gamma M_\infty^2}{2}\left[\left(\frac{V_R}{U_\infty}\right)_s^2 - 1\right] \tag{3.6}$$

Define the slot pressure coefficient, C_{Ps}, as

$$C_{Ps} = \frac{2}{\gamma M_\infty^2}\left(\frac{p_s}{p_\infty} - 1\right) \tag{3.7}$$

Then, using (3.4) and (3.6), we can write equation (3.7) as

$$C_{Ps} = -\left[\left(\frac{2u}{U_\infty}\right) + \left(\frac{v}{U_\infty}\right)^2\right]_s \tag{3.8}$$

The deviation of the longitudinal perturbation in the slot velocity, u_s, from the perturbation in the local ambient value near the wall, u_w, can come from two sources: a viscous component and an inviscid component. Therefore, the u_s velocity component may be written as

$$u_s = u_w + \Delta u_{is} + \Delta u_{vs} \tag{3.9}$$

where Δu_{is} is the rapidly varying inviscid velocity component of the flow which is accelerating into the slot due to airfoil induced streamline curvature and Δu_{vs} is the viscous velocity component in the slot due to the interaction of the slot with the wall boundary layers and the slower moving plenum air.

C. Determination of Δu_{is}

The inviscid velocity has traditionally been modelled by assuming the slot to behave as a slender body. Barnwell (ref.17) proposed writing the Δu_i in the form of a perturbation potential, $\phi(x,y,z)$. Thus,

$$\Delta u_i = \frac{\partial \phi_i}{\partial x} = \frac{\partial (v_w a \Phi)}{\partial x} \tag{3.10}$$

where v_w is the spanwise average of the far-field velocity approaching the slot, a, the slot-flow length scale, is the periodic slot spacing, and $\Phi(x,y,z)$ is the non-dimensional potential of the rapidly varying flow near the wall. Since the length scale of the flow is much greater in the longitudinal direction than in the crossflow direction, $\Phi(x,y,z)$ will, at most, be a weakly varying function of x. Differentiation of (3.10) yields

$$\Delta u_i = a \frac{\partial \Phi}{\partial x} v_w + a \Phi \frac{\partial v_w}{\partial x} \tag{3.11}$$

After evaluating (3.11) in the slot and dividing by U_∞, the resulting expression for the inviscid contribution to the slot pressure drop coefficient is

$$\frac{\Delta u_{is}}{U_\infty} = a\frac{\partial K}{\partial x}\left(\frac{v_w}{U_\infty}\right) + aK\frac{\partial}{\partial x}\left(\frac{v_w}{U_\infty}\right) \tag{3.12}$$

where

$$K = \Phi(x, y_s, 0) \qquad \text{and} \qquad \frac{\partial K}{\partial x} = \frac{\partial \Phi(x, y_s, 0)}{\partial x} \tag{3.13}$$

The parameter K is the slotted-wall coefficient which is obtained by evaluating the potential Φ in the slot at y_s. Since a non-dimensional potential was used, these terms are functions of the geometry of the slotted wall. For slowly varying slot width and fully developed flow, the gradient should be negligible, and equation (3.12) reduces to

$$\frac{\Delta u_{is}}{U_\infty} \approx aK\frac{\partial}{\partial x}\left(\frac{v_w}{U_\infty}\right) \tag{3.14}$$

D. Determination of Δu_{vs}

As previously noted, the slotted wind-tunnel wall is a composite of two types of wind-tunnel walls: a solid wall and an open jet. Ramaswamy (ref.19) examined the effects of viscosity in the region of a slot in the absence of longitudinal flow curvature and by analogy with the development of the sheared flow at an open-jet boundary concluded that a linear relationship between Δu_{vs} and the crossflow velocity should exist when the pressure drop across the wall is small. His reasoning is as follows. For an ideal open-jet wind tunnel with no plenum suction, i.e. $p_p = p_\infty$, the flow at the jet boundary will have constant total pressure, will be approximately parallel and, for incompressible flow, can be represented by the Bernoulli equation as

$$p_{t\infty} = p_\infty + \tfrac{1}{2}\rho U_\infty^2 = p_p + \tfrac{1}{2}\rho U_\infty^2$$

where $p_{t\infty}$ is free-stream total pressure, ρ is the density, U_∞ is the free-stream velocity, and p_∞ and p_p are the free-stream and plenum pressures, respectively. Reducing the plenum pressure slightly will cause an increase in the boundary velocity and force the flow to curve so that the centrifugal and pressure forces remain in equilibrium. Similarly, in the vicinity of a slot, the shear layer will behave as in an open jet; however, unlike the ideal jet boundary, the total pressure will vary through the slot shear layer.

For the case of no crossflow, the flow along the streamline at a point A near the slot is defined by

$$p_{tA} = p_w + \tfrac{1}{2}\rho U_A^2$$

where the ambient pressure, p_w, is equal to the plenum pressure. If the plenum pressure is decreased slightly, the streamline originally at A will move to a point s in the slot. This shift will induce a change in the longitudinal velocity Δu_{vs} and a normal component v_s. Thus,

$$p_{tA} = p_w + \tfrac{1}{2}\rho U_A^2 = p_s + \tfrac{1}{2}\rho\left[\left(U_A + \Delta u_v\right)_s^2 + v_s^2\right]$$

$$\approx p_s + \tfrac{1}{2}\rho\left(U_A^2 + 2U_A\Delta u_{vs} + v_s^2\right)$$

to the present approximation. For small crossflow velocities,

$$p_A + \tfrac{1}{2}\rho U_A^2 \approx p_s + \tfrac{1}{2}\rho\left(U_A^2 + 2U_A\Delta u_{vs}\right)$$

Furthermore, we know that under these conditions that Δu_{vs} is proportional to v_s. Thus,

$$\Delta u_{vs} = B' v_s \tag{3.15}$$

and

$$\frac{p_A - p_s}{\frac{1}{2}\rho U_\infty^2} = 2B' \frac{U_A}{U_\infty}\left(\frac{\Delta u_s}{U_\infty}\right) = B\left(\frac{v_s}{U_\infty}\right) \tag{3.16}$$

For large crossflows, the shear layer is pushed completely out of the slot region and free-stream total pressure is realized in the slot. This results in

$$p_{t\infty} = p_\infty + \frac{1}{2}\rho U_\infty^2 = p_s + \frac{1}{2}\rho\left(U_\infty^2 + v_s^2\right)$$

since the lateral effects of the tunnel-wall boundary layer will not allow the longitudinal slot flow to exceed the free-stream velocity. Therefore,

$$\frac{p_\infty - p_s}{\frac{1}{2}\rho U_\infty^2} = \left(\frac{v_s}{U_\infty}\right)^2 \tag{3.17}$$

and the flow is dominated by the quadratic term.

E. Slot-Flow Boundary Condition

Combining equations 3.8, 3.9, 3.14, and 3.15 gives

$$C_{Ps} = -2\frac{u_w}{U_\infty} - 2aK\frac{\partial}{\partial x}\left(\frac{v_w}{U_\infty}\right) - B\left(\frac{v_s}{U_\infty}\right) - \left(\frac{v_s}{U_\infty}\right)^2 \tag{3.18}$$

Now define

$$\theta_s = \frac{v_s}{U_\infty} \qquad \theta_w = \frac{v_w}{U_\infty} \qquad C_P = -2\frac{u_w}{U_\infty} \tag{3.19}$$

where θ_s is the slot flow angle, θ_w the far-field wall flow angle, and C_{Pw} is the pressure coefficient of the flow near the wall. Then the slotted-wall boundary condition (eqn. 3.18) can be written as

$$C_{Pw} - C_{Ps} = 2aK\frac{\partial \theta_w}{\partial x} + B\theta_s + \theta_s^2 \tag{3.20}$$

Away from the slot, the condition of irrotationality with equation 3.19 may be used to obtain

$$\frac{\partial C_{Pw}}{\partial y} = -2\frac{\partial \theta_w}{\partial x} \tag{3.21}$$

Equation 3.21 may be used to re-write (3.20) to give

$$C_{Pw} - C_{Ps} = -aK\frac{\partial C_{Pw}}{\partial y} + B\theta_s + \theta_s^2 \tag{3.22}$$

Either of equations 3.20 or 3.22 may be used as the boundary condition depending on the application. The coefficient K on the right-hand-side of equations 3.20 and 3.22 is the wind-tunnel-wall geometry-dependent proportionality coefficient which relates the pressure drop across the wall to the streamline curvature of the flow about a model in the tunnel. The coefficient B is the wall shear coefficient which is dependent not only on the geometry of the wall but also on the interaction of the wall flow and the plenum flow.

In the material to follow, a chapter will be devoted to a presentation of existing available experimental studies which will be analyzed in the light of understanding the fluid physics in the vicinity of a slotted wall and also to support assumptions which are made in the present analysis. This will be followed by a description of a series of experiments conducted in the Langley Research Center's 6- by 19-inch Transonic Tunnel for the present study which had a systematic variation of free-stream parameters and wall geometries. Results from these tests will then be presented along with some analysis of the experimental data. Following this will be a theoretical and analytical study of the 6- X 19-inch transonic tunnel experimental results which will put substance to the values of the unknown wall boundary-condition coefficients.

CHAPTER IV

ANALYSIS OF PAST EXPERIMENTAL INVESTIGATIONS

In this chapter, existing experimental data will be examined with the intent of understanding the physics of the fluid motion in the vicinity of a slotted wall. Several studies of "slot-flow/wall-interference" conducted by different researchers in different wind tunnels will be examined. These are followed by an analysis of some previously unpublished data obtained during a slotted-wall study conducted in the Langley Research Center's Diffuser Flow Apparatus (DFA) (ref. 20).

A. Chen and Mears Experiment

In a paper published in 1957 (ref. 11), Chen and Mears (referred to hereafter as CM) presented a combined theoretical and experimental study of the slotted-wall boundary condition. Three slot experiments were conducted in the Brown University 22" x 32" Low-Speed Wind Tunnel. In the first (Test 1), a 24-inch Joukowsky airfoil was placed on the lower solid wind-tunnel wall with its leading edge 12 inches downstream of the slot origin (see figure 3). In the second experiment (Test 2), the same airfoil was moved such that its leading edge was 22 inches downstream of the slot origin. And finally (Test 3), a similar 12-inch chord version of the Joukowsky airfoil was placed in the center of the tunnel between two slotted walls with its leading edge 17 inches downstream of the slot origin. Each slotted wall had 9 slots and an openness of 14.1 percent. The slots originated at 3 inches downstream of the beginning of the test section and terminated at station 47. In each case, the airfoil spanned the 32 inch dimension of the tunnel and had a chord-to-tunnel semi-height ratio of 1.09. This ratio is generally large for conventional

airfoil studies which typically fall in the range of 0.2 to 0.35 but the large size helped accentuate the airfoil/wall interaction. These test configurations are shown in figure 3, which has been taken from the Chen and Mears report.

The test velocity for each experiment was 93 feet per second. All pressure measurements were referenced to the atmospheric plenum pressure. Pressure and flow angle measurements were made both over the slot and over the slat at a position 2 inches above the plane of the wall along the length of the slotted wall. It should be noted that all of the CM data presented here have had the axial coordinate translated to the x station corresponding to the leading edge of the airfoil and are then normalized with respect to airfoil chord length.

The CM pressure measurements taken over the slot are presented in figure 4a with the corresponding flow angle measurements in figure 4b. It is to be noted that the pressure coefficient is the drop across the wall since the reference pressure is the plenum pressure. While generally good agreement appears to exists over the front of the airfoil, closer examination reveals that this is not the case. The pressure coefficients for the 12-inch and 24-inch airfoils diverge upstream to different levels beginning at $x/c = -0.5$. This disagreement is possibly due to the differences in the growth of the tunnel-wall boundary layers but more likely to finite tunnel effects being manifested in the short length of slot length upstream of the airfoil leading edge. The short slot length would not allow the flow to become fully developed prior to the imposition of airfoil-induced flow disturbances. Discrepancies in the pressure drop downstream of the leading edge begin appearing immediately but are clearly evident in the data in the vicinity of and downstream of the point of maximum thickness ($x/c \approx 0.30$). For Test 2,

the trailing edge of the airfoil extended past the end of the slots giving a finite-tunnel effect which is evident in both the pressures and flow angles (fig. 4b).

The flow angles presented in figure 4b, again, show the effects of the finite length of the slots. Data from Test 1 and Test 2 are similar in their development upstream of the maximum thickness but diverge significantly downstream. Interestingly, the measurements on the small airfoil compare very well with the Test 1 results beginning slightly upstream of the leading edge throughout the extent of the measurement region.

Since the theory requires the gradient of the flow angle, this was computed for each test and is presented in figure 4c. It can be seen that ahead of the airfoil leading edge all results are essentially the same. The data from Test 1 and Test 3 give similar results over the whole range of the measurements with Test 2, again, showing significant finite-tunnel effects downstream of maximum airfoil thickness.

Based on these observations, it is felt that the Test 3 measurements are more representative of true airfoil/slot interactions which should occur in a typical airfoil wind tunnel even though the chord-to-tunnel semi-height ratio is probably excessive. These data demonstrate the influence of finite tunnel effects on wall pressure data and the need to maintain enough upstream and downstream slot openness to allow the flow in the slot region to stabilize.

Chen and Mears made flow angle measurements both over the slat and over the slot which are presented here in figures 5a, 6a, and 7a with the corresponding gradients presented in figures 5b, 6b, and 7b. The measurements are "practically the same except in the rear portion" for all the tests. They also had similar results for their pressure measurements but "to avoid congestion of the graphs" they did not present them. The similarity of the

streamwise variation of the flow angle and pressure over the slot and slat indicate a nearly two dimensional flow across the tunnel and in the "far-field" of the slots.

B. Berndt's Experiment

Berndt (ref. 15) conducted an experiment to determine the flow conditions in the vicinity of a slotted wall occurring at a high transonic Mach number of 0.903. The general layout of his test facility and wall configuration is shown in figure 8, which was taken from the cited reference. His wall had three 4 mm. wide slots with a slot spacing of 80 mm. giving a wall-openness ratio of 5 percent. Berndt chose a relatively deep slot of 6 mm. giving a slot depth-to-width ratio of 1.5. A circular arc airfoil with a chord length of 90 mm. was chosen as a disturbance model. The chord-to-tunnel-semi-height ratio for his study was 0.72.

Figure 9a presents Berndt's wall pressure drop measurements. Both model-in and tunnel-empty pressure data are presented along with the increment between the two conditions. For reference, the airfoil leading edge is located at tunnel station 0 mm. and the trailing edge is at station 90mm. An examinination of the increment curve shows the airfoil influence to have two major effects on the wall pressure difference. The first of these is a global influence. For matched free-stream Mach numbers the far-field upstream pressure in the tunnel with the model installed will be the same as that for the tunnel-empty case. However, the pressure increment equilibrates at a constant value which is different from the tunnel-empty value indicating a negative shift in the reference plenum pressure because of the airfoil interaction with the "tunnel/plenum system". Because of this shift, the plenum pressure is a very poor choice for the reference calibration pressure

for transonic wind tunnels. This pressure shift will be discussed again in chapter V for the 6X19 experiments. The second major airfoil effect is a region of large local pressure variations between plus and minus 1 chord of the model leading and trailing edges. The terminology "local" is used to indicate the immediate vicinity of the model where large changes in some flow property (pressure in this instance) are occuring.

Flow-angle data measured in the slot are presented in figure 9b. At approximately 1/2 chord upstream of the leading edge, the flow angle flattens and becomes insensitive to the presence of the airfoil model. Unfortunately, data are unavailable downstream of the trailing edge station and the nature of the flow returning to the tunnel through the slot is not known. Berndt states that the measurements downstream of station 80 mm. are unreliable due to their small size. It is important to note the magnitude of the flow angles in the slot. At station -40 mm., the tunnel-empty values are about 13 degrees while airfoil-in values are about 18 degrees. Berndt's setup is such that large outflow occurs over most of the airfoil test region.

Figure 9c presents the gradient in the flow angle as determined from the data presented in figure 9b. The influence of the airfoil is clearly seen as is the uncertainty in the flow angle measurements beginning at station 80 mm. It is evident that the local presence of the airfoil on the slot flow is felt only in the region beginning at approximately 1/2 chord length upstream of the airfoil leading edge.

Berndt measured the total pressure both along and through the slot on its centerplane. His model-in results are reproduced here as figure 9d. It is to be noted that probe height 1 mm. is just below the slot entrance and probe height 6 mm. is at the slot exit. The total pressure of the slot-entry flow from a position 2/3 chord upstream of the airfoil leading edge to one near the

airfoil trailing edge is very near that of the free stream. The drop in the total pressure through the slot, particularly in the vicinity of the model, is an indication (contrary to Berndt) of the viscous shearing which exists in the slot and the return of lower-energy plenum air to the slot as the flow reverses direction. Berndt states that "the slot flow under consideration is one with fairly small effects of inflow from the wall boundary layer and of viscous stress in the slot ...". Statements such as this prompted the slot-flow shearing analysis of Ramaswamy (ref. 19) which has been included in the present analysis. For the tunnel-empty data, Berndt states that "When there is no model present the level of the total pressures (not shown) is somewhat reduced, while the losses towards the rear are absent."

D. DFA Experiment

An abbreviated, unpublished study of the development of the flow in the vicinity of a slotted wall was conducted in the Langley Research Center's Diffuser Flow Apparatus (DFA) by W. B. Igoe and S. G. Flechner. This facility, which is a small scale version of the contraction, test section, and diffuser region of the National Transonic Facility (NTF), is described in detail in reference 20. The test-section region of the tunnel is shown schematically in figure 10a. The tunnel is 18.26 inches square with slotted upper and lower walls and solid sidewalls. For this study, each slotted wall was composed of 6 rectangular slots each of which has a constant width of 0.25 inches and thickness of 0.24 inches. The slots originate at tunnel station 0 and terminate in the re-entry region at tunnel station ≈45. The slot coordinate system and cross-sectional shape are shown figures 10b and 10c.

During the experiment, flow angles were measured with a three-tube flow angularity probe, a schematic of which is shown in figure 11. To minimize

interference, the probe width was 0.02 inches compared to the 0.25-inch width of the slot. Measurements were made through the slot on the centerplane at a fixed longitudinal station and also along the slot at fixed vertical distance from the slot. Test results were obtained at free-stream Mach numbers of 0.6, 0.725, and 0.85. The data were acquired with various amounts of plenum suction ranging from 0 to 2 percent of free-stream mass flux; however, only those data with 0 percent plenum suction will be presented. It is important to note that not all combinations of test conditions were acquired for each case.

The test model used in the study was a 5.4-inch chord NACA 0012-64 airfoil with leading edge at station 22.6 and trailing edge at station 28. Maximum thickness of the airfoil is at $x/c = 0.30$ which corresponds to tunnel station 24.65. The chord-to-tunnel-semi-height ratio is 0.60 which is typical for two-dimensional airfoil testing. Only airfoil data at zero lift were obtained and then not at all test conditions. Because of problems incurred during data reduction, pressure data on the airfoil and on the slotted wall were not available for analysis.

The development of the tunnel-empty slot flow parameters both normal to and along the slot are shown in figures 12 for a free-stream Mach number of 0.6. In each case the local flow angle measured in degrees, the local Mach number, and the local total-pressure ratio are plotted against the normalized distance from the wall. This normalized distance is the distance from the wall divided by the slot width where 0 is at the slot entrance and positive displacements are into the tunnel. Since the slot width is 0.25 inches, $y/d = 8$ corresponds to 2 inches into the free stream while $y/d = -4$ corresponds to 1 inch into the plenum. The flow angle is measured positive out of the tunnel into the plenum. It can be seen in figure 12a that the flow

angle in the tunnel is very small, increases rapidly as the slot is approached, and reaches a value of about 7 degrees of outflow at the slot entrance. The flow angles increase almost linearly from $y/d = 0.4$ to the vena contracta which occurs between $y/d = -0.3$ and $y/d = -0.5$ in all cases. Measured variations of the local Mach number and local total pressure in figures 12b and 12c show the expected decrease due to viscous shearing of the flow in the vicinity of the wall. At the slot entrance, the total pressure in the slot is about 91 percent of its free-stream value. An increase in the shear along the slot is evident as the flow develops indicating increasing communication of the lower-energy plenum air with the high-energy tunnel free stream.

The effects of changing the free-stream Mach number on the slot flow parameters are demonstrated in figures 13. In these figures, the local flow angle, local Mach number, and local total-pressure ratio at tunnel station 24 are plotted versus normal displacement from the wall, y/d, for free-stream Mach numbers of 0.6 and 0.85. Virtually no differences in the flow angle results exist except in the region between $0.4 \leq y/d \leq 4$. Differences in the Mach number profiles shown in figure 13b are as expected and indicate the penetration depth of the tunnel flow into the plenum. The viscous slot flow is contained in a very narrow region near the wall. For the higher Mach numbers, the total-pressure ratio (fig. 13c) indicates a greater loss in the total head in the slot. Increasing the Mach number from 0.6 to 0.85 causes the total-pressure ratio in the slot to decrease from 0.91 to 0.82. Again, a much thicker shear layer exists for the higher Mach number.

Comparison of the airfoil results with the tunnel-empty results at tunnel station 24 is shown in figures 14 for a free-stream Mach number of 0.6. At this station all of the slot variables with the airfoil installed are smaller

than the corresponding tunnel-empty values. This occurs because this tunnel station is very near the station corresponding to maximum airfoil thickness and, thus, is near the station where the flow angle around the airfoil should be reversing sign. This reversal of the flow brings the lower momentum air from the plenum further into the slot decreasing the local Mach number (fig. 14b) and local total pressure (fig. 14c). Similar results are evident in Berndt's total pressure data presented in figure 9d. It should be noted that the vena contracta of the airfoil data occurs at approximately the same location as the tunnel-empty data.

An interesting phenomenon occurs in the flow-angle data (fig. 14a) between $1 \leq y/d \leq 2$. In this region, the flow begins reversing direction and the flow angle approaches zero before it again accelerates into the slot. Unfortunately, this was the only tunnel station where measurements were made normal to the wall through the slot with the airfoil installed and the exact reason for this behavior is unknown. One plausible explanation is found in data presented by Wu (ref. 21). In his experiment, flow field measurements were made normal to the wall at four spanwise stations. The wall contained a single centerline slot which was 0.36m (14.2 inches) long by 6.6×10^{-3}m (0.26 inches) wide and had zig-zag shaped baffles making a 14 degree angle to the vertical. A schematic of the experiment taken from reference 21 is shown in figure 15. Measurements were made at various free-stream Mach numbers and amounts of plenum suction. The u, v, and w velocity components were obtained with a five-port flow angularity probe. While not a true slot (because of the baffles), the character of the data for the flow into the slot should be representative of that over a slotted wall. It is to be noted that w/U_e is the normal velocity and v/U_e is the spanwise velocity in this case.

Figure 16 presents Wu's data for $M_\infty = 0.81$ at a spanwise station 1.27 cm from the slot. Comparing the normal component with the DFA flow angles presented in figure 14a shows quantitatively similar characteristics. The flow accelerates toward the slot, reverses direction (this time going negative), and then accelerates toward the slot. Wu projected the v and w components from the four spanwise stations onto the traverse plane and his results are presented in figure 17 for a free-stream Mach number of 0.6 at two different levels of plenum suction. In figure 17a with no applied suction, an apparent vortex-like secondary motion exists. However, when suction is applied (fig. 17b) the vortex is removed and the flow is directed strongly toward the slot.

By analogy with Wu's results, for the tunnel-empty DFA data the pressure drop across the wall is strong enough for the normal velocity to increase monotonically through the slot to the vena contracta. However, when the airfoil is present it tends to act as a sink thereby reducing the local wall pressure drop. This would allow the formation of a vortex giving the flow angle results of figure 14a.

Longitudinal measurements in the DFA were made along the slot at different heights and the results are shown in figure 18. On each of the figures data obtained inside the tunnel at 1 and 2 inches above the slot are shown as are data in the slot and at a position in the plenum beyond the vena contracta. It is important to note that the flow angles measured inside the tunnel are increasingly positive up to the leading edge of the model whereas the flow angles measured in the slot are almost constant upstream of approximately 1/2 chord in front of the airfoil leading edge. That is, the upstream character of the flow in the slot is different from that inside the tunnel. The slot does not appear to recognize the presence of the airfoil

except in a localized region in the vicinity of the airfoil. This effect is more apparent in the flow-angle gradient, which was computed from the data of figure 18a and is plotted for each measurement height in figure 18d. The gradient in the tunnel away from the slot is approximately constant except in the vicinity of the airfoil. In the slot and plenum, however, there are large variations upstream which are attributable to slot opening and stabilization of the flow. The gradient then assumes a constant value different from that in the tunnel prior to feeling the influence of the airfoil.

For future reference, the transverse and longitudinal mass flux have been computed from the data of figure 18 and shown in figures 19a and 19b. It is interesting to note that in the vicinity of the airfoil the longitudinal mass flux in the slot is approximately linear in its behavior, which yields an almost constant gradient.

D. Summary

From the analysis of the different sets of data presented in this chapter several groups of observations can be made. The first of these concerns the influence of the wall geometry on the measurements. The data indicate that there should be sufficient slot length both ahead of and behind the model for the flow in slot to become fully developed. Otherwise the influence of finite-length slots will become an important consideration. It was also found, for "larger" numbers of slots when "sufficiently" far from the wall, that the flow angles and pressures measured over the slot are very close to those measured over the slat. Thus, in the far-field of the slot there exists an averaging of the spanwise flow across the tunnel as predicted by slender-body theory. This is also known as a "homogeneous-wall" flow field. A comparison of the computed flow-angle gradients over the slot with those

over the slat, again, shows that nearly the same values were obtained. Therefore, sidewall measurements of the longitudinal pressure variation and its resulting gradients along and over the slotted wall should yield a sufficient representation of the average pressure level and gradients across the slotted wall.

Another observation concerns the influence of the model on the static pressures at the wall. The model had only a small effect on the pressure drop across the wall after about 1 chord upstream of the leading edge indicating a localized effect of the model on the slot flow. However, the presence of the airfoil appears to decrease the plenum pressure below the tunnel-empty value indicating a global shift in the "undisturbed" pressure drop over the entire extent of the slotted wall.

Measurements of the total pressure entering the slot show it to be very near free-stream total pressure, particularly with the airfoil installed. A large drop in the slot total-pressure occurs while the fluid passes through the slot indicating the existence of strong viscous shearing in the slot.

A final observation concerns the flow angle measurements in and around the slot. The magnitude of upstream slot flow angles (both tunnel-empty and airfoil-in) is large enough to negate the small crossflow assumptions of the classical ideal-slot theory. When the airfoil is installed, its presence does not significantly impact the local behavior of the slot flow upstream of about 1/2 chord ahead of the airfoil leading edge. The flow angle measurements in the slot may have a totally different character (as evidenced by the behavior of the flow angle gradients) from those in the tunnel away from the slot. For outflow, the location of the vena contracta appears almost fixed both with and without the airfoil. This indicates only a small deviation of the interface between the tunnel and plenum flows from the plane of the slotted wall.

CHAPTER V

DESCRIPTION OF THE 6- BY 19-INCH TRANSONIC TUNNEL EXPERIMENT

In this section a general description of the test facility and its operational capabilities will be discussed. This will be followed by a description of the models, both airfoil and slotted wall, for which data will be presented. A section will be devoted to a discussion of the locations of the pressure orifices on the tunnel sidewall since these data are used extensively in the analysis. The different types of instrumentation and the associated accuracies will then be discussed followed, finally, by a delineation of the test conditions.

A. Facility Description

The experimental portion of this study was conducted in the Langley Research Center's 6- by 19-inch Transonic Tunnel (6X19) which is primarily used for testing airfoils. A general description of the tunnel is found in reference 22. An exterior view of the facility showing the enclosure surrounding the tunnel and one of the compressed air storage tanks is shown in figure 20a. Figure 20b is an old NACA photograph of the facility which was taken prior to the installation of the enclosure and shows the general location of the vertical test section and the downstream diffuser. The wind-tunnel control room is located in the building at the end of the catwalk leading to the tunnel. Figure 20c shows details of the plenum chamber and model service area surrounding the test section which is in the center of the figure. The test section has slotted top and bottom walls and solid sidewalls and is shown with the near slotted wall removed. Each of the sidewalls have movable turntables for installing the airfoil models and changing the airfoil

angle of attack. The top and bottom walls are easily removed for modifications and access to the model. Cross-sectional dimensions of the test section are 6 inches wide by 19 inches high with a length of about 50 inches. A schematic of the facility is given in figure 21a and the test section in 21b.

A photograph of the tunnel control panel is shown in figure 22. Operational control of the Mach number is done hydraulically by either manual or automatic adjustment of the total pressure in the settling chamber upstream of the test section (fig. 21a). The operating Mach number is computed from the measured free-stream total pressure and the reference static pressure which is measured in the plenum chamber. The test Mach number is computed from the measured free-stream total pressure and an upstream reference static pressure at the -30 inch station (fig. 21b). Since this is an atmospheric facility, the reference static is not too different from that measured in the plenum chamber. This location of the tunnel reference static was used because of its insensitivity to the presence of the model, changes in its attitude, and the tunnel wall geometry. The operating Mach number range is from about 0.1 to 1.2 with unit Reynolds number varying up to about 9 million per foot at the highest Mach numbers. Typical operational characteristics of the 6- by 19-inch tunnel are shown in figure 23.

The typical method of operating the facility when testing an airfoil (and also during the conduct of this experiment) is to make runs of about 15 test points consisting of a Mach number sweep starting at the highest and continuing to the lowest desired Mach number at a fixed airfoil angle of attack. Operating in this manner will give a run time of about 4 minutes. Compressed air is supplied to the tunnel at a rate such that continuous flow can be maintained at Mach numbers of approximately 0.4 and below.

B. Models

1. Airfoil model.- Airfoil models used in the 6X19 typically have chord lengths of 4 or 6 inches and are instrumented for obtaining surface pressure data. Two such models of an NACA 0012 airfoil are shown in figure 24. Since the general purpose of this study is to examine wall/slot flow, the larger of the two was chosen to increase the magnitude of the disturbance at the wind tunnel wall. The model was instrumented chordwise with 47 (23 upper surface/23 lower surface/1 leading edge) 0.0137-inch i.d. pressure orifices along the mid-span of the airfoil. These pressure data were integrated to give normal force and pitching moment. No drag measurements were made. All data were acquired allowing free transition of the model boundary layer. Coordinates of the model taken at the orifice locations are given in table I. The tunnel-spanning model was mounted in the center of the tunnel on turntables in the tunnel sidewall. Station $x = 0$ is taken at the model mid-chord.

2. Wall configurations.- During the experiment-design phase of this study, it was necessary to take into consideration not only those wall geometries which would be practical in wind tunnels of similar construction to the 6X19 but also those geometries on which, due to scale effects, accurate and pertinent data could be obtained. Clearly, the slots had to be large enough to allow for meaningful measurements of the flow angle; that is, the wider slots would minimize the interference between the flow-angle probe and the wind-tunnel wall. In addition, due to the numerous, possible variations in geometric parameters, only those parameters which were deemed to be the most significant would be studied. Based on these "common sense" considerations, it was decided to establish a baseline slot configuration

which, for each configuration, was rectangular in cross section, had constant openness, and constant thickness.

Figure 25 shows the variation of the number of slots tested with the wall openness ratio. A solid wall was also tested and is indicated by the solid symbol at the origin. Note that in the subsequent discussions the wall-symbol notation used in this figure will be strictly adhered to (for instance, open circles correspond to 1-slot configurations). The slotted walls have slot widths which range from a maximum of 0.90 inches for the 15 percent open wall with 1 slot to 0.09 inches for the 6 percent open wall with 4 slots. The thickness of the slat is 0.125 inches in all cases.

Three 15-percent open wall configurations which were constructed having 1, 2, and 4 slots are shown in figure 26. The 2- and 4-slot configurations each have one-half of a slot on each side at the theoretical reflection plane formed by the sidewall of the tunnel. The wall assembly is demonstrated in figure 27. These walls are then installed in the tunnel between stations -29.0 and 19.5 inches. All walls were constructed such that the slots opened linearly from 0-percent open at station -23.0 to full openness at -17.0. Constant slot width (openness ratio) was maintained to the 19.5 inch tunnel station where the flow enters the diffuser (see fig. 21b). The wall slats were constructed of 0.125 inch thick aluminum sheet and have sharp edges. Shop drawings showing details of the construction are shown in figures 28a, 28b, and 28c.

Orifices for slot-flow pressure measurements were installed on one slat from each configuration as shown in figure 29a. Each slat had 15 0.020-inch i.d. orifices placed on the centerline of the slat sidewall. The orifices were more closely spaced in the region directly below the position of the airfoil. A limited number of slats had orifices installed both on the top

(tunnel side), centerline of the slat and also on the bottom (plenum side) of the slat as indicated in figure 29b. The orifice location and the manner in which the orifices were installed for each case is as indicated in figures 29 and table II.

In subsequent sections it will be necessary to refer repeatedly to the different wall configurations being considered. For the sake of brevity, a short-hand notation will be established consisting of the slot openness followed by the number of slots with a hyphen separating the two. For example, a 15 percent open wall with 4 slots will be denoted as 15-4. Likewise, a 7.5 percent open wall with 2 slots will be denoted as 7.5-2.

C. Sidewall Pressure Measurements

A view of the sidewall of the wind-tunnel test section is shown in figure 30. This view gives a good indication of the scale of the facility and the number and general location of the pressure measurements made on the sidewall of the tunnel. The top wall of the tunnel is taken as the left-hand slotted wall and upstream is downward toward the floor. The circular region in the center of the sidewall is the turntable for installing the airfoil. There is a 6-inch ruler at the top of the turntable for reference. In this figure, the airfoil turntable has been replaced with a blank which is instrumented for wind-tunnel Mach number calibration purposes. Centerline calibration orifices are clearly visible upstream and downstream of the model location as are three rows of pressure orifices on the left-hand-side of the turntable near the slotted wall. Pressures obtained from these orifices were used for the near-field analysis of the slot flow field. At the extreme left of the sidewall are two brackets. The upper bracket is a mounting bracket for the

slotted wall while the lower bracket is for mounting the slot flow-angle probe.

A shop drawing detailing the installation of the sidewall orifices is show in figure 31. The three rows of slot-flow orifices are shown at the top of the figure with each containing 21 0.020-inch i.d. orifices. These rows are located at 8.5, 8.0, and 7.5 inches. The orifices are located so that the closest spacing is in the region directly below the model position. Table III gives the location of the sidewall pressure orifices near the slotted wall.

D. Instrumentation

A detailed schematic of the data acquisition system (DAS) and the instrumentation hookup is shown in figure 32. Details of the individual components are described in subsequent paragraphs.

1. Data acquisition system.- The data acquisition system is shown in figure 33. This system is composed of two major pieces of hardware: the Hewlett Packard 9845B computer and the Innovative Data Technologies GPIB 1050 9-track tape drive. The 9845B was used to acquire the data from all associated instrumentation while testing and then used to process the data post-run to obtain engineering units. Only a limited capability to do post-run data analysis was available on the system with the major portion of the data reduction and analysis done on Langley's central computing facilities. All of the data were recorded for post-run processing on the 9-track tape drive.

2. Pressure instrumentation.- The data acquired during the tests were obtained using several different types of pressure instrumentation. Absolute readings for the tunnel reference conditions of total pressure and plenum chamber pressure were made with 30 psi differential Datametrics pressure

transducers which had the reference side of the gauge reduced to vacuum. These instruments have a quoted accuracy of 0.25 percent of reading. Two 1085A Electronic Manometers (fig. 34) were used to condition the signals prior to sending the information to the DAS. The total pressure was measured in the tunnel settling chamber while the plenum static is the "far-field" measurement of the pressure in the plenum chamber. The latter pressure is hydraulically averaged in the plenum by venting a large diameter (1/4 inch i.d.) tube at several places around the interior plenum chamber wall prior to its measurement by the pressure gauge. This near-atmospheric pressure was used as the reference for all the differential measurements. As a consistency check on the other measurements, the difference between total and plenum pressure was measured with a 30 psi. Datametrics gauge and was continuously monitored on an HP 3478A Multimeter.

All measurements on the airfoil surface, along the tunnel sidewall, and on the flow angularity probes were acquired as differential pressures using an electronically scanned pressure (esp) system manufactured by Pressure Systems Incorporated. These instruments have a quoted accuracy of 0.07 percent of full scale. The high degree of accuracy of these gauges is obtained by their capability of online, anytime calibration. This feature was used prior to each run during these tests to minimize error. The system included 2 10-psi. and 3 5-psi. pressure modules (each with 32 pressure ports) for a total of 160 differential pressure measurements (fig. 35), the 780B Pressure Calibrator Unit (fig. 35), and the 780B Data Acquisition and Control Unit (fig. 34). The esp's are capable of acquiring up to 20,000 samples per second.

3. Temperature instrumentation.- Total temperature was obtained from a Type K thermocouple located in the settling chamber. Temperature was

displayed on a Fluke 2190A Digital Thermocouple and then sent to a HP 3478A Multimeter prior to being given to the DAS.

4. Flow angularity probes.- The flow angle was measured with three-tube flow angularity probes manufactured by United Sensor, Incorporated which are shown schematically in figure 36. Two views of one of the probes mounted on a wind-tunnel wall are shown figures 37a and 37b. These probes have 0.015 i.d. orifices with the outer tubes sloped to give an included angle of 90 degrees on the probe head. The tip of the probe is approximately 0.030 inches wide by 0.090 inches high with a total probe length of 4 inches from tip to base. These probe dimensions were selected to minimize the probe-slot interference while the probe orifices were sized according to reference 23 to reduce the response time associated with making pressure measurements through a small volume system.

Calibration of the probes was done in the 6X19 over a range of Mach number from 0.1 to 0.95 and over a pitch range of from -15 to 15 degrees with more detailed calibration data being acquired between -5 and 5 degrees. A detailed discussion of the calibration procedure is contained in Appendix A. When in use, a preliminary measurement was made at the expected slot-flow angle for zero airfoil angle of attack. Then, the probe axis was adjusted to something close to this measured angle. This procedure gives a quasi-nulling effect on the probe and, hopefully, keeps the succeeding measurements within the higher resolution portion of the probe-calibration table.

Accuracy and repeatablity of the flow angles was a primary concern during this study. A series of 10 repeat runs was made to determine how well the flow angles could be determined in the free stream. The average flow angle and the standard deviation computed from these measurements are presented as a function of free-stream Mach number in figure 38. Based on these results,

then, it is believed that over the Mach number range considered that the angles measured will have a maximum standard deviation of less than 0.1 degree. Likewise, local Mach number and the standard deviation of the local Mach number are presented in figure 39 and, over the range considered, the maximum standard deviation of the Mach number is less than 0.0026. Two repeat runs with the probe in the slot were made and a sample result for flow angle is presented in figure 40. The repeatability of these results was similar to those in the free stream.

E. Test Conditions

1. Mach number and Reynolds number.- The plenum reference Mach number in the 6X19 is computed from the total pressure measured in the settling chamber upstream of the test section and the plenum reference static pressure. The plenum pressure is obtained from a mechanically averaged value measured in a large volume tube which has been vented at several places around the interior of the plenum chamber. Based on this value of Mach number, the tunnel-empty Mach number at the model station is then adjusted to the required free-stream Mach number. The free-stream Mach number at the model station with the model installed is taken as the tunnel-empty model-station value calibrated with an upstream value at the -30.0 inch tunnel station. This upstream value has been found to be insensitive to both the presence of the model and changes in wind-tunnel-wall geometry. Because the 6X19 is an atmospheric wind tunnel, Mach number cannot be varied independently of the Reynolds number. The relationship between the two is shown in figure 23. For a free-stream Mach number of 0.7, the chord Reynolds number for the 6-inch chord NACA 0012 is about 3.25 million.

As part of the study, it was found necessary to make multiple tunnel runs both with and without the flow-angle probe due to probe interference on wall- and slot-pressure data measured in the vicinity of the probe. In order to determine the repeatability of the test conditions, the standard deviation of the tunnel Mach number was determined from the same 10 consecutive runs used for the probe analysis. The results are shown in figure 41. It can be seen that the standard deviation of the free-stream Mach number is typically less than 0.0017 and for free-stream Mach numbers in the vicinity of 0.7 it is about 0.001. Both repeatability values are considered good for transonic wind tunnels.

2. Mach number calibrations.- Tunnel-empty centerline values of the local Mach number plotted against tunnel station for each wall configuration studied are shown in figures 42. In each case, the data begin their acceleration to test section Mach number far upstream in the converging portion of the nozzle, plateau between stations -36 and -30, accelerate through the slot-development region between stations -23 and -17, and remain essentially flat through the rest of the tunnel. When installed, the model is between stations -3 to 3. The effect of the diffuser section on the centerline data downstream of the model appears to be small except possibly for some of the smaller openness-ratio walls at the higher Mach numbers. In all cases, the Mach number distribution is flat at the model station except, again, at the very highest Mach numbers. Because the upstream Mach number consistently plateaus at the same location and because prior experience in this facility has shown this region to be insensitive to the presence of the model, measurements made at tunnel station -30 have been chosen as the upstream reference position.

Based on the preceeding conclusions, the subsequent calibration procedure was applied to each wall configuration. At each setting of the reference Mach number, a least-squares fit of the data lying between stations -6 to 6 was made and evaluated at station 0 to give a calibration Mach number. The calibration value was then plotted against the reference value and a least-squares parabolic curve fit was then determined. Typical results are as shown in figure 43 for the 15 percent open wall with one slot. It was anticipated that only those data between free-stream Mach numbers of 0.1 and 0.9 would be analyzed; therefore, any deviations from the curve fit outside of this range were deemed inconsequential. The least-squares coefficients for each wall are shown in Table IV.

3. Angle of attack.- The model angle-of-attack is set manually by rotating the turntables to the desired pitch. This angle is determined from inclinometer readings on a reference surface attached to the model turntable. During the experiment, data were acquired at 0, ±0.5, ±1, and ±2 degrees on all wall configurations. Data were acquired at ±4 degrees on some configurations. The angles were generally set to within ±3 minutes of arc (0.05 degrees).

CHAPTER VI

ANALYSIS OF THE 6- BY 19-INCH TRANSONIC TUNNEL DATA BASE

In this section, data acquired in the 6X19 as a part of the present study will be analyzed. Initially, the tunnel sidewall-pressure data will be examined. This is followed by a discussion of what the slot/plenum pressure is and where it is determined. Measurements made with the flow-angle probe in the slot region will be analyzed in detail yielding important conclusions regarding the determination of the flow angle in regions with small flow curvature. Finally, the influence of the different wall configurations on the measured airfoil pressures and force coefficients will be presented.

A. Wall Pressure Data

1. General observations.- Typical wall pressure data from the 6X19 experiment are shown in figures 44 and 45. Given in these figures are the tunnel-empty and airfoil-in wall pressures for the 6-percent and 15-percent open, four-slot wall configurations at a free-stream Mach number of 0.7. These data are plotted versus tunnel station with an expanded pressure scale to accentuate the differences between the different rows of sidewall pressures. In these figures, the pressure data on the slat ($y = 9.5$), along sidewall rows 1 ($y = 8.5$), 2 ($y = 8$), and 3 ($y = 7.5$) have been plotted. The far-field measurement of the plenum pressure is also shown. Data along row 1 for the tunnel-empty configurations were not acquired because the instrumentation was used to measure the tunnel-empty centerline pressures. For all walls, the slots open linearly beginning at $x = -23$ inches and go to constant width at $x = -17$ inches. When the airfoil is installed, the leading edge is located at $x = -3$ inches and the trailing edge at $x = 3$ inches. In

each of the figures, the pressure changes due to the opening of the slots is evident downstream of $x = -23$. The spike in the data for $x \geq 5$ is caused by the presence of a flow angle probe mounted inside of the tunnel, 2 inches above the wall, over the center slot.

The pressure data for both tunnel-empty cases (figs. 44a and 45a), show virtually no difference between rows 2 and 3. For the airfoil-in cases (figs. 44b and 45b), there is a significant shift in the level of the measurements along row 1 relative to that of rows 2 and 3. This indicates that row 1 (which is closest to the wall) is highly influenced by the presence of the slot and the large flow gradients that might exist there. Rows 2 and 3 therefore are a better indicator of the inviscid, far-field (or average), wall pressure field. Berndt (ref. 24) and Kemp (ref. 25) each have made analyses that indicate that flow-field measurements should be made at $y/a \geq 0.75$. This is to insure that flow-field measurements are not adversely affected by the presence of the rapidly varying flow in the slot. The data obtained along row 1 do not in general meet this requirement.

2. Airfoil influence.- The influence of the airfoil on the pressure data measured along the tunnel sidewall is shown in figure 46 for a free-stream Mach number of 0.7. To enable correlation between the different wall configurations, the pressure scaling has been chosen such that a comparison can be made with respect to the wall with the largest pressure variations, that is, the solid-wall configuration. For clarity, only those data along row 3 are plotted. It should be noted that, given a symmetrical airfoil, an indication of both the top- and bottom-wall pressure distributions is available by combining the positive and negative angle-of-attack data.

In figure 46a, the tunnel-empty solid wall is compared with that for the airfoil at angles of attack of $-4^{0} \leq \alpha \leq 4^{0}$. These data indicate that even

for the larger lift values (for the solid wall) the major deviation from the undisturbed-tunnel flow is contained within approximately ±3 chords of the airfoil. The upstream quickly approaches the undisturbed-tunnel value while the downstream appears to approach the no-lift value. The lack of pressure recovery is an indication of the large blockage caused by the presence of the airfoil wake in a solid-wall wind tunnel, even at small values of lift.

When the walls are opened (figs. 46b to 46g), the tunnel blockage is greatly reduced. The zero-lift minimum pressure coefficient goes from $C_p \approx -0.08$ for solid walls to $C_p \approx -0.025$ for the 15-4 slot configuration. The major deviation from the undisturbed tunnel flow is reduced to within ±2 chords of the airfoil. The flow in the tunnel with the airfoil installed appears as a perturbation about the well-established tunnel-empty flow. This is especially evident if the pressures around the downstream probe are considered. Here, the spike in the data moves as a reference-shift in the data when changing the model pitch angle.

B. Slot Pressure Data

The development of the slotted-wall theory indicates that the pressure drop across the slot is a required parameter for determining the wall characteristics. This requirement poses the dilemma of where the slot pressure should be measured. To resolve the question, all of the slotted walls were equipped with pressure orifices on the sidewall of the slat in the slot (slat-sidewall) and several wall configurations were equipped with orifices on the back of the slat in the plenum (slat-plenum). Tunnel-empty pressures from these orifices are compared with a far-field measurement of the plenum pressure, $C_{p,plenum}$, in figure 47 for three different slotted walls at $M_\infty \approx 0.7$. In each case, the slat-plenum pressure results are very near that

measured in the far-field of the plenum while the slat-sidewall measurements are significantly different. It also appears that the greater the number of slots (compare fig. 47b with fig. 47c), the better the agreement between the slat-plenum and the far-field-plenum. The reason for the large disagreement between the slat-sidewall and the far-field is most likely the result of large flow acceleration in the slot. In general, the pressures measured on the slat sidewall do not equal those measured either in the tunnel above the slots or in the far-field of the plenum. However, the far-field measurement of the plenum pressure is a sufficient representation of that measured on the back of the slat in the plenum (slat-plenum). Therefore, when determining the wall pressure drop, the far-field measurement of the plenum pressure, $C_{p,plenum}$, will be used as the local slot pressure.

C. The Effect of the Airfoil on Plenum Pressure

The effect of the airfoil on the pressure drop across the wall as determined by the "far-field" reference pressure upstream of the slots (x = -30 in.) and the average "far-field" pressure in the plenum chamber are compared in figure 48 for a free-stream Mach number of 0.7. This pressure drop is plotted versus the wall openness. For matched free-stream Mach numbers, the presence of the airfoil causes a global decrease in the pressure of the plenum relative to the corresponding tunnel-empty case. This effect is present for all slot geometries tested; however, the difference decreases with increasing openness. For openness ratios greater than 10 percent, the difference in the measurements is negligible. This phenomenon indicates that the tunnel is approaching open-jet conditions where the free-stream static is equal to that of the surrounding plenum. These observations are consistent with those of Berndt (ref. 15)

D. Slot Flow Measurements

Flow-field measurements were made on the slot centerplane normal to the wall for the 15-1 wall for both tunnel-empty and zero-lift airfoil conditions. This wall was chosen because of the large slot-to-probe-width ratio which reduced the probe/wall interference. Due to the lack of an automatic probe-traversing mechanism and the large amount of time and effort required to make these measurements, this was the only wall configuration where detailed measurements of this type were made. However, measurements were made in the slot at ≈1/2 chord upstream of the airfoil leading edge for all wall configurations.

While slot data were obtained for all openness ratios, the accuracy of the data is suspect for the smallest values of openness for two reasons. First, as the slot-to-probe-width ratio becomes small, the possibility of large measurement errors due to blockage at the higher Mach numbers increases. More importantly, however, because the vena contracta of the flow occurs at 0.3 to 0.5 slot widths into the plenum (fig. 12a), the height of the probe from the top tube to the bottom tube covers an increasingly significant portion of the measurement region. For the 15-1 slot configuration, the vena contracta should occur around 0.45 inches into the plenum whereas for the 5-2 slot configuration, the vena contracta should occur around 0.08 inches into the plenum. If the flow separates at the slot-entry edge for 0.125-inch thick walls, the vena contracta will be in the plenum for the 15-1 slots but it will be in the slot for the 5-2 slots. Due to the large changes in the magnitude of the flow angle and its gradient which occur near the vena contracta, small errors in probe positioning are critical and much care is required to prevent error.

1. Flow-angle measurements.- Flow angle measurements from the 6X19 are shown in figure 49 for free-stream Mach numbers of 0.3 and 0.7. These measurements were made at x = -6 which corresponds to a tunnel station 3 inches (1/2 chord) upstream of the airfoil leading edge. The flow angle, θ, which is measured positive out of the tunnel is plotted versus the normalized distance from the wall, y', which is measured positive into the tunnel. Comparison of figure 49a with 49b shows the flow angles to be somewhat insensitive to changes in the free-stream Mach number. For the airfoil and tunnel-empty cases, at both Mach numbers, the value of the flow angle in the slot is ≈7 degrees, while the maximum is ≈12 degrees. The presence of the airfoil only slightly increases the maximum angle achieved at the vena contracta. This indicates that the outflow in the upstream portion of the tunnel is dominated by the tunnel-wall boundary layer which is not too different from the tunnel-empty case. Comparison of the total-pressure ratios (figs. 50a and 50b) indicates that the presence of the airfoil tends to reduce the total-head losses in the middle of the slot by forcing higher energy fluid through the slot. For the airfoil case, the fuller total-pressure ratio indicates a thinner shear layer. This effect is again obvious in figure 51 where the local Mach numbers are higher for the airfoil cases.

Flow angles measured in the slot of the different wall configurations are shown in figure 52 for $M_\infty = 0.7$. These measurements were, again, made at tunnel station x ≈ -6. The generally decreasing angle with increasing openness and decreasing slot number is intuitively correct. Smaller values of openness at constant slot number would tend to have larger values of normal crossflow velocity for constant normal mass flux due to the reduced slot area. Likewise, a greater number of slots at constant openness ratio would decrease the crossflow area.

The increasing uncertainty in the measurements is evident for the smaller openness ratios, particularly for the 5-2 and 6-4 walls. Interestingly, the difference between the airfoil and tunnel-empty measurements for each openness are very small across the range of openness ratios considered. This, again, is an indication of the dominance of the tunnel-empty crossflow attributable to the boundary layer.

2. Total-pressure measurements.- The ratio of the slot total pressure to the free-stream total pressure for the different slot walls is shown in figure 53 for $M_\infty = 0.4$ and $M_\infty = 0.7$. For the tunnel-empty case (fig. 53a), the higher Mach number increases the shear in the slot resulting in larger total head losses at the wall. For the airfoil case, the effect of increased Mach number has little impact on the total pressure losses in the slot. The presence of the airfoil tends to decrease the slot losses upstream of the airfoil leading edge station due to the reduction in the plenum pressure (thereby increasing the wall pressure drop) over that for the corresponding tunnel-empty case. The larger wall pressure drop forces more, higher energy mass through the slot.

3. Crossflow with negligible streamwise curvature.- The pressure drop across the wall as expressed by equation 3.20 is

$$C_{Pw} - C_{Ps} = 2aK\frac{\partial \theta_w}{\partial x} + B\theta_s + \theta_s^2 \tag{6.1}$$

For small streamwise, free-stream curvature, as would exist in an empty tunnel or far upstream of the leading edge of an airfoil, $\partial\theta_w/\partial x \approx 0$. For large values of crossflow in the absence of streamwise, free-stream curvature, Ramaswamy (ref. 19) hypothesized that the linear crossflow velocity component

should be negligible and that the pressure drop across the wall should be governed by the quadratic component of the crossflow velocity. If these two assumptions are true, then equation 6.1 will reduce to

$$C_P - C_{Ps} = \theta_s^2 = \left(\frac{v_s}{U_\infty}\right)^2 \tag{6.2}$$

In order to verify this equation, the longitudinal and transverse mass-flux quantities were determined from the tunnel-empty flow-field measurements on the largest, and hence, most interference-free wall configurations. For the 15-1 configuration where detailed measurements were made, these quantities were also determined at the vena contracta which is located at the maximum of the ρv curves shown in figure 54a. Longitudinal mass flux at this location was then computed. The results for each of the 15-percent-open walls are plotted for various values of M_∞ in figure 55. A first-order least-squares-fit of the data (solid lines in figure 55) was then made. The results for the 15-1 slot are

$$(\rho U)_\infty = 2.644\ M_\infty \tag{6.3a}$$

$$(\rho U)_s = 2.215\ M_\infty \tag{6.3b}$$

$$(\rho U)_{vc} = 1.914\ M_\infty \tag{6.3c}$$

$$(\rho v)_s = 0.263\ M_\infty \tag{6.3d}$$

$$(\rho v)_{vc} = 0.358\ M_\infty \tag{6.3e}$$

Using (6.3a) and (6.3d),

$$\theta_s = \left[\frac{v_s}{U_\infty}\right] \approx \frac{(\rho v)_s}{(\rho U)_\infty} = 0.099 \text{ rad.} = 5.70^0 \tag{6.4}$$

Using (6.3a) and (6.3e),

$$\theta_{vc} = \left[\frac{v_{vc}}{U_\infty}\right] \approx \frac{(\rho v)_{vc}}{(\rho U)_\infty} = 0.135 \text{ rad.} = 7.73^0 \tag{6.5}$$

Both of equations (6.4) and (6.5) serve to demonstrate the Mach number insensitivity of the flow angle in the slot and at the vena contracta. For the 15-2 slots (fig. 56), the procedure yields

$$(\rho U)_\infty = 2.574\ M_\infty \tag{6.6a}$$

$$(\rho U)_s = 2.081\ M_\infty \tag{6.6b}$$

$$(\rho v)_s = 0.255\ M_\infty \tag{6.6c}$$

giving

$$\theta_s = 0.099 \text{ rad.} = 5.70^0 \tag{6.7}$$

Likewise, for the 15-4 wall (fig. 57), the results are

$$(\rho U)_\infty = 2.701\ M_\infty \tag{6.8a}$$

$$(\rho U)_s = 1.898\ M_\infty \tag{6.8b}$$

$$(\rho v)_s = 0.318\ M_\infty \tag{6.8c}$$

and

$$\theta_s = 0.118 \text{ rad.} = 6.76^0 \tag{6.9}$$

As discussed earlier, the measurements for the θ_s should be more representative of the θ_{vc} for smaller slots due to probe-height-to-slot-depth ratio considerations.

It should be noted here that published values (ref. 26) of the discharge coefficient, ϵ, place the orifice coefficient in the range of 0.61 to 0.90, depending on the "sharpness" (cross-sectional geometry) of the opening. The walls in this study had "sharp" edges. Shop fabrication instructions were to break the edges 0.005R (fig. 28); but, the actual slot-entry radius is unknown. If cross-flow continuity in the slot region is written as

$$(\rho vd)_s = (\rho vd)_{vc} = (\rho v)_{vc}(\epsilon d_s)$$

and changes in the density of the fluid in the slot region are considered negligible, then,

$$v_s = \epsilon v_{vc}$$

which gives

$$\epsilon = \frac{v_s}{v_{vc}} = \frac{\theta_s}{\theta_{vc}} \approx 0.74 \tag{6.10}$$

for the 15-1 wall. This is consistent with results of reference 26 and also with empirical values used by Sedon (ref. 27) which were required to match theoretical computations with experimental measurements.

Next, the pressure drop across the wall at the probe measurement station was determined. This was computed by taking the average of the pressure coefficient obtained on rows 2 and 3 and then subtracting the far-field measurement of the plenum pressure coefficient. The results are shown in figure 58 for each of the 15 percent open walls. The different symbols represent repeat runs. In all cases, the very low Mach number results are scattered due to the low values of free-stream dynamic pressure; that is, the resolution of the instrumentation is being taxed. Additionally, the tunnel is not as steady at these low values of free-stream Mach number (fig. 41). The pressure drop is constant except for the very wide 15-1 wall where it appears to decrease slightly at the higher Mach numbers. Average values of the pressure drop, ΔC_p, obtained for these data are

$$\Delta C_p = C_{Pw} - C_{P,plenum} = 0.0188, \quad \text{for 15-1} \tag{6.11a}$$

$$\Delta C_p = C_{Pw} - C_{P,plenum} = 0.0145, \quad \text{for 15-2} \tag{6.11b}$$

$$\Delta C_p = C_{Pw} - C_{P,plenum} = 0.0125, \quad \text{for 15-4} \tag{6.11c}$$

The flow angles from 6.5, 6.7, and 6.9 and the ΔC_p from 6.11 have been plotted in figure 59 along with results from other 6X19 measurements. Also

shown are data acquired by Berndt (ref. 15) and two points which were available from the DFA experiment described in chapter IV. A modified version of the Gardenier and Chew data (discussed below) originally published by Goethert (ref. 28) is shown as the dashed curve. The theory given by equation 6.2 is shown as the solid line. Experimental agreement with the theory is very good indicating a valid correlation.

4. Gardenier and Chew data.- Data originally presented as "unpublished AEDC transonic model tunnel data" by Goethert (ref. 28, fig. 11.25a) have been reproduced here as figure 60a. In the figure, the wall-pressure drop is plotted versus the average transverse mass flux in the slot normalized by the free-stream longitudinal mass flux. These data were obtained on a wall with a single, sharp-edged, longitudinal slot which was 1.3-in. wide (11 percent open) and 0.125-in. thick. The free-stream Mach number was varied from 0.75 to 1.20. It can be seen that the Mach number has negligible (if any) influence on the results. Goethert states that

> "Several tests (results unpublished) were conducted in the same model tunnel using a wall thickness increased considerably beyond the 1/8 in. of the wall presented in Fig. 11.25a. Also, slots with the edges beveled to increase their sharpness and with rounded edges were studied. In all cases, basically similar characteristics were obtained, that is, a remarkable independence of Mach number existed as well as a predominantly linear characteristic of the cross-flow pressure drop."

For comparison purposes, the expression

$$\left(\frac{\Delta p}{q_\infty}\right) = 0.2254\left(\frac{\rho v_h}{\rho U_\infty}\right) + 1.7460\left(\frac{\rho v_h}{\rho U_\infty}\right)^2, \text{ for } \left(\frac{\rho v_h}{\rho U_\infty}\right) \geq 0 \qquad (6.12)$$

where the subscript h denotes the average, gives a good representation of the data shown in the figure.

Several velocity distributions reproduced from reference 28 are shown in figure 60b. These data correspond to measurement stations 0.74 slot widths above the slot, in the slot, and 0.74 slot widths below the slot. The later distribution is well beyond the expected location of the vena contracta and, therefore, beyond the maximum transverse mass flux where the local plenum pressure should be felt. A conservative estimate of the slot-average to the slot-centerline velocity is obtained from the mid-slot results as

$$U_h \approx 0.62\ U_p \tag{6.13}$$

where the subscript p denotes "at the slot center". The reduction in the "effective" slot width represented by equation 6.13 when substituted into 6.12 yields the curve labelled "Modified Gardenier and Chew" of figure 59.

E. Boundary Layer Growth

In this section, an estimate of the velocity at the wall will be determined by two different methods. First, the results of an adaptive, solid, flexible-wall experiment (ref. 29) which was conducted in the 6X19 will be used to estimate the velocity normal to the tunnel wall at the model station. Second, the flow angle measurements on the 15-1 wall will be used to obtain a corresponding velocity for comparison.

1. Flexible-wall experiment.- It was determined during the conduct of the experiment described in reference 29 that the boundary layer grew as

$$\frac{\delta^*}{x} = 0.0643\ R_x^{-1/5}$$

with a virtual origin of -48 in. Differentiation gives

$$\frac{d\delta^*}{dx} = 0.0514 R_x^{-1/5}$$

At $M_\infty = 0.7$, the 6X19 has $R/l \approx 6.6 \times 10^6$/ft. Thus, at the measurement station, the boundary layer has grown such that the effective normal velocity at the wall is given by

$$\left(\frac{v_w}{U_\infty}\right) = \frac{d\delta^*}{dx} = \frac{0.0514}{\left(2.3 \times 10^7\right)^{1/5}} = 0.0017 \text{ rad.} \tag{6.14}$$

2. 6X19 slot experiment.- By assuming that the boundary layer grows equally on all walls but recognizing the thickening that occurs in the slot region due to shear, we can write

$$a\left(\frac{v_w}{U_\infty}\right) \approx d\epsilon\left(\frac{v_s}{U_\infty}\right) \tag{6.15}$$

For the 15-1 tunnel-empty case

$$a = (6 + 19) \text{ in.} = 25 \text{ in.}$$

and

$$d = 0.9 \text{ in.}$$

From the tunnel-empty measurements,

$$\left[\frac{v_s}{U_\infty}\right] = 5.7^\circ = 0.099 \text{ rad.}$$

From equation 6.10

$$\epsilon = 0.74$$

Making the substitutions in equation 6.15

$$\left[\frac{v_w}{U_\infty}\right] = \frac{d\delta^*}{dx} = \frac{(0.099)\ (0.74)\ (0.9)}{(25)} = 0.0026 \text{ rad.} \qquad (6.16)$$

By comparing equations 6.14 and 6.16, it is seen that the tunnel-empty outflow with slots is consistent with that determined by an alternate method. The close agreement lends additional credibility to the analysis and measurement techniques used in the study.

Some indication of the magnitude of δ^* can be obtained from an experiment conducted in the 6X19 by Sewall to study the sidewall boundary layer effects on transonic airfoil data (ref. 30). The following values of sidewall boundary layer thickness at the model station were measured:

$$M_\infty = 0.50, \quad \delta^* = 0.0866 \text{ in.}$$

and

$$M_\infty = 0.89, \quad \delta^* = 0.0827 \text{ in.}$$

By assuming that δ^* is constant on each wall, the boundary layer is found to reduce the effective cross-sectional area of the tunnel by 3.8 percent at $M_\infty = 0.5$. To maintain a constant centerline Mach-number distribution when the tunnel walls are parallel, the mass corresponding to this area deficit would have to be removed from the test section through the slots. A more rational and common approach is to adjust the wall divergence angle.

F. Effect of the Slotted Wall on the Airfoil Measurements

In this section the airfoil data will be examined to determine how variations in slot geometry affect the results.

1. General observations.- A typical set of pressure distributions on the upper surface of the NACA 0012 airfoil are shown in figure 61. These data, and those subsequently presented in this section, were acquired with the 15-1 slots. The data show the behavior of the pressures when the free-stream Mach number varies from 0.70 to 0.85. These data cover the range of conditions from no local supersonic flow to a condition where supersonic flow extends over a substantial portion of the upper surface of the airfoil. Since the airfoil is symmetrical, the lower surface has similar behavior.

The effect of Mach number and model geometric angle-of-attack on the measured values of the normal force coefficients are shown in figure 62. Normal force coefficient is used instead of lift coefficient because the lift requires a knowledge of the angle-of-attack correction. This corrected quantity is dependent on the wall-geometry-influenced boundary condition and its unknown coefficients. However, it is to be noted that the normal force is almost identical to the lift force when the angle is small. The data are symmetrical about the zero-lift results. Maximum normal force occurs in the Mach number range of 0.82 to 0.83 which corresponds to the onset of drag

divergence for this airfoil. A smoothing spline, represented by the solid line, was used for interpolation at $M_\infty = 0.7$.

Similar results for the pitching moment about the quarter-chord are shown in figure 62b. As with the normal force, the data are symmetrical with angle of attack and are well represented by the smoothed, solid curve. The spike in the data occurs due to large pressure losses on one airfoil surface as a result of the formation of a very strong shock wave. While the NACA 0012 was a good airfoil for the experiment because of its symmetry and "standardness", the magnitude and variation of the pitching moment with angle of attack leaves much to be desired for correlation purposes. As can be seen in the figure, the pitching moment about the quarter-chord is very small over the region of interest and as a result small errors in pressure measurements can make significant error in the moment.

The interpolated normal force and pitching moment coefficients for each angle at $M_\infty = 0.7$ are shown in figure 63. A linear least squares fairing of the results is given by the solid line. For a symmetrical NACA 0012 airfoil, any deviation of the intercept values from zero is a result of inaccuracies in the experimental measurements, model fabrication, or the different development of the upper and lower surface boundary layers. For these and all subsequent wall configurations, the integrated coefficients of normal force and pitching moment will be represented by

$$C_n = A\,\alpha \quad \text{and} \quad C_m = B\,\alpha \tag{6.17}$$

where the coefficients A and B are determined from the least squares fairing of results from the corresponding wall under consideration and the intercept has been neglected.

2. Force coefficient variation with wall openness.- The variations of the slopes of the normal force and pitching moment curves for each of the tested wall configurations are presented in figure 64. These values were obtained from the measured data as described above for the 15-1 slot configuration. A modified free-air (MFA) solution which accounts for the effects of the development of the sidewall boundary layer on the wind tunnel walls is also shown for reference. The MFA solution is discussed in Appendix B. According to classic wall-interference theory (ref. 4), the lift interference attributable to upwash in a closed-wall tunnel is zero so that the difference between this value and the MFA is due to the top- and bottom-wall induced effects of streamline curvature. The application of classic solid-wall corrections to these data is presented in Appendix B as are the more recent corrections for the effects of the sidewall boundary layer (refs. 31, 30, and 32).

Streamline curvature is the rate of change of the local flow angle. Due to the constraints imposed on the flow about the model by the slotted-wall boundaries, streamline-curvature interference will result and cause an effective recambering of the airfoil. This recambering will appear as a change in the airfoil pitching moment and, thus, as a shift in the location of the aerodynamic center. With the moment center at the quarter chord the pitching moment is related to the location of the aerodynamic center by (ref. 33)

$$\frac{C_m}{C_n} = \frac{1}{4} - \frac{x_{ac}}{c} \tag{6.18}$$

for a symmetrical airfoil. Using equations (6.17) and (6.18), the presence of streamline-curvature interference and its influence on the measured airfoil data can be demonstrated through

$$\frac{C_m}{C_n} = \frac{B}{A} = \frac{1}{4} - \frac{x_{ac}}{c} \tag{6.19}$$

Note that this equation will yield a finite value at zero incidence angle where (for a symmetrical airfoil) the normal force and pitching moment are both zero. Evaluating the shift in the aerodynamic center in this fashion also helps remove some of the above mentioned experimental uncertainty. Its variation with wall openness is shown in figure 65. It is again interesting to note that the data flatten beginning at approximately 10 percent open indicating a near open-jet condition.

3. Shock variations with Mach number and openness.- The movement of the shock wave on an airfoil is a direct indication of the variation of wind tunnel blockage interference at transonic speeds. This movement was determined for all wall configurations and is shown in figure 66 plotted against free-stream Mach number at zero lift. The closed tunnel result is shown for reference as a solid line against which the corresponding values for different openness ratios may be gauged. The figures indicate that openness values greater than 7.5 percent have minimal influence on the blockage in this wind tunnel.

To further highlight the effect of the wall geometry, the closed-tunnel Mach number where the shock went to the trailing edge was determined to be 0.8227. The airfoil shock location for each wall was then determined for this Mach number and is plotted in figure 67 against openness ratio. It is seen,

again, that the most significant shock movement occurs in the first 5 percent of wall opening and that after approximately 7.5 percent there is negligible influence of wall-openness on the blockage. For all practical purposes, the tunnel appears to operate as an open jet.

G. Experimental Conclusions

The slot feels the presence of the airfoil in two major ways. First, there is a global interaction of the airfoil, tunnel, and plenum which sets the far-field behavior of the flow development in the slot and in the tunnel. This interaction determines the first-order mass flux through the wall and also the "undisturbed far-field" pressure drop across the wall. The upstream, small, almost constant, pressure gradient thickens the boundary layer in the tunnel which in turn increases the mass flux through the wall in the regions where the streamline curvature is negligible. The other interaction is a local phenomenon which occurs in the near-region about the model approximately 1/2 chord both upstream and downstream of the model. In this region, the flow is driven by the inviscid pressure imposed on the wall by the airfoil and is highly dependent on the strong variations in streamline curvature. The limits of this flow region are determined by the onset of large changes in the wall flow-angle gradients.

Measurements of the pressures in the slot region indicate that the local variation on the back (plenum) side of the slat is not significantly different from that measured in the far-field of the plenum. This, then, is the appropriate quantity for determining the pressure drop across the wall.

The flow angles measured around and through the slot in this test are consistent in both magnitude and variation with those measured in the DFA experiment. These data show that the effective depth of the slot occurs at

the vena contracta for outflow to the plenum. A lack of information for inflow to the tunnel does not allow one to draw similar definitive conclusions, however, it will be assumed that such is the case for later theoretical analyses of the data.

It has been demonstrated that pressure drop across the wall is well represented by the square of the quadratic cross-flow velocity for large outflow with negligible flow curvature within the tunnel. The presence of a linear cross-flow velocity term, while not excluded for small cross flow, does not appear necessary.

Finally, consistent variations in the slopes of the normal force and pitching moment curves, and the shift in the location of the aerodynamic center with openness were shown giving an indication of the degree of the lift and streamline curvature interference. The presence of blockage interference was demonstrated through the variation of airfoil shock position with openness and number of slots.

CHAPTER VII

ANALYSIS OF THE SLOTTED-WALL BOUNDARY CONDITIONS

In this chapter, a method will be developed which combines the general theory described in chapter III with the experimental observations of chapters IV and VI to determine the unknowns in the wall-boundary condition. Several illustrative calculations are presented and analyzed to give a more complete understanding of the wall-boundary condition and the importance of the individual terms in it. The chapter will then conclude by analyzing the development of the slot flow using the concept of dynamic similarity of viscous flows.

A. Wall Pressure Data

A typical set of the wall pressure data for the 15-4 slot configuration is shown in figure 68. These data were acquired at a free-stream Mach number of 0.70. The different symbol types represent measurements along different rows of sidewall pressure orifices with the open symbols corresponding to the case with the airfoil at 0 degrees angle of attack while those with the solid symbols correspond to the tunnel-empty values. Far-field measurements of the plenum pressures are also shown. The pressure plotted at the -30 inch station is the upstream reference pressure.

While the pressure data are reasonably consistent and accurate, the necessity to calculate normal derivatives using adjacent rows of data required that the data be smoothed to remove experimental error. This error or noise was caused by instrumentation inaccuracies and hardware deficiencies such as roughness around the orifice. Smoothing the data was done in three steps. First, the tunnel-empty pressure at a given orifice was subtracted from the

airfoil-in pressure obtained at the same orifice for matched free-stream Mach numbers. This was to separate the airfoil-induced increment in the pressure signature from that measured in the empty tunnel. The second step was to input both pressure signatures to a computer program written explicitly for smoothing data. The actual smoothing was done using CSDS (ref. 34) which is a cubic-spline "smoother" (as opposed to "fitter") implementing the method of reference 35. Finally, the smoothed results were additively re-combined at each orifice location for further analysis. The smoothed data for row 3 with the airfoil and tunnel-empty are plotted in figure 69 as are the corresponding measurements of the far-field plenum pressure. It should be noted that an accurate representation of the data was not obtained downstream of stations greater than 6 inches owing to the presence of a flow-angle probe and its support. Only the general trend of the data was enforced in this region during the smoothing process.

B. Determination of the Streamline-Curvature Gradient

Calculating derivatives from experimental data is extremely difficult especially when the required derivative is that normal to two, closely-spaced, parallel rows of data which are themselves only slightly different. Under these circumstances any small experimental error will be magnified tremendously. The accuracy of computing the derivatives was greatly increased by fitting a cubic spline to the previously smoothed data in the longitudinal direction. The second derivative of the pressure coefficient with respect to x was then computed and used to determine the corresponding second derivative with respect to y using the following procedure.

First, it is assumed that the measurements are far enough away from both the slotted wall and the model that the small-disturbance form of the continuity equation

$$\beta^2 \frac{\partial u}{\partial x} + \frac{\partial v}{\partial y} + \frac{\partial w}{\partial z} = 0 \tag{7.1}$$

is a reasonable approximation of the flow. This equation is then differentiated with respect to x giving

$$\beta^2 \frac{\partial^2 u}{\partial x^2} + \frac{\partial^2 v}{\partial x \partial y} + \frac{\partial^2 w}{\partial x \partial z} = 0 \tag{7.2}$$

Next, the flow above the wall is assumed to be irrotational so that it can be described by

$$\frac{\partial u}{\partial y} = \frac{\partial v}{\partial x} \tag{7.3a}$$

$$\frac{\partial u}{\partial z} = \frac{\partial w}{\partial x} \tag{7.3b}$$

$$\frac{\partial w}{\partial y} = \frac{\partial v}{\partial z} \tag{7.3c}$$

Differentiation of (7.3a) with respect to x and (7.3b) with respect to z yields

$$\frac{\partial^2 u}{\partial x^2} = \frac{\partial^2 v}{\partial x \partial y} \tag{7.4a}$$

and

$$\frac{\partial^2 u}{\partial z^2} = \frac{\partial^2 w}{\partial x \partial z} \tag{7.4b}$$

Substitution of (7.4) into (7.2) results in

$$\beta^2 \frac{\partial^2 u}{\partial x^2} + \frac{\partial^2 u}{\partial y^2} + \frac{\partial^2 u}{\partial z^2} = 0 \tag{7.5}$$

The flow region where this equation is to be applied is fundamentally two-dimensional, meaning that the changes in the streamwise and normal directions dominate the spanwise changes across the tunnel. Thus, approximately,

$$\beta^2 \frac{\partial^2 u}{\partial x^2} + \frac{\partial^2 u}{\partial y^2} = 0 \tag{7.6}$$

Inherent in the further evaluation of this equation is the assumption that the measurements along the sidewall represent an average of the spanwise pressure variations across the tunnel. Support for this is found in the discussion of the Chen and Mears experiment and data presented in chapter III.

Finally, to the present approximation, the pressure coefficient is given by

$$C_p = -2\frac{u}{U_\infty} + \left(\frac{v}{U_\infty}\right)^2$$

which reduces to

$$C_P = -2\frac{u}{U_\infty}$$

far from the slot where the cross flow component is very small. Substitution of this into (7.6) gives

$$\beta^2\frac{\partial^2 C_P}{\partial x^2} + \frac{\partial^2 C_P}{\partial y^2} = 0 \tag{7.7}$$

The second derivative with respect to y, the normal direction to the wall, is now determined.

With the value of both C_p and $\partial^2 C_p/\partial y^2$ known along each data row, the coefficients a_1 to a_4 of

$$C_p(x,y) = a_1 + a_2\left(y-y_0\right) + a_3\left(y-y_0\right)^2 + a_4\left(y-y_0\right)^3 \tag{7.8}$$

may be determined at each x location and

$$\frac{\partial C_p(x,y)}{\partial y} = a_2 + 2a_3\left(y-y_0\right) + 3a_4\left(y-y_0\right)^2 \tag{7.9}$$

may be computed. The subscript "0" merely indicates the y location of one of the rows of pressure data. The normal pressure gradient computed in this fashion for the data set of figure 68 is shown in figure 70. The gradient has been computed at a distance from the wall corresponding to that of row 3, the furthest pressure measurements from the wall.

While this was found to be the "best" method of determining the gradient, there are two notes which should be made concerning accuracy. First, the

results for gradient calculations at stations greater than 6 inches are inaccurate due to the presence of the flow-angle probe. Second, the gradient computed for stations upstream of -22 inches are less accurate than those downstream due to the sparseness of the data there and also because the pressure at -30 inches is the tunnel-centerline pressure as opposed to a pressure measured along either of the near-slot sidewall rows. This pressure was added to increase the amount of data along the upstream portion of the walls and to enforce the far-field behavior of the flow. It should again be noted that the slots start opening at station -23 and do not reach their constant-width value until station -17.

C. Viscous Considerations

In chapter III it was shown that the angles measured in the slot were considerably smaller than those measured at the vena contracta where the minimum effective slot width is achieved. This viscous effect will be accounted for through the use of an orifice coefficient, ϵ. The value of this coefficient for sharp-edged circular orifices is given as 0.65 to 0.85 in reference 26. A value of 0.74 was calculated for these walls for the 15-1 wall configuration (eqn. 6.10).

D. Calculation of Slot Flow Angles

Determination of the slot flow angle is an important part of the evaluation of equation 3.22 and must be done prior to the determination of the boundary-condition coefficients. Analysis of existing data indicates that there are at least two flow-angle regimes which must be considered: those with small free-stream curvature which occur away from the model and those

C-2

with significant free-stream curvature found in the immediate vicinity of the model. These two regimes will now be analyzed.

1. Flow angle where curvature is small.- The pressure drop across the slotted wall as expressed by equation 3.22 is rewritten as

$$C_{Pw} - C_{Ps} = \theta_s^2 - aK\frac{dC_{pw}}{dy} + B\theta_s \tag{7.10}$$

For the empty tunnel and for locations sufficiently far enough upstream and downstream of the model, it has been shown that the pressure drop across the wall is denominated by the θ_s^2 term rather than the $B\theta_s$ term. In addition, it was demonstrated in chapter VI that the slot does not significantly recognize the airfoil-induced curvature except in the immediate vicinity of the model. Therefore, for those regions outside of that where large variations in curvature occur, the gradient term describing the streamline curvature may be neglected. Elimination of the $B\theta_s$ and the $aK\frac{dC_P}{dy}$ terms gives

$$C_{Pw} - C_{Ps} = \theta_s^2 \tag{7.11}$$

which allows θ_s to be determined to good approximation.

2. Regions with significant changes in flow angle.- In the vicinity of the model the linear flow-angle term becomes important (θ becomes small and $B\theta >> \theta^2$) and there can be significant model-induced changes in the streamline curvature. Thus, in this region, an alternate means of determining θ_s must be used. Historically (see refs. 13, 14, and 15), slender body theory has been used to model the flow near a slot in a wind tunnel. If this assumption is

made, the velocity in the slot would be governed by cross-flow continuity as expressed by

$$\rho_s v_s d\epsilon = \rho_w v_w a$$

where the slot width has been reduced by the orifice coefficient, ϵ, to account for the presence of viscosity in the slot. However, measurements from Berndt's experiment, the DFA experiment, and the present experiment indicate that determining the slot velocity using this form of cross-flow continuity is inaccurate due to the "cushioning" effect of the wall boundary layers. Modifications (see ref. 15) to the crossflow velocity in the slot to account for the mass flux due to the wall boundary layer are possible but require a detailed understanding of the viscous development of the flow over the slotted wall. Note that the formulation used here is different from that used previously in that, there, only the immediate vicinity of the slot and vena contracta was considered.

Examination of the data from the Berndt and DFA experiments clearly shows that the inviscid phenomena are the driving mechanism for the slot flow in the vicinity of the model (see figs. 9 and 18) and changes in the wall flow-angle gradients will be reflected in slot flow-angle gradients. Specifically, the ratio of the rate of change of flow angle in the slot to that above the slot is given roughly by the ratio of the slot spacing to the effective slot width. That is,

$$\frac{\dfrac{d\theta_s}{dx}}{\dfrac{d\theta_w}{dx}} \approx \frac{a}{d\epsilon} \tag{7.12}$$

In order to evaluate equation 7.12, we first examine the pressure coefficient. To the present approximation

$$C_P = -2\frac{u}{U_\infty} + \left(\frac{v}{U_\infty}\right)^2 \tag{7.13}$$

Differentiation with respect to y gives

$$\frac{\partial C_P}{\partial y} = -2\frac{\partial}{\partial y}\left(\frac{u}{U_\infty}\right) + 2\left(\frac{v}{U_\infty}\right)\frac{\partial}{\partial y}\left(\frac{v}{U_\infty}\right) \approx -2\frac{\partial}{\partial y}\left(\frac{u}{U_\infty}\right) + 2\theta\frac{\partial \theta}{\partial y} \tag{7.14}$$

since

$$\frac{v}{U_\infty} = \tan^{-1}\theta \approx \theta$$

From the continuity equation we can write

$$\beta^2\frac{\partial}{\partial x}\left(\frac{u}{U_\infty}\right) + \frac{\partial \theta}{\partial y} = 0$$

which when substituted into 7.14 gives

$$\frac{\partial C_P}{\partial y} = -2\frac{\partial}{\partial y}\left(\frac{u}{U_\infty}\right) - 2\beta^2\theta\frac{\partial}{\partial x}\left(\frac{u}{U_\infty}\right) \tag{7.15}$$

It is assumed that the flow can be approximated as irrotational and as such can be described by

$$\frac{\partial}{\partial x}\left(\frac{v}{U_\infty}\right) = \frac{\partial}{\partial y}\left(\frac{u}{U_\infty}\right) - \frac{\partial \theta}{\partial x} \tag{7.16}$$

Using equation 7.16 in 7.15 results in

$$\frac{\partial \theta}{\partial x} = -\frac{1}{2}\frac{\partial C_P}{\partial y} - \beta^2 \theta \frac{\partial}{\partial x}\left(\frac{u}{U_\infty}\right) \tag{7.17}$$

The second term on the right-hand-side of 7.17 is typically small inside of the tunnel away from the wall; however, when the expression is evaluated in the slot, the data indicate that it may become significant. Thus, it will be retained for the slot analysis.

Evaluating equation 7.17 at the wall and substituting it into 7.12 gives

$$d\epsilon \frac{d\theta_s}{dx} \approx -a\left[\frac{1}{2}\frac{\partial C_P}{\partial y} + \beta^2 \theta \frac{\partial}{\partial x}\left(\frac{u}{U_\infty}\right)\right]_w \tag{7.18}$$

The second term on the right-hand-side of 7.18 will now be evaluated. From figure 19a, the variation of u ($\rho \approx$ constant) can be approximated by the linear relationship

$$\frac{u}{U_\infty} \approx \left.\frac{u}{U_\infty}\right|_0 + (x - x_0)\frac{d}{dx}\left(\frac{u}{U_\infty}\right)_0$$

for $x_0 \leq x \leq x_1$ where x_0 is some point upstream of the airfoil leading-edge station and x_1 is some point near the airfoil trailing-edge station. Differentiation gives

$$\frac{d}{dx}\left(\frac{u}{U_\infty}\right) \approx \frac{d}{dx}\left(\frac{u}{U_\infty}\right)_0 \tag{7.19}$$

Likewise, using figure 18a, similar observations can be made for the flow angle and

$$\theta \approx \theta_0 + \left(x-x_0\right)\frac{d\theta_0}{dx} \tag{7.20}$$

Using equations 7.19 and 7.20, the second term of equation 7.18 may be rewritten as

$$\beta^2\theta_w\frac{\partial}{w\partial x}\left(\frac{u_w}{U_\infty}\right) \approx \beta^2\left[\theta_{w0} + \left(x-x_0\right)\frac{d\theta_{w0}}{dx}\right]\frac{d}{dx}\left(\frac{u_w}{U_\infty}\right)_0$$

This expression varies linearly in the vicinity of the model and is rewritten as

$$\beta^2\theta_w\frac{\partial}{w\partial x}\left(\frac{u_w}{U_\infty}\right) = \lambda_0 + \lambda_1(x-x_0) \tag{7.21}$$

where λ_0 and λ_1 are coefficients which must be evaluated. If this expression is substituted into 7.18 we get

$$d\epsilon\frac{\partial\theta_s}{\partial x} \approx a\left[\frac{1}{2}\frac{\partial C_p}{\partial y} + \lambda_0 + \lambda_1(x-x_0)\right]_w \tag{7.22}$$

Examination of the DFA and Berndt data shows that the slot flow angles are approximately constant upstream of about 1/2 chord in front of the leading edge of the model where the slot angle approaches its undisturbed (or far-field) value. Because of the lack of appropriate data with which to evaluate its character downstream of the airfoil trailing edge, the behavior of the flow angle in this region is assumed to behave in a similar manner to

that upstream of the leading edge. For slots of infinite length this is a very realistic assumption since the flow must return to some undisturbed far-field value; however, for slots which end soon after the airfoil trailing edge, the re-entry region of the tunnel could exert a large influence on the downstream flow in the slot. Thus, upstream at some point x_0 and downstream at some point x_1, equation 7.22 gives

$$d\epsilon \frac{\partial \theta_s}{\partial x} \approx 0 \quad \text{at} \quad x = x_0 \quad \text{and} \quad x = x_1$$

or

$$\left[\frac{1}{2}\frac{\partial C_{Pw}}{\partial y} + \lambda_0 + \lambda_1(x-x_0)\right]_{x_0,\ x_1} \approx 0$$

which when used to solve for λ_0 and λ_1 results in

$$\lambda_0 = -\frac{1}{2}\left.\frac{\partial C_{Pw}}{\partial y}\right|_{x_0} \tag{7.23a}$$

and

$$\lambda_1 = -\frac{1}{2}\left[\left.\frac{\partial C_{Pw}}{\partial y}\right|_{x_1} + \left.\frac{\partial C_{Pw}}{\partial y}\right|_{x_0}\right]\frac{1}{(x_1 - x_0)} \tag{7.23b}$$

The gradient of the flow angle in the slot is now defined by using equation 7.22 in conjunction with 7.23. It is now possible to compute the flow angle in the slot between x_0 and x_1 by integration using

$$\theta_s(x) = \theta_{s0} + \int_{x_0}^{x} \frac{\partial \theta_s}{\partial x} \, dx \tag{7.24}$$

where θ_{s0} is the slot flow angle evaluated at x_0 and is determined by using equation 7.11.

Since a distribution of the slot flow angle was not measured for the 6X19 experiments, the limits x_0 and x_1 must be approximated from the tunnel sidewall measurements. Examination of the DFA results shown in figure 18d indicate that the slot location where the presence of the airfoil is felt correlates with rapid streamline curvature changes. For the 6X19 data, this will be taken as the bottom of the "bucket" at the point shown on figure 70. The location of this point will vary from case to case. A corresponding point will exist downstream of the airfoil trailing edge; however, due to the uncertainty existing in the value of the gradient here (because of the probe), the slope, λ_1, in equation 7.21, will be taken as zero. Flow-angle sensitivity studies conducted with this parameter showed only minimal upstream dependence on its value.

The variation of the flow angle computed from the data presented in figure 69 and the computed gradient shown in figure 70 using the method outlined here is presented in figure 71. Since the maximum thickness point of the NACA 0012 occurs at the 30-percent chord station on the airfoil which corresponds to tunnel station x = -1.2 inches, the flow angle should be very near zero. This is indeed the case as can be seen in the figure.

E. Ideal Form of the Slotted-Wall Boundary Condition

One method of estimating the value of the slotted-wall coefficient, K, is to evaluate

$$C_{Pw} - C_{Ps} = -aK\frac{dC_{Pw}}{dy} + B\theta_s + \theta_s^2 \tag{7.25}$$

from the measurements using information at only two points. These two points are chosen as follows. The first point is taken upstream where the outflow is large. At this point, the analysis indicates the $B\theta_s$ term to be negligible. The second point will be taken near the point of maximum thickness on the airfoil where θ_s becomes very small. Writing equation 7.25 at these two points gives

$$\left(C_{Pw} - C_{Ps}\right)_1 = -aK\left.\frac{dC_{Pw}}{dy}\right|_1 + \theta_{s1}^2 \tag{7.26a}$$

and

$$\left(C_{Pw} - C_{Ps}\right)_2 \approx -aK\left.\frac{dC_{Pw}}{dy}\right|_2 \tag{7.26b}$$

Subtracting (7.26b) from (7.26a) yields

$$C_{Pw1} - C_{Pw2} = -aK\left[\left.\frac{dC_{Pw}}{dy}\right|_1 - \left.\frac{dC_{Pw}}{dy}\right|_2\right] + \theta_{s1}^2 \tag{7.27}$$

Now, define

$$\Delta C_P = C_{Pw1} - C_{Pw2} \tag{7.28a}$$

$$\Delta\frac{dC_P}{dx} = \left[\left.\frac{dC_{Pw}}{dy}\right|_1 - \left.\frac{dC_{Pw}}{dy}\right|_2\right] \tag{7.28b}$$

and

$$A = \theta_{s1}^2 \tag{7.28c}$$

Therefore, substituting (7.28) in (7.29) gives

$$\Delta C_P = A - aK\Delta\frac{dC_P}{dy} \tag{7.29}$$

which is solved for K using the procedure just described.

A measure of the performance of the DM/CM formulation of the boundary condition may be obtained by substituting K into equation 1.1 and adding A to the equation. For this form of the boundary condition, the A is taken as a constant over the model position and must be interpreted as a correction to the reference pressure. Equation 1.1 is re-written using equation 3.21 as

$$C_{Pw} - C_{Ps} = A_I - aK_I\frac{dC_{Pw}}{dy} \tag{7.30}$$

where the subscript I denotes the ideal form of the equation. The analysis of the CM Test 3 data (figs. 4 and 7) yields values of 0.041 and 1.94 for the A_I and K_I, respectively. Since the slot flow angle was not measured, the K_I was obtained by matching the change in the gradient with the pressure drop between stations 9 inches and 16 inches while the A_I was obtained by shifting the curves to match the minimum values. An estimate of the upstream value of the flow angle in the slot is obtained by using equation 7.11. This value is computed as 11.6^0 which is comparable in magnitude to that measured for the DFA, Berndt, and 6X19 experiments. The results are shown in figure 72. D represents the left-hand-side, or "known" side, of equation 7.30 while D_F

represents the right-hand-side, or "fitted" side. Recall that the airfoil extends from station 17 inches to 29 inches.

Some results for equation 7.30 are shown in figure 73 for the four-slot configurations from the 6X19 experiment. As with the CM data, this representation of the boundary condition appears to approximate the pressure drop across the wall reasonably well upstream of the maximum thickness of the model; however, large discrepancies exist aft of the maximum thickness point where inflow to the tunnel occurs.

F. Berndt's Form of the Slotted-Wall Boundary Condition

The performance of Berndt's form of the boundary condition

$$C_{Pw} - C_{Ps} = \theta_s^2 - aK_B \frac{dC_{Pw}}{dy} \tag{7.31}$$

is shown in figure 74 for the data of figure 9. A value of K_B has been determined using the theory of reference 15. Berndt's form of the boundary condition appears to contain discrepancies similar to those for the Ideal analysis shown in figure 72. This form of the boundary condition was applied to the four-slot walls tested during the 6X19 experiment and the results are shown in figure 75. The fact that curves match upstream as well as they do for both the Berndt and 6X19 experiment is a result of the streamline curvature in the slot becoming small and the wall-pressure drop being equated to the quadratic cross-flow term.

G. Alternate Method of Analysis

Further analysis of the data showed that greatly improved correlations could be achieved if a tunnel-empty tare was removed from the boundary condition. This not only removes some of the effects of the tunnel-empty pressure distribution but also negates the effect of orifice irregularities and, to some degree, systematic measurement error. Most importantly, subtracting the tunnel-empty data removes the gross effects of tunnel-empty outflow and highlights the influence of the model on the wall. Rewriting equation 3.22

$$C_{Pw} - C_{Ps} = - aK\frac{dC_{Pw}}{dy} + B\theta_s + \theta_s^2 \tag{7.32}$$

removing the streamline curvature term due to the airfoil, and assuming the tunnel-empty flow angles to be large enough for the θ_s^2 to dominate results in

$$C_{Pw,te} - C_{Ps,te} = \theta_{s,te}^2 \tag{7.33}$$

If equation 7.33 is subtracted from 7.32, then

$$\left(C_{Pw} - C_{Pw,te}\right) - \left(C_{Ps} - C_{Ps,te}\right) = -aK\frac{\partial C_{Pw}}{\partial y} + B\theta_s + \left(\theta_s^2 - \theta_{s,te}^2\right) \tag{7.34}$$

From the previous discussion it is known that the θ_s^2 term is dominated by the tunnel-empty flow. Nevertheless, if we assume that there is an increment due to the presence of the airfoil, we can write

$$\Delta\theta_s = \theta_s - \theta_{s,te} \tag{7.35}$$

Then

$$\theta_s^2 - \theta_{s,te}^2 = 2\theta_{s,te}\Delta\theta_s + \left(\Delta\theta_s\right)^2 \tag{7.36}$$

Using the definition of $\Delta\theta_s$ (eq. 7.35) and the fact that $\theta_{s,te}$ has only small variation with respect to x (i.e. $\approx$ constant), equation 7.36 can be written functionally as

$$\theta_s^2 - \theta_{s,te}^2 \approx A + B'\theta_s \tag{7.37}$$

which can be substituted in 7.34 to give

$$\left(C_{Pw} - C_{Pw,te}\right) - \left(C_{Ps} - C_{Ps,te}\right) \approx A - aK\frac{\partial C_{Pw}}{\partial y} + B\theta_s \tag{7.38}$$

where the $B'\theta$ term of 7.37 is absorbed into the $B\theta$ term of 7.34. It is worthwhile to note that $B\theta_s$ has the same functional form as the $\partial K/\partial x$ term in equation 3.12 and as such may absorb any minor inviscid variations attributable to changes in the slot width.

Far upstream with respect to the model, the streamline curvature is negligible and the $B\theta_s$ term may become negligible. Data obtained in the 6X19, DFA, and by Berndt support this since they show upstream total pressures in the slot to be not too different from those in the free stream when the model is in the tunnel. Since the free-stream Mach number, as opposed to plenum Mach number, is matched with and without the model

$$C_{Pw} - C_{Pw,te} \approx 0$$

far upstream. However, in general, as noted in the 6X19 data and also in Berndt's data,

$$C_{Ps} - C_{Ps,te} \neq 0$$

because of the shift in the plenum pressure which occurs due to the interaction of the airfoil with the plenum. The coefficient A which results from equation 7.35 will account for this shift. The A, which acts like an airfoil-induced zero shift in the plenum pressure coefficient, may also accommodate any discrepancies due to experimental error, particularly those associated with the upstream gradients caused by extremely small pressure differences. Equation 7.38 is the equation which will be analyzed to determine the wall boundary-condition coefficients in the succeeding sections.

H. Determination of Coefficients by the Method of Least Squares

The method of Linear Least Squares (LLS) as developed in Appendix C was used to determine the value of the unknown coefficients in equation 7.38. This technique is simple, powerful, and, above all else, consistent in its application. A measure of the "goodness of fit", the multiple correlation coefficient, R^2, is a by-product of the method and is used to assess the quality of the analysis.

Prior to discussing the results, the following definitions are made:

$$D = \left(C_{Pw} - C_{Pw,te}\right) - \left(C_{Ps} - C_{Ps,te}\right) \tag{7.39a}$$

$$B_1 = - a\frac{\partial C_{Pw}}{\partial y} \tag{7.39b}$$

and

$$B_2 = \theta_s \tag{7.39c}$$

so that equation 7.38 becomes

$$D = A + KB_1 + BB_2 \tag{7.40}$$

As discussed in the Appendix, by letting the unknown coefficients A, K, and B assume arbitrary values, the above equation is written as

$$D = D_F + e \tag{7.41}$$

where the subscript "F" indicates the fitted value of D. The term e is the resulting local error between the left-hand-side which is known and the right-hand-side which contains the unknown (and as yet arbitrary) coefficients. The LLS method determines the value of the A, K, and B coefficients contained in D_F which minimize its error with respect to the known function D.

Since D_F is itself composed of functions B_1 and B_2, it is instructive to examine them, collectively, along with D. Figure 76 shows the variation of D, B_1, and $B_2/2$ with x. It is seen that B_1 is very similar to D (as predicted by the Ideal-slot theory) and that they are nearly symmetric about their minimum values. However, the two curves are skewed with respect to each other: their minimum values are typically displaced. The B_2 is asymmetrical over the model and any re-alignment of B_1 with D will have to occur by including the contribution of B_2.

Results of applying the statistical reduction technique to equation 7.40 and retaining all of the coefficients are shown in figure 77 for the four slot configurations. The limits of the region over which the curves are matched are indicated on the figure as XBC1, the upstream limit, and XBC2, the downstream limit. Analysis of the data was typically terminated at an XBC2 value of approximately 3 inches because this corresponds to the trailing-edge station of the model and also because of interference due to the presence of a probe installed at tunnel station 6 inches. The analysis gives a good correlation of the known curves with the fitted curves. Multiple correlation coefficients of 0.999, 0.980, and 0.991 were computed for the 15%, 10%, and 6% open walls, respectively. A summary and discussion of the resulting coefficients is given in a subsequent section.

The effect of excluding the linear $B\theta_s$ contribution is shown in figure 78. Agreement of the curves is not very good even though the trends are similar. Dropping this term reduces the correlation to 0.787, 0.574, and 0.754 for the 15%, 10%, and 6% open walls, respectively.

Changes in the length of the evaluation region had minimal effect on the values of the wall boundary-condition coefficients as long as the correlation remained high. Figure 79 demonstrates this with the 15-4 wall which should be compared with the results of figure 77a. The changes in the coefficients are shown in the following table.

XBC1,XBC2	-6.01, 2.99	-13.02, 2.99
R^2	0.999	0.988
A	-0.003	-0.002
K	1.176	1.131
B	0.046	0.049

Berndt's data, figure 9, offered the opportunity to evaluate the performance of the method with a different set of measurements. The application of the present technique to his data is shown in figure 80. Since the flow angle was measured in the slot instead of above the wall as in the present experiment, the streamline-curvature contribution was approximated as

$$a\frac{\partial \theta_w}{\partial x} = d\epsilon\frac{\partial \theta_s}{\partial x}$$

over the entire extent of the data set even though the measurements from the DFA experiment indicate that this is not necessarily true (see fig. 18d). Errors resulting from this assumption appear in the upstream mismatch of the results. Greater correlation exists in the vicinity of the model ($0 \leq X \leq 90$mm) than with his form of the boundary condition (eqn. 7.31). The coefficients computed for this case are -0.013, 2.25, and 0.242 for A_B, K_B, and B_B, respectively.

I. Slot-Flow Similarity.

The concept of similarity is one which is fundamental to fluid-dynamics research and to the solution of the equations of fluid motion. White (ref. 36) defines a similarity solution as "one in which the number of variables can be reduced by one or more by some analytical means, usually by a coordinate transformation". Applications of this technique have had a profound impact on the understanding of fluid physics and the general solution of engineering problems. Reynolds' classic investigation of flows through pipes (ref. 37) forms the foundation of our understanding of laminar and turbulent flows. Blasius' mathematical solution of the boundary layer equations (ref. 38)

established a reference against which most other methods are gauged. Numerous extensions (refs. 36 and 39) and practical engineering solutions (ref. 40) which apply these techniques have been published.

Another area of practical application is the flow in a transonic wind tunnel which requires realistic boundary conditions for the computation of accurate wall-interference effects. Initial analysis of the DFA data set demonstrated that similarity of the flow existed along the centerline of a longitudinally slotted wall. Application of similarity methods should greatly simplify the viscous solution over walls of this type by allowing the determination of the slot-flow velocity components thus yielding the angles necessary for the application of the wall boundary conditions (eqns. 7.32 and 7.38).

In this section, a set of similarity variables applicable to the flow along and through a longitudinally-slotted wind-tunnel wall will be presented. Results which demonstrate the influence of longitudinal location, curvature of the free stream, and compressibility will be presented. The results, though not complete enough for application to the present study, open the way to further experimental and theoretical research on their application.

1. Definition of similarity variables.- Analysis of the flow-field data indicated that by using an appropriate transformation, the data would collapse to a single curve. Prior to giving the similarity variables, however, it will be necessary to discuss and define several parameters used in their definition.

Local values of the longitudinal and transverse mass flux in the vicinity of the wall were calculated from the flow angle, Mach number, and total-pressure measurements for both the DFA and 6X19 data sets (see figs. 12 and 54). The location of the maximum of the crossflow component, y_{vc}, which

occurs at the vena contracta, was determined and the longitudinal mass flux values at these locations were then interpolated. The position, $y_{1/2}$ is in the plenum where one half of the transverse mass flux at the vena contracta is achieved.

Free-stream mass-flux values were determined at the locations $y_{u,fs}$ and $y_{v,fs}$ where, for the longitudinal component,

$$\frac{(\rho U)}{(\rho U)_\infty} = 0.995$$

and, for the transverse component,

$$\frac{(\rho V) - (\rho V)_{vc}}{(\rho V)_1 - (\rho V)_{vc}} = 0.995$$

The subscript "1" indicates the value of the measured data furthest from the wall into the free stream. This was used because it is unclear whether the free stream was attained for the 6X19 data (see fig. 54a).

With these definitions, it is now possible to discuss the similarity transformations. The definitions of the longitudinal variables are

$$\eta = \frac{y - y_{vc}}{y_{u,fs} - y_{vc}} \tag{7.42}$$

and

$$f(\eta) = \frac{(\rho U) - (\rho U)_{vc}}{(\rho U)_{fs} - (\rho U)_{vc}} \tag{7.43}$$

Examination of the transverse mass flux indicated the existence of at least two regions in the crossflow. The first of these is an acceleration into the slot up to the vena contracta and the second is a deceleration from the vena contracta into the plenum. The similarity variables describing the first region are

$$\xi_1 = \frac{y - y_{vc}}{y_{v,fs} - y_{vc}} \tag{7.44}$$

and

$$f(\xi_1) = \frac{(\rho V) - (\rho V)_{vc}}{(\rho V)_{fs} - (\rho V)_{vc}} \tag{7.45}$$

Similarity variables for the second region are given by

$$\xi_2 = \frac{y_{vc} - y}{y_{1/2} - y_{vc}} \tag{7.46}$$

and

$$f(\xi_2) = \frac{(\rho V) - (\rho V)_{vc}}{(\rho V)_{1/2} - (\rho V)_{vc}} \tag{7.47}$$

2. Results.- The tunnel-empty DFA data presented in chapter IV have been used to demonstrate the validity of the similarity transformations and their dependence on axial location. Results for a free-stream Mach number of 0.6 are presented in figure 81 for both the longitudinal and crossflow variables

which were acquired at different tunnel stations. Excellent correlation is achieved using this formulation.

Mach-number effects on the tunnel-empty results are examined in figure 82 using data from both the DFA and the 6X19. The longitudinal similarity variable, again, gives excellent agreement as does the transverse variable except for a region $0 \leq \xi \leq 1$ where the 6X19 data differs slightly from the DFA data. The mismatch is attributable to not having a good definition of the 6X19 transverse free-stream conditions.

The influence of free-stream curvature induced by the airfoil and the effect of Mach-number variations are shown in figure 83. In figure 83a, longitudinal similarity results for both data sets are presented along with a tunnel empty comparison. The correlation for the longitudinal component is excellent. Two correlations of the crossflow variable with free-stream curvature are shown in figures 83b for $M_\infty = 0.6$ and 83c for $M_\infty = 0.725$. The correlation is not as good for these two cases deep in the plenum ($\xi_2 < -1.5$) because the instrumentation could not resolve small values of dynamic pressure. Disagreement between $0.5 \leq \xi_1 \leq 1$ is expected but unexplained for reasons previously discussed in chapter IV while analyzing the Wu data. The lack of experimental data permits only speculation that there exists another region between $0.5 \leq \xi_1 \leq 1$ where similar flows and similarity parameters may be shown to exist. The scaling in this region may be dependent on some value of the local shear stress or some value of the boundary-layer thickness on the wall.

3. Concluding Remarks.- These analyses have shown that the shear layer in the wall region of a longitudinally-slotted wind tunnel can be described using the concept of flow similarity. The similarity variables defined by equations 7.42 and 7.47 show excellent correlation of the longitudinal and

transverse flow components in the absence of free-stream curvature and in the longitudinal component with curvature. Crossflow correlations in the presence of free-stream curvature, while generally good, indicate the possible existence of an additional region of similarity. The results indicate the choice of similarity parameters to be insensitive to the effects of compressibility.

Formulation of the similarity variables in the manner presented, while not firmly established for the crossflow component with free-stream curvature, open the way for a simplified solution of the viscous slot flow existing in wind tunnels with these types of walls. These results may be digitized for table lookup or curve fit to obtain a functional form for use in a similarity solution of the viscous flow near the wall. Further experimental research should be conducted using non-intrusive measurement techniques to tie the present results to those existing over the solid portions of the wall and to further examine the behavior of the flow with curvature of the free stream. The influence of the cross-sectional geometry of the slot should be evaluated as should the thickness of the wall boundary layer over the slot.

CHAPTER VIII

CORRELATION OF THE BOUNDARY-CONDITION COEFFICIENTS

This chapter summarizes the slotted-wall boundary-condition coefficients obtained using the analysis techniques described in chapter VII. The first section discusses the results of the Ideal slotted-wall analysis. Wall corrections using this form of the boundary condition have been extensively analyzed elsewhere and expressions for the blockage and lift interference (among others) may be obtained from a classical reference such as that of Garner et. al (ref. 4) or Pindzola and Lo (ref. 5). The second section details the coefficients obtained with the boundary condition as given by the present analysis. It has been shown that the nonlinear form of the boundary condition as given by equation 3.22 can be reduced to a linear boundary condition which is given by equation 7.38. This equation differs by only a constant (which may be assimilated in C_{ps}) from that of reference 4 where the blockage and lift interference are given for an arbitrary set of boundary-condition coefficients. Results detailing the effect of variations in the openness ratio and number of slots are presented for a constant free-stream Mach number for all baseline wall configurations. The Mach-number influence on the coefficients obtained at zero lift and the airfoil lift influence at constant Mach number for the 15-4 wall configuration are presented.

Berndt (ref. 40) mathematically analyzed the inviscid slotted-wall interference problem in three-dimensions using slender body theory to show that the slots could be treated in the crossflow plane. The resulting K coefficient is a second-order approximation for small openness ratio to the two-dimensional value which he derived in an earlier paper (ref. 15).

Berndt's two-dimensional K coefficient shows an effect (also shown in an earlier work by Goethert) due to slot depth. In reference 24, Berndt proposed a presentation method which highlights the thickness parameter t/d. A discussion of the present set of results in this manner is given in Section C.

A. Ideal Slotted-Wall Coefficient Correlations

The Ideal slotted-wall boundary condition is given by

$$C_{Pw} - C_{Ps} = A - aK\frac{dC_{Pw}}{dy} \tag{8.1}$$

where the A and K coefficients are obtained from the two-point analysis as discussed in the previous chapter. The A coefficient is a necessary addition to the Ideal slot condition which accounts for the large amount of outflow through the slotted wall due to the growth of the tunnel-empty boundary layer. Determination of the K coefficient is made by scaling the streamline-curvature gradient upstream of the maximum thickness point of the airfoil to match the wall-pressure-drop distribution.

The K coefficient determined in this fashion is shown in figure 84 for a free-stream Mach number of 0.7. Results for the one-, two-, and four-slot walls show very consistent variations with both openness ratio and number of slots. A least squares fitting of the results is given by the dashed curves. Also shown are the classical theories (solid lines) of Davis and Moore (DM) (ref. 10) and Chen and Mears (CCM) as corrected by Barnwell (ref. 17). The agreement of the one-slot results with DM theory and the two-slot results with CCM theory is fortuitous in that these two theories were derived assuming an infinite number of slots of uniform openness. Discrepancies between the

theories are a direct result of the different methods used to model the slat shape. Data published in references 11, 15, and 16 are used to obtain the filled symbols. Berndt's result for three slots (filled circle) correlates well with the present variation in slot number in that it lies between the two- and four-slot results of the present study. Even though the trends of the CCM and DM theories are similar to the present results, quantitatively they give K values that are much smaller than those for the four-slot configuration when, in fact, they should be larger. The Chen and Mears experimental result (9 slots) and the Baronti, Ferri, and Weeks result (15 slots) have about the right magnitude relative to the present four-slot results. On the basis of the agreement of the points based on the Chen and Mears and Baronti et. al. experimental data with the four-slot results, it would seem that the homogeneous-wall condition is rapidly approached for walls with more than four-slots.

The coefficients resulting from this analysis procedure may be used when the tunnel-empty outflow through the slots is small thus negating the "zero-shift" adjustment of the pressure coefficient (as should occur when the walls are diverged to account for boundary layer growth) or when some estimate of the upstream slot-flow angle is available (for example equation 6.2). These results may also be used when estimates of the wall interference are desired but not "absolute" answers (for instance, when designing slotted walls). Expressions for correcting the interference due to model blockage and that due to lift may be obtained from a classical reference such as that of Pindzola and Lo (ref. 5) or Garner et. al. (ref. 4).

B. Present-Method Slotted-Wall Coefficients Correlations

It was shown in chapter III that the pressure drop across the slotted wall is nonlinear in θ_s and is appropriately given by

$$C_{Pw} - C_{Ps} = -aK\frac{\partial C_{Pw}}{\partial y} + B\theta_s + \theta_s^2 \tag{8.2}$$

It was then shown in chapter VII that this boundary condition could be linearized if the tunnel-empty flow given by

$$C_{Pw,te} - C_{Ps,te} = \theta_{s,te}^2 \tag{8.3}$$

was subtracted from the model-in condition of equation 8.2. The linearized form of the equation is then given by

$$\left(C_{Pw} - C_{Pw,te}\right) - \left(C_{Ps} - C_{Ps,te}\right) = A - aK\frac{\partial C_{Pw}}{\partial y} + B\theta_s \tag{8.4}$$

where the A, K, and B coefficients must be determined for a given wall geometry and set of flow conditions. Analyses of the data in chapter VII revealed that very good agreement could be achieved when using the wall boundary condition in this form.

1. Influence of openness ratio and number of slots.- Figure 85a shows the variation of the K coefficient with openness ratio for a free-stream Mach number of 0.7 and zero model angle-of-attack. The dashed line is a least-squares fitting of the present coefficients to indicate trends of those walls with the same number of slots. A value obtained from Berndt's experiment with the present evaluation technique is given by the filled

symbol. The addition of the $B\theta_s$ term absorbs part of the contribution to wall-pressure drop originally assumed in total by the streamline-curvature term and, as a result, reduces the value of the K coefficients compared to the "ideal" values of K. The variation with the number of slots is still consistent in that increased values of K are obtained with larger numbers of slots (at least up to four slots). However, the results for three and four slots are very nearly the same which indicates that the assumption of a homogeneous boundary condition is more closely modelled by these experimental results.

The corresponding B coefficients are shown in Figure 85b. Dashed lines are again a least-squares fitting of the data. The variations of the one- and two-slot results are very similar; however, the results for the walls with four slots changes slope. This is not be too surprising since one of the greatest uncertainties in the analysis method is the behavior of the boundary layer over the slotted wall and how it interacts with the flow through the slot. The 15-4 wall has a slot width of 0.225 inches while the 6-4 wall has a slot width of 0.09 inches. Any uncertainties in the flow-angle calculations will be reflected in the determination of the B coefficient. In general, the values of B are not determined as accurately as would normally be desired; more resolution would have been desirable. However, it is clear, based on the curve fits (compare figure 77 with figure 78) that a "B-term" is required in the boundary-condition equation to appropriately model the pressure drop through a longitudinally-slotted wind-tunnel wall. The present analysis demonstrates the importance of including this term and examines its parametric variation with wall geometry and test conditions. The actual numerical value of the coefficient must be determined for the given wall/slot configuration and will be dependent on the viscous nature of the flow over and

through the wall and its cross-sectional geometry. For reference, the linear coefficient in the pressure drop equation for the Modified Allen and Chew data is 0.14 (see equations 6.12 and 6.13) while that for the Berndt equation was determined here as 0.24.

The A coefficient is presented in Figure 85c for a free-stream Mach number of 0.7 at zero model lift. Consistent variations with changes in the number of slots were determined and are indicated by the dashed lines. Any scatter in the results appears to be related to the determination of the B coefficient. It is also noted that the A coefficient accounts for the decrease in the plenum pressure coefficient below the tunnel-empty value due to the presence of the airfoil. If A is assumed to result exclusively from this decrease (a distinct possibility), then, for this Mach number, an A value of ±0.02 will yield a small pressure difference of ±0.1 psi.

2. Free-stream Mach number effect.- The influence of free-stream Mach number on the K coefficient for the 15-4 wall configuration at zero angle-of-attack is shown in figure 86a. A linear least-squares fit of the coefficients is given by the dashed line. Increasing the Mach number causes a gradual increase in the K coefficient. An inviscid analysis by Goethert (ref. 28) shows that effects of changes in the Mach number should be nonexistent. The present variation could be explained through viscous changes at the wall; that is, increases in the Mach number will cause increased shearing and mixing in the slot which would tend to decrease the effective slot width.

Variations in the B coefficient, figure 86b, support this hypothesis. Increased Mach number causes the contribution of the slot-shear effect given by the linear flow-angle term to become more pronounced. The scatter at lower Mach numbers is a result of the small value of dynamic head increasing the

uncertainty in the determination of the streamline-curvature gradient, $\partial C_{pw}/\partial y$, which must be integrated to obtain the flow angle.

Figure 86c shows the A coefficient to have only a slight variation with Mach number until the higher Mach numbers are reached. Repeatability of the results is to be noted in each of the figures 86a through 86c.

3. Influence of model lift.- Results from the lift analysis are shown in figures 87 for the 15-4 wall at a free-stream Mach number of 0.7. Dashed lines in each of these figures are a linear least-squares fit of the coefficients. The model angle-of-attack was varied from -2 degrees to 4 degrees and the deviations in the K (fig. 87a) and B (fig. 87b) coefficients proved insignificant. Since the wind tunnel plenum chamber is effectively a large, open room surrounding the test section (the upper and lower slotted walls can communicate) and since the airfoil is symmetrical (the plenum pressure should be the same for positive and negative values of lift), the scatter in the A coefficient (fig. 87c) must come from the inability of the analysis method to make a precise determination of the normal pressure gradient (particularly in the upstream portion of the tunnel where the pressure differences are very small) and the flow angle which is determined from this gradient. This is particularly evident for the negative model angles-of-attack where (as previously discussed) accurate normal pressure gradients are much more difficult to obtain.

C. Comparison with Berndt's Slotted-Wall Theory

Berndt gave an elegant mathematical analysis of the three-dimensional slotted-wall interference problem in reference 41. This analysis and also that presented in an earlier paper (ref. 15) for two-dimensional tunnels shows

an effect of slot depth or slat thickness. The Berndt two-dimensional analysis yielded an analytical form of the slotted-wall coefficient given by

$$K_B = -\frac{1}{\pi} \ln\left[\sin\left(\frac{\pi d}{2a}\right)\right] + 0.462 + \frac{t}{d} \tag{8.5}$$

or

$$K_B = K_{DM} + 0.462 + \frac{t}{d} \tag{8.6}$$

where K_{DM} is the theoretical Davis and Moore form of the slotted-wall coefficient for a zero-thickness wall. In reference 42, Berndt proposed a presentation method which highlights the thickness by writing (8.6) as

$$\Delta K = 0.462 + \frac{t}{d} \tag{8.7}$$

where ΔK is defined by inspection of equation 8.6. This equation shows a linear variation of ΔK with wall thickness. Thus if the experimental K at a given openness ratio has the Davis and Moore value of K subtracted from it, then the results should scatter around the theoretical prediction of equation 8.7 (if the theory is valid). The results of applying this procedure to the Ideal boundary-condition K are shown on figure 88a as are the results from the Chen and Mears and the Berndt experiments. The Ferri, Baronti, and Weeks result could not be plotted because the slat thickness is unknown. It is to be noted that increasing thickness ratio corresponds to decreasing the wall openness ratio. It appears that K values do indeed follow some trend with slat thickness. However, this trend has a different slope than that of the theoretical prediction.

Comparable results for the present-analysis method are given on figure 88b. The present four-slot, Berndt three-slot, and Chen and Mears nine-slot values closely approximate the Berndt theory given in equation 8.7. Based on previous discussions, the one- and two-slot results would not be expected to match the theoretical prediction, which is indeed the case. This, again, adds support to the earlier observation that the four-slot wall is close to representing a homogeneous slotted wall.

An examination of the wall coefficients as summarized here does not support or disprove any one form of the physical modelling of the wall boundary condition. A judgement of the "goodness" of a particular modelling equation is found in how well it approximates the experimentally determined variation of the wall pressure drop. The Ideal form of the boundary condition (eqn. 8.1) or Berndt's extension of it for large crossflow (eqn. 7.31) appear to approximate the wall pressure drop well upstream of the maximum thickness point of the model; however, downstream of this point, where substantial inflow to the tunnel can occur, an additional contribution due to viscous shearing in the slot becomes important. The present modelling (eqn. 8.2) includes this viscous contribution and gives consistently good agreement with the measured pressure data not only in the immediate vicinity of the airfoil but, also, for an extended region upstream of its leading edge. Boundary-condition coefficients computed with the present method of analysis have been shown to have generally consistent variations with openness ratio, Mach number, and model lift.

CHAPTER IX

CONCLUSIONS

The following conclusions can be made as a result of the present research:

1. A theoretical analysis of the flow in the vicinity of a longitudinally-slotted wind-tunnel wall has been conducted. The resulting boundary-condition equation which appropriately describes the pressure drop across the wall has been determined as

$$C_{Pw} - C_{Ps} = \theta_s^2 + 2aK\frac{\partial \theta_w}{\partial x} + B\theta_s = \theta_s^2 - aK\frac{\partial C_{Pw}}{\partial y} + B\theta_s$$

where C_{Pw}, C_{Ps}, θ_w, and θ_s are the average pressure coefficient at the wall, pressure coefficient in the slot, average flow angle near the wall, and the flow angle in the slot, respectively. The a, K, and B are the slot spacing, and slotted-wall coefficients, respectively. This equation relates the pressure drop across the wall to the streamline curvature in the tunnel (as predicted by classical slotted-wall theory), the non-negligible square of the slot flow angle (as predicted by Wood), and the viscous shearing in the slot (as predicted by Ramaswamy). The controversial viscous shear contribution (which was empirically added in several previous treatments of the problem) is a necessary piece of the boundary condition and has been shown to have a theoretical, fluid-dynamic basis for its inclusion in the present formulation of the boundary condition. The slotted-wall coefficients K and B are the result of the inviscid and viscous analysis, respectively.

2. An analysis of the Chen and Mears experimental data proved (for large numbers of slots) that the flow far from the slot could indeed be assumed as homogeneous and, as a result, the data acquired on the sidewall of a two-dimensional transonic wind tunnel could approximate the average of that across the tunnel.

3. Adequate results may be obtained for the streamline curvature gradient by using parallel rows of tunnel-sidewall pressure measurements. However, extreme care must be exercised. For small values of dynamic pressure, low Mach numbers, and negative angles of attack (where the differences between rows of pressures become very small), good, reliable, estimates become difficult to make.

4. An evaluation of the 6X19 data show the plenum pressure to be a better indicator of the local far-field pressure which is felt by the slot than the measurement of the pressure in the slot even for transonic speeds with the larger values of the crossflow velocity. The larger the number of slots, the closer the correlation between those measurements made on the back of the slat and those made in the far-field of the surrounding plenum.

5. For the range of conditions considered in this study, the effect of the airfoil on the wall-pressure distribution appears as a perturbation on the existing, well-established, tunnel-empty pressure distribution. When lift is present, the "reference" level of the pressure distribution changes almost as a zero-shift.

6. Tunnel-empty data acquired in the DFA indicate that the slot flow angles are insignificantly affected by variations in the tunnel Mach number. However, data acquired with a model reveal anomalies which may (at this time) be explained only by the presence of a vortex originating at the slot-entry

edge of the slat near the point of zero slot flow angle under the model. Conclusive statements will require further experimental research.

7. Viscous effects are extremely important. Experimental results acquired by Berndt, unpublished data from the DFA, and the present 6X19 data set each indicate that the tunnel-empty growth of the wall boundary layers has significant impact on the wall-pressure drop. This effect is evident in the large values of the measured tunnel-empty slot-flow angles for each of these data sets and, in itself, negates the assumption that the square of the crossflow velocity component is negligible as has been assumed in many previous derivations of the wall boundary condition.

8. Experimental results acquired by Berndt, unpublished data from the DFA, and the present 6X19 data set each indicate that the airfoil has two major effects on the slot flow. The first is a global interaction of the airfoil and tunnel with the plenum which forces the plenum pressure to be decreased over the corresponding tunnel-empty case for matched free-stream Mach numbers. This interaction, which is felt over the entire extent of the slotted wall, is diminished with increasing openness ratio indicating a more open-jet like behavior as would be expected. The second effect is a highly localized region in the immediate vicinity of the airfoil from $-1.5 \leq x/c \leq 1.5$ where rapid variations in and large changes in the slot flow angles occur. Upstream of this, excluding the global effect, the flow angle in the slot appears to be insensitive to the presence of the model and almost completely dominated by the growth of the boundary layer. As a result of this, the flow-angle gradients which appear in the slot may have a different character upstream from those occurring inside the tunnel which are caused by model-induced changes in the streamline curvature. For instance, the "far-field" gradients may have different signs.

9. The analysis of the DFA data has clearly shown that the shear layer in the wall region of a longitudinally-slotted wind tunnel can be described using the concept of dynamic similarity of the flow. Similarity variables have been presented which show excellent correlation of the longitudinal and transverse flow components in the absence of free-stream curvature and in the longitudinal component with free-stream curvature. Crossflow correlations in the presence of free-stream curvature, while generally good, indicate the possible existence of an additional region of similarity which cannot be evaluated with the existing data. The results indicate the choice of similarity parameters to be insensitive to the effects of compressibility. Further refinement of the similarity variables by appropriate experiments would allow them to be used for the determination of the slot-flow velocity components (angles) thus simplifying the application of the wall boundary conditions.

10. For those wall configurations examined, it was experimentally verified that the wall pressure drop both for tunnel empty and for those regions of negligible free-stream curvature is well represented by

$$C_{Pw} - C_{Ps} = \theta_s^2$$

where the plenum pressure apparently "acts" at the vena contracta of the crossflow-velocity component. This indicates that the boundary layer developing on the tunnel walls is a major contributor to the pressure drop expression. This expression allows the slot flow angle in these regions to be accurately computed.

11. The Ideal form of the slotted-wall boundary condition can effectively model the wall pressure drop upstream of the point of maximum

model thickness if a zero-shift correction in the reference pressure is included. This empirical addition accounts for the growth of the tunnel boundary layers not included in the original theoretical development. Downstream of maximum model thickness, the ability of this form of the boundary condition to reproduce the wall pressure drop is poor and only the general trends are followed. Consistent variations of the ideal K coefficients with openness ratio and slot number have been demonstrated.

12. Berndt's form of the boundary condition is much the same as the "corrected Ideal" form. In this case, the constant is replaced by the square of the slot flow angle which is variable. This form of the equation gives better upstream results where the outflow is dominated by the growth of the boundary layer. However, its ability to model the flow past the maximum model thickness is not much better than the Ideal formulation. The Ideal form is generally much easier to use and appears to give more consistent results (possibly due to uncertainties which may exist in the present flow angle determination).

13. The present form of the wall-pressure drop can be linearized by subtracting the tunnel-empty boundary condition. The resulting linear form of the boundary condition is given by

$$\left(C_{Pw} - C_{Pw,te}\right) - \left(C_{Ps} - C_{ps,te}\right) = A - aK\frac{\partial C_{Pw}}{\partial y} + B\theta_s$$

where the subscript "te" indicates tunnel-empty and the A, K, and B are the slotted-wall boundary-condition coefficients. When using this, very good correlations were obtained between the measured pressure drop and that computed with the linearized formulation. The correlations were consistently

good for all of the tested openness ratios for all numbers of slots. Correlation of the computed pressure drop also improved with increasing numbers of slots, indicating that a more "homogeneous" flow was being achieved at the wind-tunnel wall. Good correlations between the experiment and the theory for variations in Mach number and angle of attack were obtained; however, a better correlation was achieved for positive angles than for negative angles due to the larger pressure differences between the parallel rows of pressure orifices. These larger differences yielded increased accuracy in determining the streamline curvature gradients which resulted in improved computations of the slot flow angles.

14. The analysis of the Ideal (classical) form of the boundary condition using the 6X19 data yielded consistent variations in the slotted-wall coefficient K for a free-stream Mach number of 0.7. The coefficients differ substantially from those predicted by the classical theory of Davis and Moore and also of Chen and Mears. Berndt's K value for 3 slots was consistent with the present results in that it was between the present 2 and 4 slot results. Comparison of other published results with those of the present study indicate the K values become insensitive to the number of slots for slot number of 4 or greater.

15. For a fixed free-stream Mach number of 0.7, all of the unknown boundary condition coefficients determined using the linearized form of the slotted-wall boundary condition were, again, found to have consistent variations with both openness ratio and number of slots. The present form of the boundary condition resulted in reduced values of the slotted-wall coefficient K as compared to the Ideal values with the most "theoretical-like" variations being those for 4 slots. The B (or viscous) coefficient has a linear variation with openness ratio for a fixed number of

slots; however, due to a lack of resolution (i.e., insufficient flow angle measurements), this coefficient has the most uncertainty and, as a result, more extensive research should be conducted to further analyze its behavior. As with the B coefficient, the A coefficient shows a small, linear variation with openness ratio.

16. An analysis of the boundary condition for the 15-percent-open wall with 4 slots at $\alpha = 0.0$ using the linearized boundary condition revealed previously unknown, consistently repeatable, linear, Mach-number variations for the K coefficient. There was effectively no variation in this coefficient for changes in lift over the α range considered for $M_\infty = 0.7$. The B coefficient was found to be repeatable and linearly increasing with Mach number while the variation with lift was very small. Mach numbers of less than 0.8 (where the model/tunnel interaction with the plenum is of small importance) had little effect on the value of the A coefficient. As with B, the effect of lift on A is very small for the range of conditions considered.

17. Berndt proposed a theoretically-based, slot-depth addition to the Davis and Moore modelling of the K coefficient. According to his theory, the depth of the slot increases the value of K linearly over that predicted by the Davis and Moore theory. This effect was examined for the Ideal and present-method evaluations of this coefficient using the present and previously acquired experimental results. The Ideal values of K indicate the effect of slot depth to be an important factor but with different slope and intercept than predicted by the Berndt theory. However, when using the present-method analysis, the results for a slot number of 3 or larger gives an excellent correlation with the Berndt theory.

CHAPTER X

RECOMMENDATIONS FOR FURTHER RESEARCH

In this chapter, some of the deficiencies which were identified in the course of the present study will be discussed as will be recommendations for follow-on research.

There are several, major areas which are ripe for both theoretical and experimental investigations. Probably the most obvious (and most important) is that of the viscous interactions on the wall and through the slot. When defining the current series of experiments, all single slot configurations had the slot located on the centerline of the tunnel; however, for those walls with multiple slots, a half slot was placed in the corner at each tunnel sidewall. This was done to maintain the symmetry (both hardware and fluid dynamic) about a centerline slot where the flow-angle measurements were made. This arrangement has the drawback that the influence of the sidewall boundary layer on the corner slots is unknown. The potential for error when determining the flow angle exists for these walls particularly those which have a small openness ratio. In this case, the mass flux through the sidewall slots may not have the same characteristics as those away from the wall.

The results reported herein did not include any variations in the thickness of the sidewall boundary layer except those due to the normal variations in free-stream Mach number and Reynolds number at fixed airfoil angle of attack. To date, all known analysis methods have assumed the top and bottom walls to be linearly separable from the sidewalls. The interaction of these surfaces should be examined, particularly for the higher Mach numbers where the equations defining the flow in the tunnel may become nonlinear.

The viscous interaction with the slot geometry is an important consideration. Analysis of the DFA data indicated that the wall boundary layer became a shear flow on the centerline of the slot. The manner in which this transition occurs could be very important for analytically modelling the flow in the tunnel and determining the mass flux (flow angle) along and through the slot. The DFA data also revealed the possibility of a vortex forming along the slot-entry edges near the point of zero slot flow angle. There is a need for an improved understanding of the flow in and around slots as a function of Reynolds number and Mach number as well as the effects of wall geometry and plenum suction on these flows.

A relatively new field of study is that of wall interference/assessment correction (WIAC) (ref. 43). These techniques use wall-pressure measurements to evaluate the "residual" interference in wind tunnel data by analytically modelling the flow in the wind tunnel. The results are then used to assess whether the data are correctible or whether some form of wall adaptation can be made to improve data fidelity. This modelling requires an appropriate formulation of the boundary condition. An implementation of the present form could greatly improve the existing wall-interference prediction techniques, particularly if the slat pressures (possibly with a correction factor) could be used as opposed to the homogeneous-wall (or far-field) pressure. The present experimental technique left open to question the applicability of using tunnel-side slat pressures as an appropriate representation of the far-field (homogeneous) wall pressure.

Owing to the lack of appropriate slot-flow data downstream of the airfoil trailing-edge station, the interaction of the flow returning to the test section with the tunnel flow and also with the wall geometry is still a cause for concern. Several important questions remain including:

What is the structure of the returning flow; Does it jet into the tunnel or does it form a separation bubble on the tunnel-side of the wall (ref. 15)?; and,

What is the behavior of the flow angle as the tunnel flow returns to its far-field state?

Adequate descriptions of the tunnel inflow conditions are required to further improve the assessment of wall interference in wind tunnels (ref. 25).

Obvious geometric extensions of this present study include the influences of slot radius-of-curvature and slot depth on the wall pressure drop. The ability to make large changes in the wall-flow characteristics by way of small changes in the slot geometry holds the promise (or future) of adaptive slotted walls for interference reduction in large wind tunnels. The ability to control the wall flow by way of slot blowing (either longitudinal or normal) may allow adjustment to the "effective" geometric shape of the slot with minimum hardware changes.

Another "geometric" observation from the present study is what appears to be the existence of a minimum number of slots for a good approximation of the homogeneous slotted-wall boundary condition. This minimum value should be investigated as should the effect of the simultaneous use of different top- and bottom-wall configurations.

Finally, the boundary condition should be evaluated under more adverse conditions. These include higher Mach numbers and larger lift coefficients.

In summary, it is first recommended that a study specifically oriented toward the viscous interaction of the slotted-wall flow field with the wall geometry be conducted. This study should be nonintrusive due to the scale

effects of the slot width and the boundary-layer displacement thickness. This study should, as a minimum, vary the boundary-layer thickness over the slotted wall, both with and without the airfoil, at several values of lift. The influence of the plenum pressure on the re-entry flow should be evaluated in order to access its importance on the wall-flow characteristics. Second, the ability to control the wall-flow characteristics by way of slot blowing and/or suction should be examined. This is fundamental to validating whether this technique can be used as a simple "add-on fix" to existing wind tunnels for implementing adaptive slotted walls. Finally, it is recommended that the number of slots be systematically increased for fixed wall openness ratio to examine their ability to yield a homogeneous form of the slotted-wall boundary condition and that the effects of slot depth and slot radius-of-curvature be evaluated.

REFERENCES

1. Glauert, H.: The Elements of Aerofoil and Airscrew Theory. Second ed. Cambridge University Press, 1947, pp. 189-198.

2. Theodorsen, T.: The Theory of Wind-Tunnel Wall Interference. NACA Report No. 410, 1931.

3. Allen, H. Julian; and Vincenti, Walter G.: Wall interference in a Two-Dimensional-Flow Wind Tunnel, With Consideration of the Effect of Compressibility. NACA Report No. 782, 1944.

4. Garner, H. C.; Rogers, E. W. E.; Acum, W. E. A.; and, Maskell, E. C.: Subsonic Wind Tunnel Wall Corrections. AGARDograph 109, October, 1966.

5. Pindzola, M.; and Lo, C. F.: Boundary Interference at Subsonic Speeds in Wind Tunnels with Ventilated Walls. AEDC TR-69-47, 1969.

6. Pope, Alan; and Harper, John J.: Low-Speed Wind Tunnel Testing. John Wiley & Sons, Inc., 1966.

7. Pankhurst, R. C.; and Holder, D. W.: Wind-Tunnel Technique, An Account of Experimental Methods in Low- and High-Speed Wind Tunnels. Sir Isaac Pitman & Sons LTD., 1952 (reprinted with corrections 1965).

8. Wright, Ray H.; and Ward, Vernon G.: NACA Transonic Wind-Tunnel Test Sections. NACA Report 1231, 1955.

9. Hansen, James R.: Engineer in Charge: A History of the Langley Aeronautical Laboratory, 1917-1958. NASA SP-4305, 1987.

10. Davis, Don D., Sr.; and Moore, Dewey: Analytical Studies of Blockage and Lift-Interference Corrections for Slotted Tunnels Obtained by the Substitution of an Equivalent Homogeneous Boundary for the Discrete Slots. NACA TM-L-53E075, 1953.

11. Chen, C. F.; and Mears, J. W.: Experimental and Theoretical Study of Mean Flow Boundary Conditions at Perforated and Longitudinally Slotted Wind Tunnel Walls. Arnold Engineering and Development Center, TR-57-20, 1957.

12. Baldwin, Barrett S., Jr.; Turner, John B.; and Knechtel, Earl D.: Wall Interference in Wind Tunnels with Slotted and Porous Boundaries at Subsonic Speeds. NACA TN 3176, 1954.

13. Goethert, B. H.: Properties of Test Section Walls with Longitudinal Slots in Curved Flow for Subsonic and Supersonic Velocities (Theoretical Investigations). AEDC TN-55-56, 1957.

14. Wood, W. W.: Tunnel Interference from Slotted Walls. Quart. J. Mech. Applied Math., vol 17, 1964.

15. Berndt, S. B.; and Sorensen, Hans: Flow Properties of Slotted Walls for Transonic Test Sections. AGARD Conference Proceedings No. 174, Paper No. 17, 1975.

16. Baronti, P.; Ferri, A.; and Weeks, T.: Analysis of Wall Modifications in a Transonic Wind Tunnel. Advanced Technology Laboratories, TR-181, 1973.

17. Barnwell, Richard W.: Improvements in the Slotted-Wall Boundary Condition. Proceedings, AIAA Ninth Aerodynamic Testing Conference, 1976, pp. 21-30.

18. Liepmann, H. W.; and Roshko, A: Elements of Gasdynamics. John Wiley & Sons, Inc., c.1957.

19. Ramaswamy, M. A.: A New Hypothesis on the Cross Flow Characteristics of Slotted Walls. 1st Asian Conference on Fluid Mechanics, Bangalore, India, December, 1980.

20. Gentry, Garl L.,Jr.; Igoe, William B.; and Fuller, Dennis E.: Description of 0.186-Scale Model of High-Speed Duct of National Transonic Facility. NASA TM 81949, 1981.

21. Wu, J. M.; and Collins, F. G.: Investigations of Flow Field Perturbations Induced on Slotted Transonic-Tunnel Walls. Proceedings, Wind Tunnel Wall Interference Assessment/Correction 1983 Workshop. NASA Conference Publication 2319, 1984.

22. Ladson, Charles L.: Description and Calibration of the Langley 6- by 19-inch Transonic Tunnel. NASA TN D-7182, 1973.

23. Sinclair, Archibald R.; and Robins, A. Warner: A Method for the Determination of the Time Lag in Pressure Measuring Systems Incorporating Capillaries. NACA TN-2793, 1952.

24. Berndt, S. B.: Measuring the Flow Properties of Slotted Test-Section Walls. FFA Report 135, 1982.

25. Kemp, William B.: Computer Simulation of a Wind Tunnel Test Section with Discrete Finite-length Wall Slots. NASA CR-3948, 1986.

26. Baumeister, Theodore; and Marks, Lionel S., ed.: Mechanical Engineers' Handbook. Sixth Edition, McGraw-Hill Book Company, 1964.

27. Sedin, Y. C.-J.; and Sorensen, H.: Computed and Measured Wall Interference in a Slotted Transonic Test Section. AIAA 22nd Aerospace Sciences Meeting, 1984.

28. Goethert, B. H.: Transonic Wind Tunnel Testing. Edited by W. C. Nelson. AGARDograph 49. Pergamon Press, 1961.

29. Everhart, Joel L.: A Method for Modifying Two-Dimensional Adaptive Wind-Tunnel Walls Including Analytical and Experimental Verification. NASA TP-2081, 1983.

30. Sewall, William G.: Application of a Transonic Similarity Rule To Correct the Effects of Sidewall Boundary Layers in Two-Dimensional Transonic Wind Tunnels. M.S. Thesis, The George Washington University, 1982.

31. Barnwell, Richard W.: Similarity Rule for Sidewall Boundary-layer Effect in Two-Dimensional Wind tunnels. AIAA J. vol. 18, no. 9, Sept. 1980, pp. 1149-1151.

32. Murthy, A. V.: Effect of Aspect Ratio on Sidewall Boundary-Layer Influence in Two-Dimensional Airfoil Testing. NASA CR-4008, 1986.

33. Von Mises, Richard: Theory of Flight. Dover Publications, Inc., 1959.

34. Mathematical and Statistical Software at Langley. Central Scientific Computing Complex, Document N2-3b, March 1987.

35. Reinsch, C. H.: Smoothing by Spline Functions. Numerische Mathematik, vol. 10, no. 3, 1967.

36. White, F. M.; Viscous Fluid Flow. McGraw-Hill, Inc., 1974.

37. Reynolds, O.: An Experimental Investigation of the Circumstances Which Determine Whether the Motion of Water Shall Be Direct or Sinuous, and of the Law of Resistance in Parallel Channels. Phil. Trans. Roy, Soc., London, 174, 935-982 (1883) or Scientific Papers II, 51.

38. Blasius, H.: Grenzschichten in Flüssigkeiten mit kleiner Reibung. Z. Math. u. Phys. 56, 1-37 (1908). Engl. Transl. in NACA TM 1256.

39. Schlichting, H.: Boundary Layer Theory. Sixth Edition. McGraw-Hill, Inc., 1968.

40. Goradia, Suresh H.: Confluent Boundary Layer Flow Development With Arbitrary Pressure Distribution. Ph. D. Thesis, Georgia Institute of Technology, 1971.

41. Berndt, S. B.: Inviscid Theory of Wall Interference in Slotted Test Sections. AIAA J., vol.15, no 9, September 1977, pp. 1278-1287.

42. Berndt, Sune B.: Flow Properties of Slotted-Wall Test Sections. Agard Fluid Dynamics Panel Specialist Meeting on Wall Interference in Wind Tunnels, Paper No. 6, 1982.

43. Wind Tunnel Wall Interference Assessment/Correction - 1983. NASA CP 2319, 1984.

44. Harris, Charles D.: Two-Dimensional Aerodynamic Characteristics of the NACA 0012 Airfoil in the Langley 8-Foot Transonic Pressure Tunnel. NASA TM-81927, 1981.

45. Melnik, R. E.; Mead, H. R.; and Jameson, A.: A Multi-grid Method for the Computation of Viscid/Inviscid Interaction on Airfoils. AIAA 83-0234, Jan. 1983.

46. Brownlee, K. A.: Statistical Theory and Methodology in Science and Engineering. Second ed. John Wiley & Sons, Inc., 1965.

TABLE I
NACA 0012 AIRFOIL ORIFICE ORDINATES

ORIF	X	Y	ORIF	X	Y
801	0.0000	-0.0002			
802	0.0719	-.1127	825	0.0733	0.1110
803	0.1490	-.1584	826	0.1533	0.1582
804	0.2980	-.2149	827	0.2958	0.2121
805	0.4514	-.2539	828	0.4535	0.2529
806	0.6022	-.2829	829	0.6085	0.2835
807	0.9048	-.3226	830	0.9008	0.3222
808	1.2018	-.3450	831	1.1971	0.3445
809	1.5000	-.3568	832	1.4959	0.3562
810	1.7992	-.3602	833	1.7961	0.3598
811	2.0981	-.3579	834	2.0980	0.3577
812	2.3969	-.3495	835	2.3693	0.3498
813	2.6983	-.3361	836	2.6967	0.3364
814	2.9949	-.3190	837	2.9965	0.3191
815	3.2939	-.2984	838	3.2963	0.2985
816	3.5932	-.2745	839	3.5946	0.2754
817	3.8928	-.2476	840	3.8925	0.2500
818	4.1919	-.2188	841	4.1951	0.2215
819	4.4939	-.1879	842	4.4934	0.1911
820	4.7924	-.1560	843	4.7940	0.1586
821	5.0893	-.1231	844	5.0937	0.1247
822	5.3899	-.0884	845	5.3911	0.0896
823	5.6881	-.0501	846	5.6880	0.0527
824	5.8428	-.0293	847	5.8332	0.0330

TABLE II
SLOT AND SLAT ORIFICES

SIDE			TOP			BOTTOM		
ORIF	X	Y	ORIF	X	Y	ORIF	X	Y
001	-16.0	9.5	016	-16.0	9.5	031	-16.0	9.5
002	-13.0	9.5	017	-13.0	9.5	032	-13.0	9.5
003	-10.0	9.5	018	-10.0	9.5	033	-10.0	9.5
004	-8.0	9.5	019	-8.0	9.5	034	-8.0	9.5
005	-6.0	9.5	020	-6.0	9.5	035	-6.0	9.5
006	-4.5	9.5	021	-4.5	9.5	036	-4.5	9.5
007	-3.0	9.5	022	-3.0	9.5	037	-3.0	9.5
008	-1.5	9.5	023	-1.5	9.5	038	-1.5	9.5
009	0.0	9.5	024	0.0	9.5	039	0.0	9.5
010	1.5	9.5	025	1.5	9.5	040	1.5	9.5
012	5.0	9.5	027	5.0	9.5	042	5.0	9.5
013	7.5	9.5	028	7.5	9.5	043	7.5	9.5
014	10.5	9.5	029	10.5	9.5	044	10.5	9.5
015	14.0	9.5	030	14.0	9.5	045	14.0	9.5

TABLE III
SIDEWALL ORIFICES

ROW 1			ROW 2			ROW 3		
ORIF	X	Y	ORIF	X	Y	ORIF	X	Y
101	-22.002	8.482	201	-22.020	7.955	301	-22.019	7.454
102	-18.996	8.475	202	-19.020	7.955	302	-19.017	7.460
103	-16.002	8.500	203	-16.018	7.967	303	-16.017	7.464
104	-13.012	8.489	204	-13.017	7.972	304	-13.016	7.474
105	-9.998	8.498	205	-10.017	7.980	305	-10.013	7.479
106	-7.999	8.497	206	-8.018	7.984	306	-8.016	7.485
107	-6.007	8.493	207	-6.007	7.994	307	-6.006	7.493
108	-5.007	8.493	208	-5.007	7.994	308	-5.006	7.494
109	-4.007	8.493	209	-4.007	7.995	309	-4.006	7.496
110	-3.007	8.494	210	-3.006	7.995	310	-3.006	7.497
111	-2.007	8.494	211	-2.007	7.997	311	-2.006	7.497
112	-1.005	8.495	212	-1.006	7.997	312	-1.006	7.497
113	-0.006	8.496	213	-0.006	7.997	313	-0.008	7.491
114	0.994	8.497	214	0.992	7.997	314	0.994	7.500
115	1.995	8.497	215	1.995	7.999	315	1.995	7.500
116	2.993	8.498	216	2.994	7.999	316	2.995	7.501
117	4.995	8.501	217	4.995	8.000	317	4.995	7.501
118	6.995	8.502	218	6.996	8.002	318	6.995	7.501
119	8.993	8.502	219	8.995	8.004	319	8.997	7.504
120	10.985	8.508	220	11.001	8.009	320	10.987	7.505
121	12.987	8.513	221	12.974	8.005	321	12.996	7.503

Table IV
WIND-TUNNEL-WALL MACH-NUMBER-CALIBRATION COEFFICIENTS

WALL	ALS	BLS	CLS
15-1	0.000688	0.970948	0.076716
15-2	.000997	.965892	.090900
7.5-1	.000398	.975668	.078477
solid	.000208	.989451	.079178
15-4	.000650	.976335	.060428
7.5-2	.000427	.992203	.033086
3.75-1	.000090	1.006190	.011167
10-4	.000531	.983785	.047933
5-2	.000604	.990582	.053354
6-4	.000789	.987352	.056231
3-2	.000299	1.008190	.030300
10-2	.000692	.976066	.069774

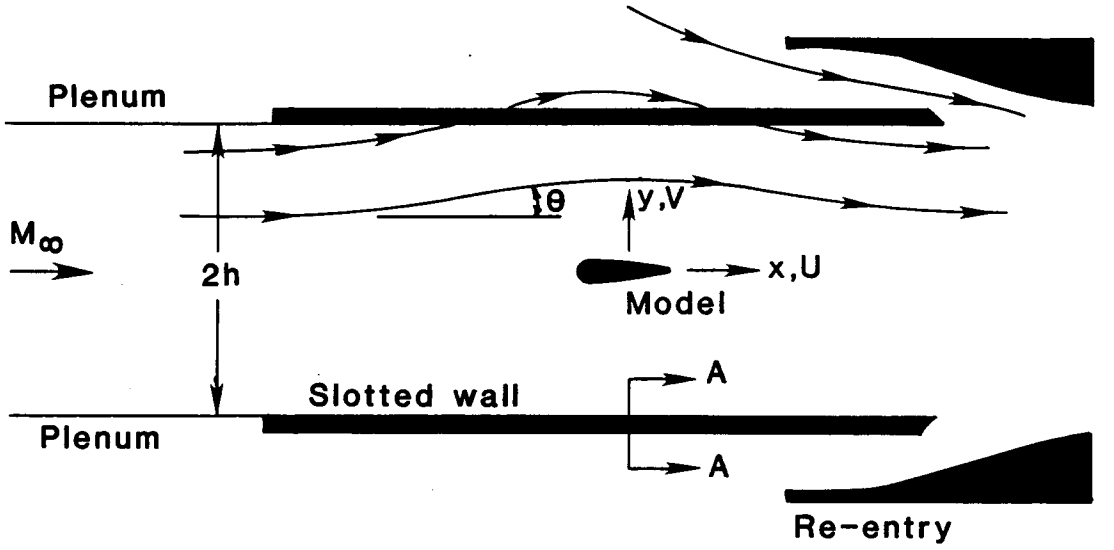

(a) Tunnel cross section.

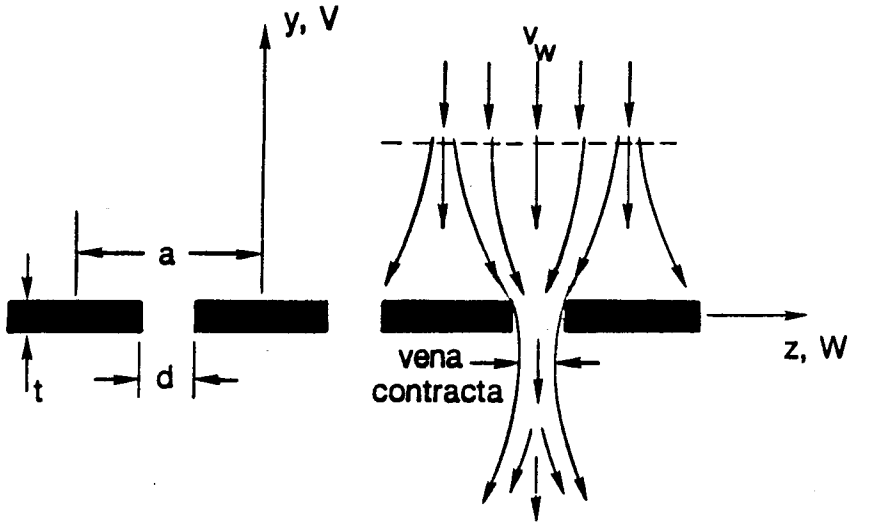

(b) Cross-sectional view of a slotted wall, section A-A of figure a.

Figure 1.- Typical slotted-wall wind tunnel.

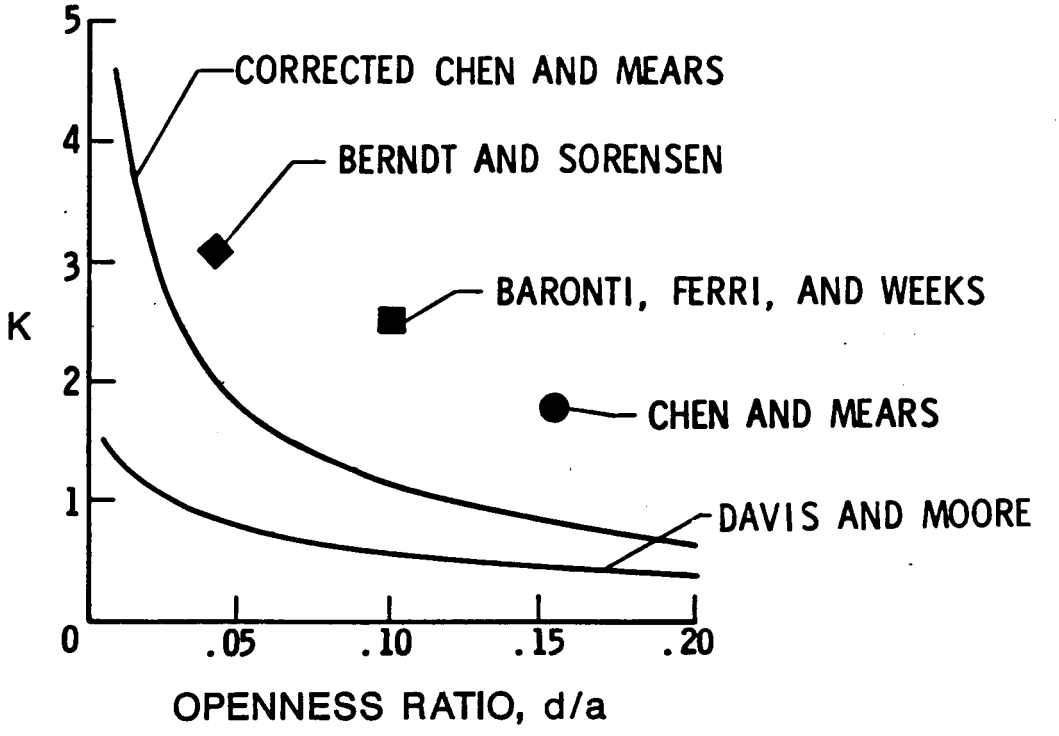

Figure 2.- Published values of the slotted-wall coefficient K.

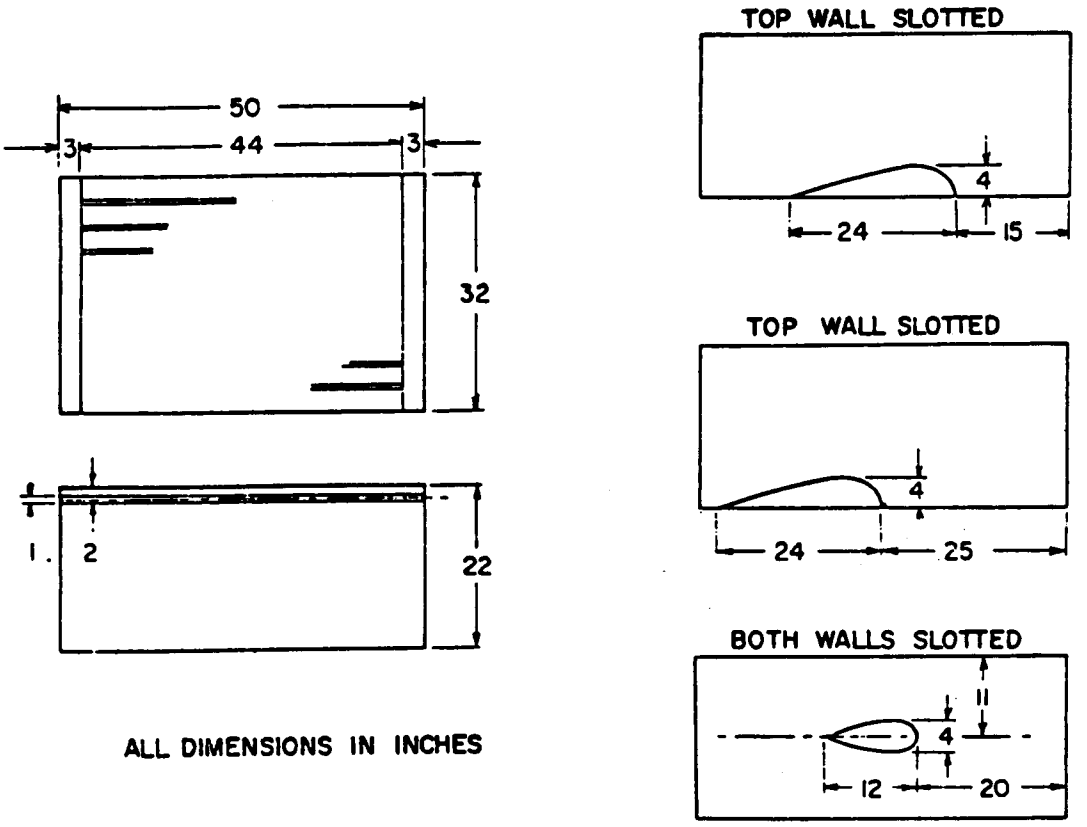

Figure 3.- Chen and Mears' experimental setup.

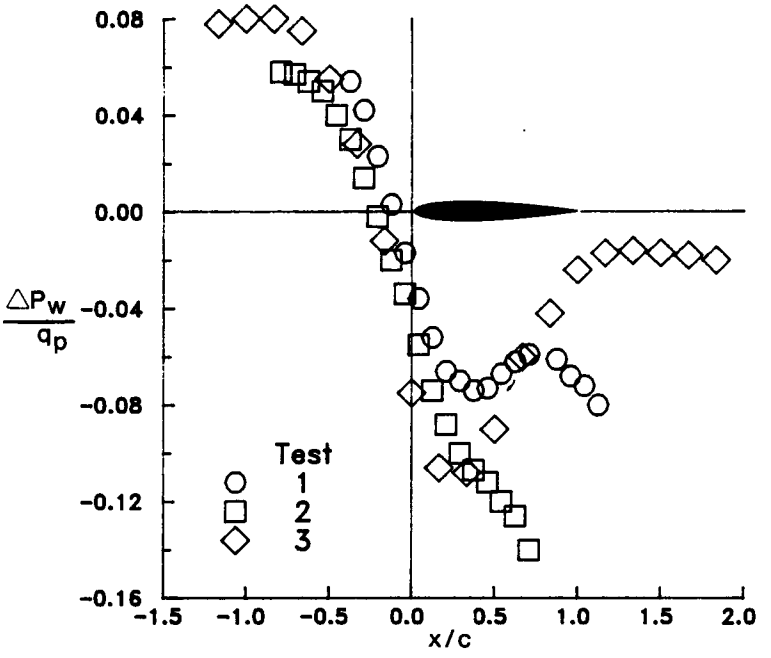

(a) Measured wall-pressure drop over the slot.

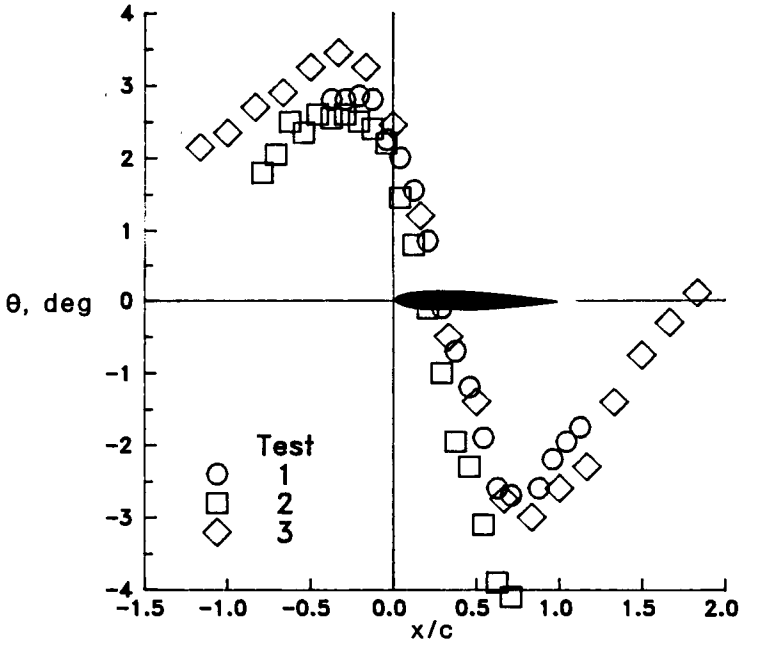

(b) Measured flow angle over the slot.

Figure 4.- Chen and Mears' over-slot data for all tests.

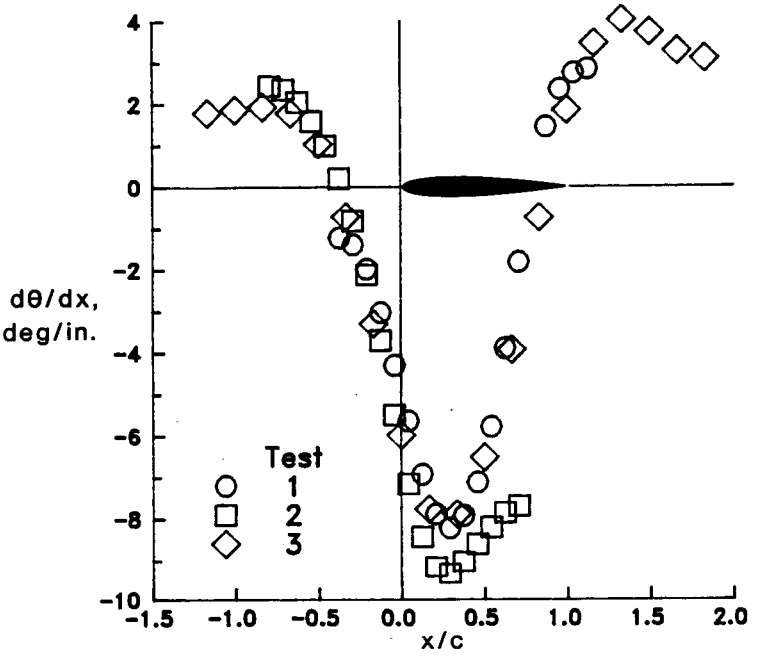

(c) Computed flow-angle gradient over the slot.

Figure 4.- Concluded.

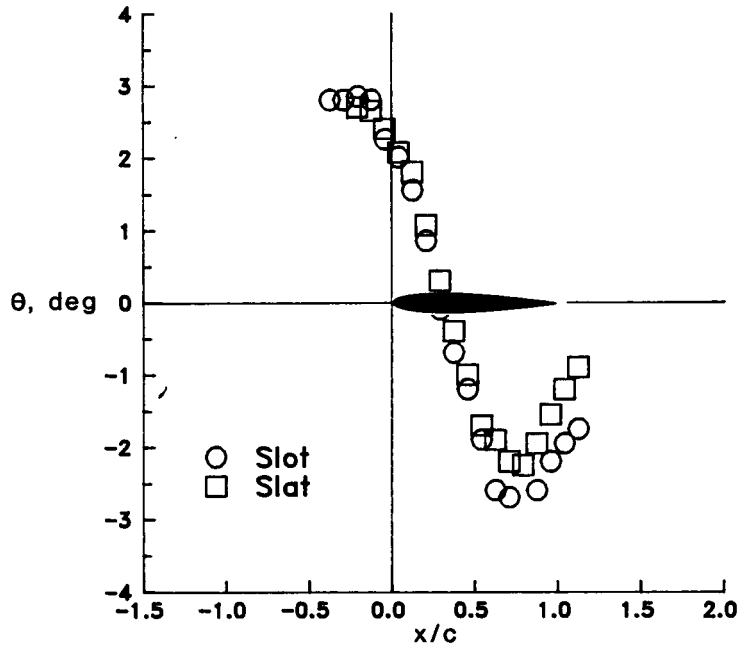

(a) Test 1.- Measured flow angles.

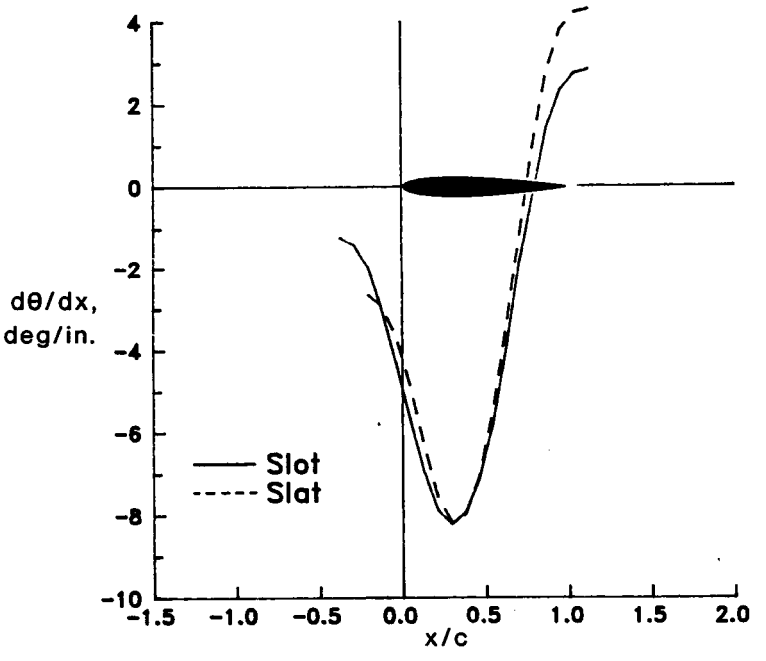

(b) Test 1.- Computed flow-angle gradient.

Figure 5.- Chen and Mears' Test 1 data over the slot and slat.

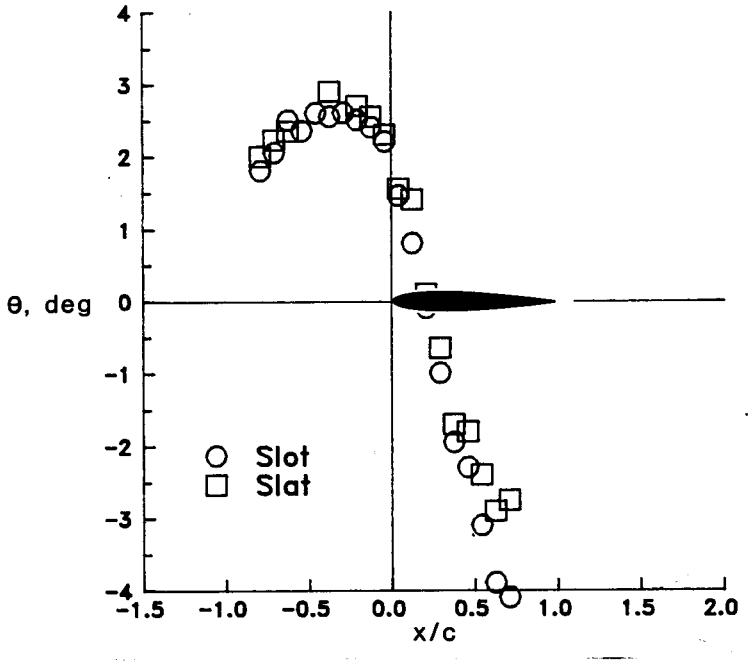

(a) Test 2.- Measured flow angles.

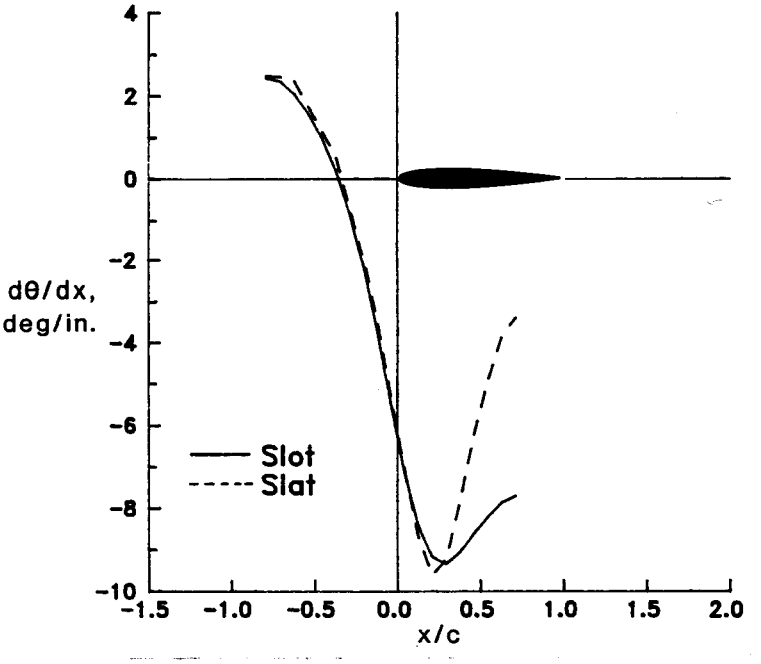

(b) Test 2.- Computed flow-angle gradient.

Figure 6.- Chen and Mears' Test 2 data over the slot and slat.

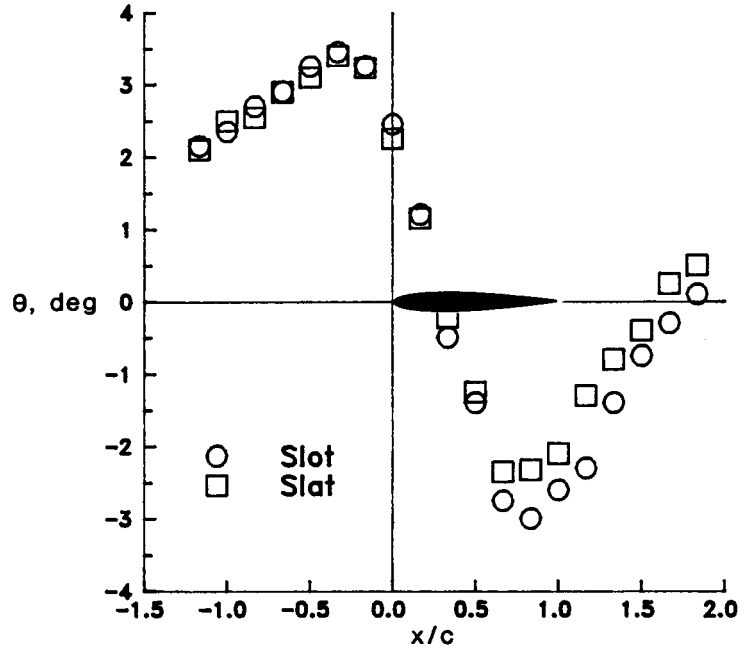

(a) Test 3.- Measured flow angles.

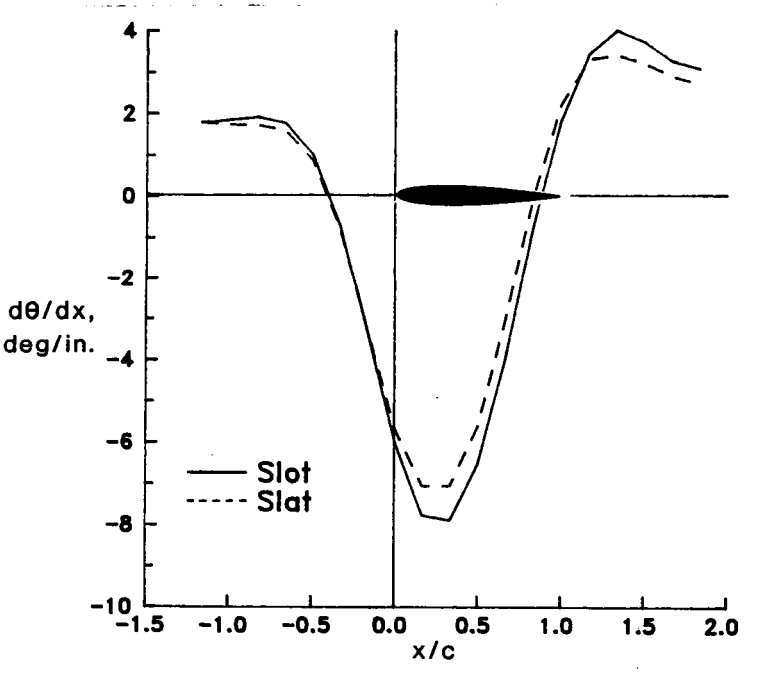

(b) Test 3.- Computed flow-angle gradient.

Figure 7.- Chen and Mears' Test 3 data over the slot and slat.

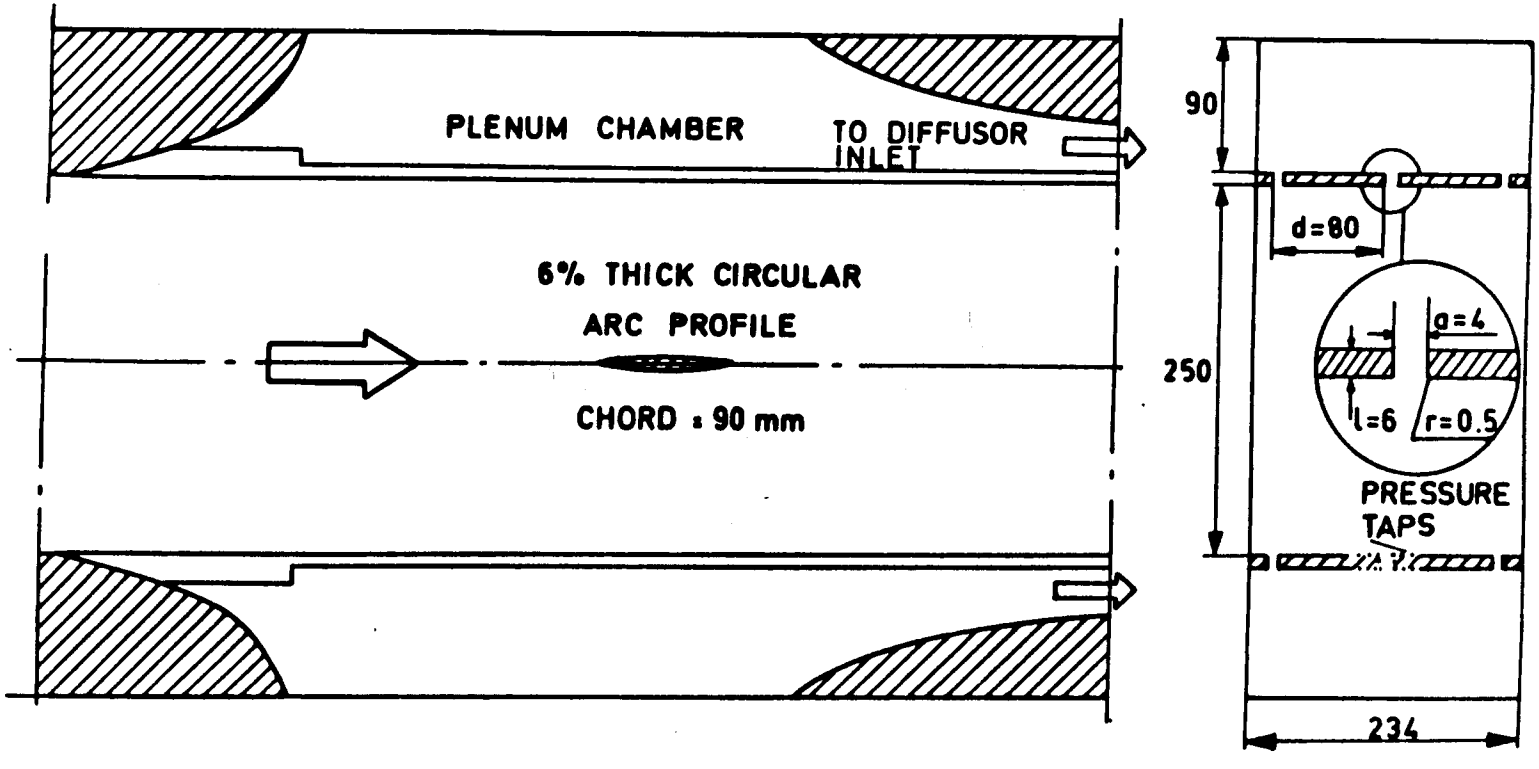

Figure 8.- Berndt's experimental setup.

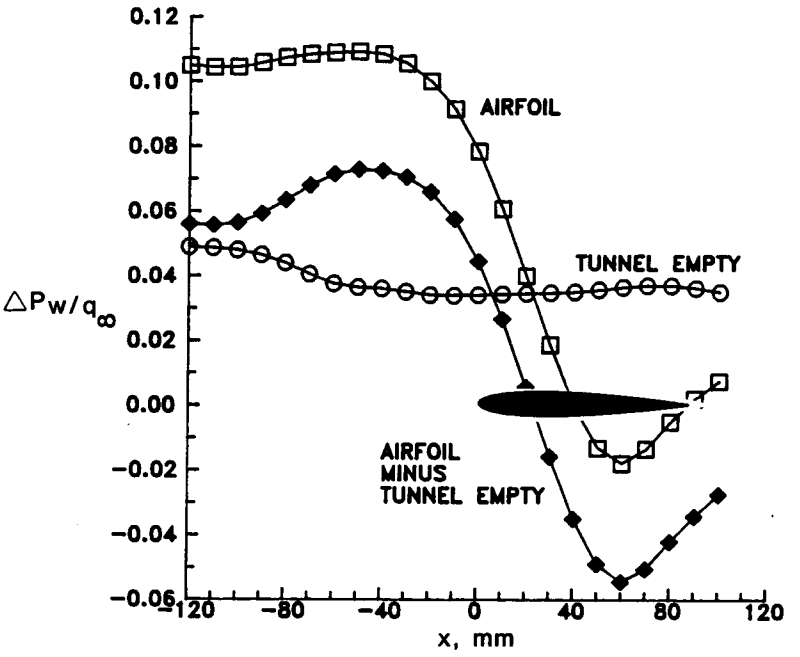

(a) Measured wall-pressure drop.

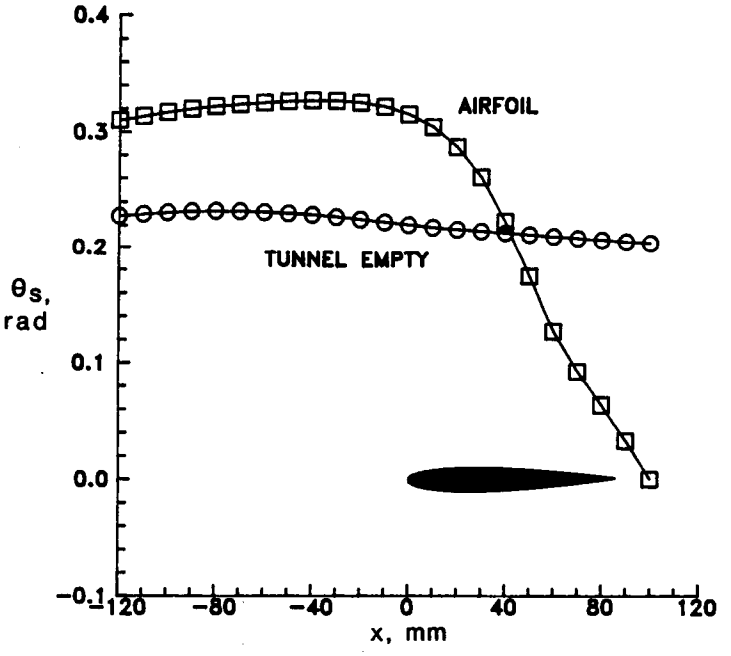

(b) Measured flow angle in the slot.

Figure 9.- Berndt's data.

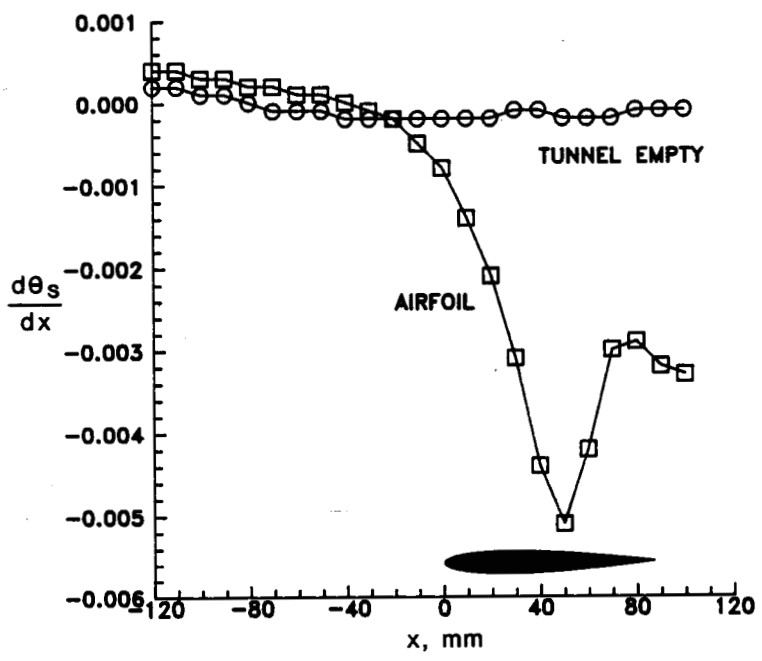

(c) Computed flow-angle gradient in the slot.

Figure 9.- Continued.

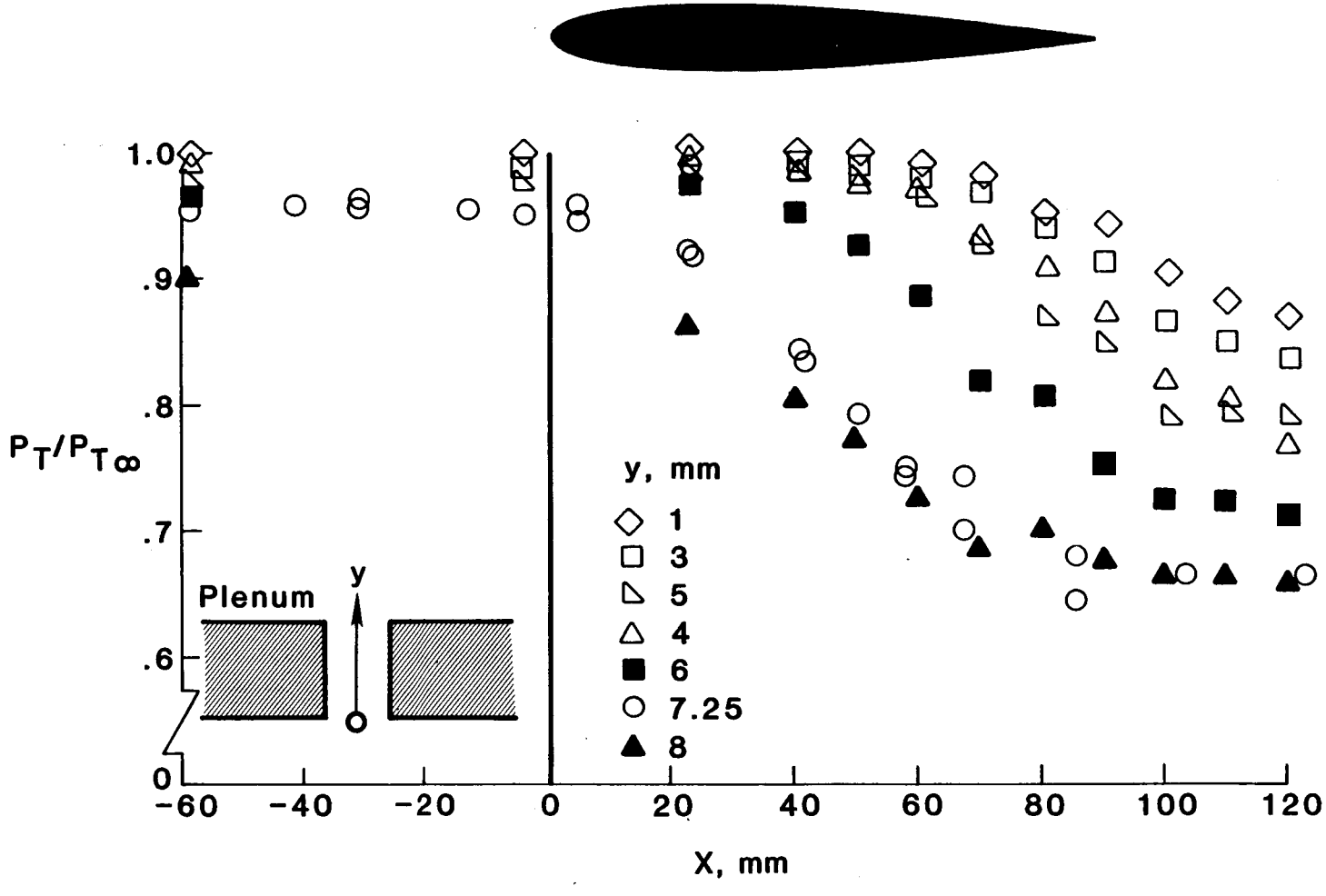

(d) Measured total-pressure distribution in the slot.

Figure 9.- Concluded.

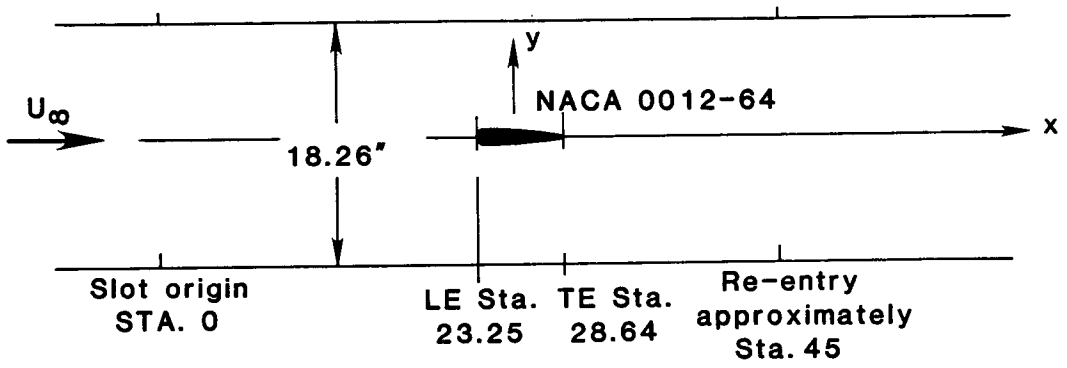

(a) Cross section of DFA.

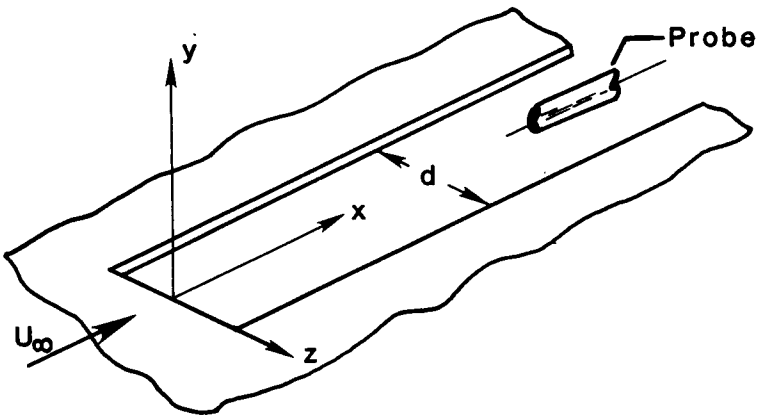

(b) Slot coordinate system.

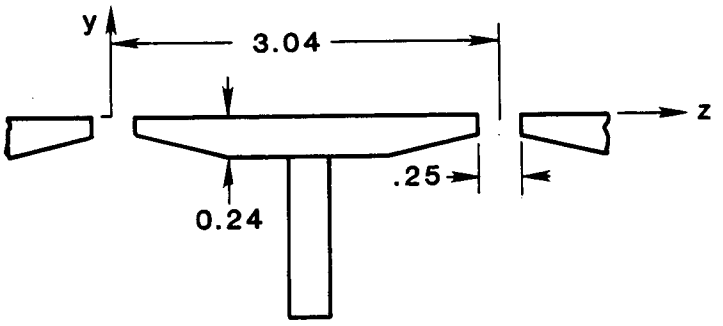

(c) Cross-sectional view of the wall.

Figure 10.- DFA experimental setup.

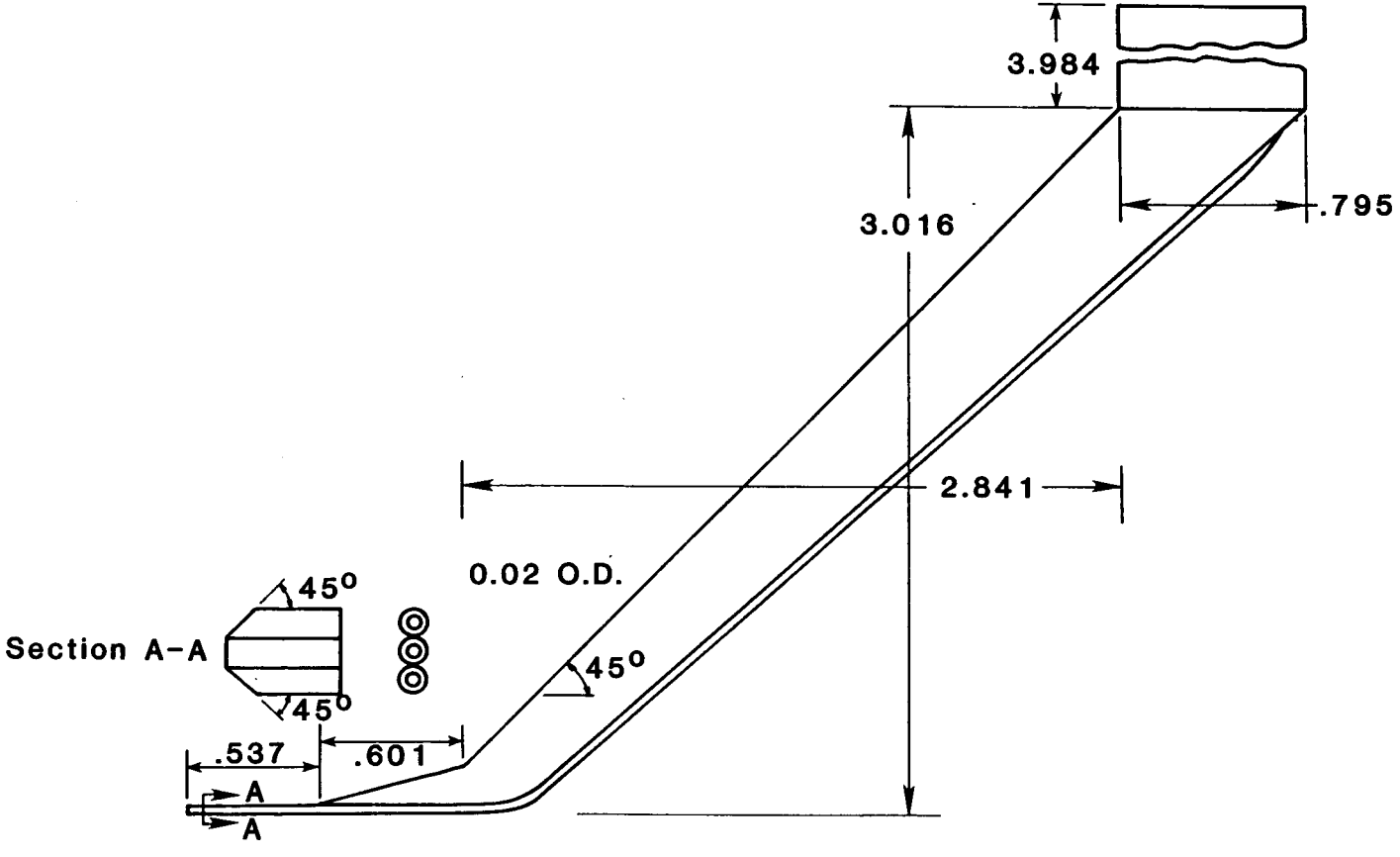

Figure 11.- Schematic of the DFA flow-angle probe.

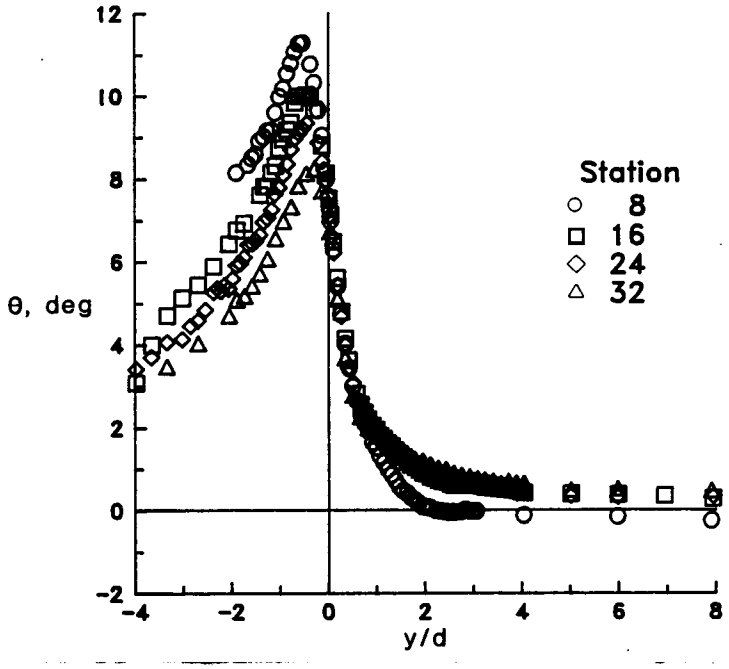

(a) Flow angle.

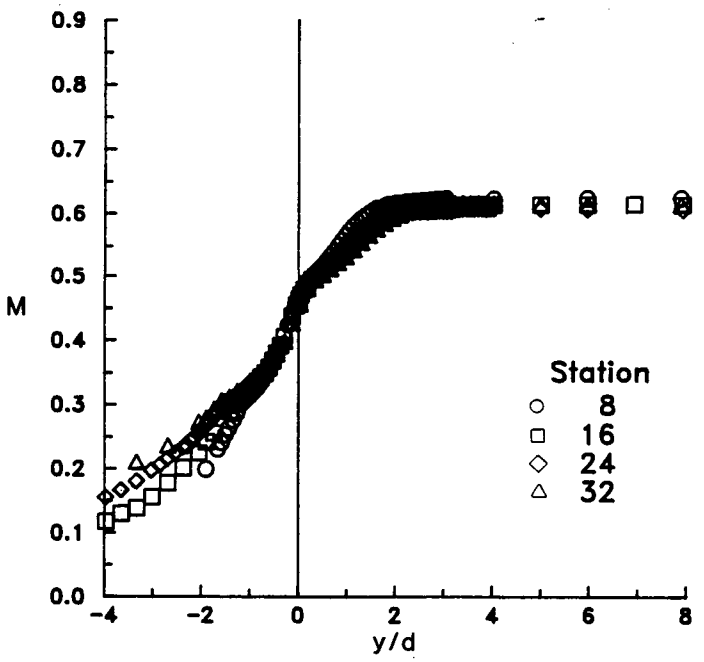

(b) Mach number.

Figure 12.- Variation of DFA-probe measurements with tunnel station.

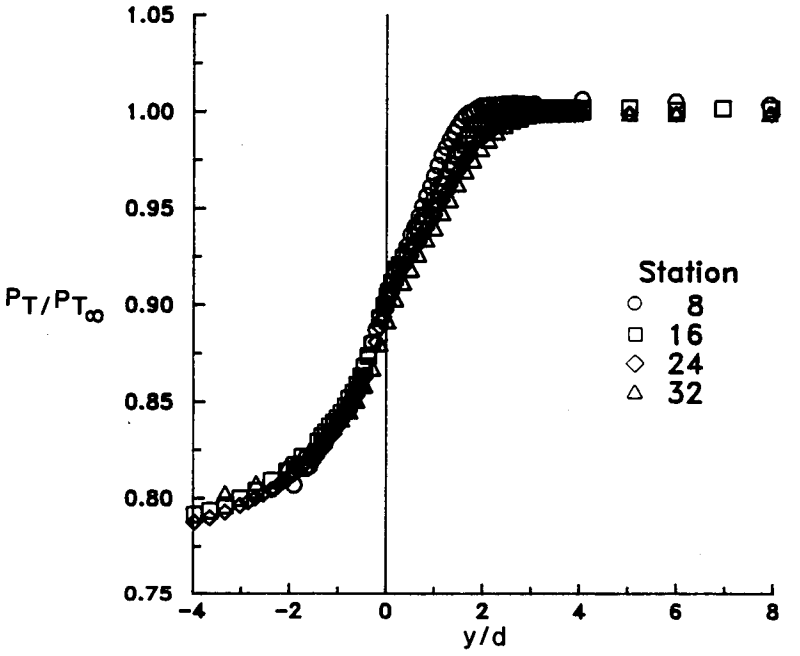

(c) Total-pressure ratio.

Figure 12.- Concluded.

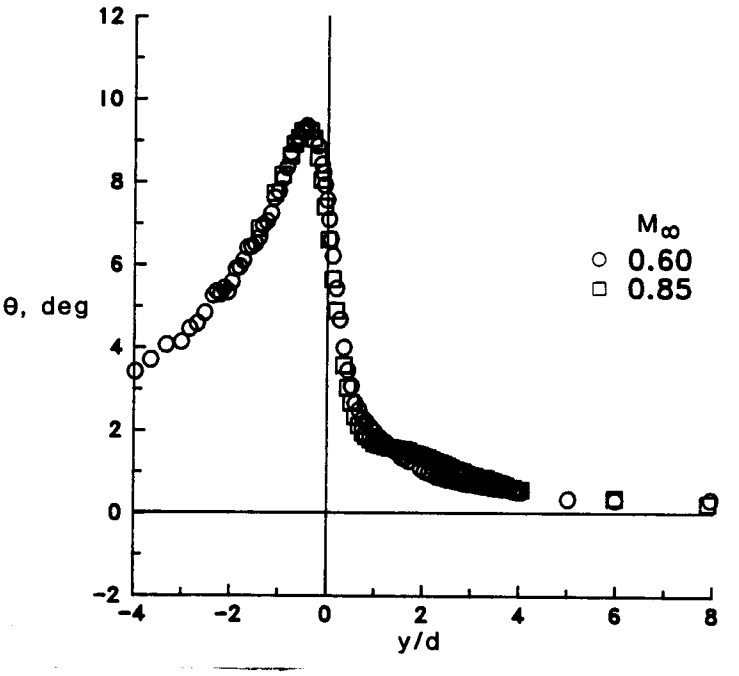

(a) Flow angle.

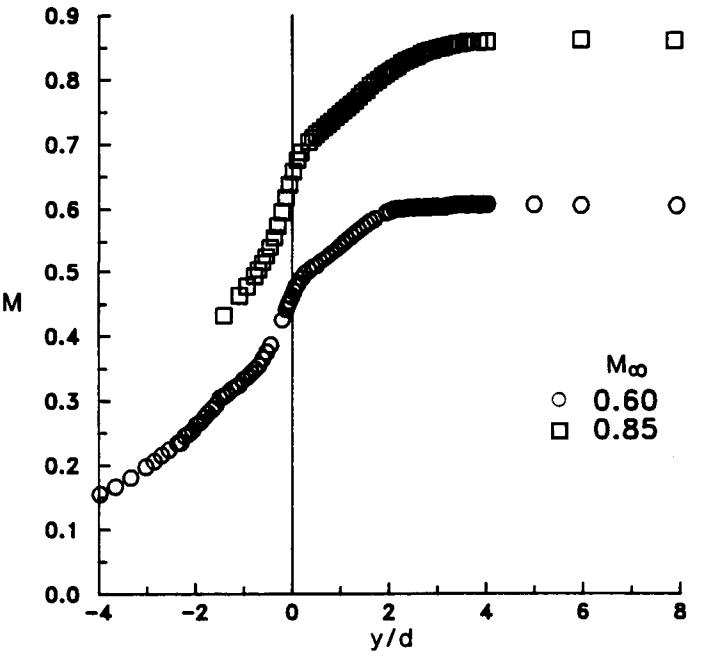

(b) Mach number.

Figure 13.- Influence of Mach number on the DFA-probe measurements.

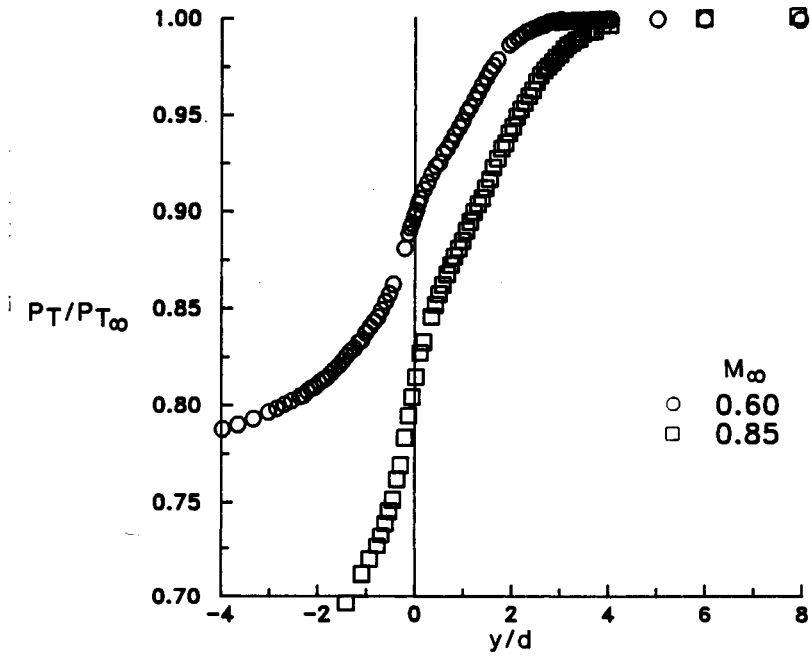

(c) Total-pressure ratio.

Figure 13.- Concluded.

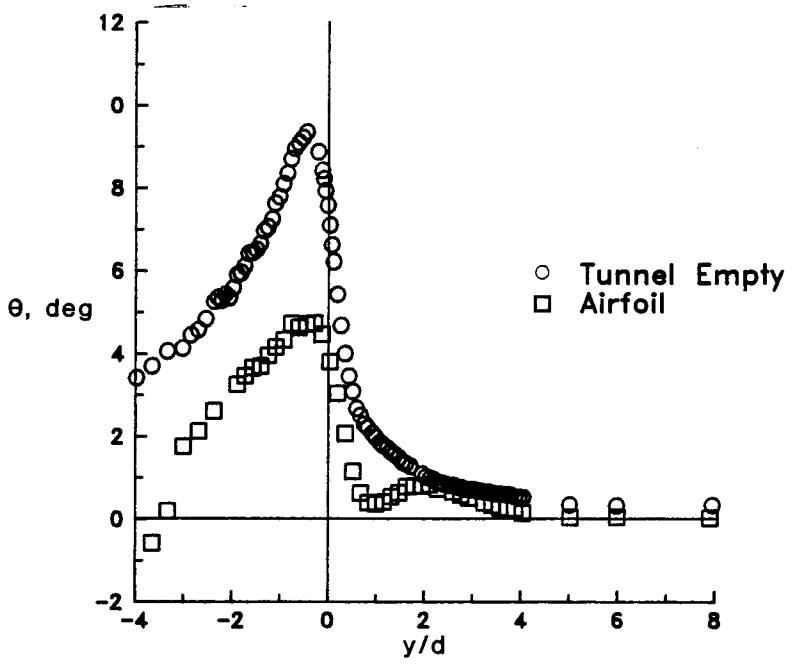

(a) Flow angle.

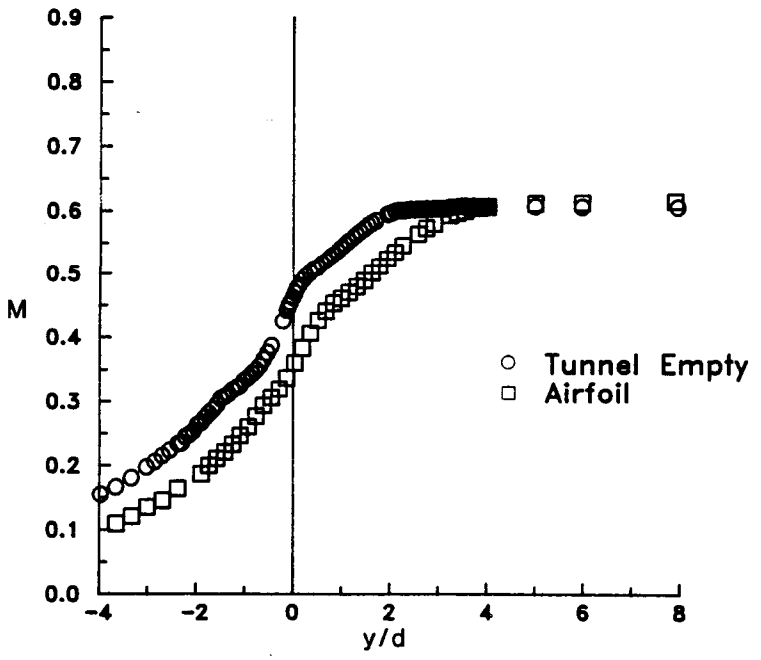

(b) Mach number.

Figure 14.- Comparison of tunnel-empty DFA-probe measurements to those with the airfoil.

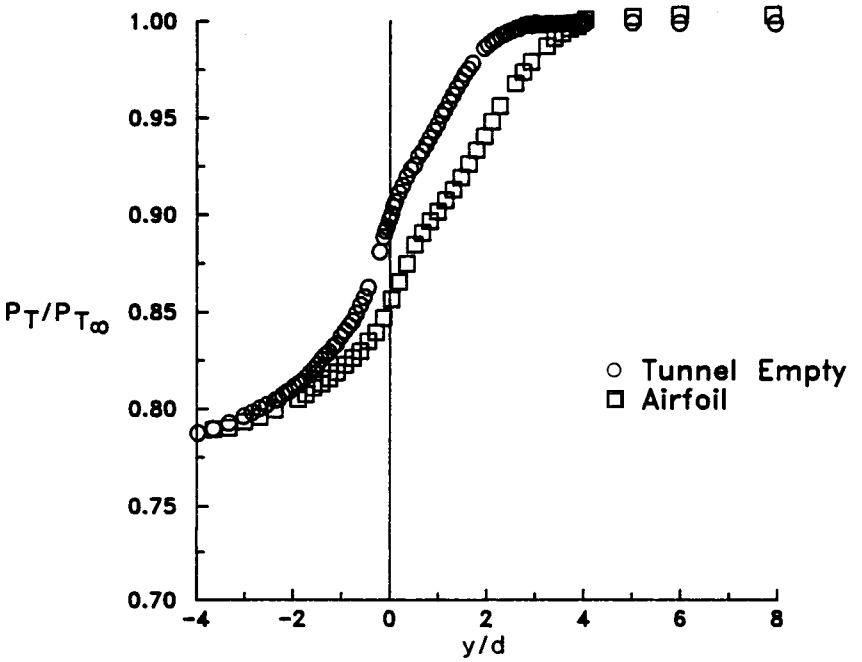

(c) Total-pressure ratio.

Figure 14.- Concluded.

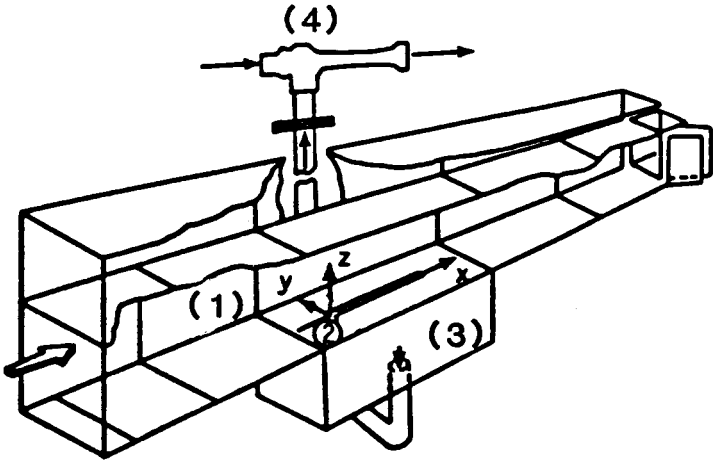

1. Wind tunnel test section
2. Slotted model wall
3. Auxillary suction/plenum chamber
4. Ejector (suction) system

(a) Schematic of model mounting on the tunnel floor.

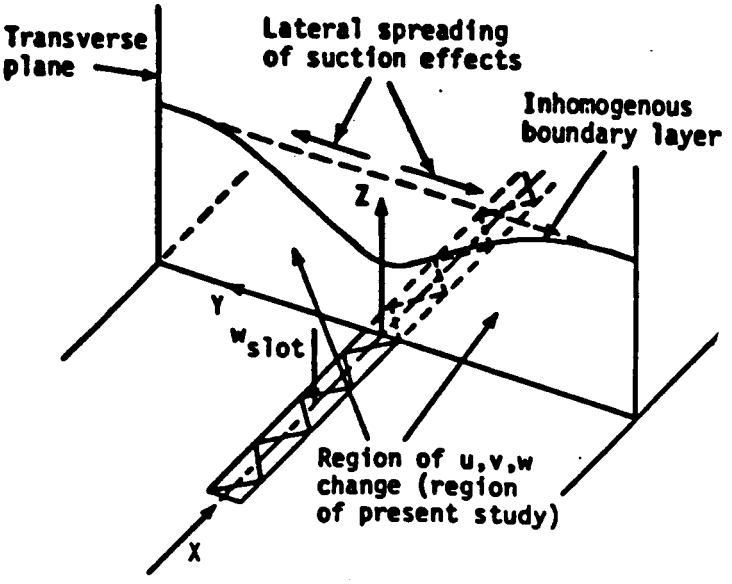

(b) Schematic of wall flow and measurement plane.

Figure 15.- Wu's experimental setup.

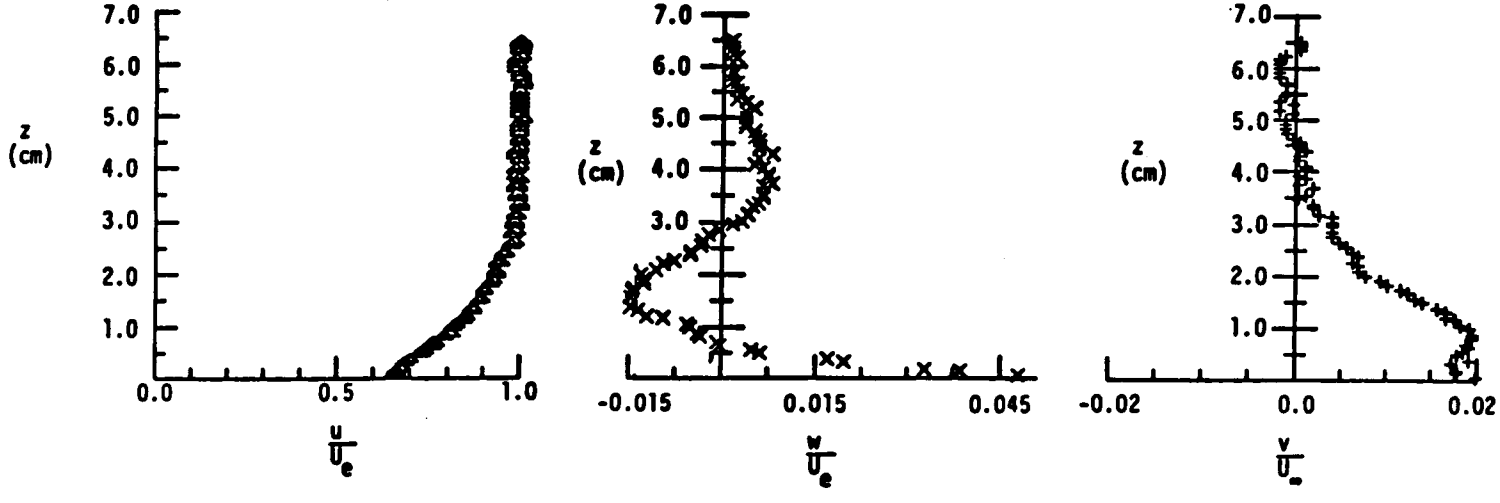

Figure 16.- Velocity component distribution on the single slotted wall model. M = 0.81, Re/m. = 2.67 x 10^7, Q = 1.65 m^3/min., Y = -1.27cm.

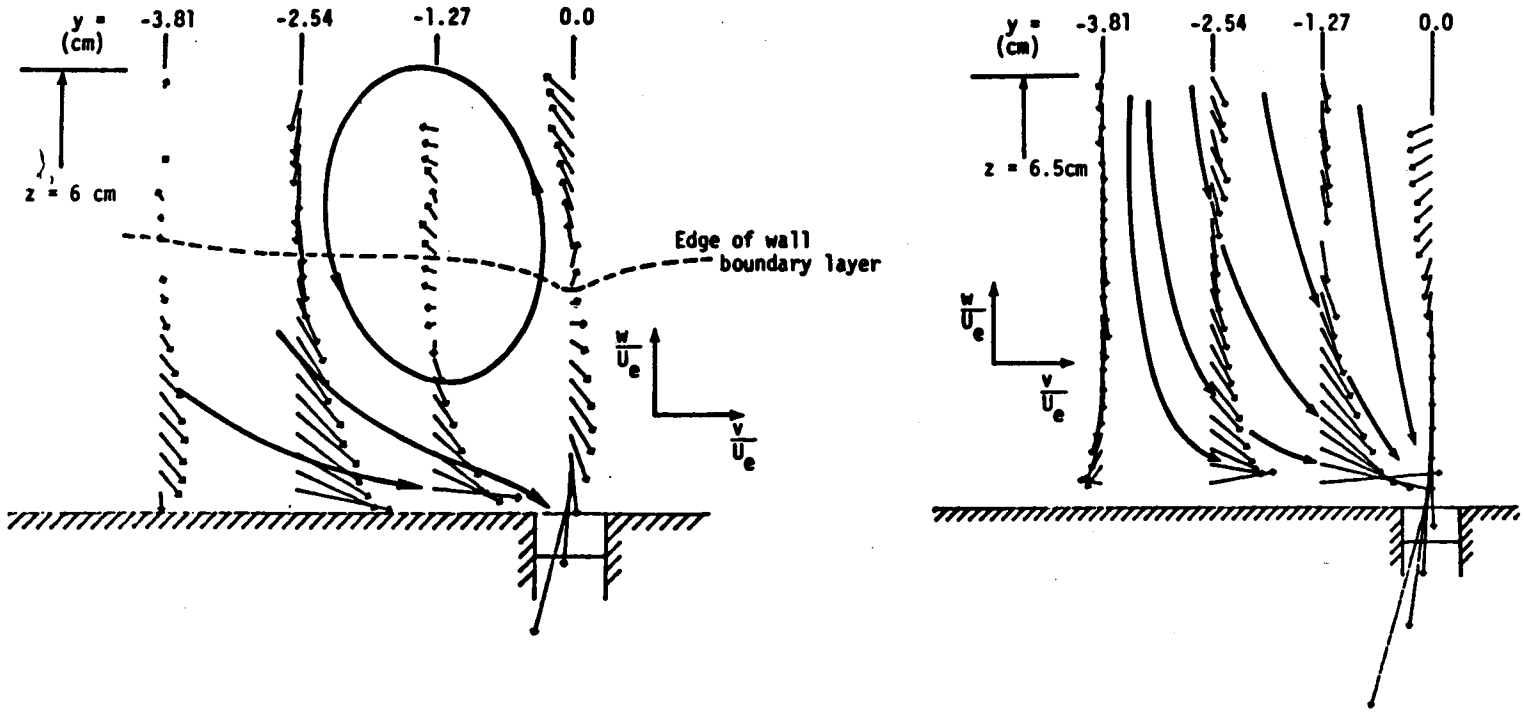

(a) Re/m = 2.2 x 10^6, Q = 0.0.

(b) Re/m = 1.78 x 10^6, Q ≈ 7.1m^3/min.

Figure 17.- Velocity vectors projected on the crosflow plane and schematic of the streamline patterns for M_∞ = 0.6.

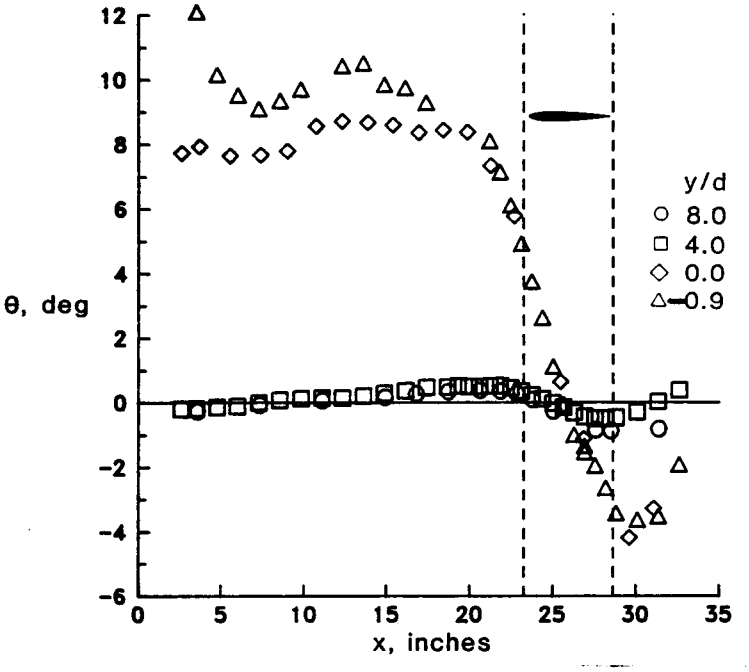

(a) Flow angle.

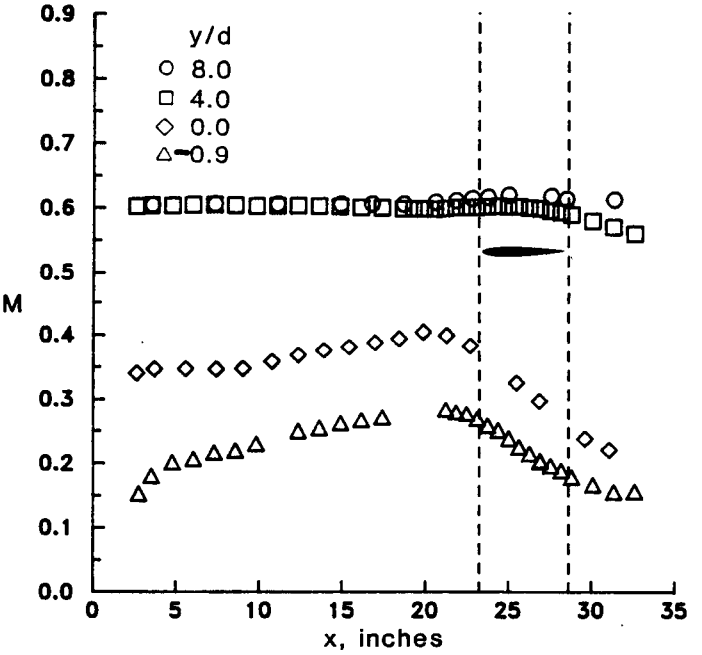

(b) Mach number.

Figure 18.- Longitudinal probe measurements in the DFA at various distances from the slot.

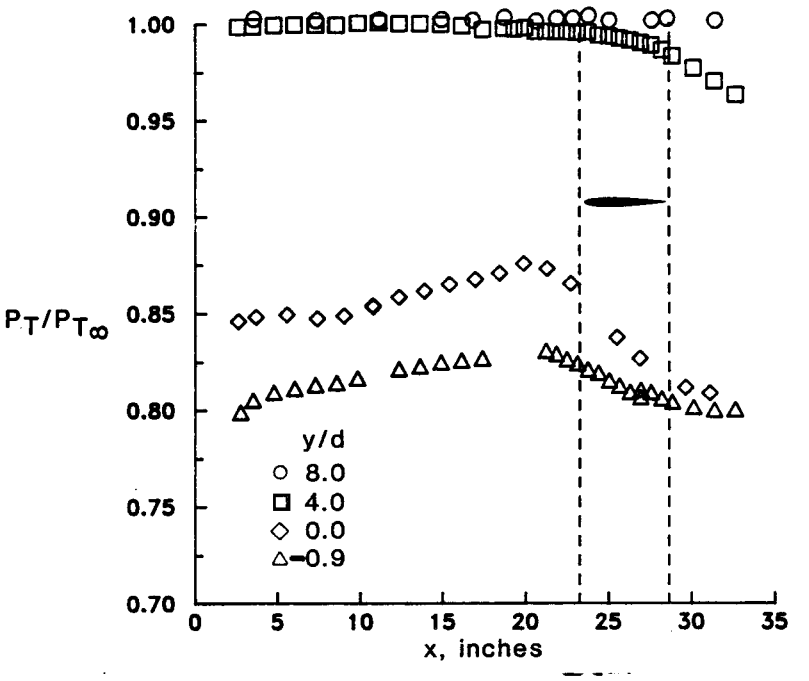

(c) Total-pressure ratio.

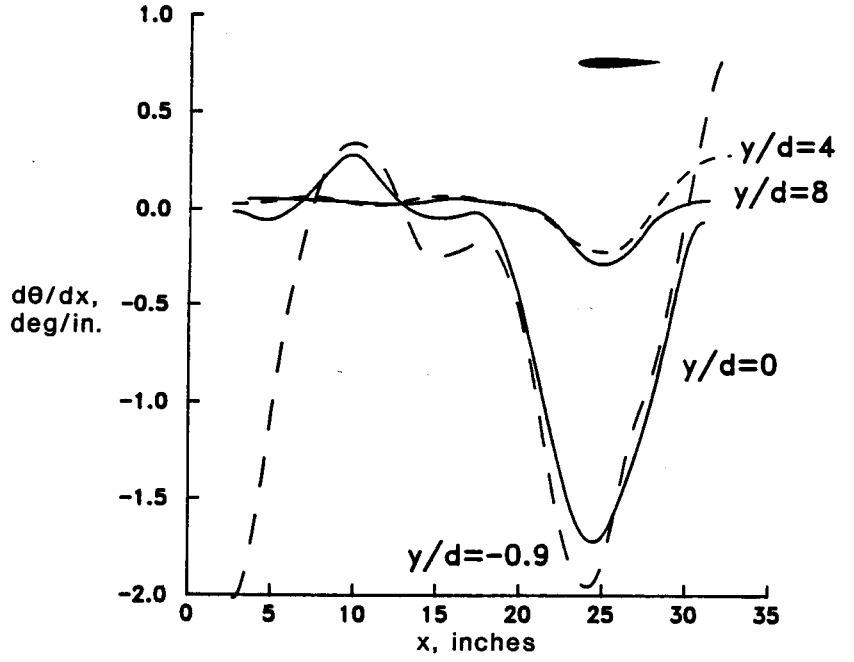

(d) Computed flow-angle gradient.

Figure 18.- Concluded.

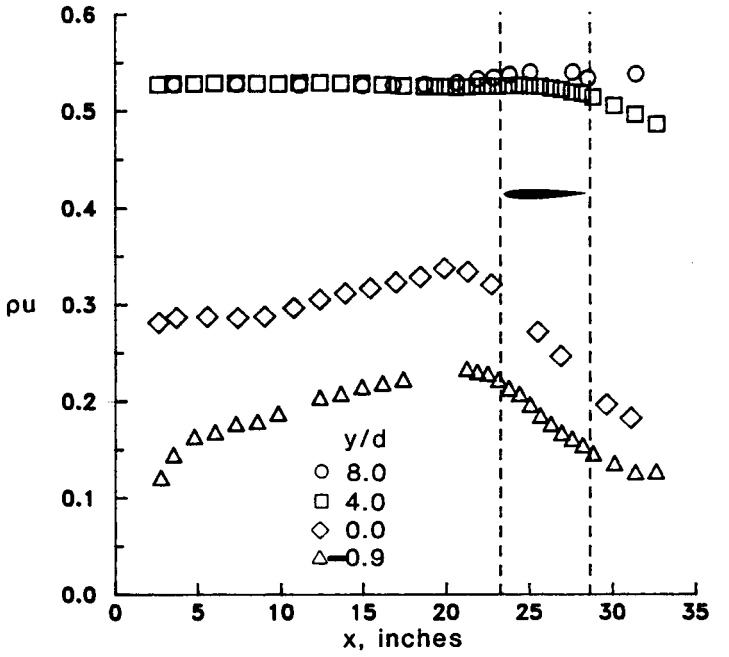

(a) Longitudinal mass flux.

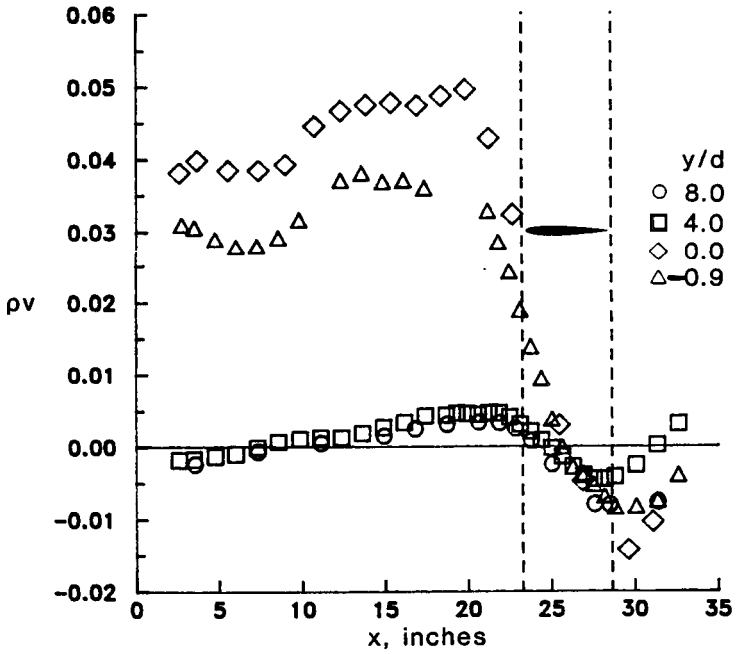

(b) Transverse mass flux.

Figure 19.- Mass flux computed from DFA probe measurements.

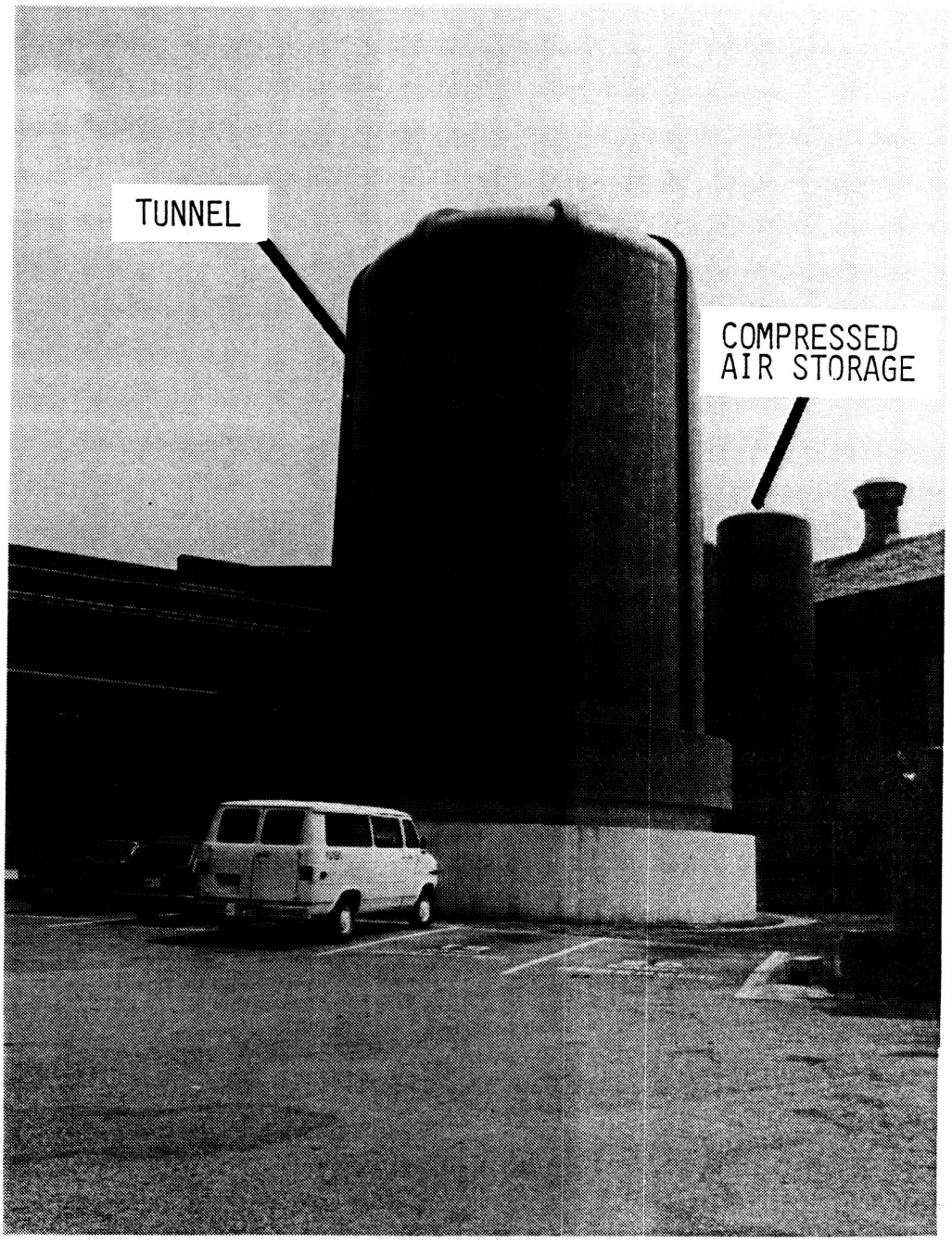

(a) Present-day exterior view of the tunnel.

Figure 20.- Langley Research Center 6- by 19-inch Transonic Tunnel.

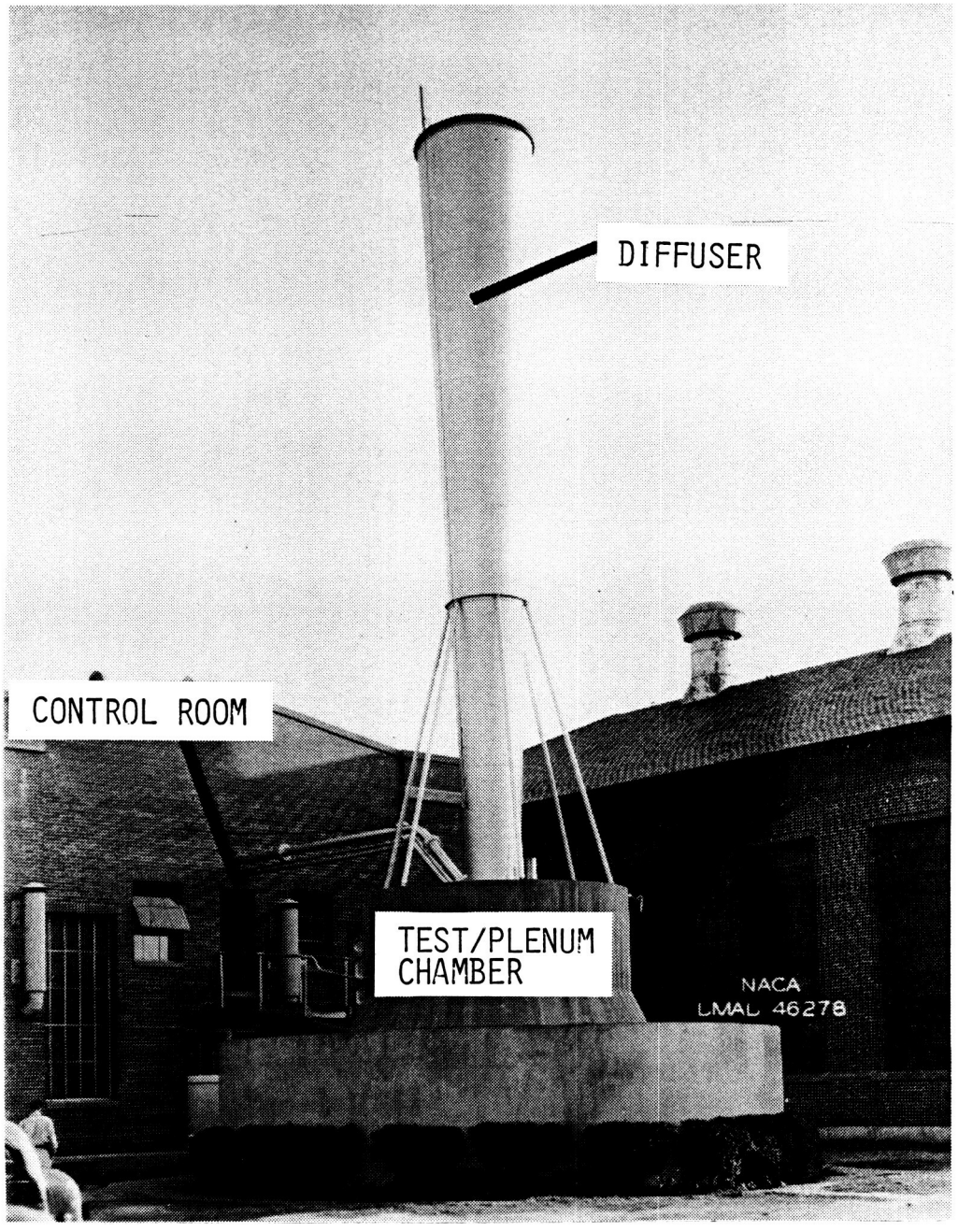

(b) Early view of the tunnel showing the location of plenum, test region, diffuser.

Figure 20.- Continued.

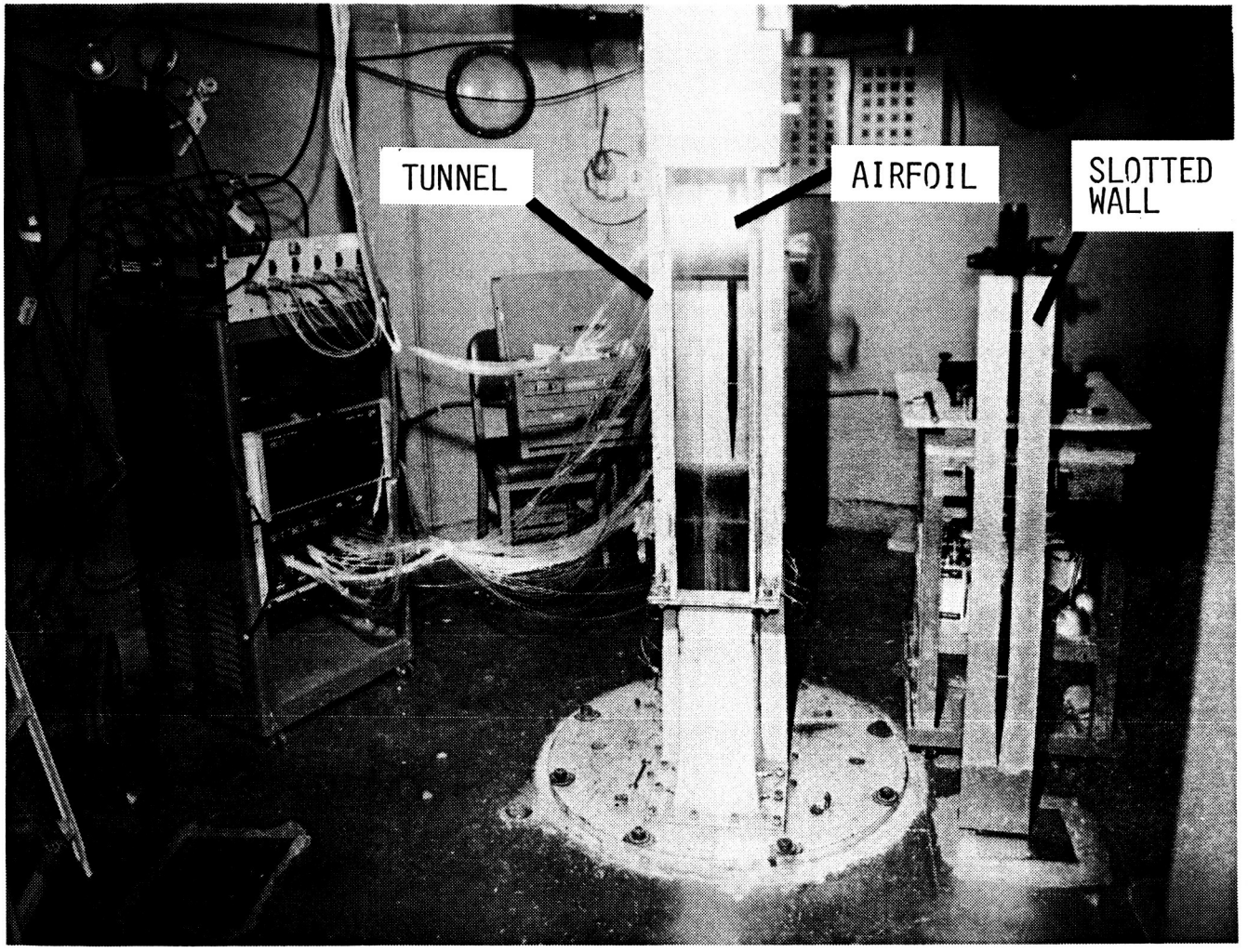

(c) View of the test section and plenum chamber.

Figure 20.- Concluded.

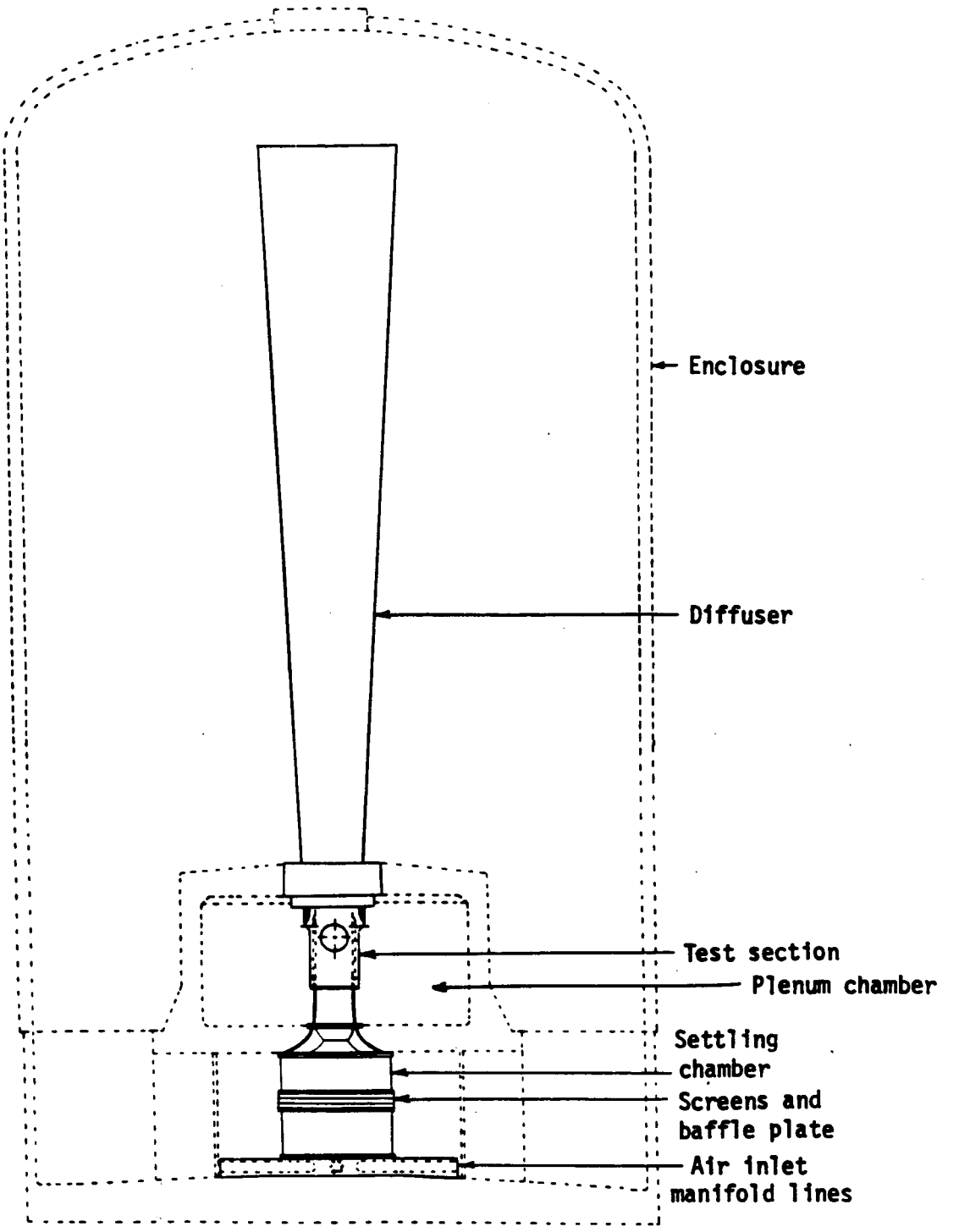

(a) Overall view.

Figure 21.- Schematic of the 6- by 19-inch Transonic Tunnel.

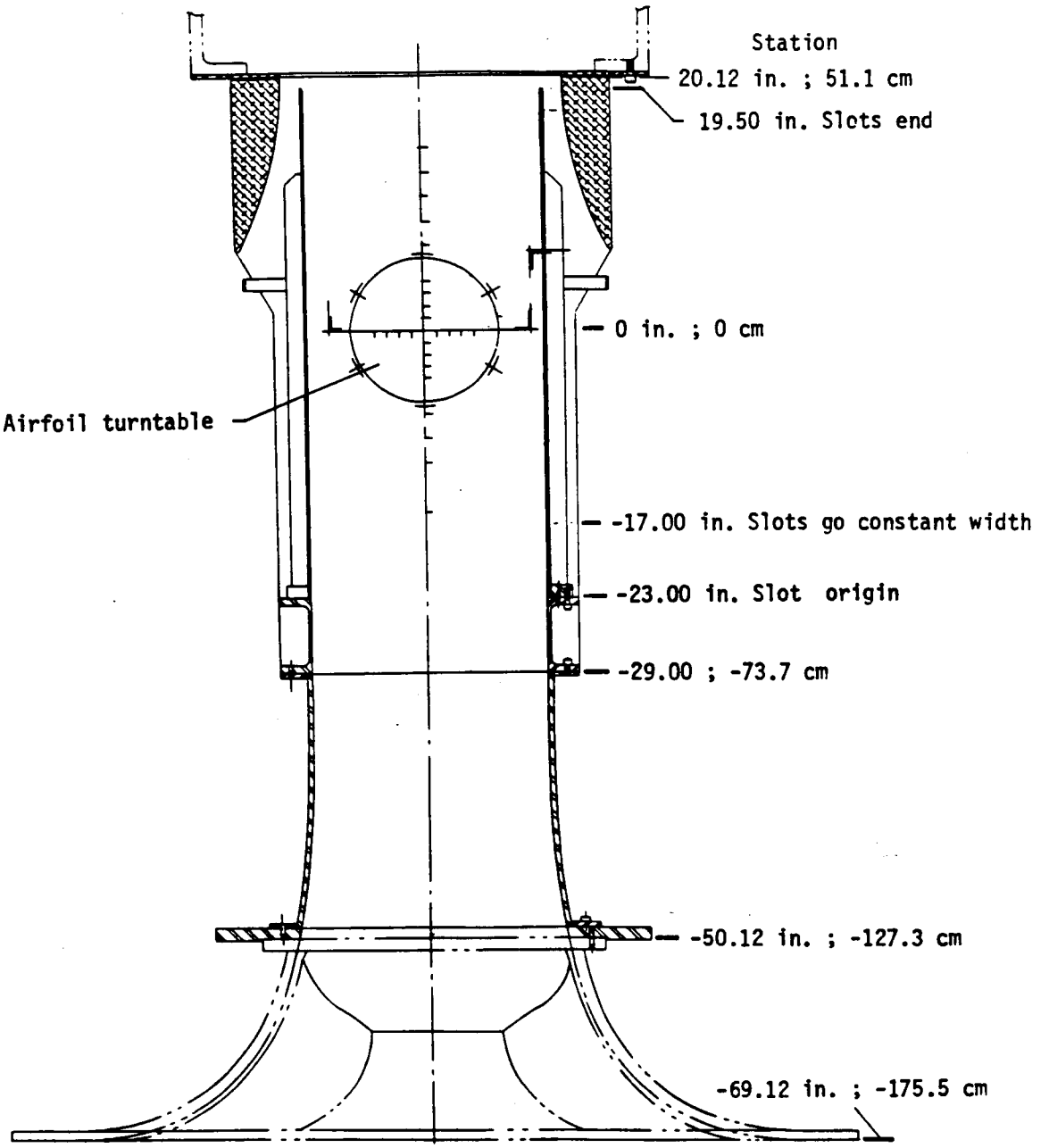

(b) Test-section details.

Figure 21.- Concluded.

Figure 22.- View of the 6- by 19-inch Tunnel control panel.

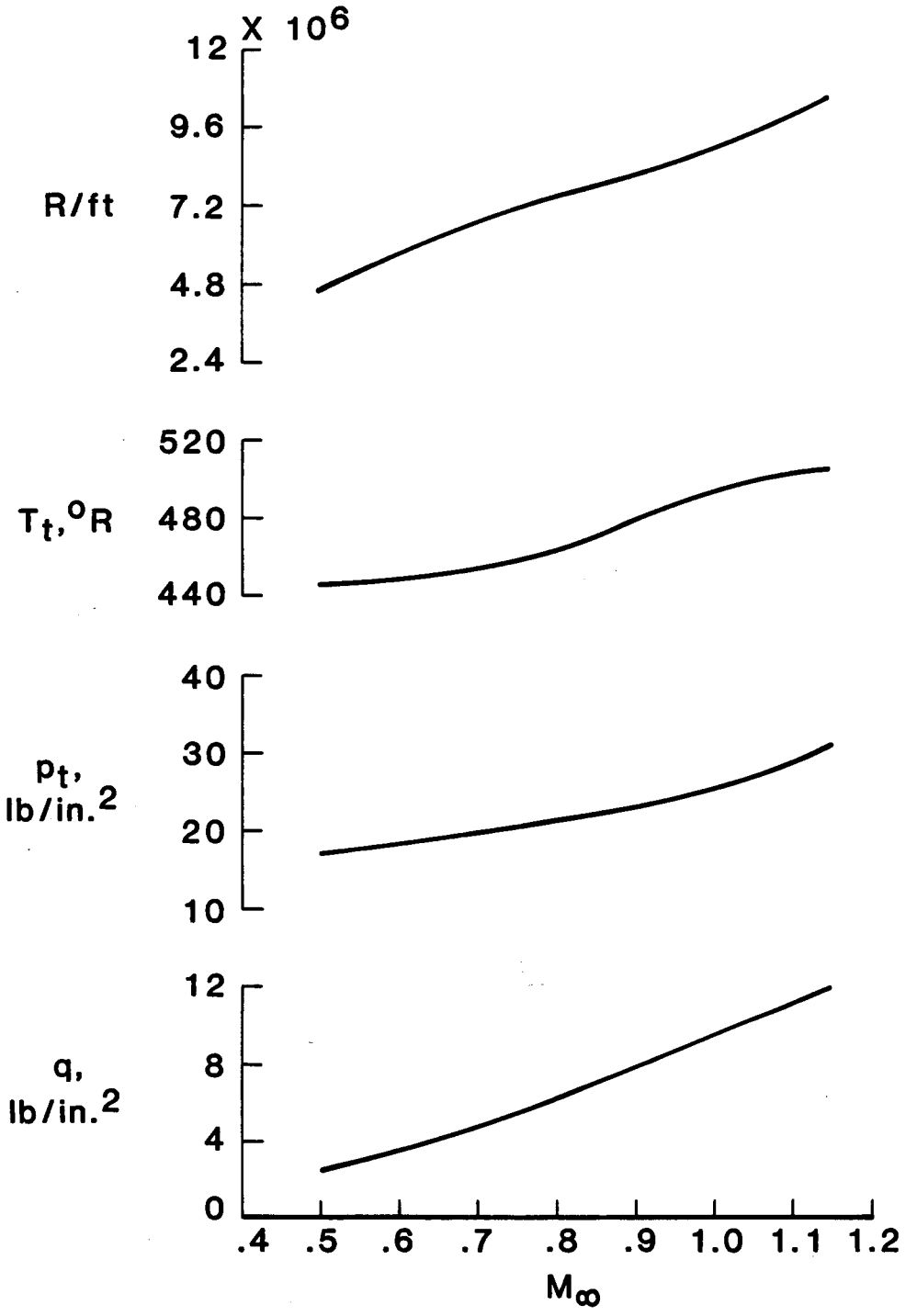

Figure 23.- Typical operational characteristics of the 6- by 19-inch Transonic Tunnel.

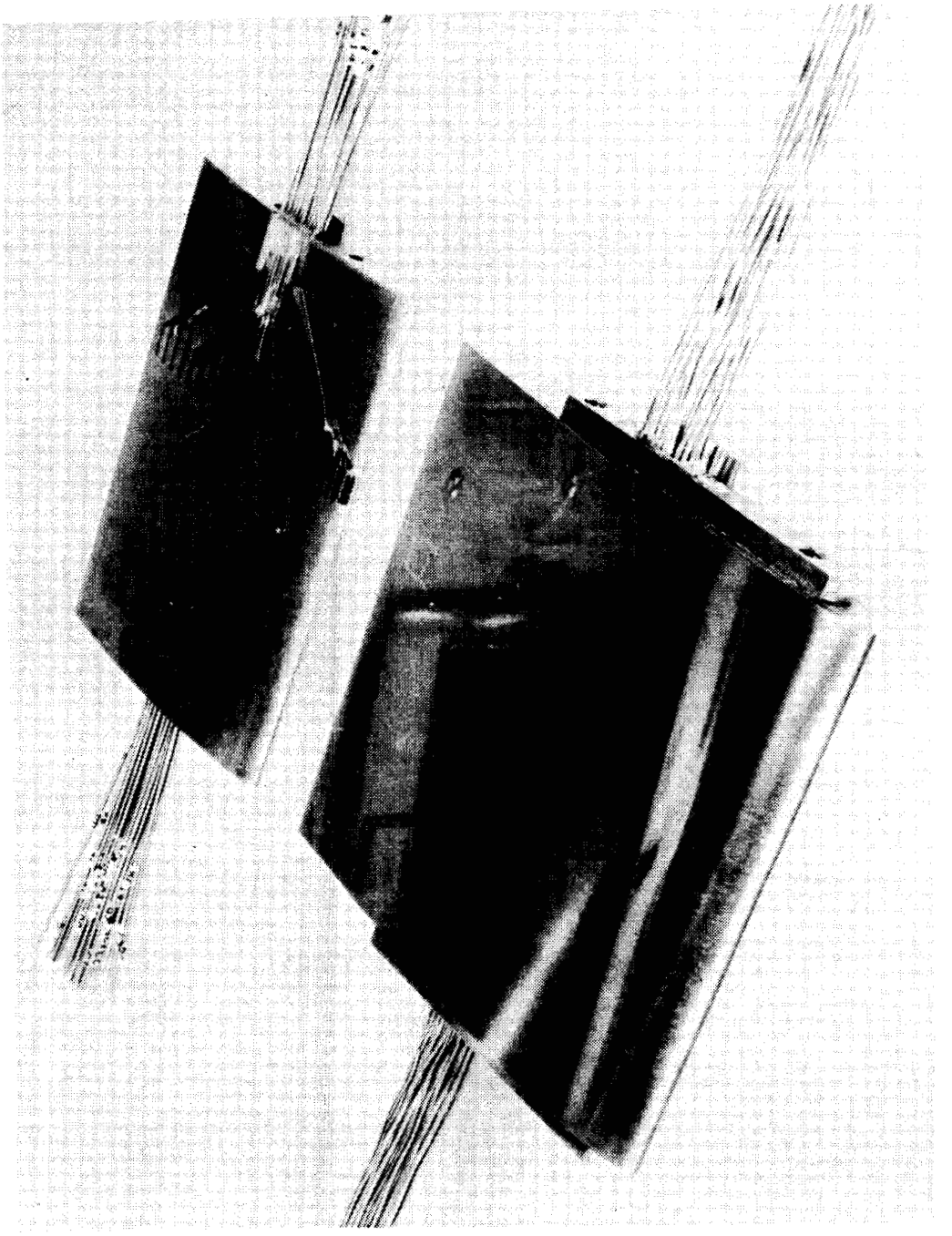

Figure 24.- Typical pressure-instrumented airfoil models.
6-inch chord in foreground, 4-inch chord in background.

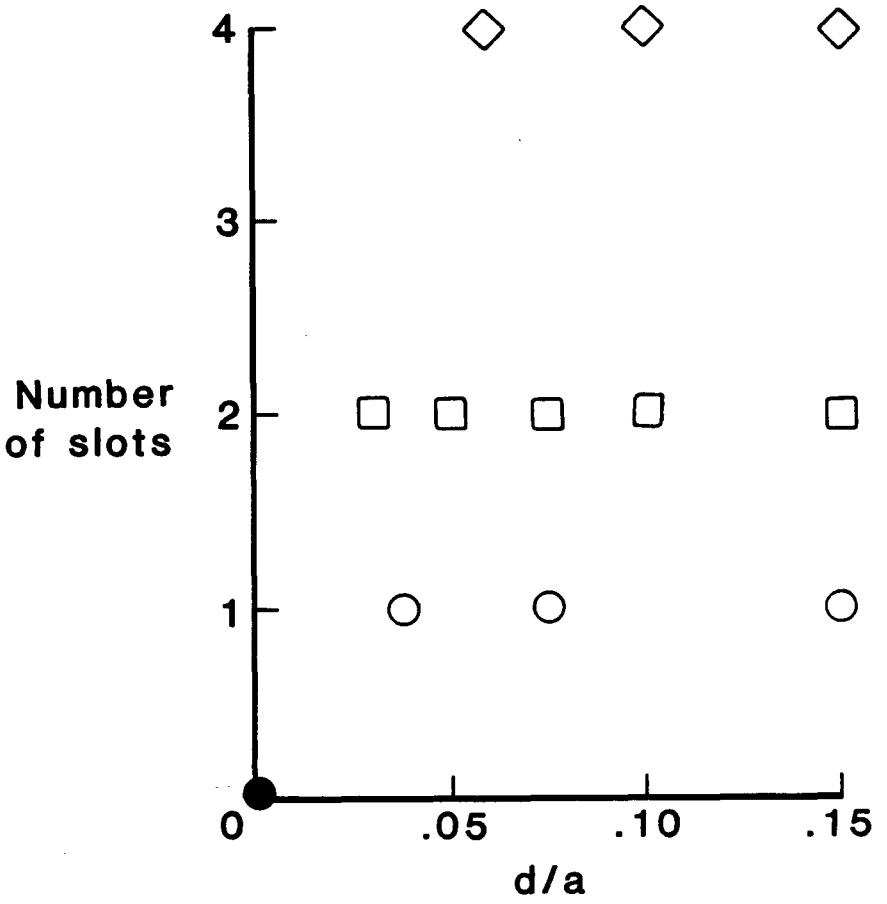

Figure 25.- Wall-geometry test matrix.

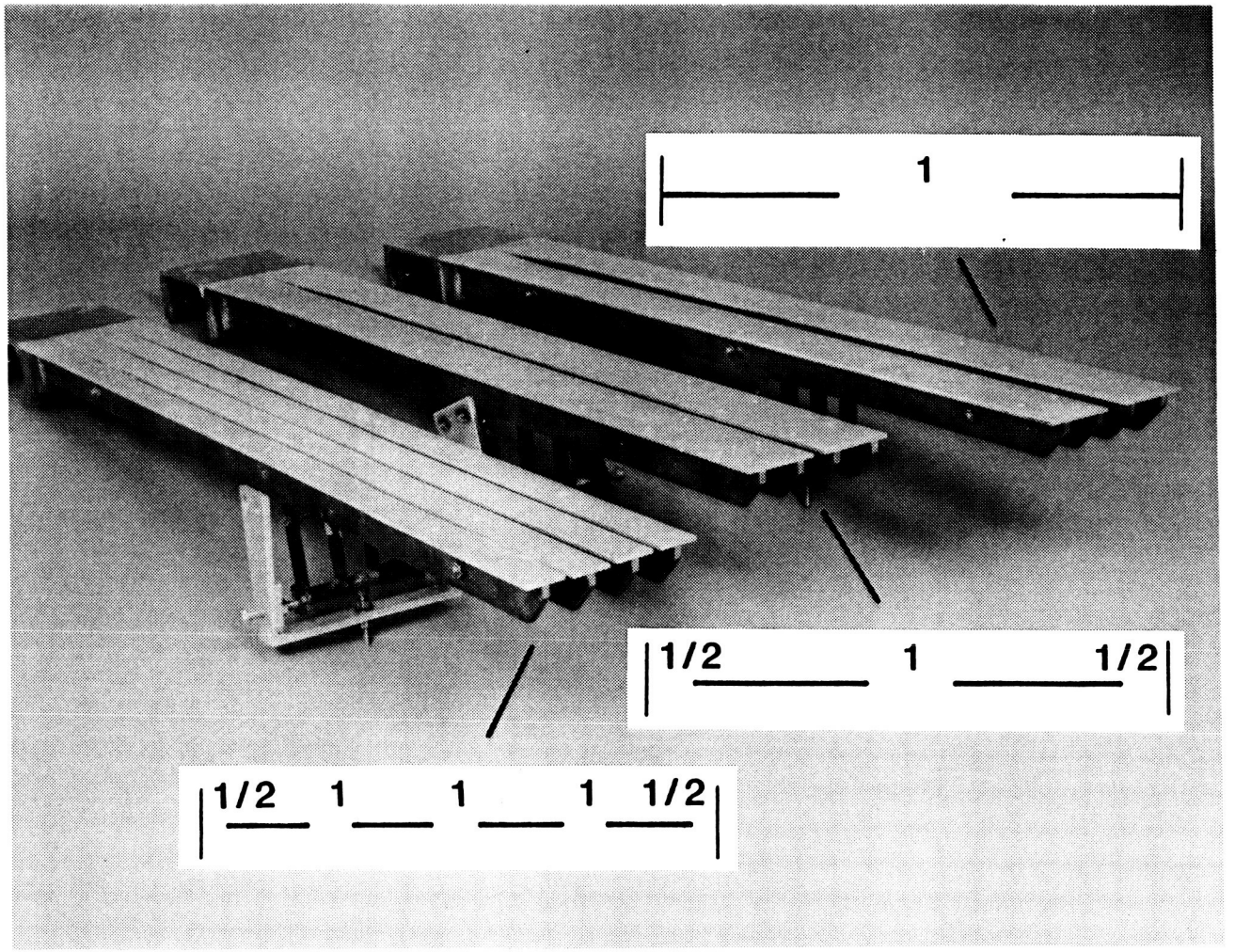

Figure 26.- Photograph of the 15-percent-open wall configurations.

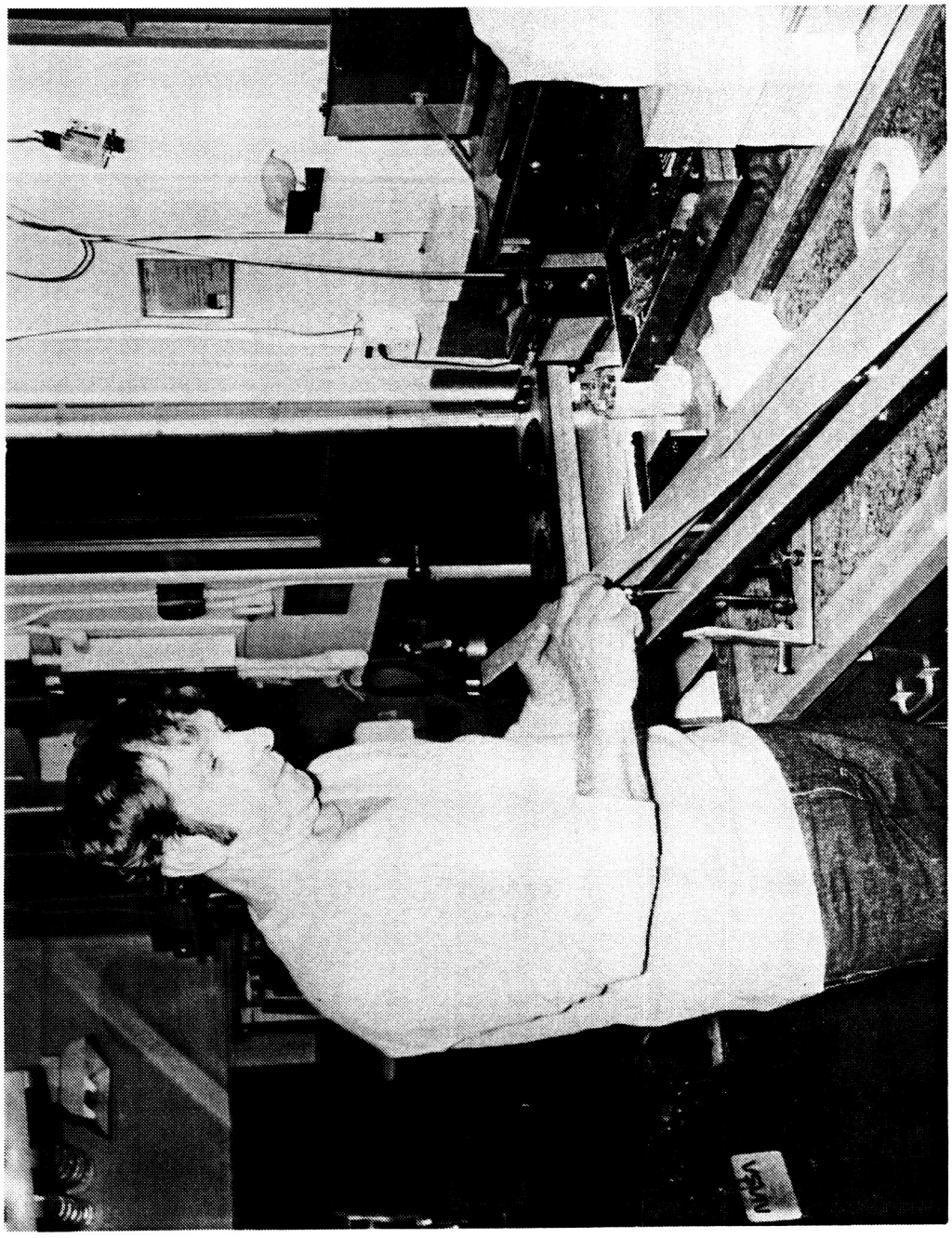

Figure 27.- Typical slotted-wall assembly.

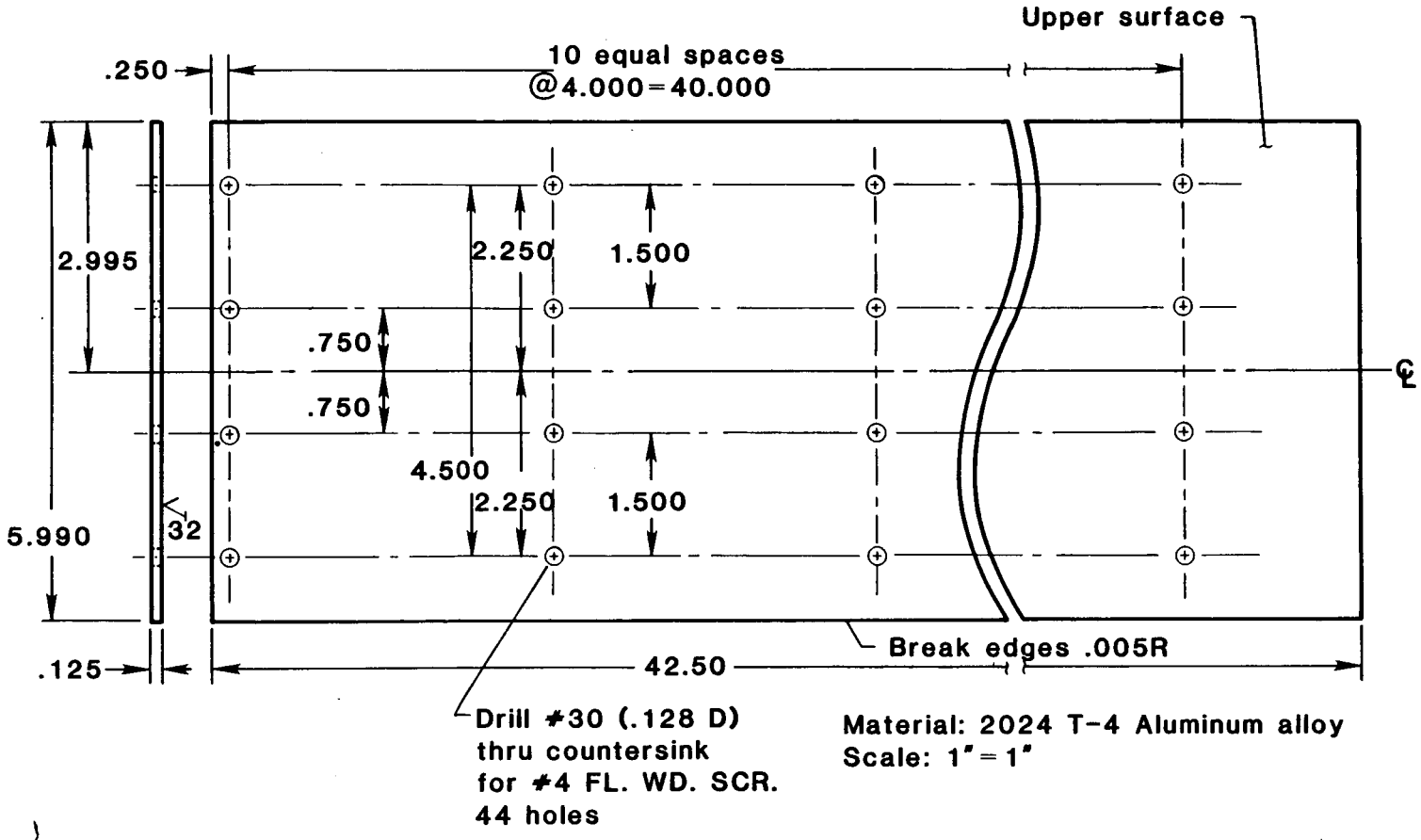

(a) Solid wall.

Figure 28.- Shop drawings showing details of slat construction.

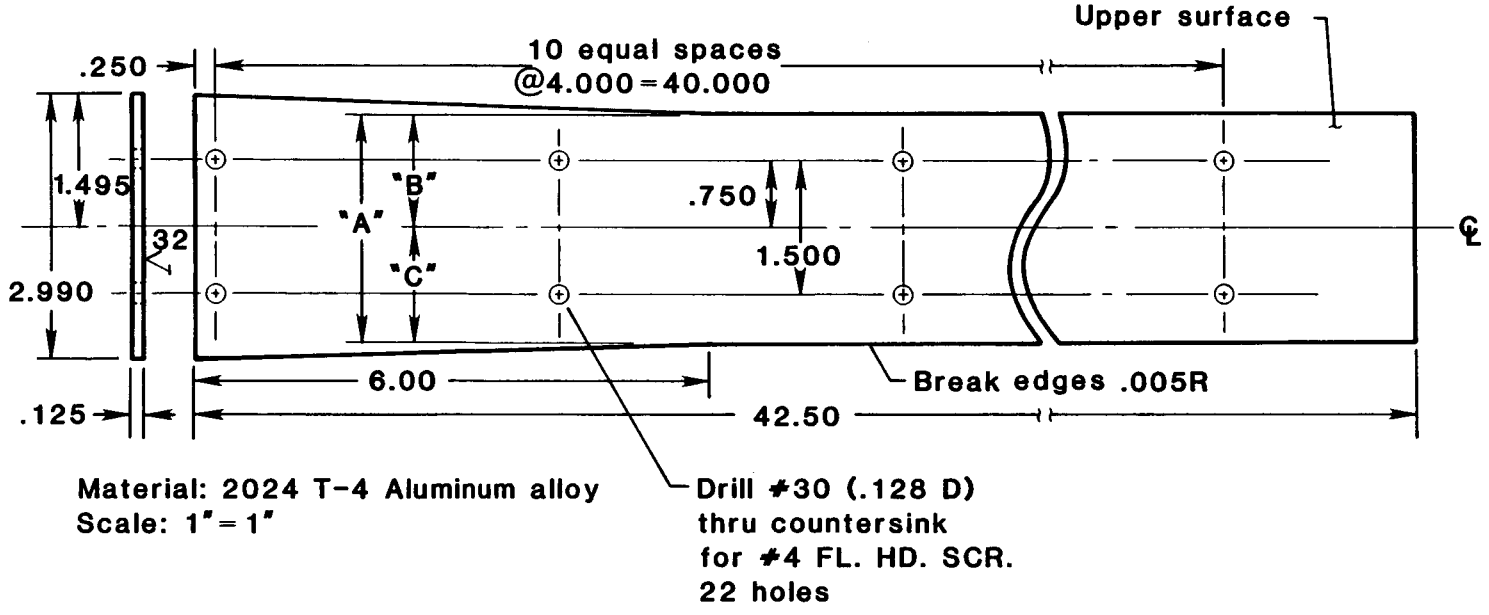

Configuration	A (Inches)	B (Inches)	C (Inches)	Number Required
2	2.990	1.495	1.495	10
3A	2.800	1.495	1.205	3
3B	2.700	1.205	1.495	2
4A	2.550	1.495	1.055	3
4B	2.550	1.055	1.495	2
5	2.700	1.350	1.350	5

(b) One- and two-slot walls.

Figure 28.- Continued.

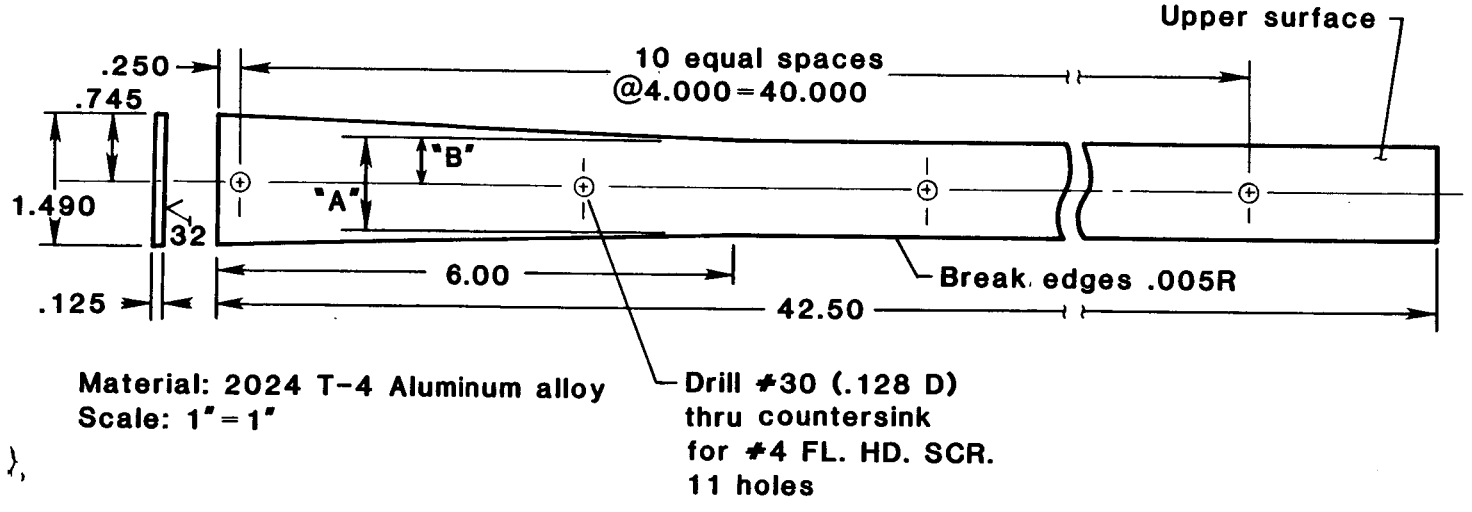

Configuration	A (Inches)	B (Inches)	Number Required
6	1.490	.745	10
7	1.410	.705	9
8	1.350	.675	9

(c) Four-slot walls.

Figure 28.- Concluded.

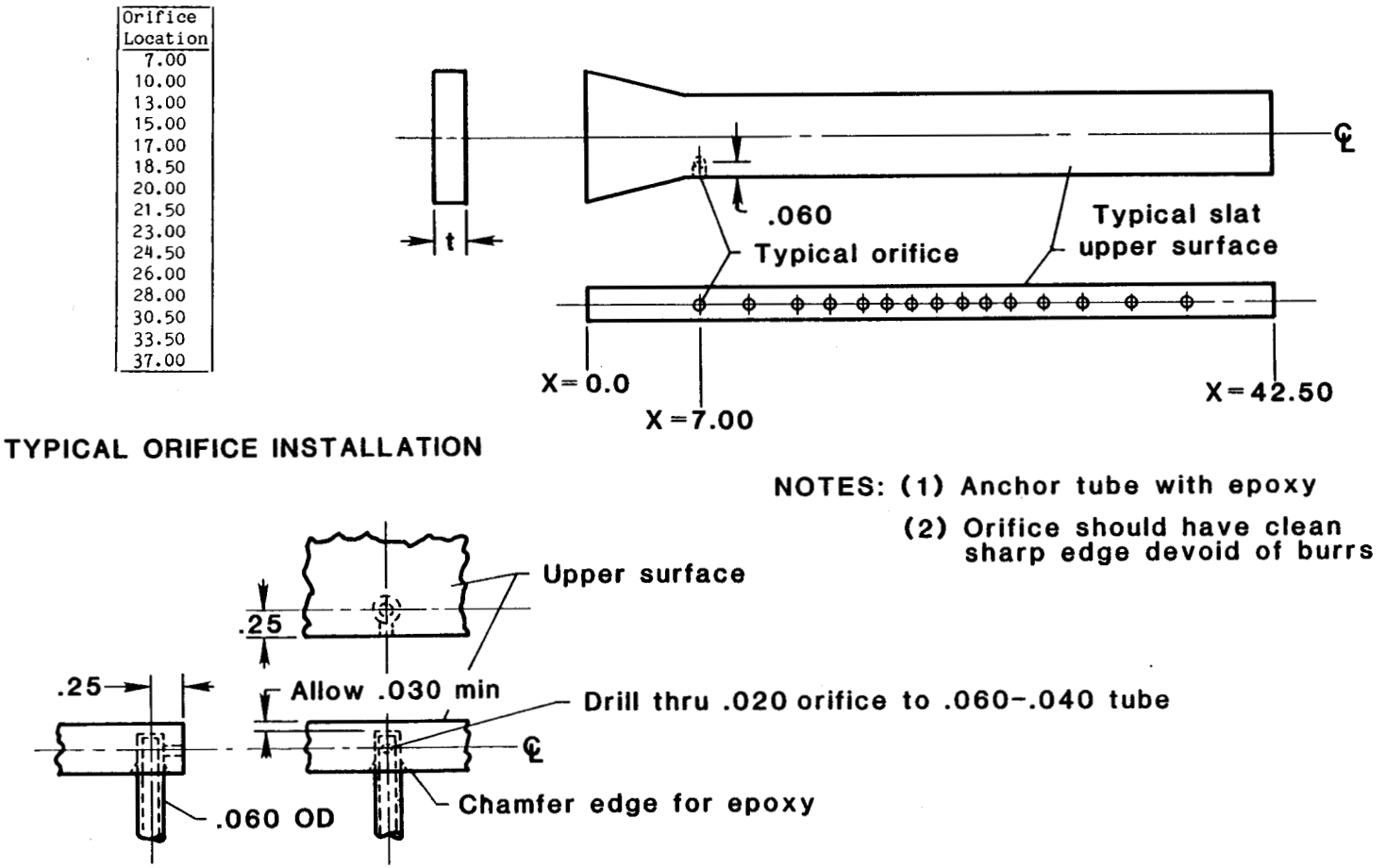

(a) Slat-sidewall orifice installation.

Figure 29.- Typical slat orifice installation.

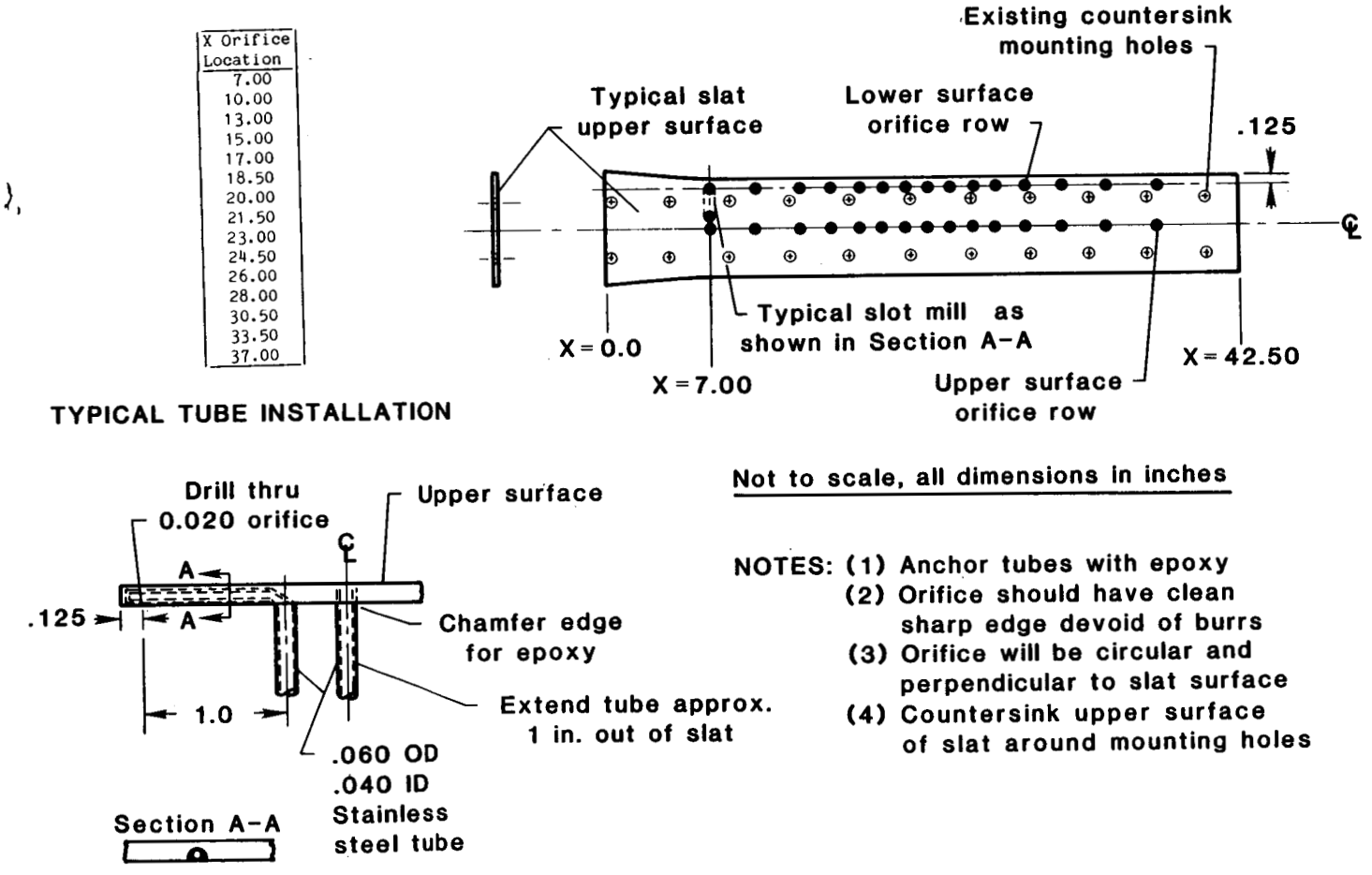

(b) Slat top- and bottom-wall orifice installation.

Figure 29.- Concluded.

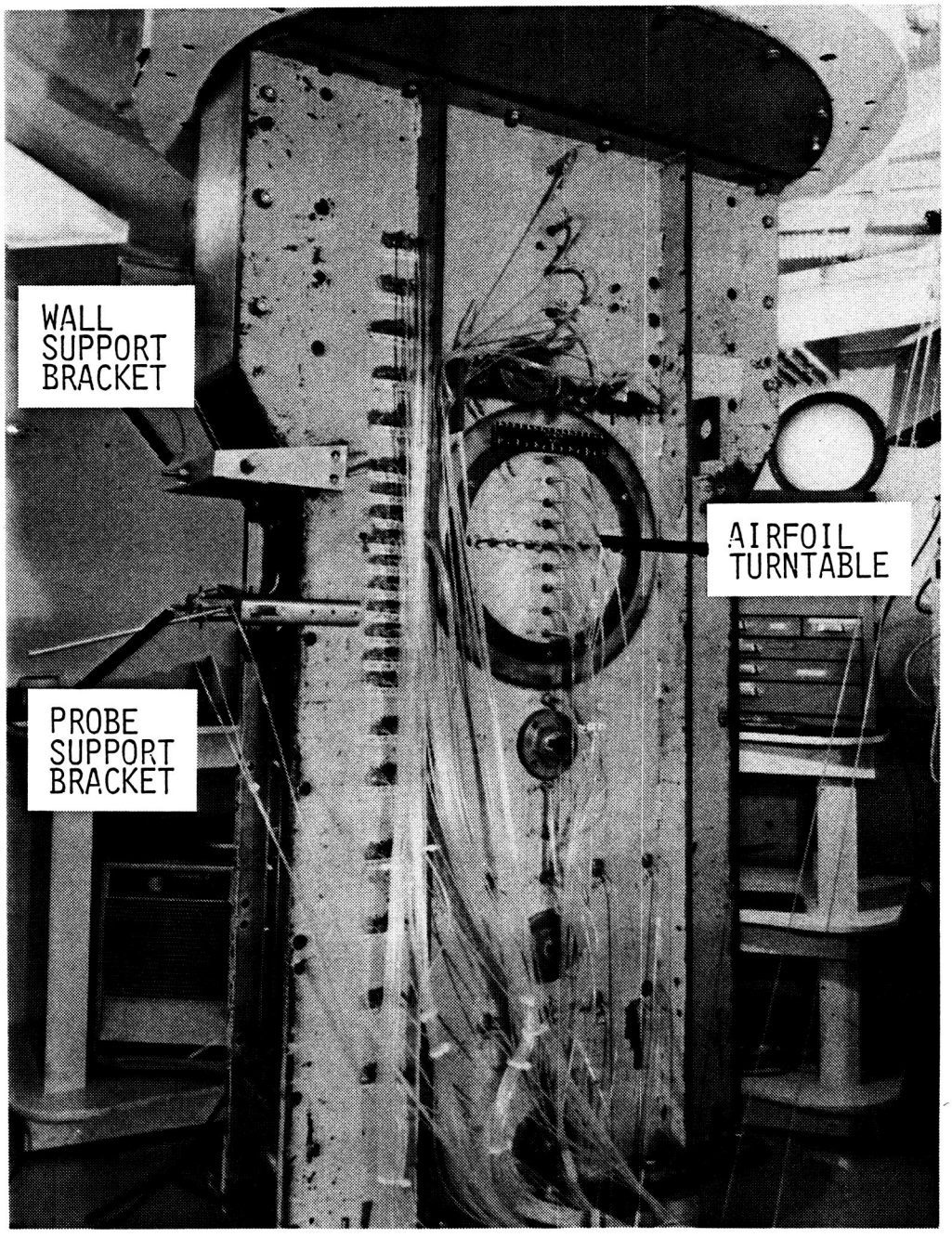

Figure 30.- Photograph of the tunnel sidewall showing the orifice layout and location of the airfoil turntable.

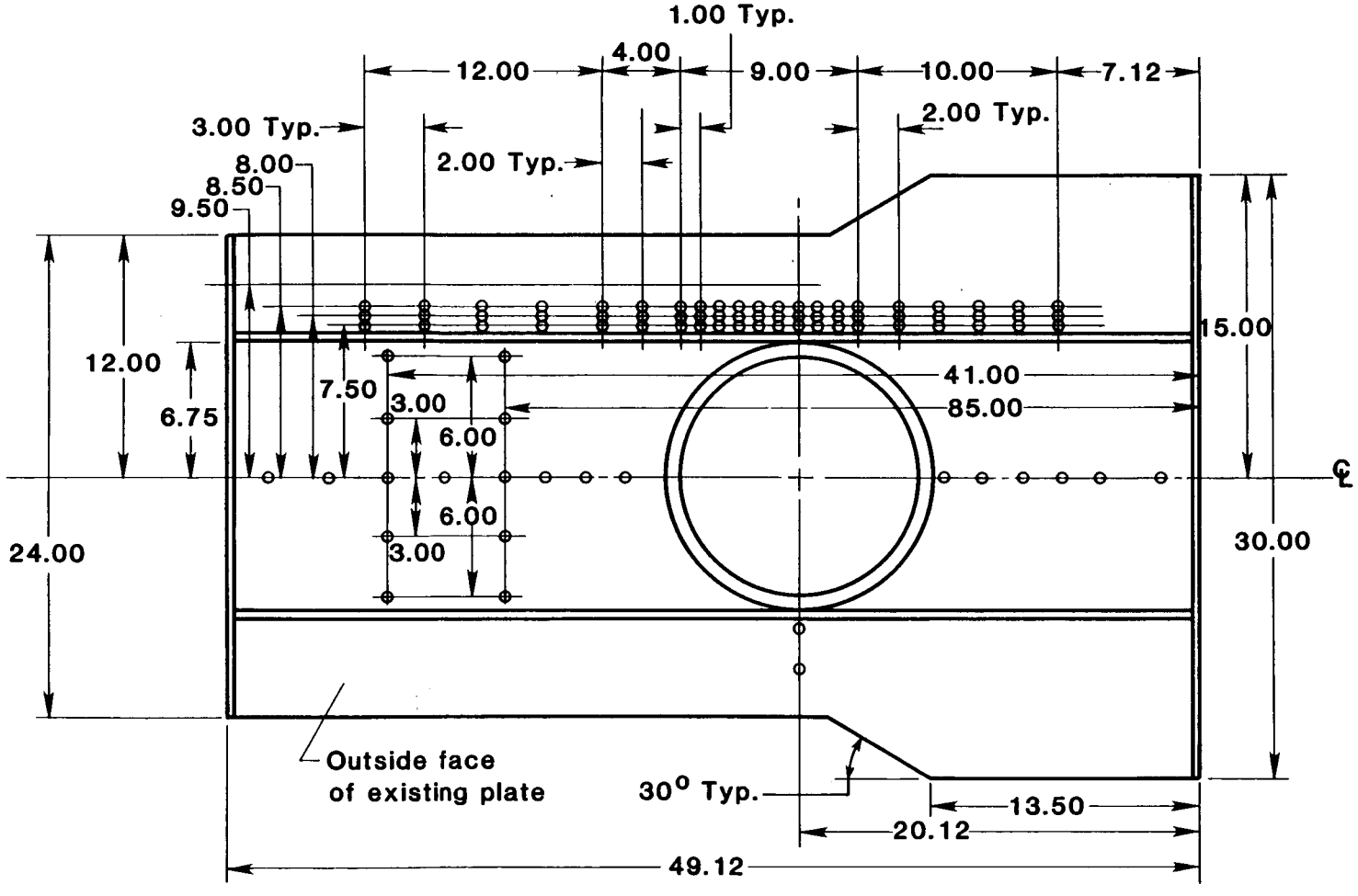

Figure 31.- Shop drawing detailing sidewall orifice installation.

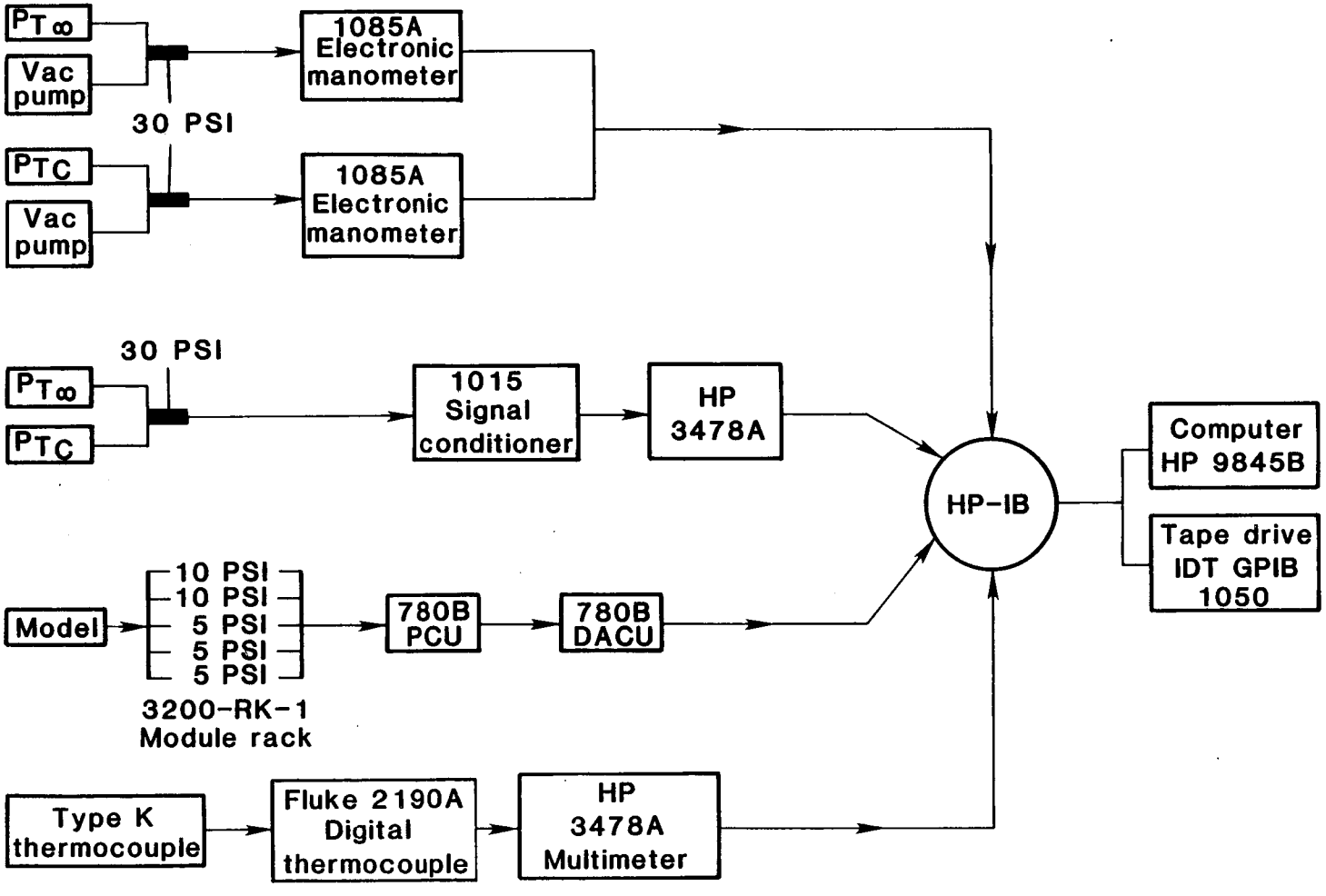

Figure 32.- Schematic of the data system and instrumentation.

Figure 33.- The data acquisition computer and magnetic tape drive.

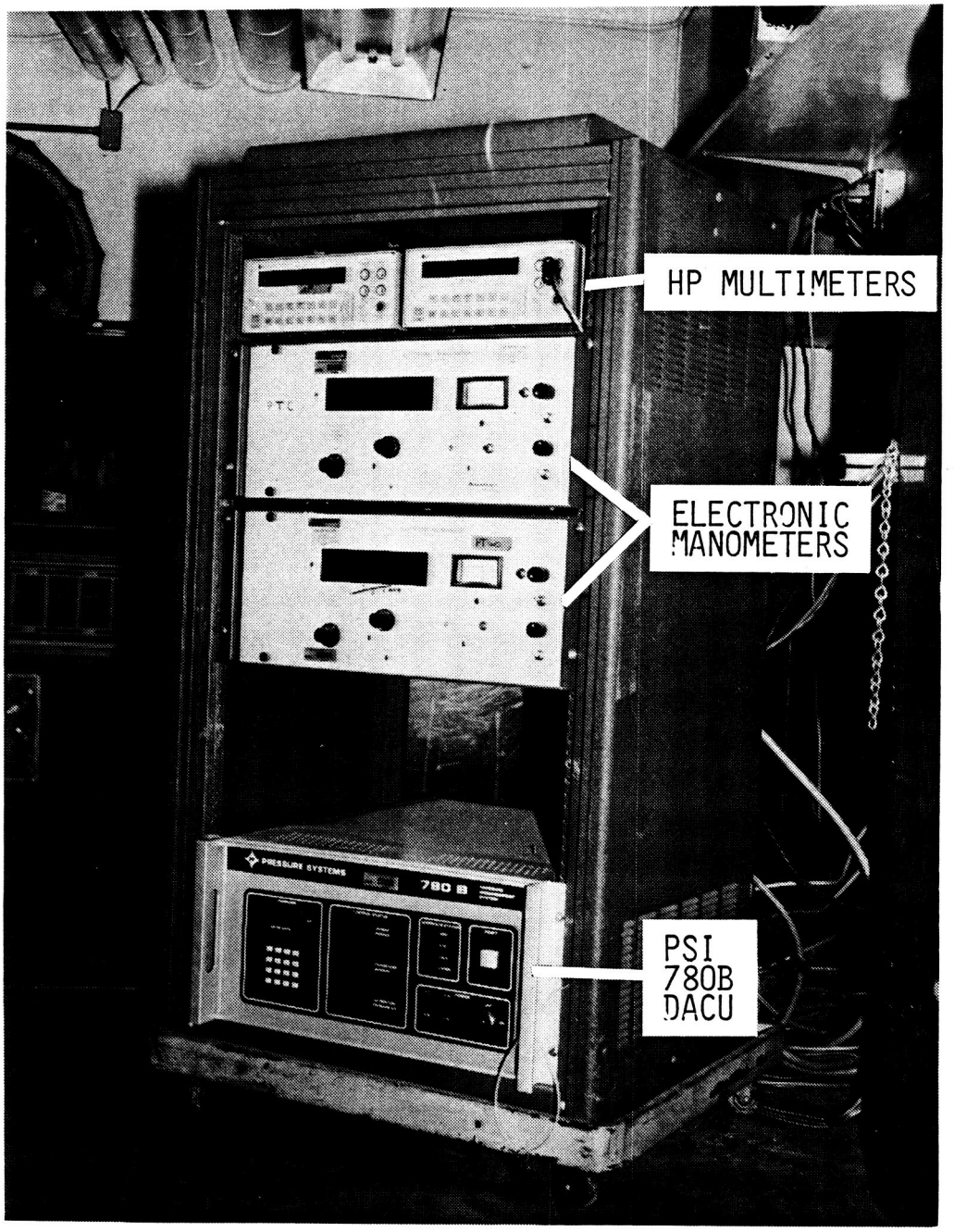

Figure 34.- The electronic manometers, multimeters, and the electronically scanned pressure system.

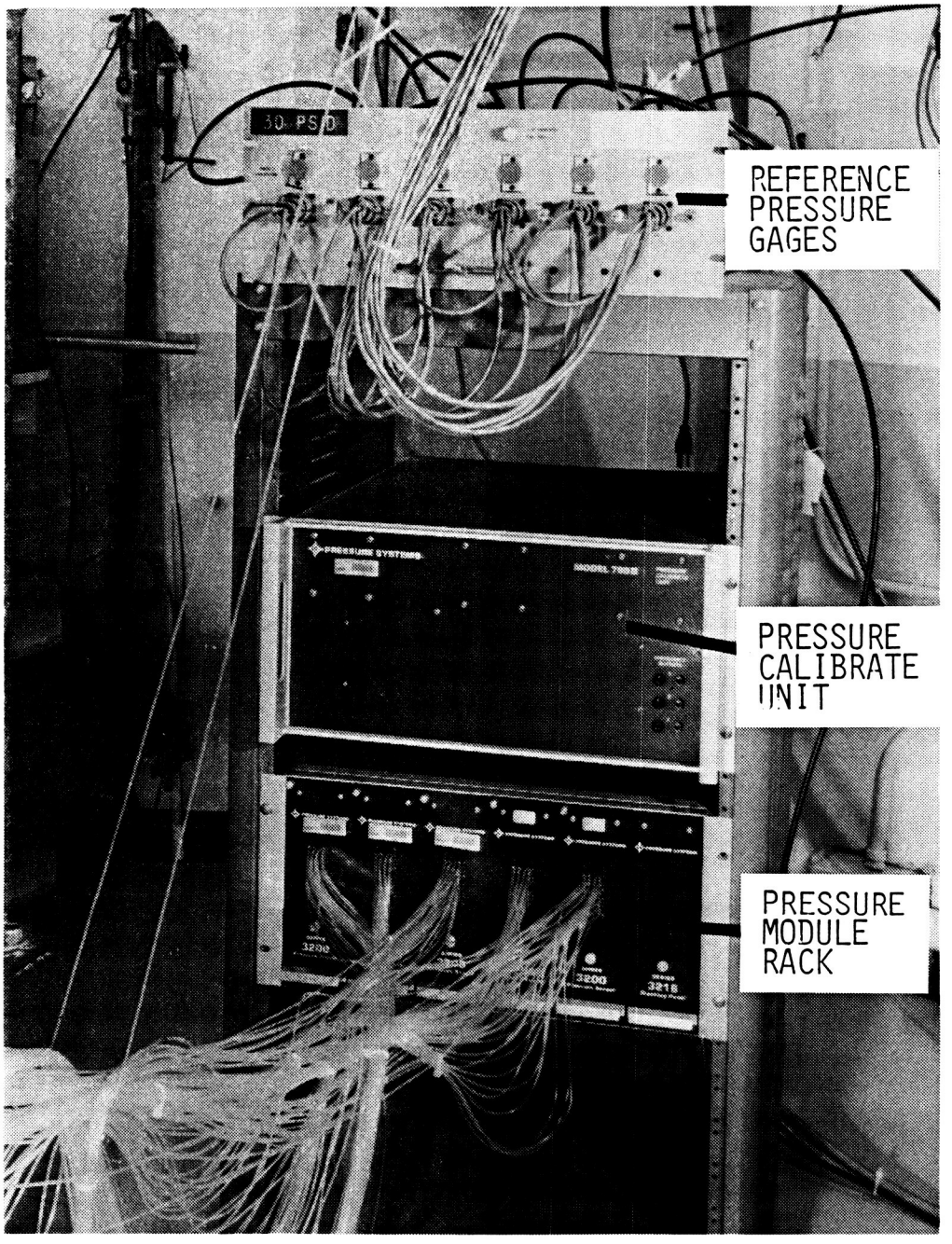

Figure 35.- The pressure calibrator unit and pressure modules.

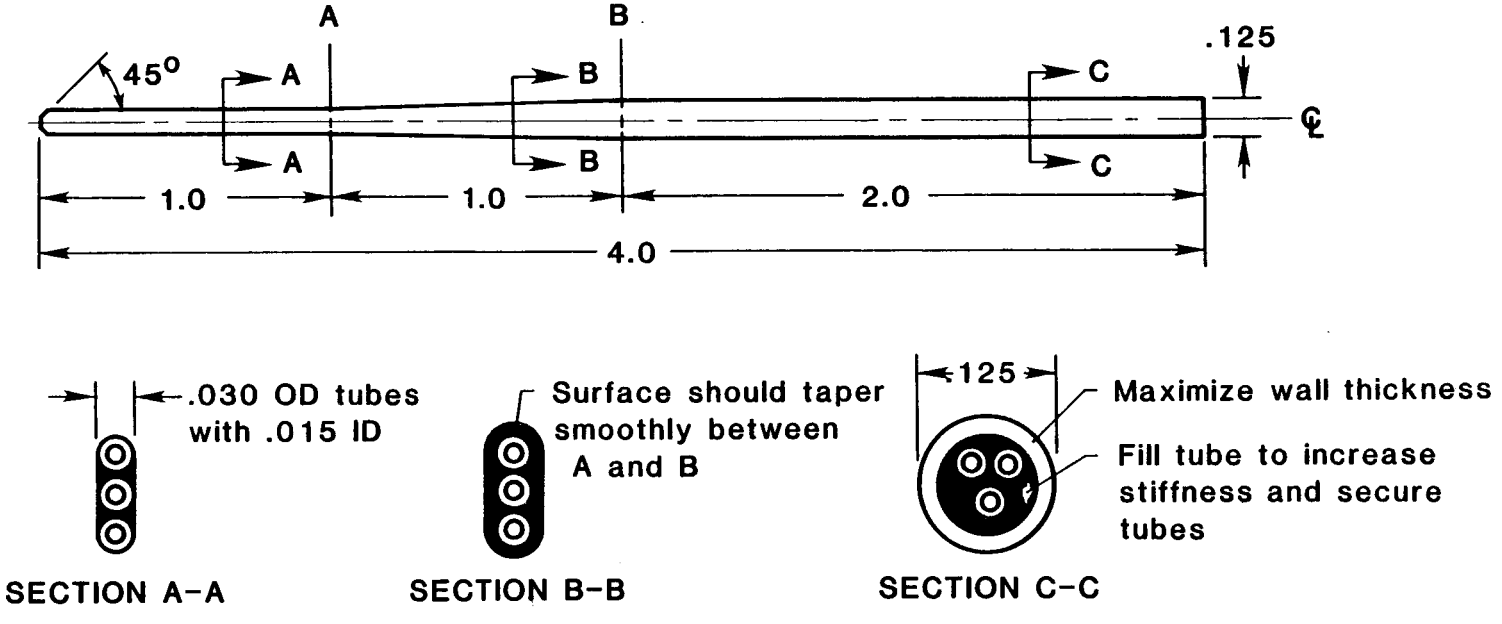

C-3

Figure 36.- Schematic of the 6- by 19-Inch Tunnel flow-angle probe.

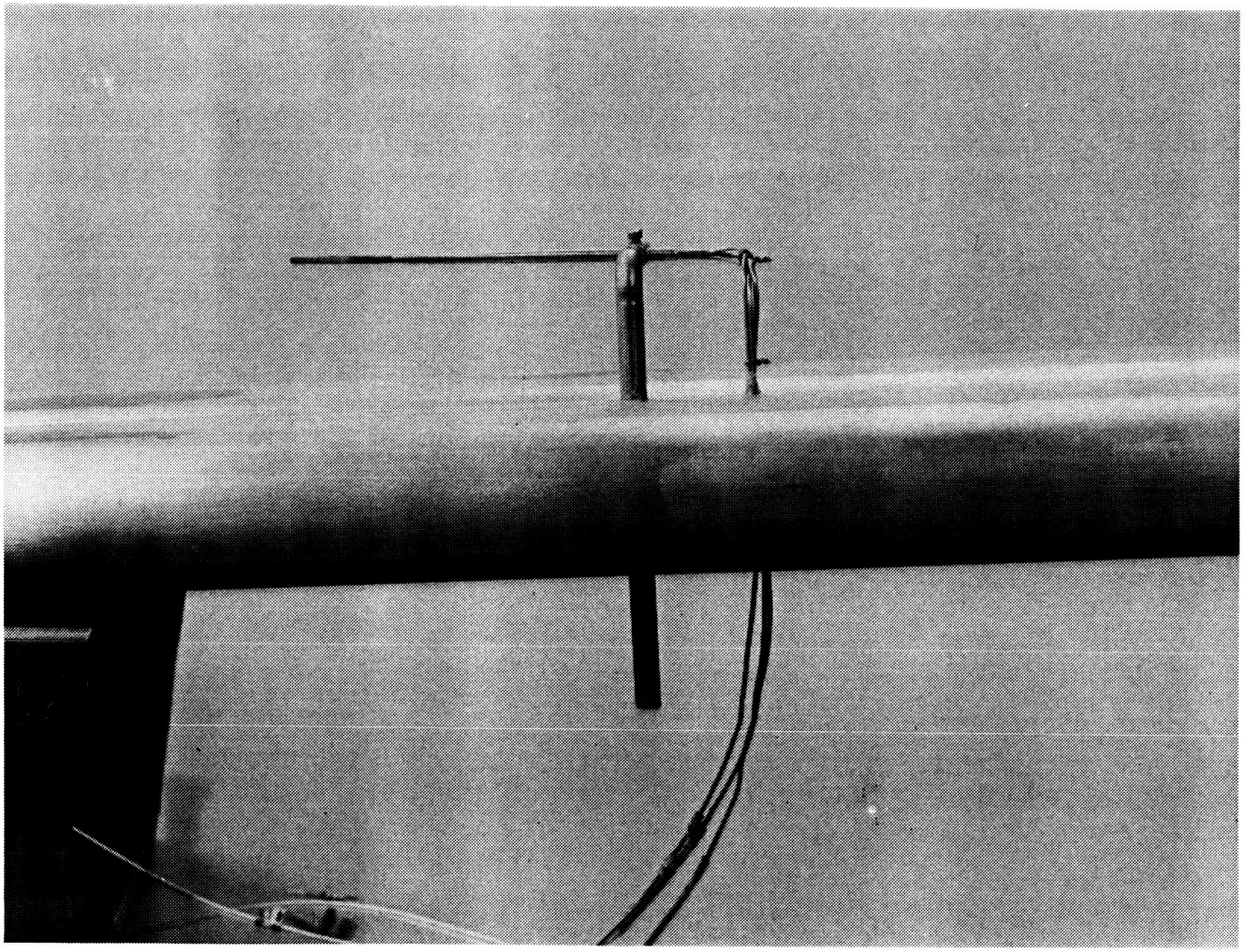

(a) Side view of probe mounted on wall.

Figure 37.- Photograph of the flow angle probe.

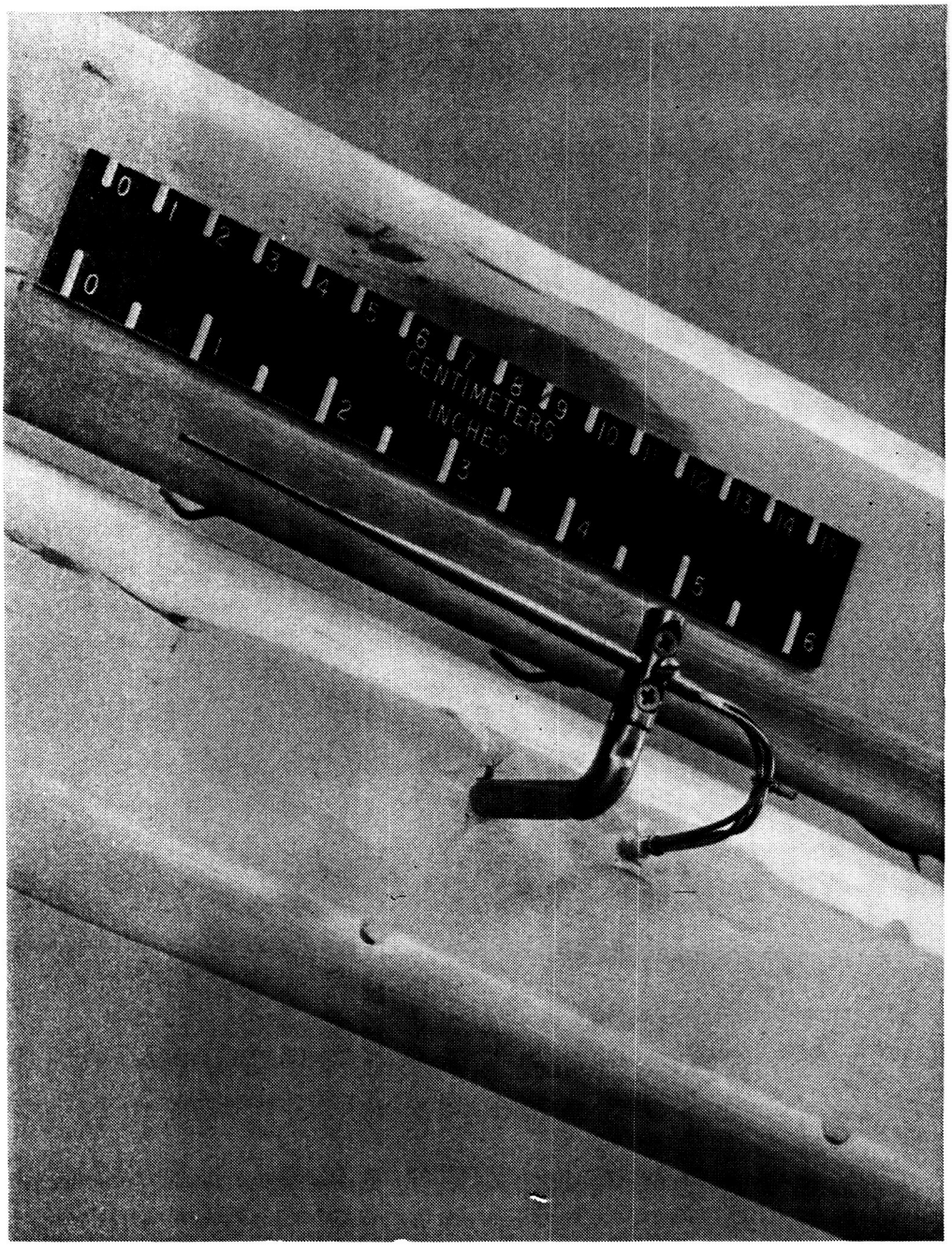

(b) Top view of probe mounted over slot.

Figure 37.- Concluded.

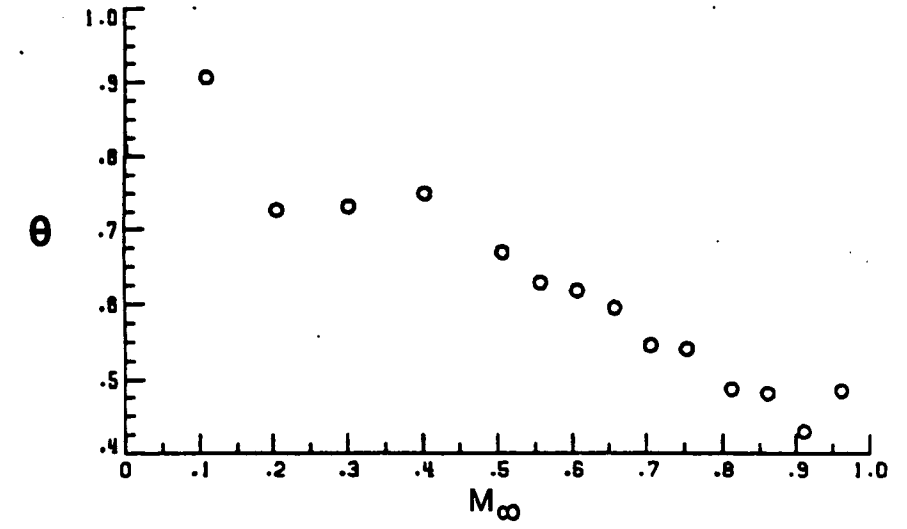

(a) Average of the flow-angle measurements.

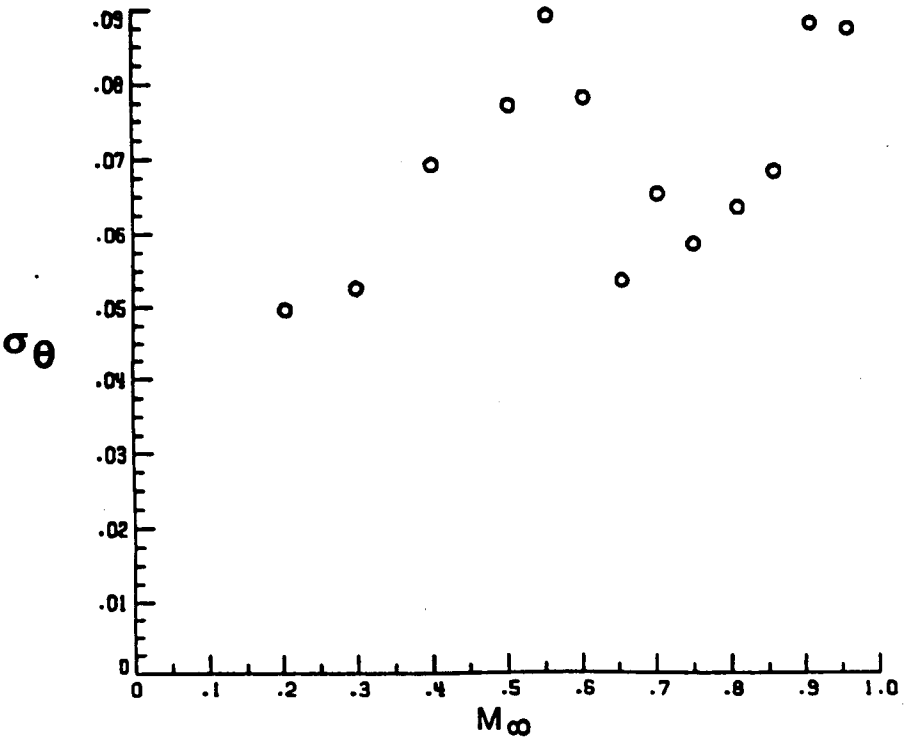

(b) Standard deviation of flow-angle measurements.

Figure 38.- Accuracy of the flow-angle measurements.

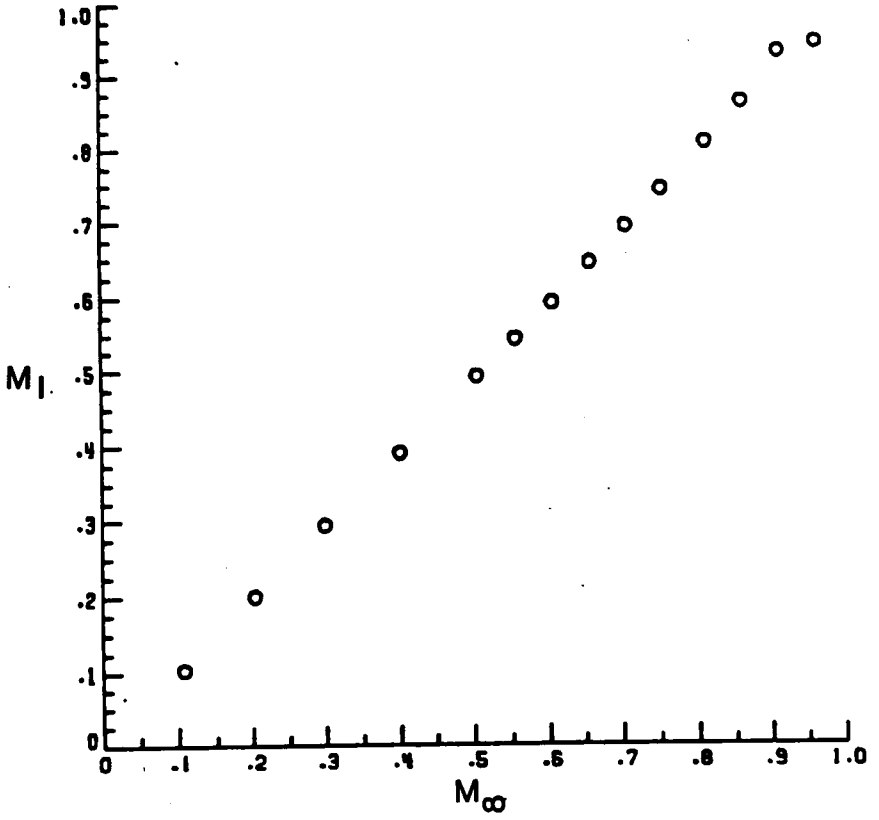

(a) Average of the local Mach number.

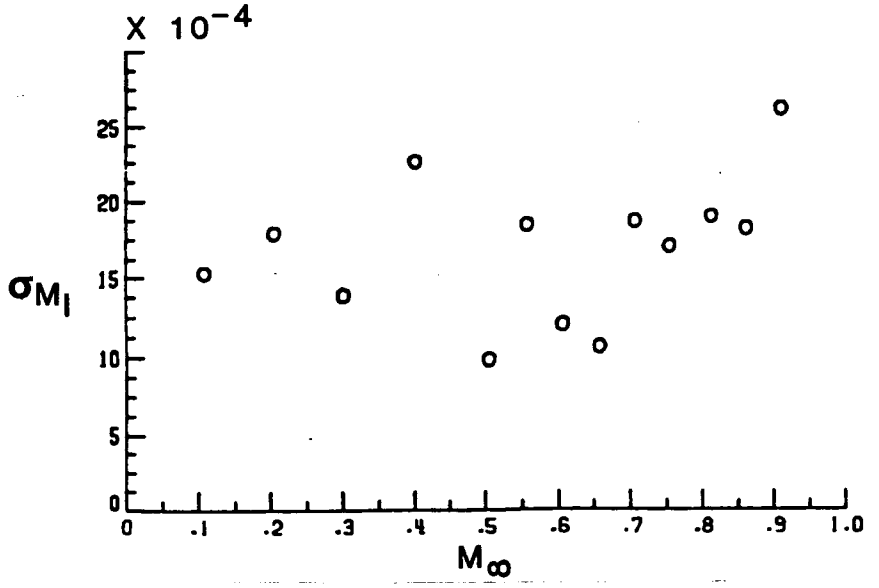

(b) Standard deviation of the local Mach number.

Figure 39.- Accuracy of the local Mach-number measurements.

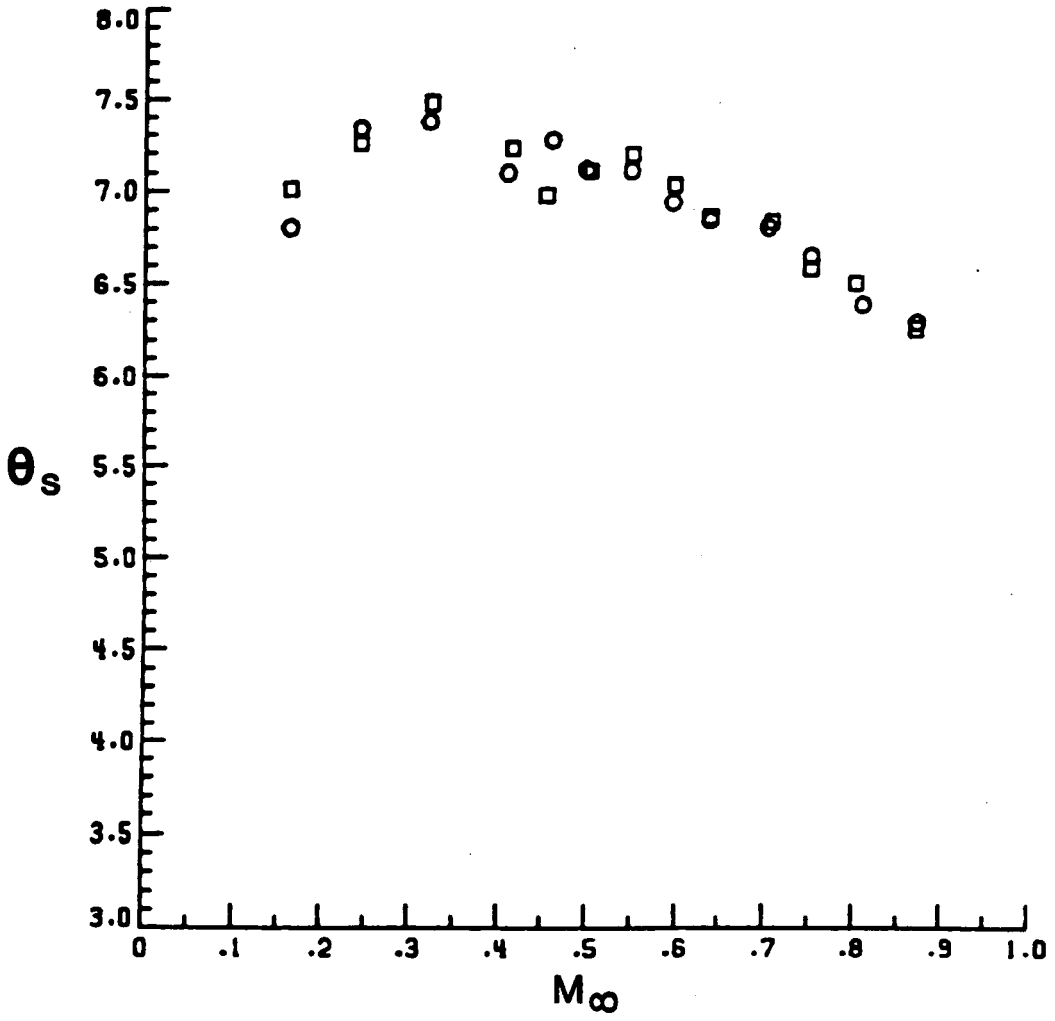

Figure 40.- Repeatability of slot flow angle.

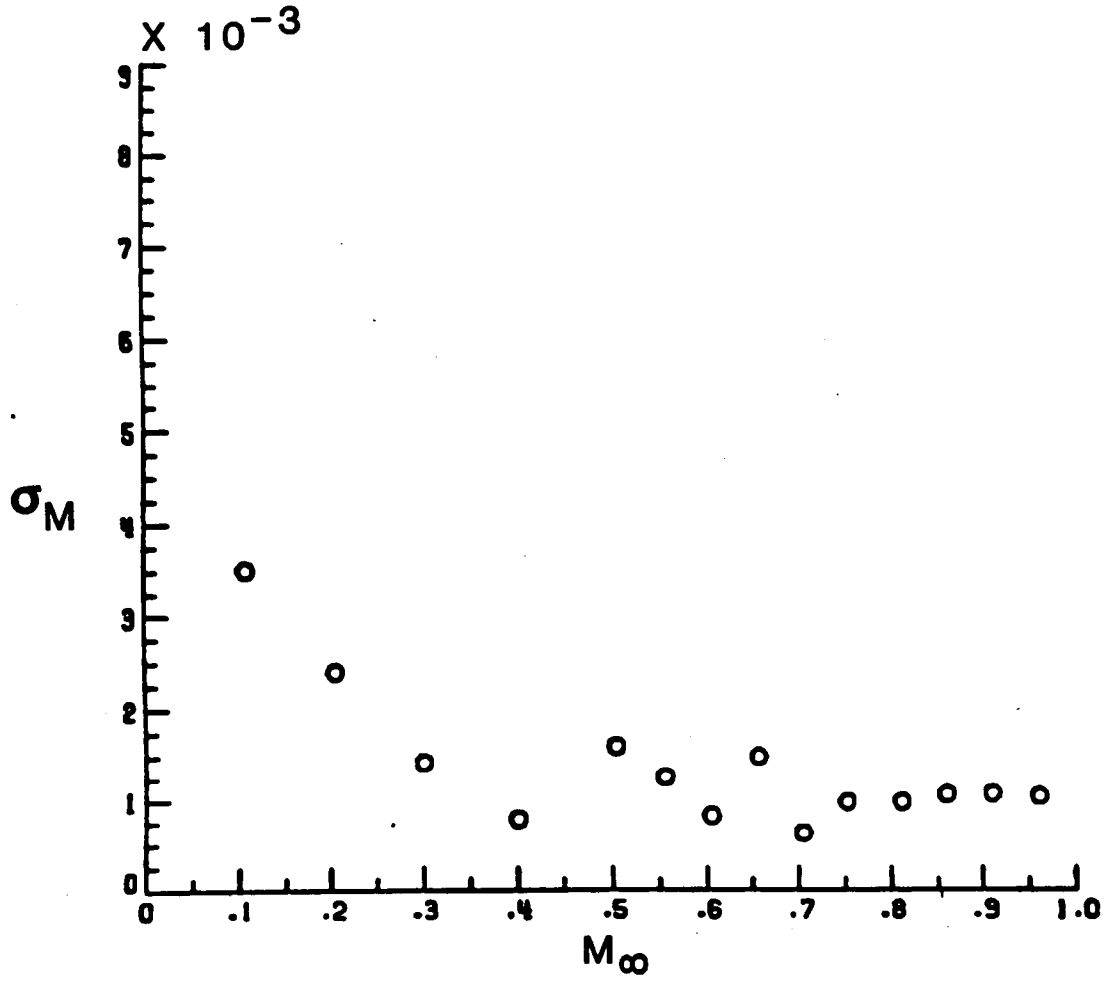

Figure 41.- Repeatability of free-stream Mach number.

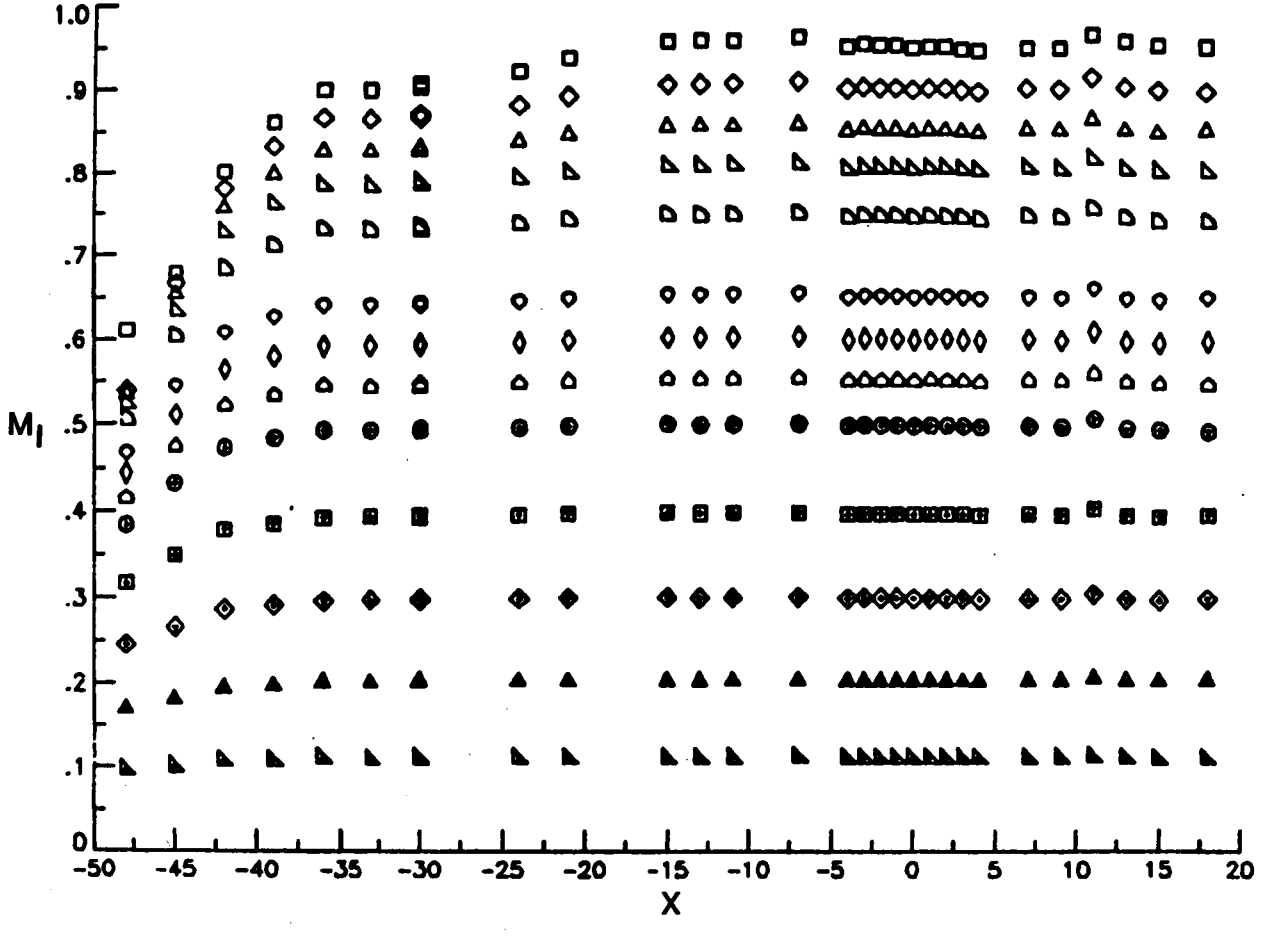

(a) 15-1 wall.

Figure 42.- Centerline Mach number calibration.

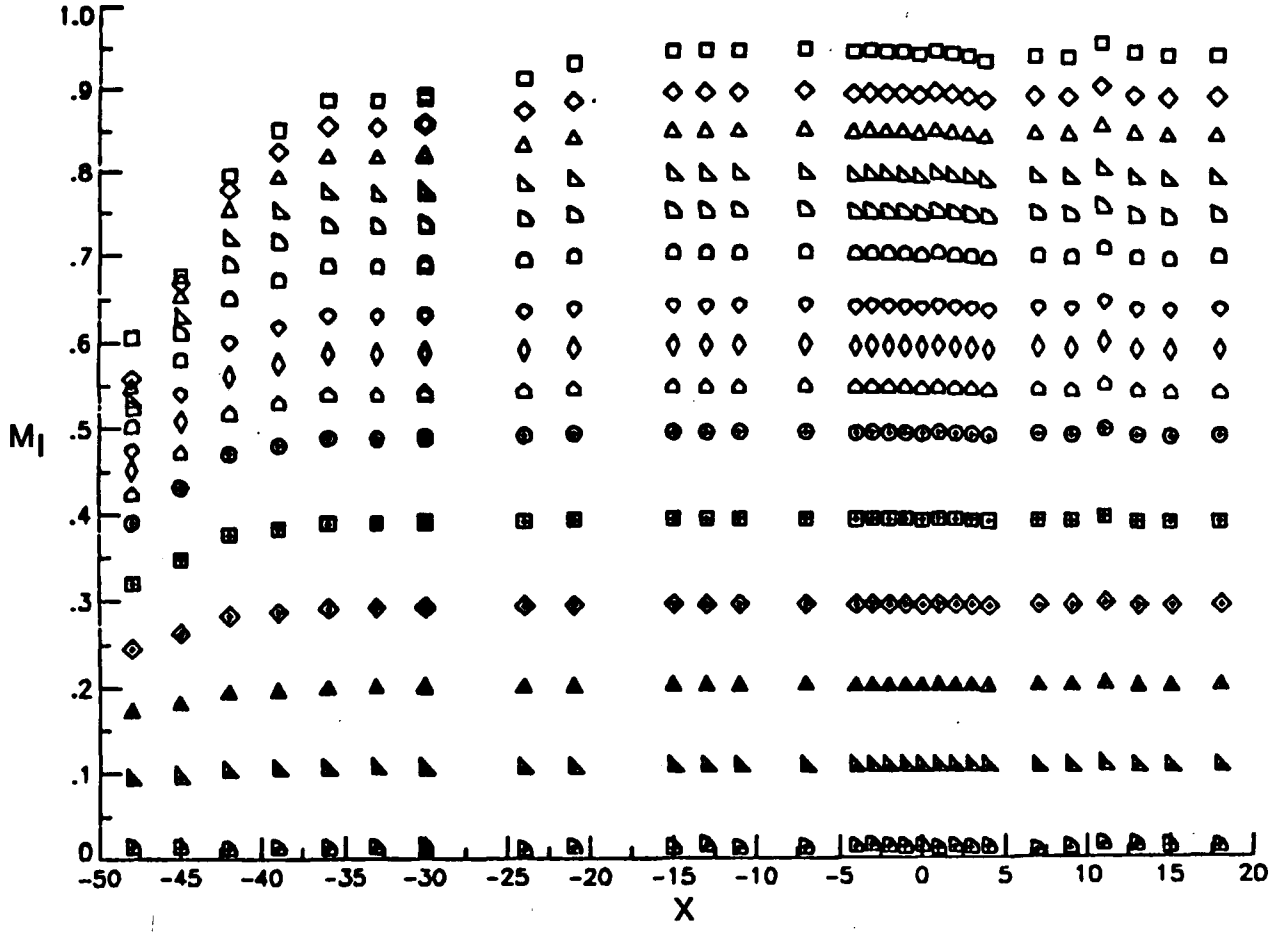

(b) 15-2 wall.

Figure 42.- Continued.

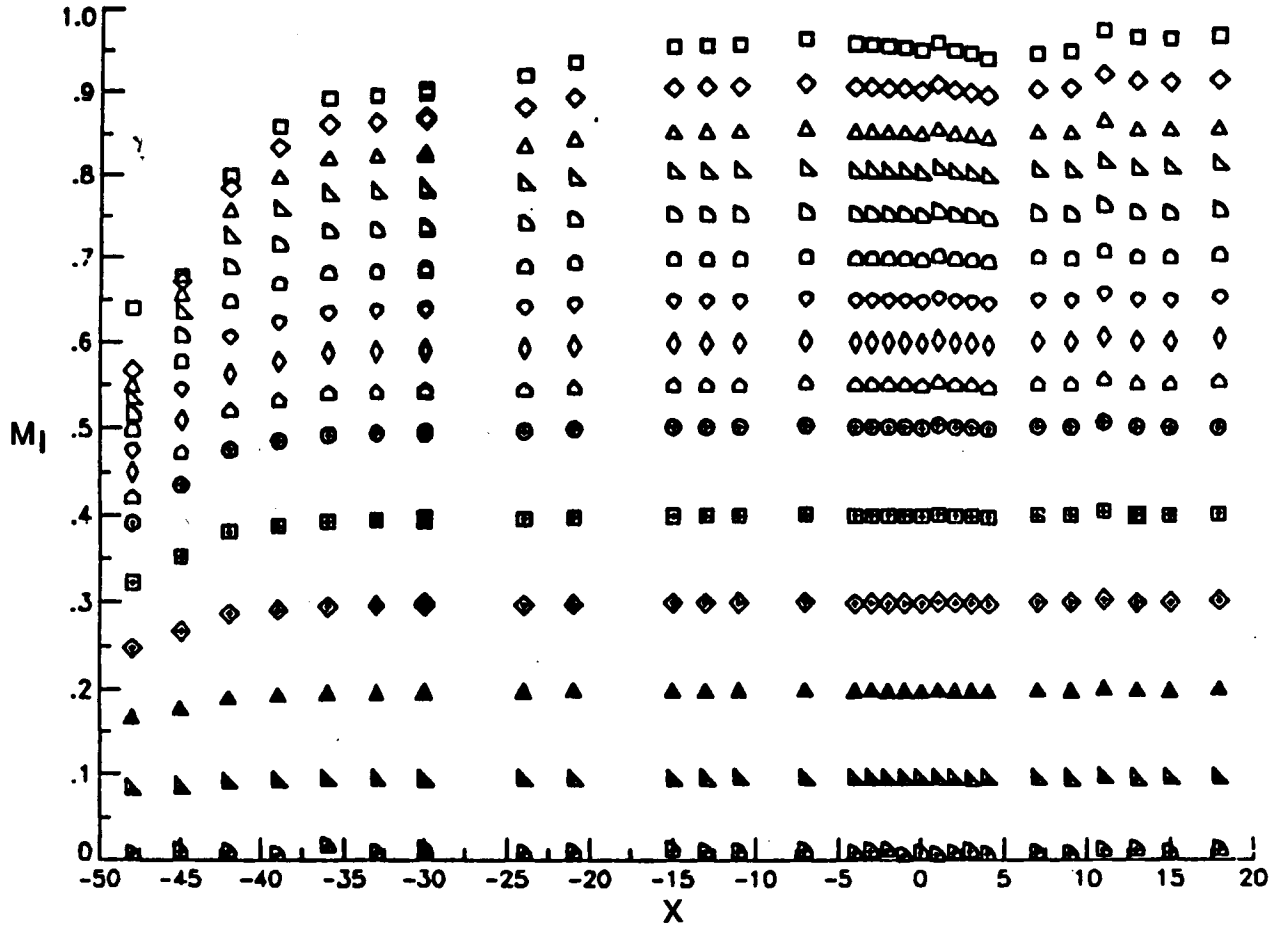

(c) 7.5-1 wall.

Figure 42.- Continued.

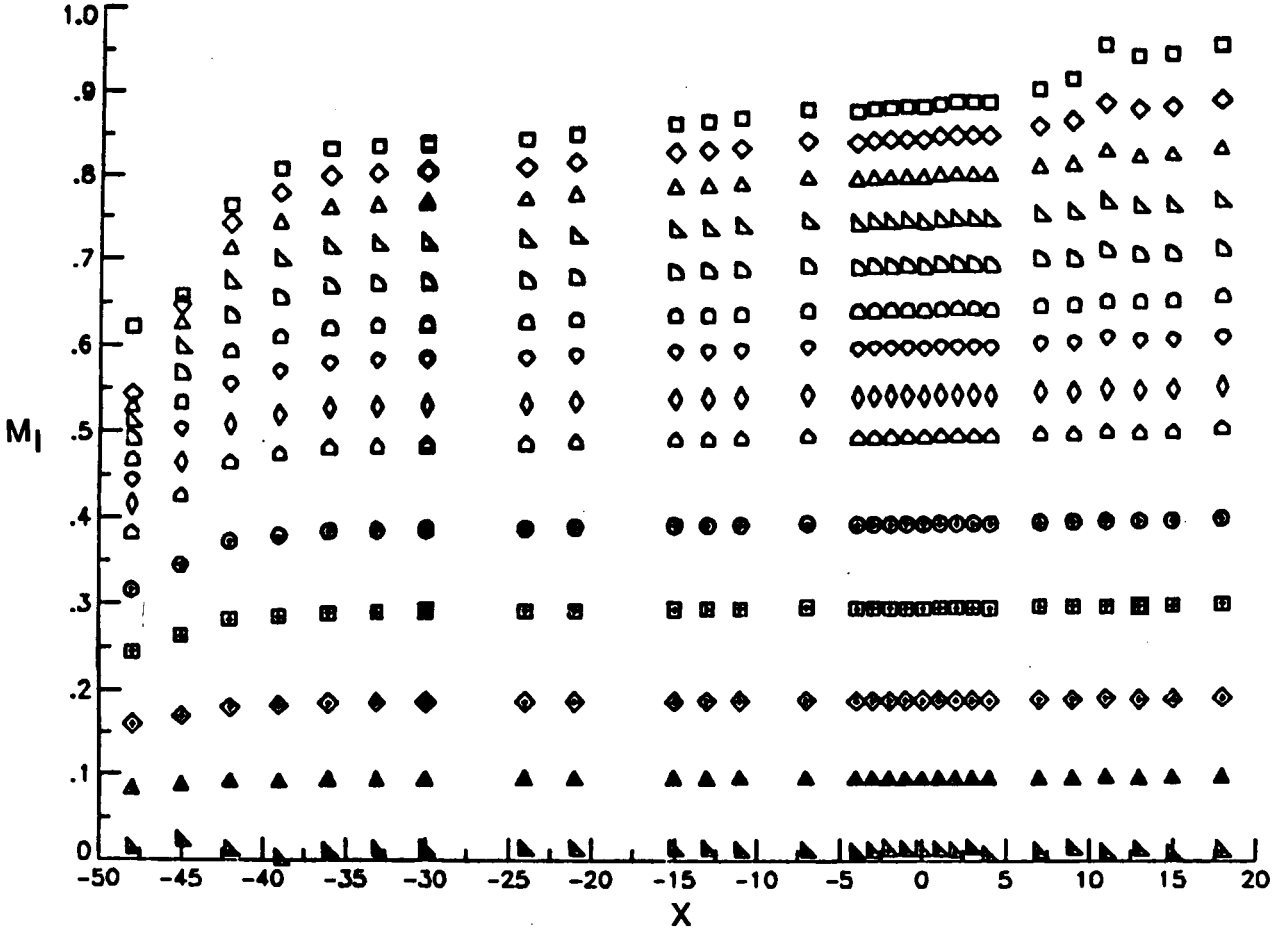

(d) Solid wall.

Figure 42.- Continued.

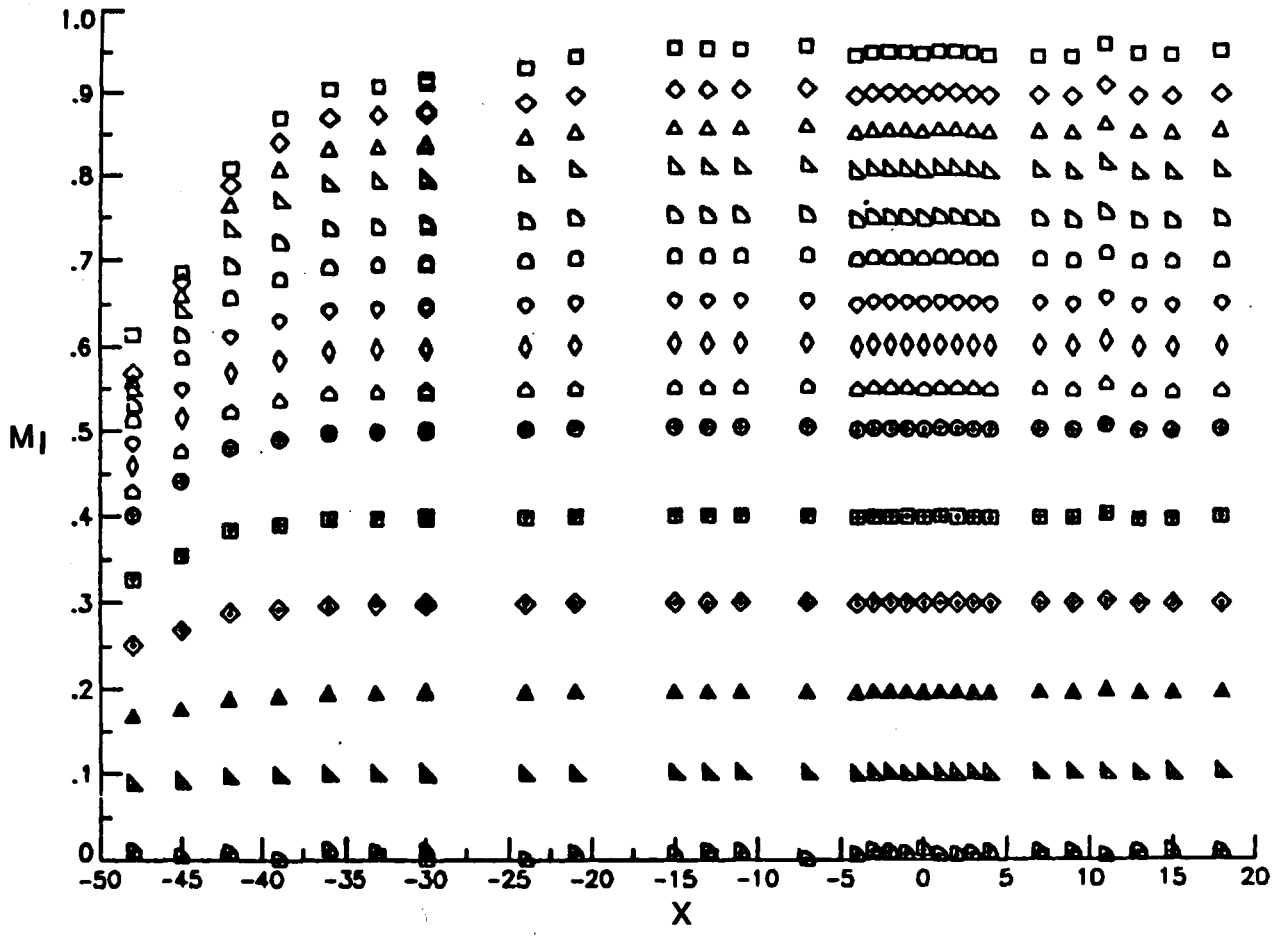

(e) 15-4 wall.

Figure 42.- Continued.

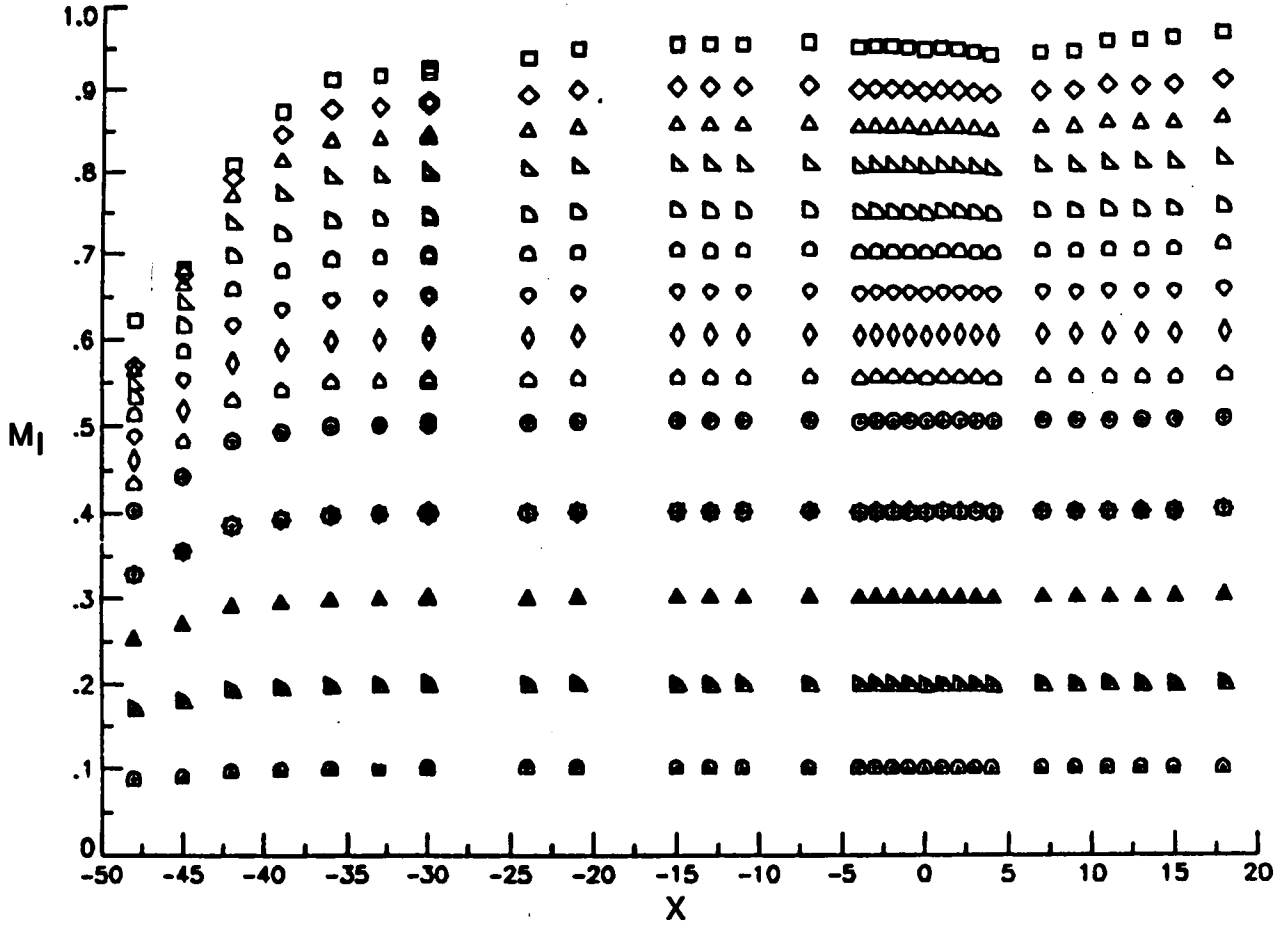

(f) 7.5-2 wall.

Figure 42.- Continued.

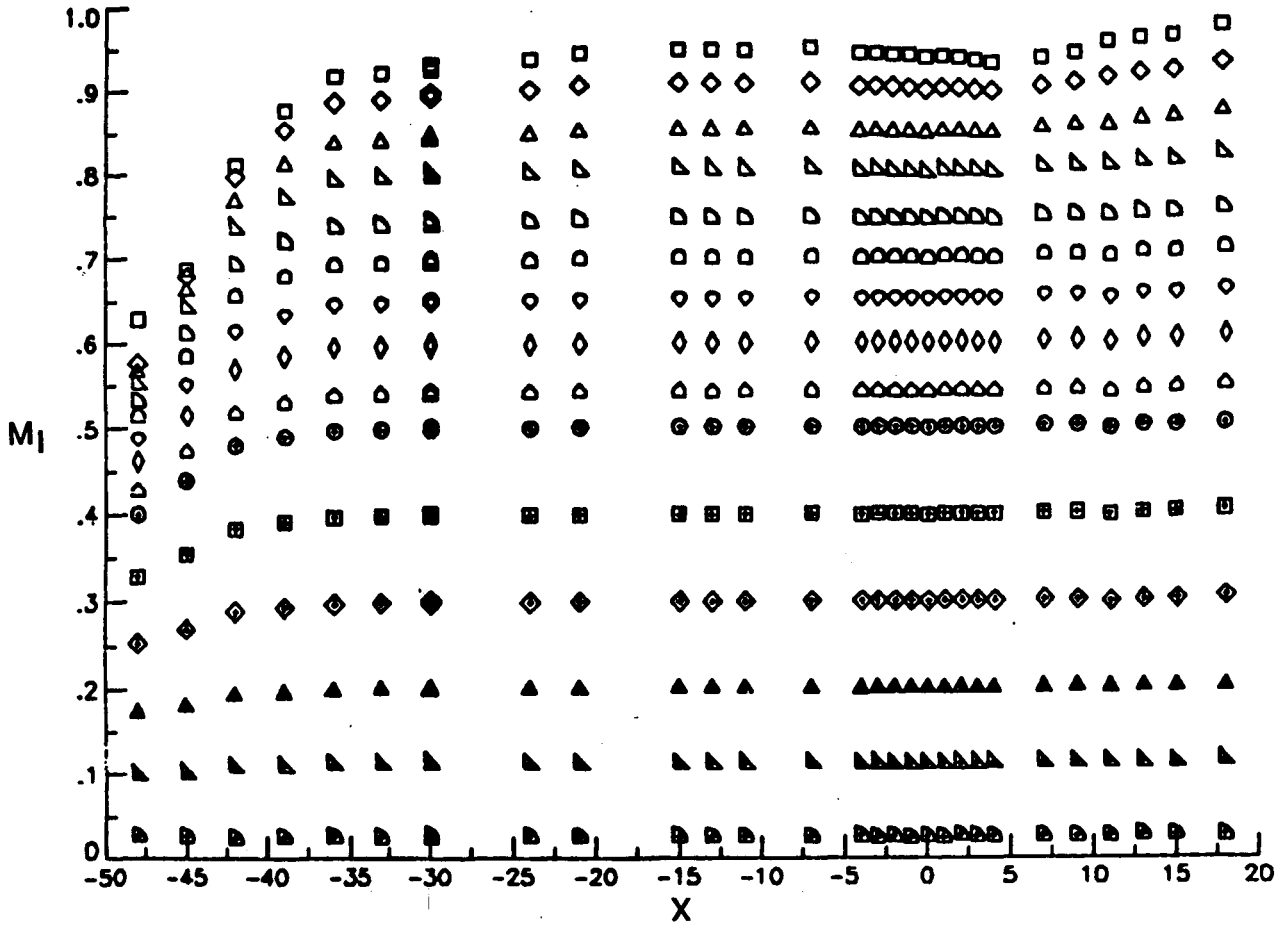

(g) 3.75-1 wall.

Figure 42.- Continued.

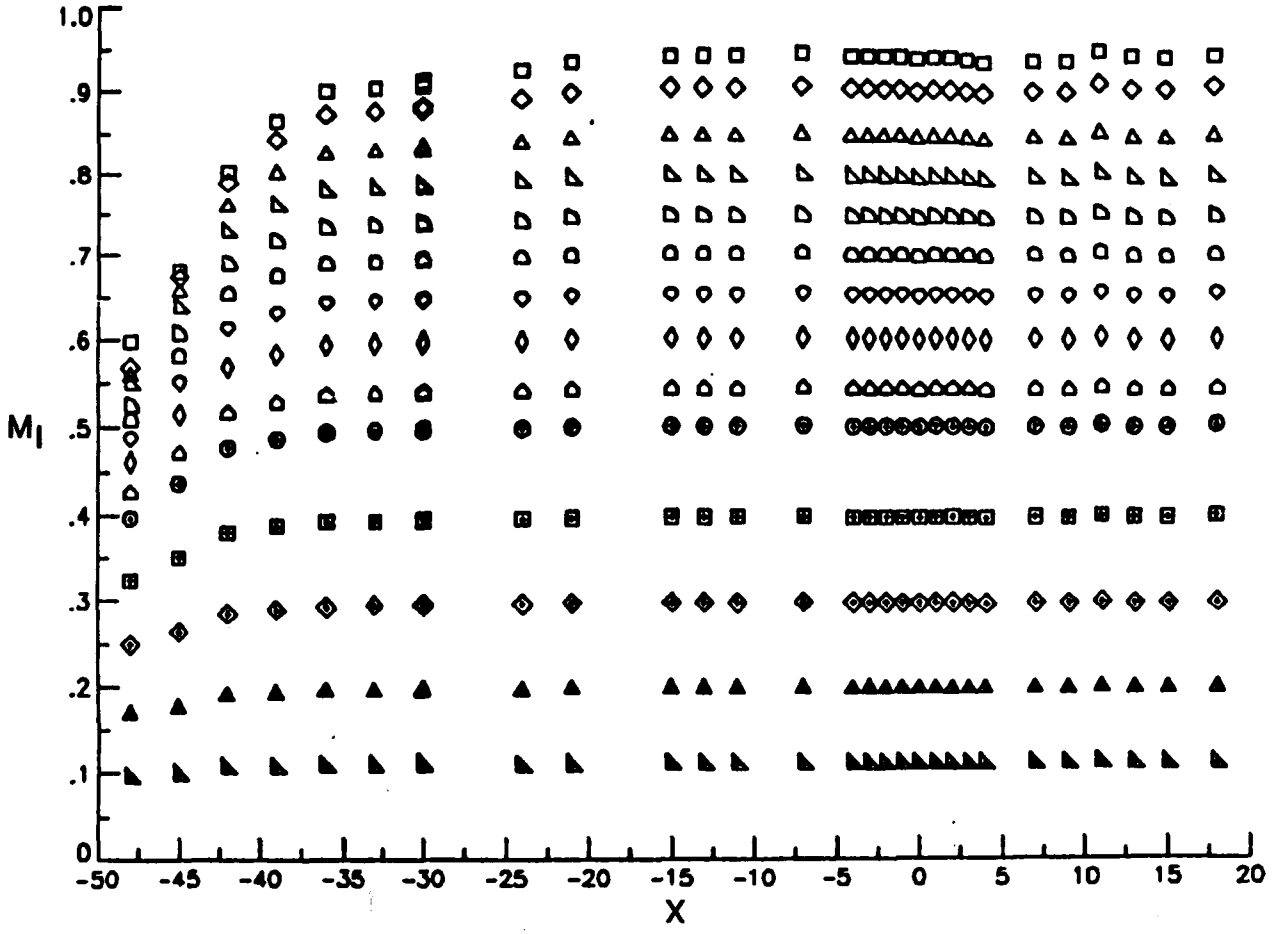

(h) 10-4 wall.

Figure 42.- Continued.

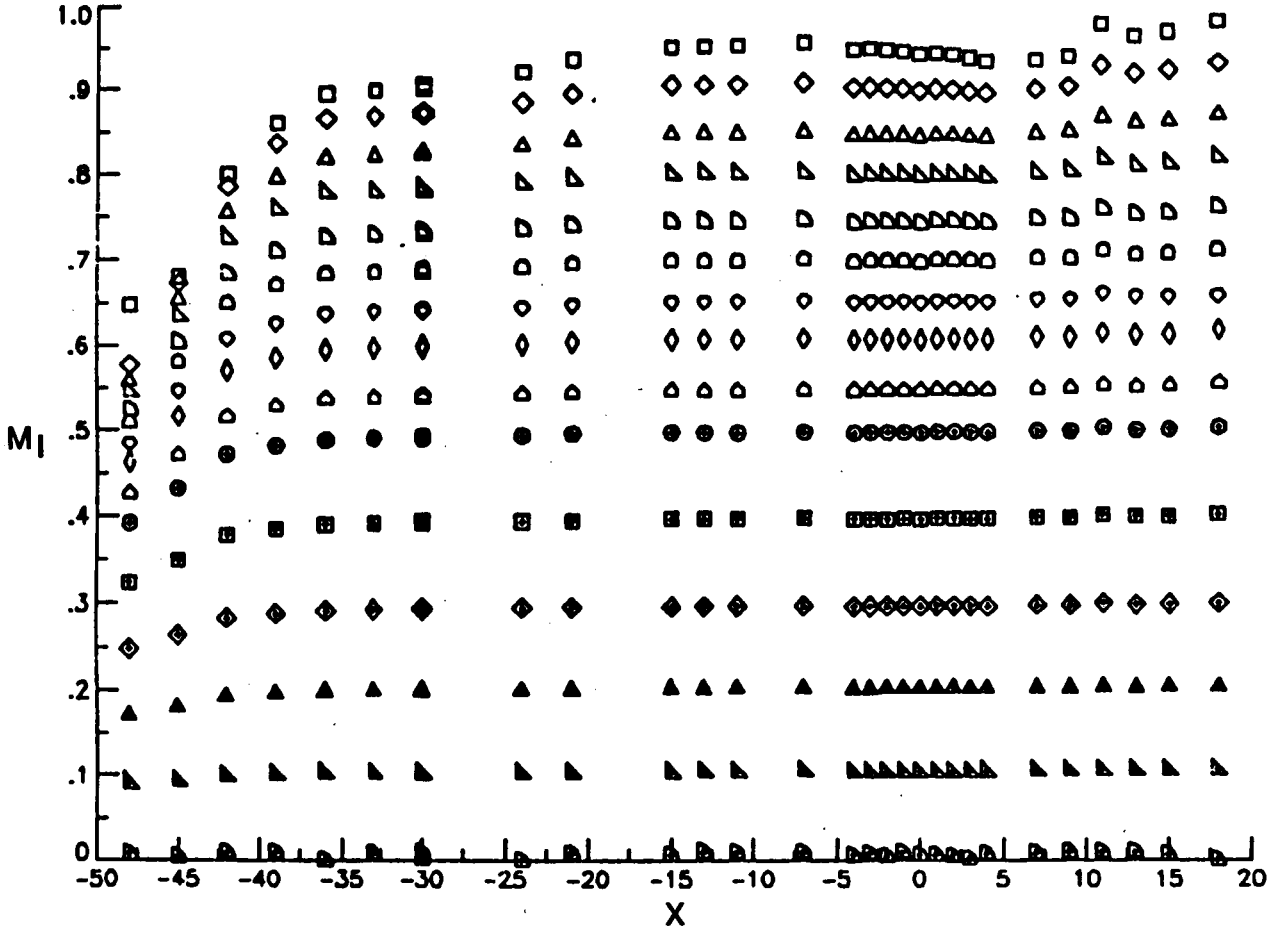

(i) 5-2 wall.

Figure 42.- Continued.

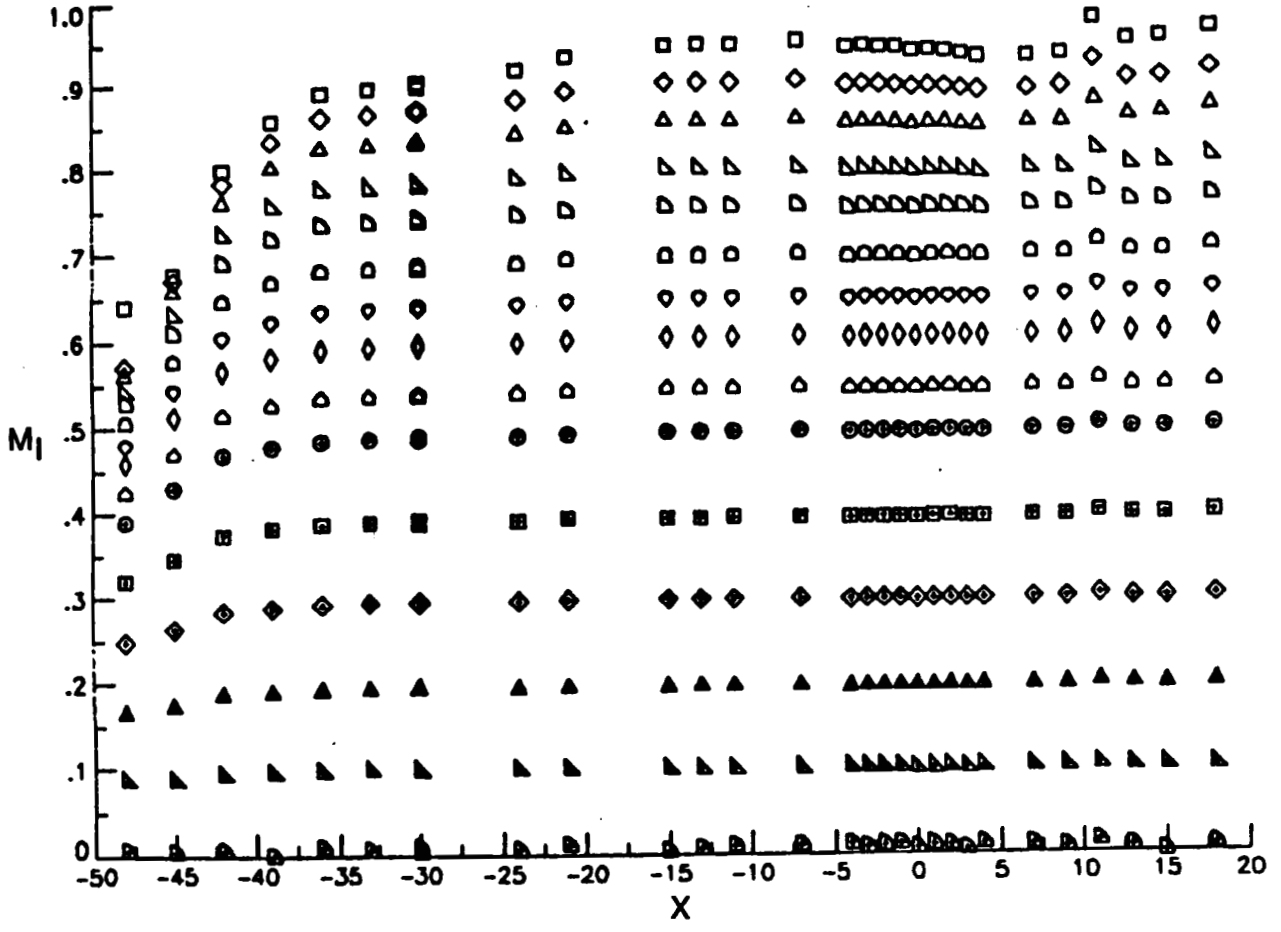

(j) 6-4 wall.

Figure 42.- Continued.

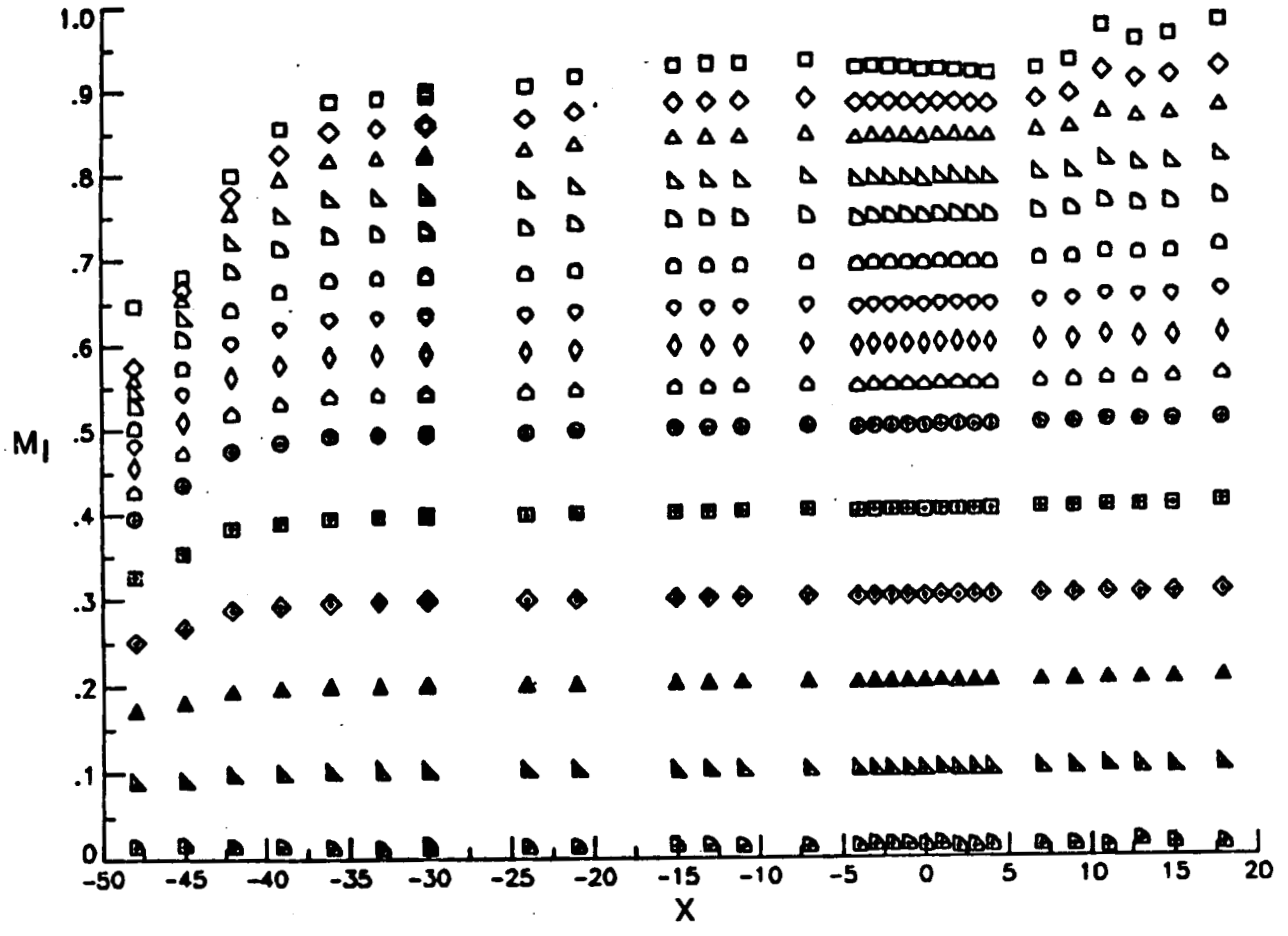

(k) 3-2 wall.

Figure 42.- Continued.

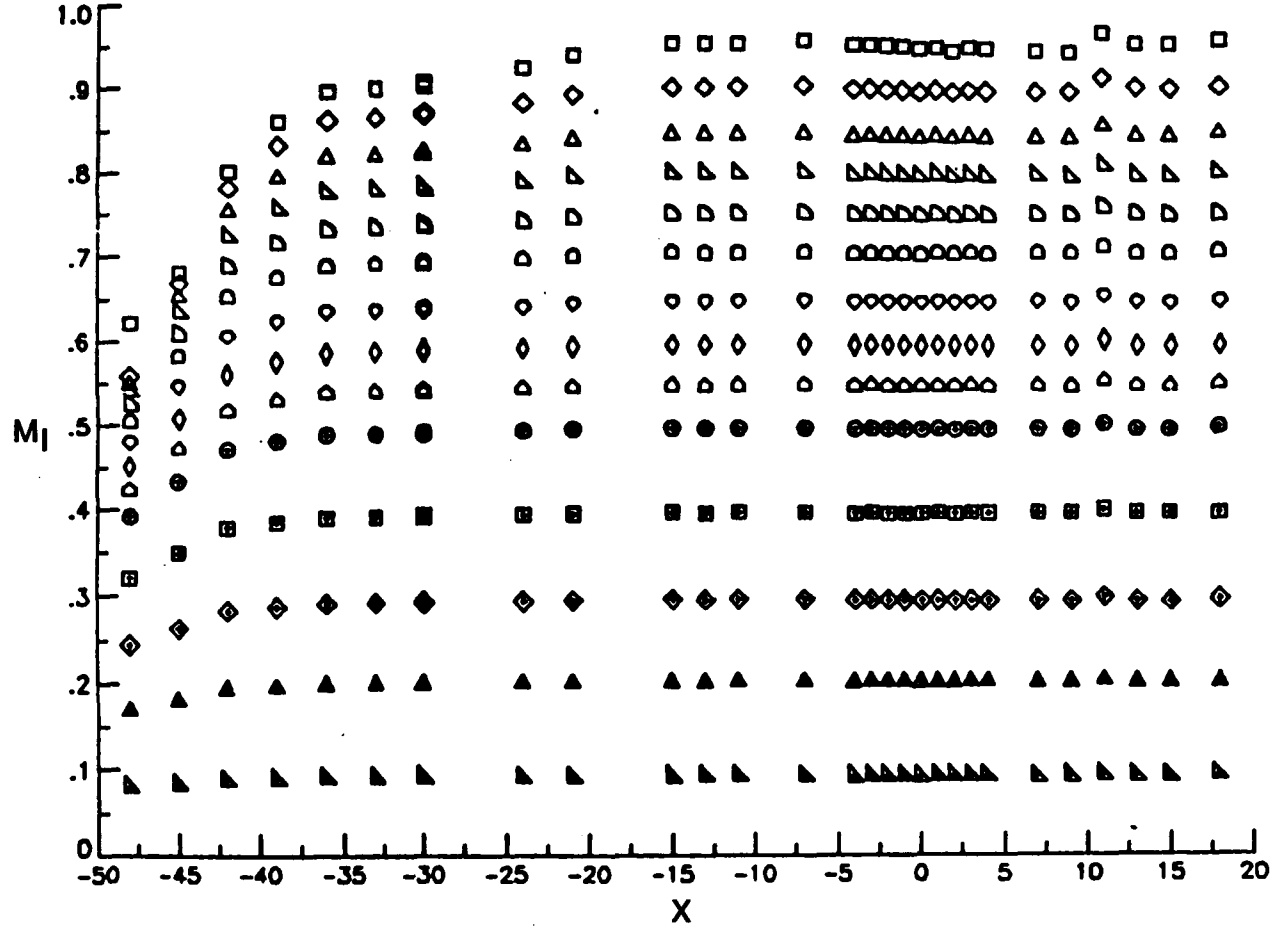

(l) 10-2 wall.

Figure 42.- Concluded.

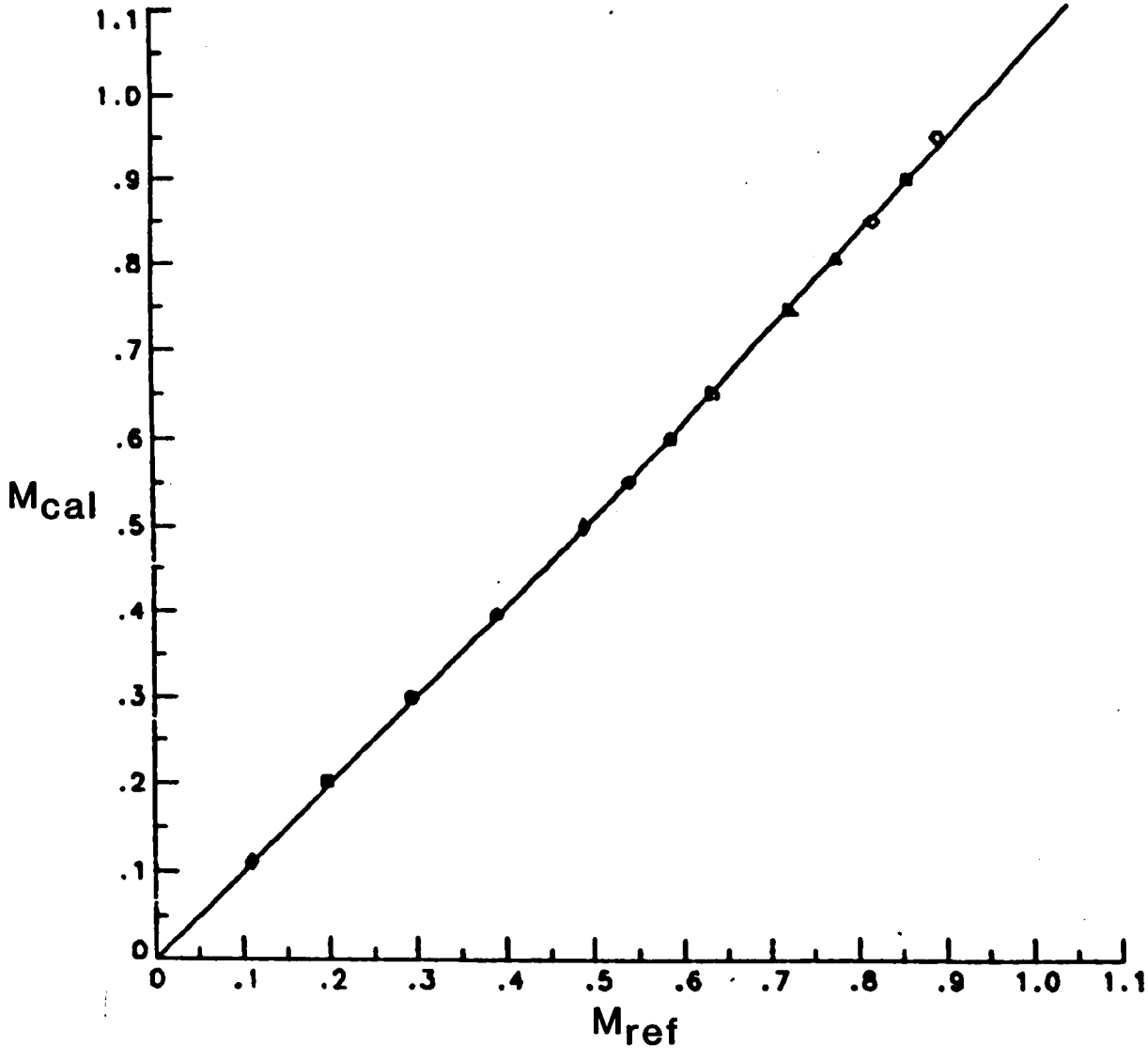

Figure 43.- Wind-tunnel wall calibration for the 15-1 wall.

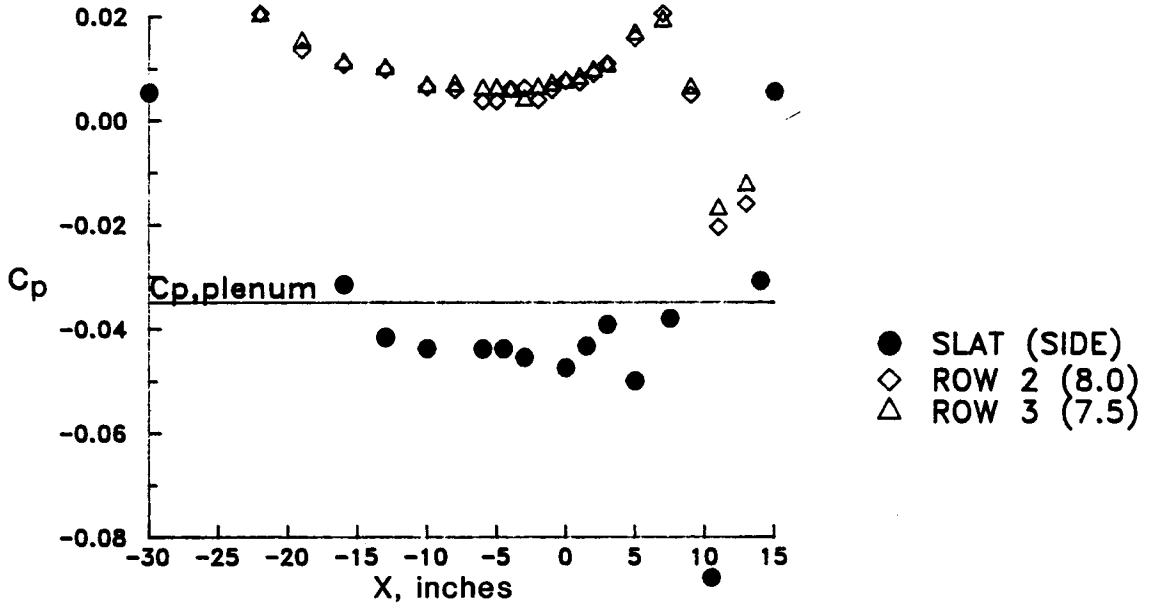

(a) Tunnel empty.

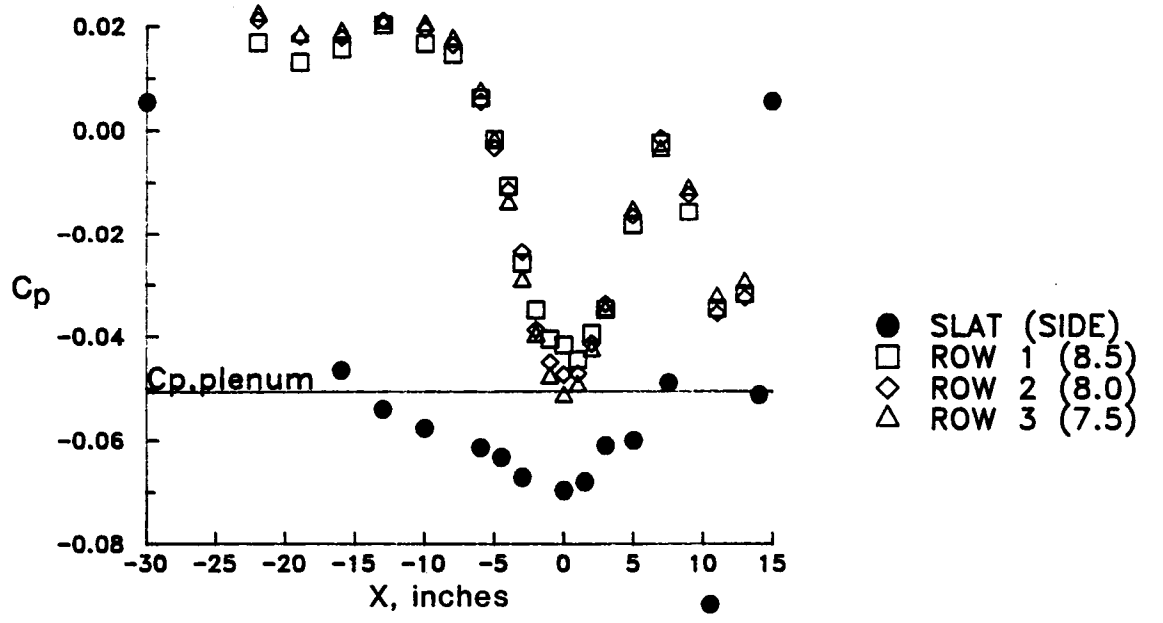

(b) Airfoil installed.

Figure 44.- Pressure distributions near the 6-4 slotted wall. $M_\infty = 0.7$.

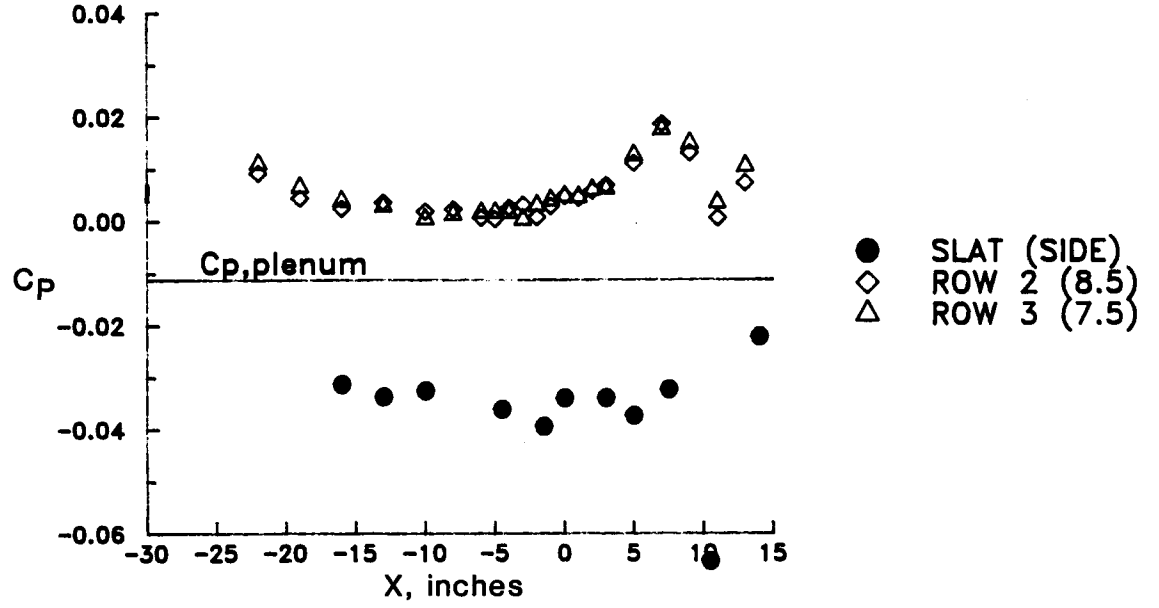

(a) Tunnel empty.

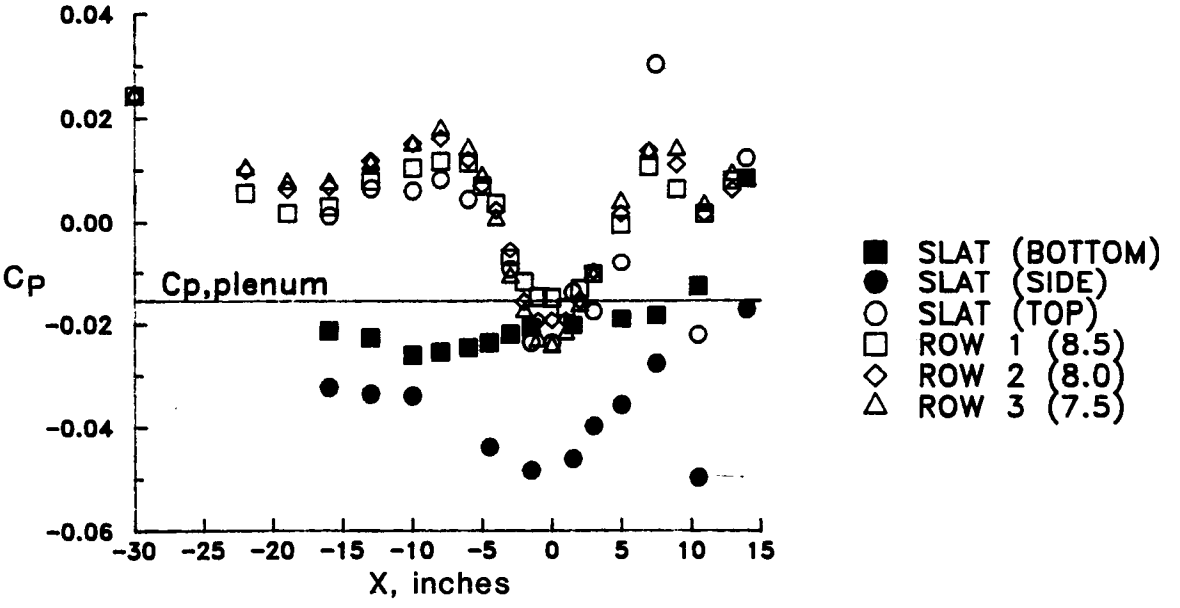

(b) Airfoil installed.

Figure 45.- Pressure distributions near the 15-4 slotted wall. $M_\infty = 0.7$.

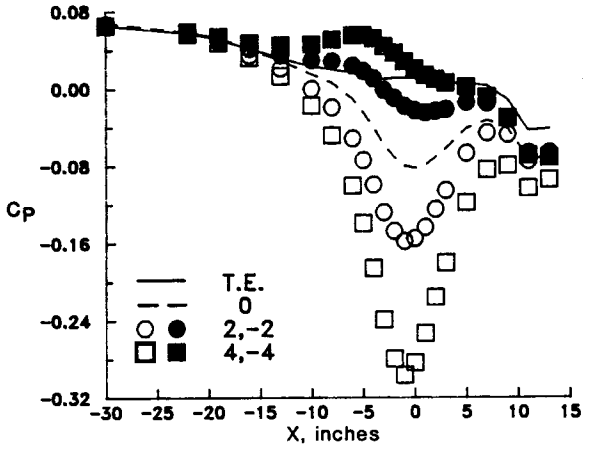

(a) Solid wall.

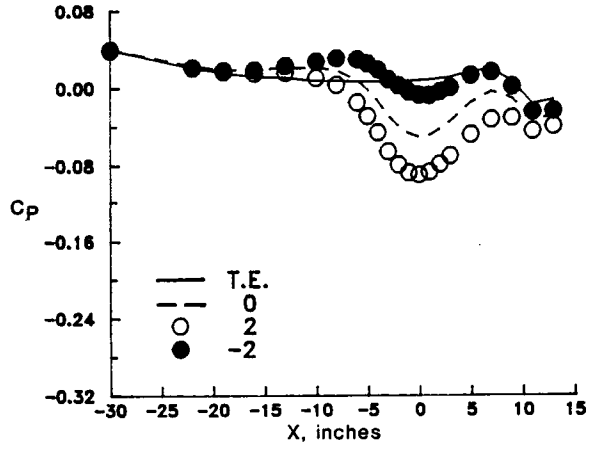

(b) 6-4 wall.

Figure 46.- Pressure distributions along row 3, $M_\infty = 0.7$.

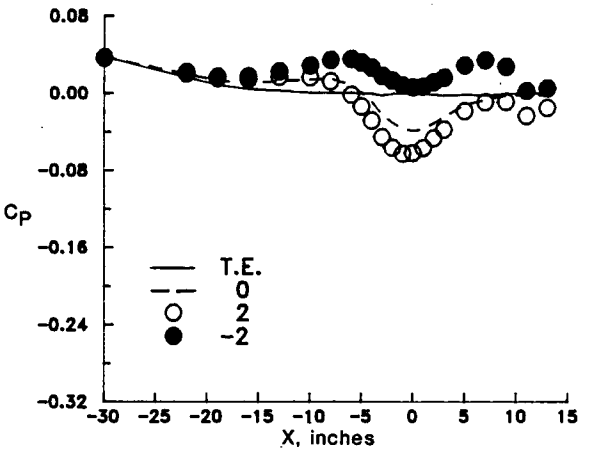

(c) 10-2 wall.

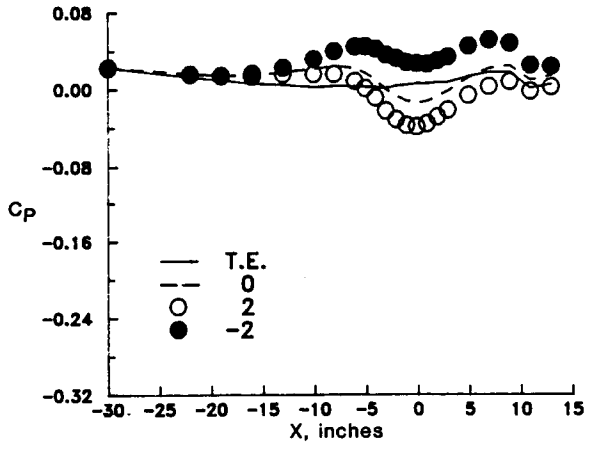

(d) 10-4 wall.

Figure 46.- Continued.

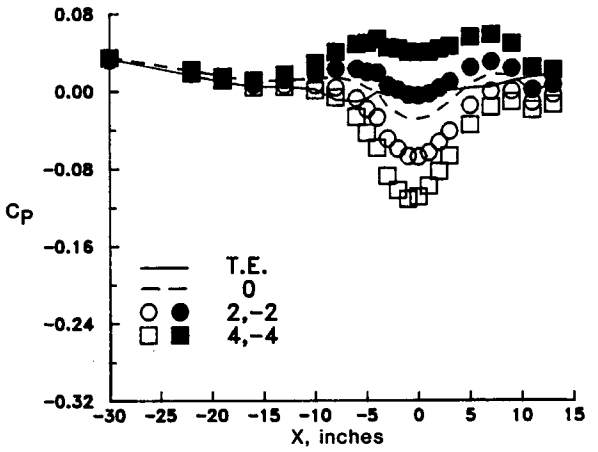

(e) 15-1 wall.

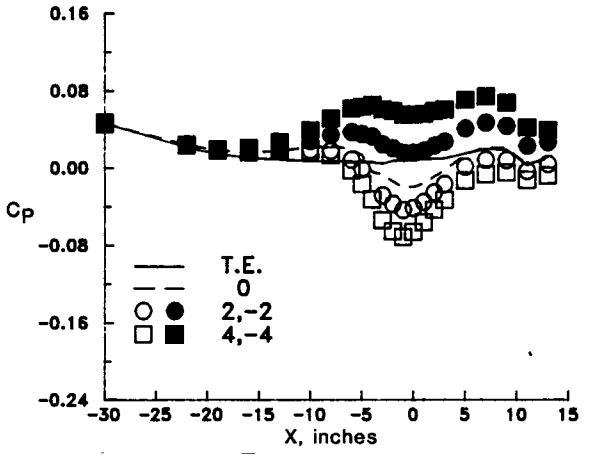

(f) 15-2 wall.

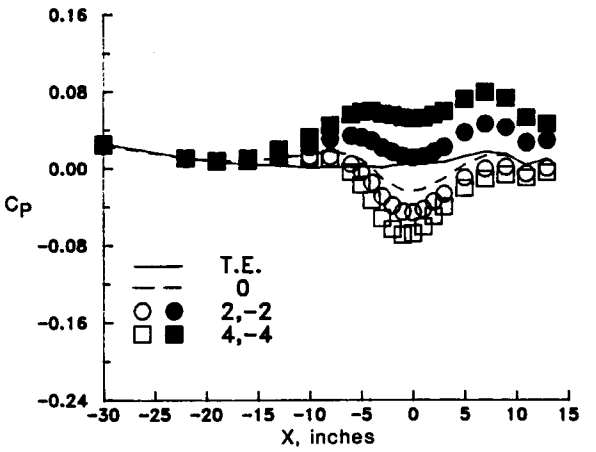

(g) 15-4 wall.

Figure 46.- Concluded.

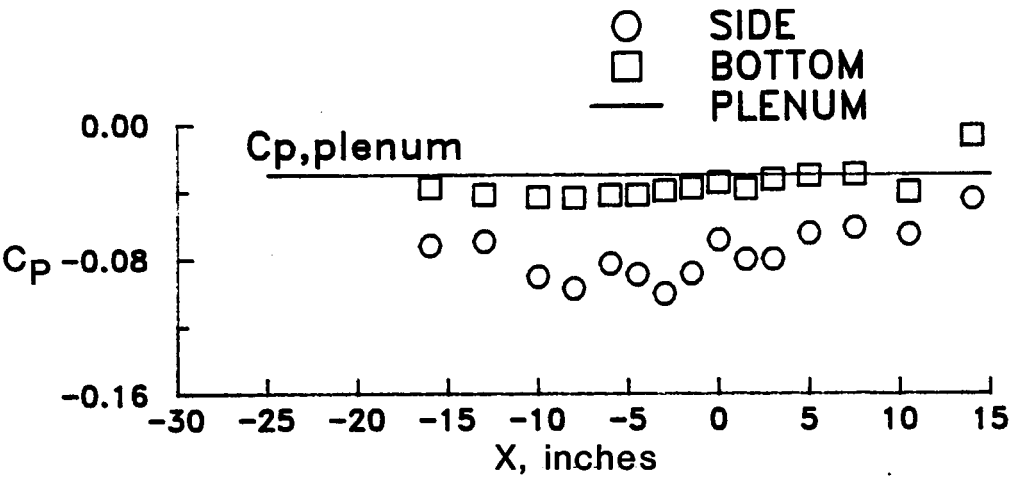

(a) 10-2 wall.

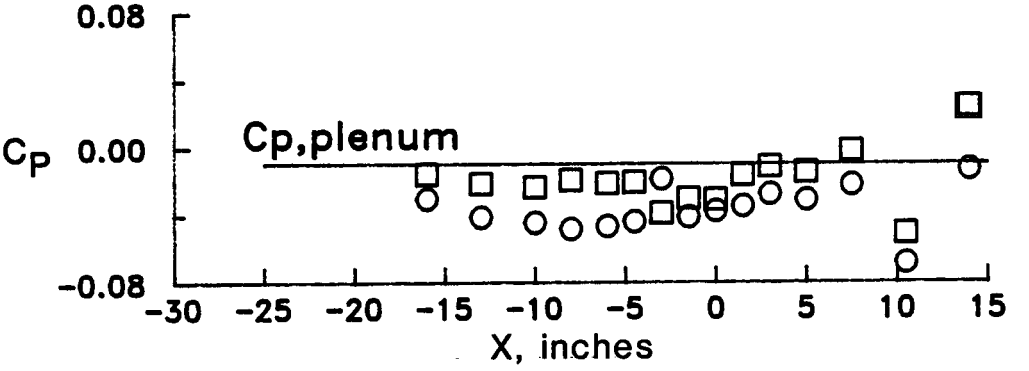

(b) 15-2 wall.

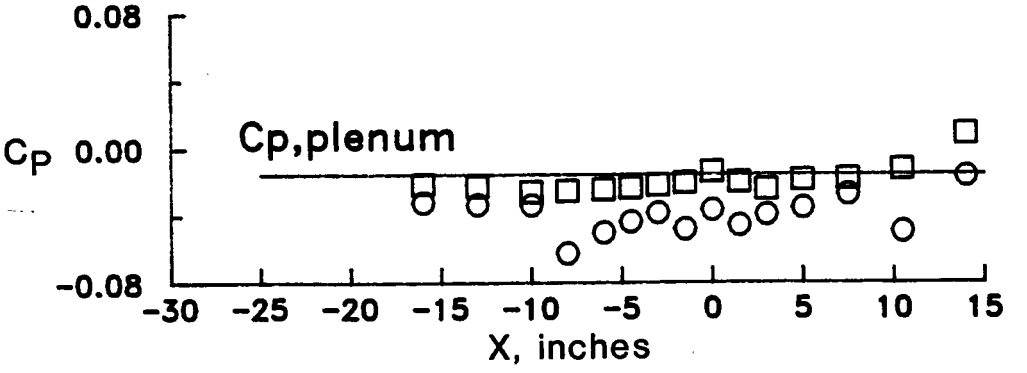

(c) 15-4 wall.

Figure 47.- Pressure measurements in the slot region.

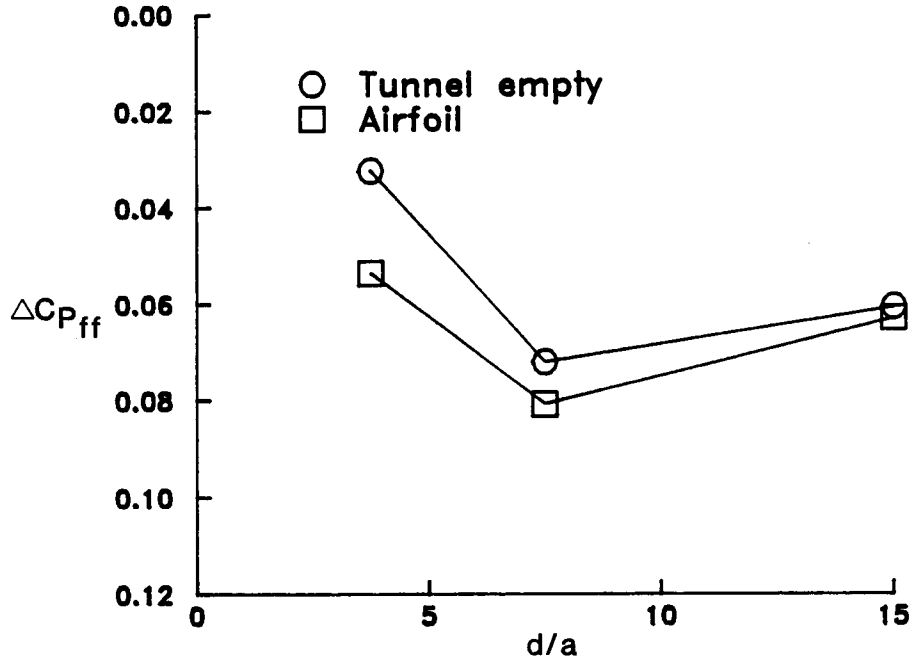

(a) One-slot walls.

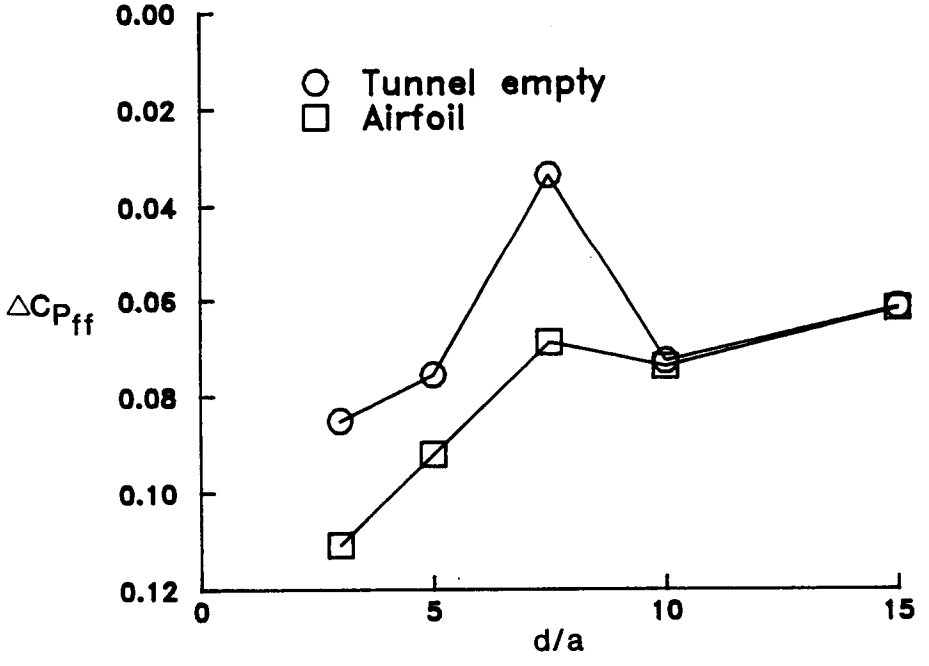

(b) Two-slot walls.

Figure 48.- Far-field wall-pressure drop, $M_\infty = 0.7$.

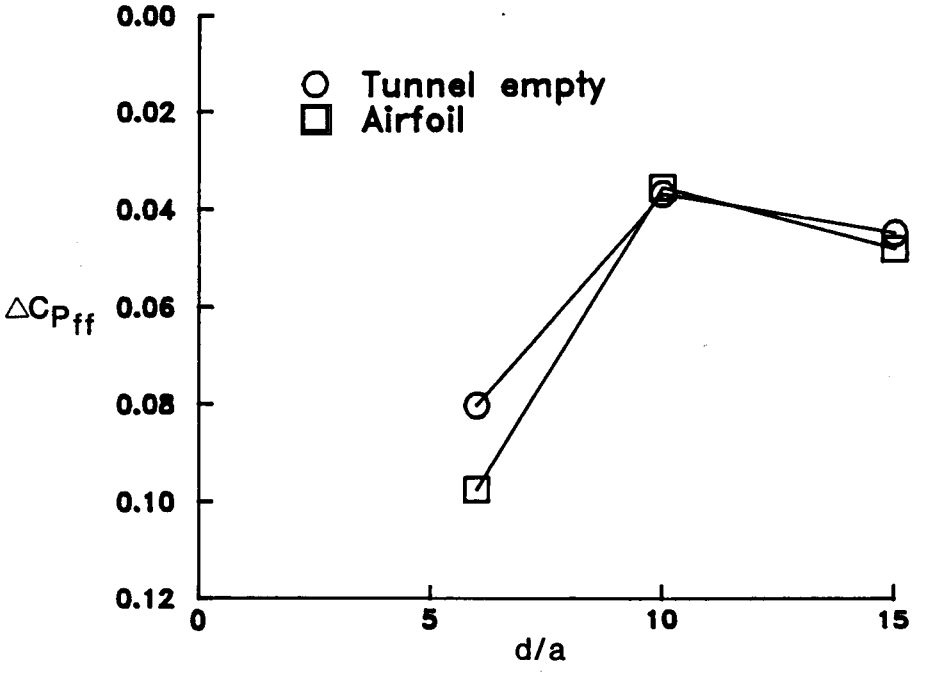

(c) Four-slot walls.

Figure 48.- Concluded.

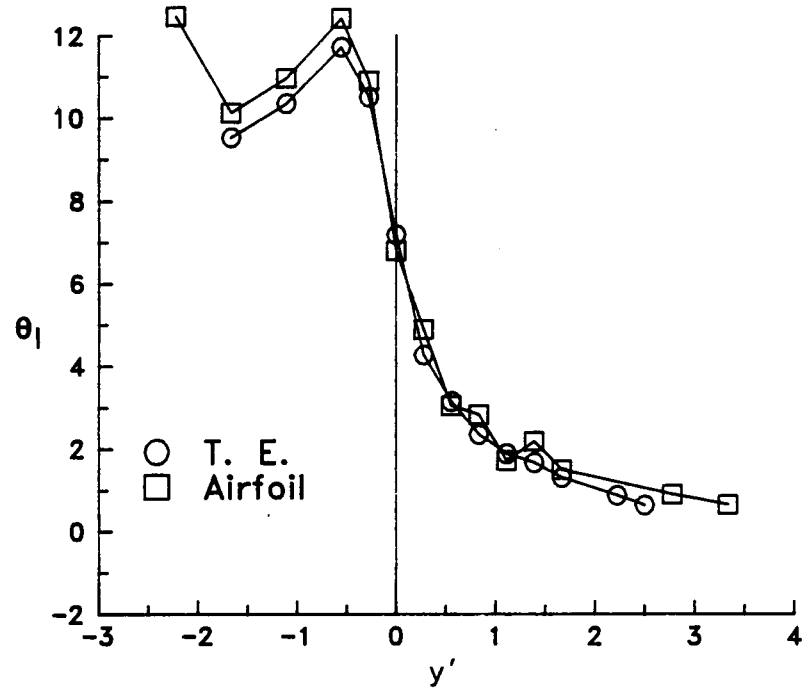

(a) $M_\infty = 0.3$.

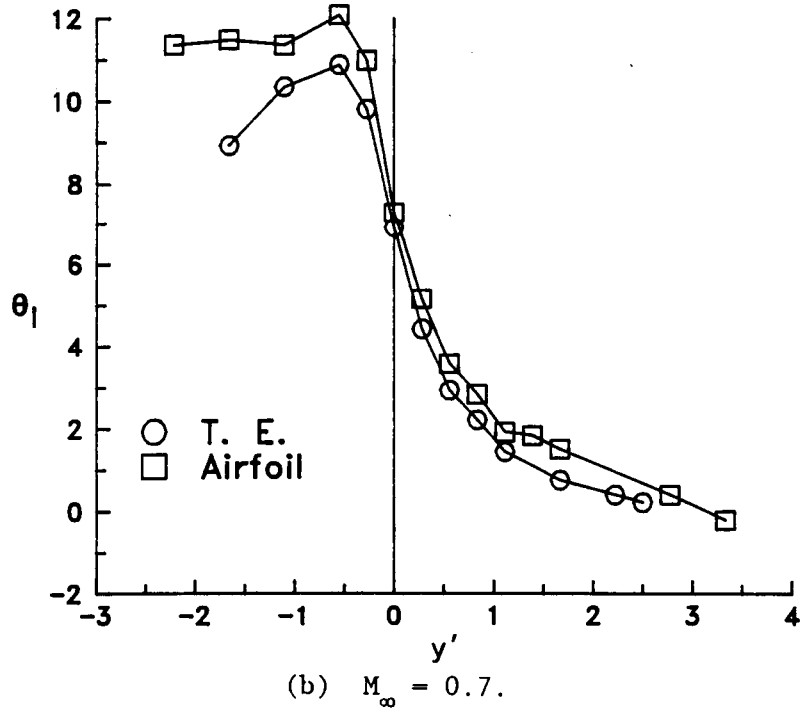

(b) $M_\infty = 0.7$.

Figure 49.- Comparison of tunnel-empty and airfoil flow angles measured through the slot in the 6- By 19-Inch Tunnel.

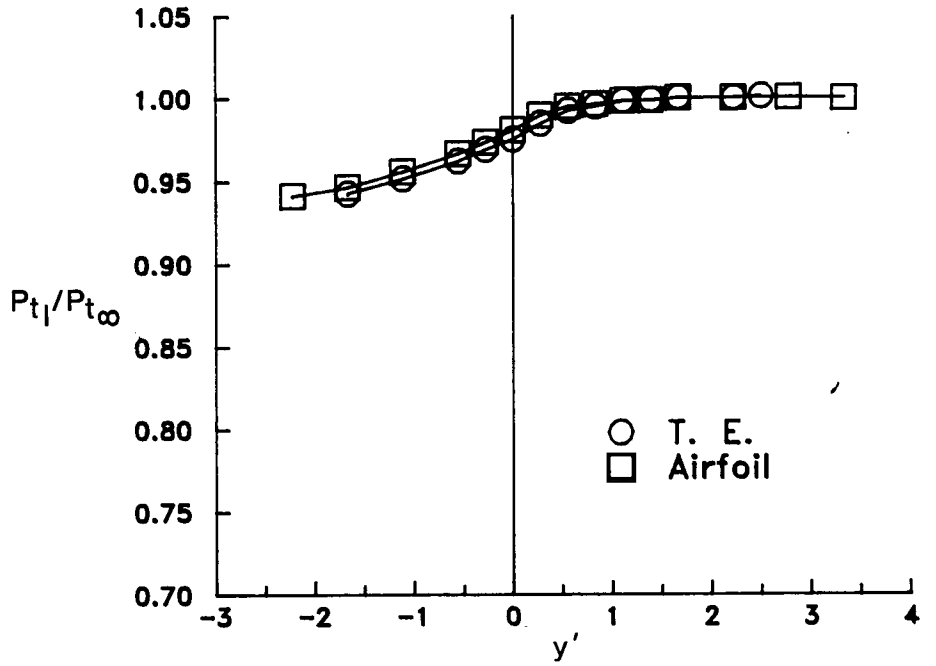

(a) $M_\infty = 0.3$.

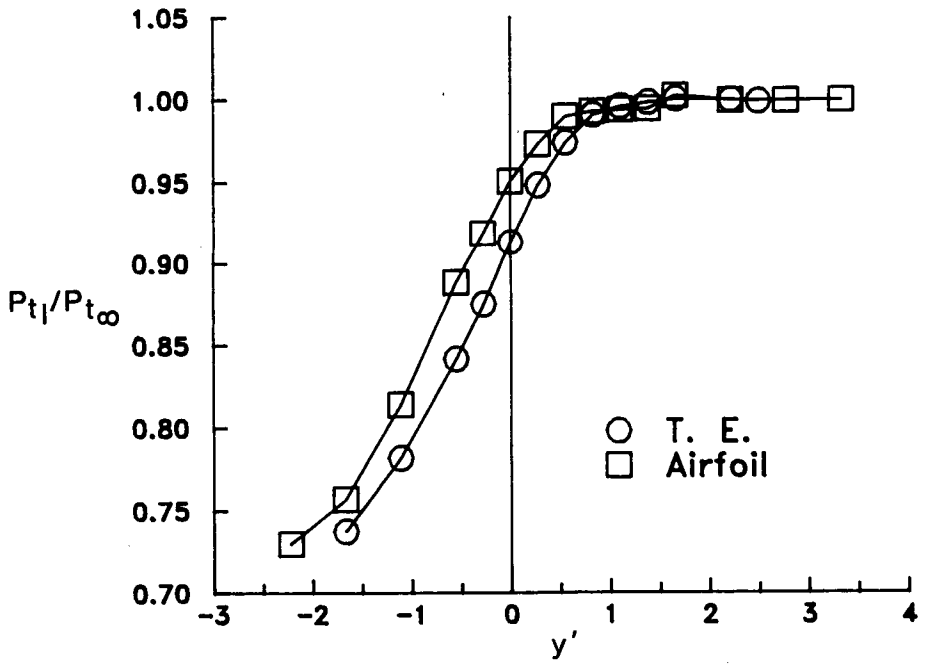

(b) $M_\infty = 0.7$.

Figure 50.- Comparison of tunnel-empty and airfoil total pressures measured through the slot in the 6- By 19-Inch Tunnel.

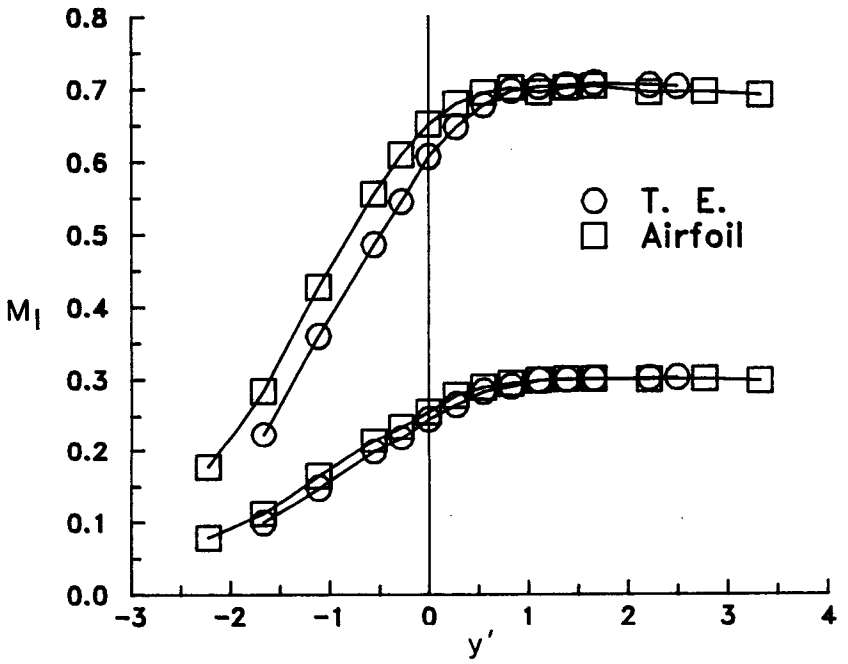

Figure 51.- Comparison of tunnel-empty and airfoil Mach numbers measured through the slot in the 6- By 19-inch Tunnel.

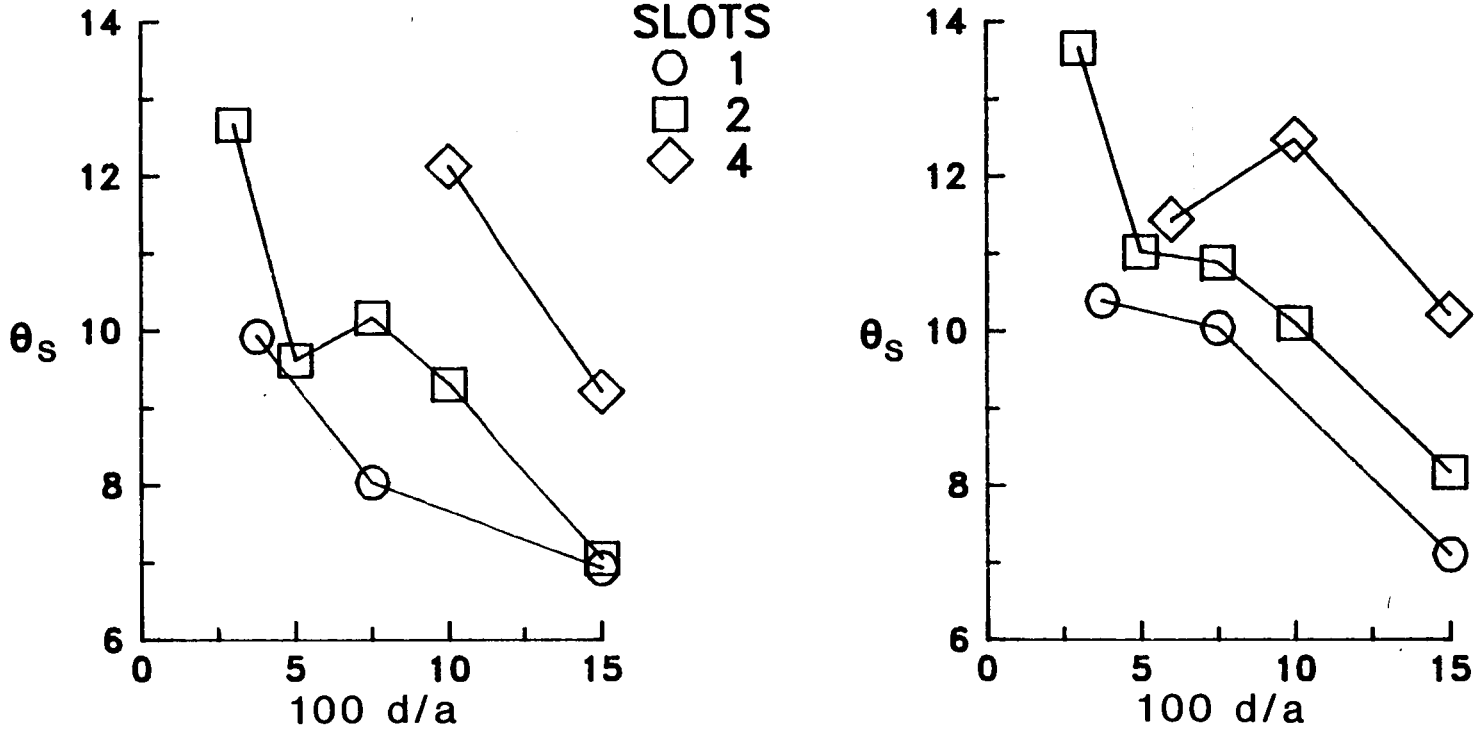

(a) Tunnel empty.

(b) Airfoil.

Figure 52.- Summary of measured flow angles in the slot, $M_\infty = 0.7$.

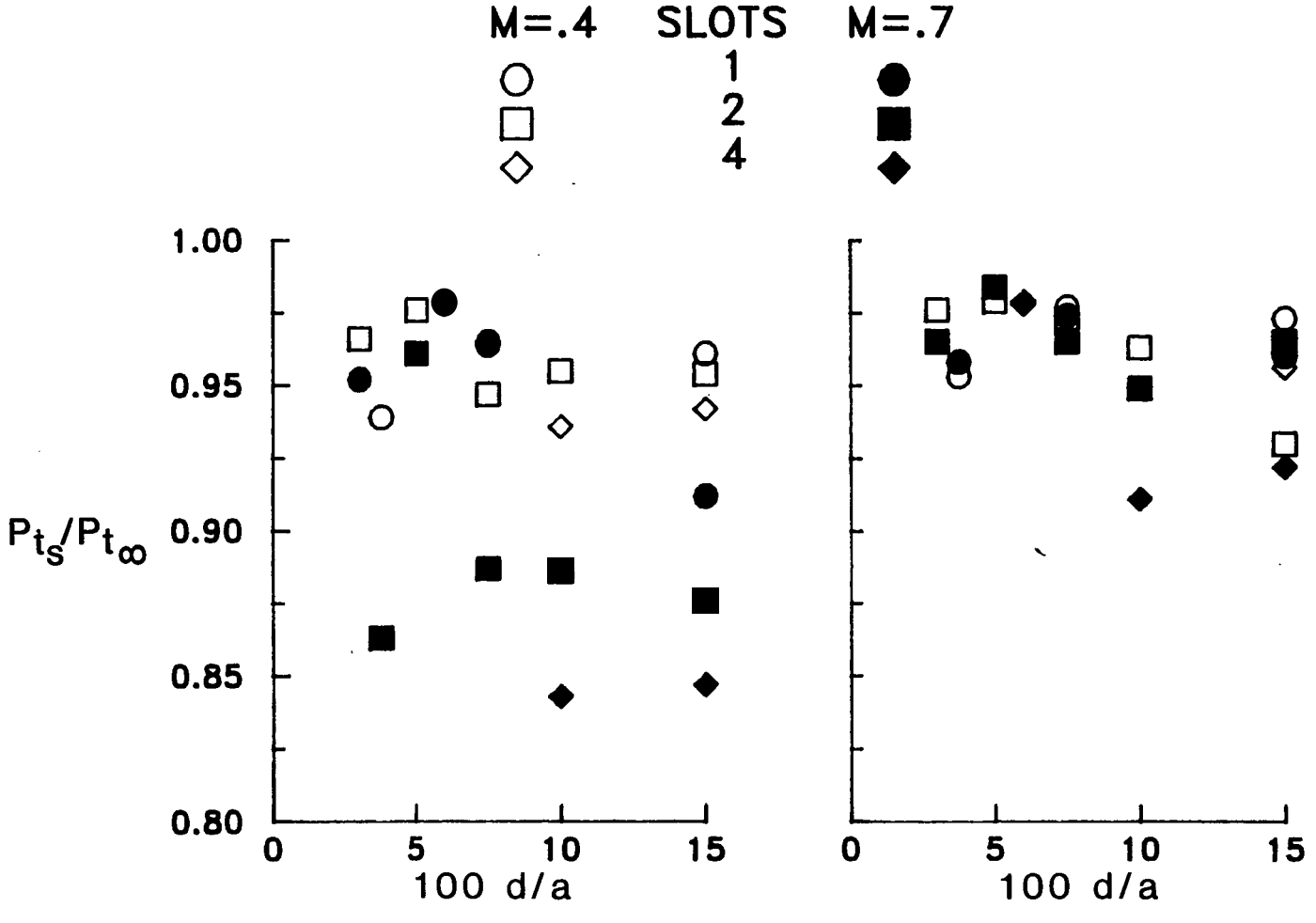

(a) Tunnel empty.

(b) Airfoil.

Figure 53.- Summary of measured total pressures the slot.

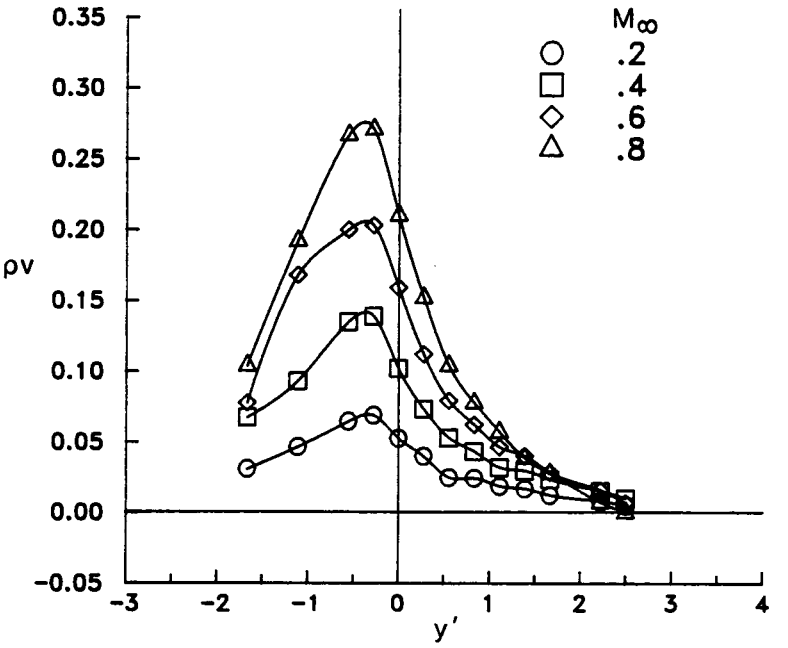

(a) Transverse mass flux.

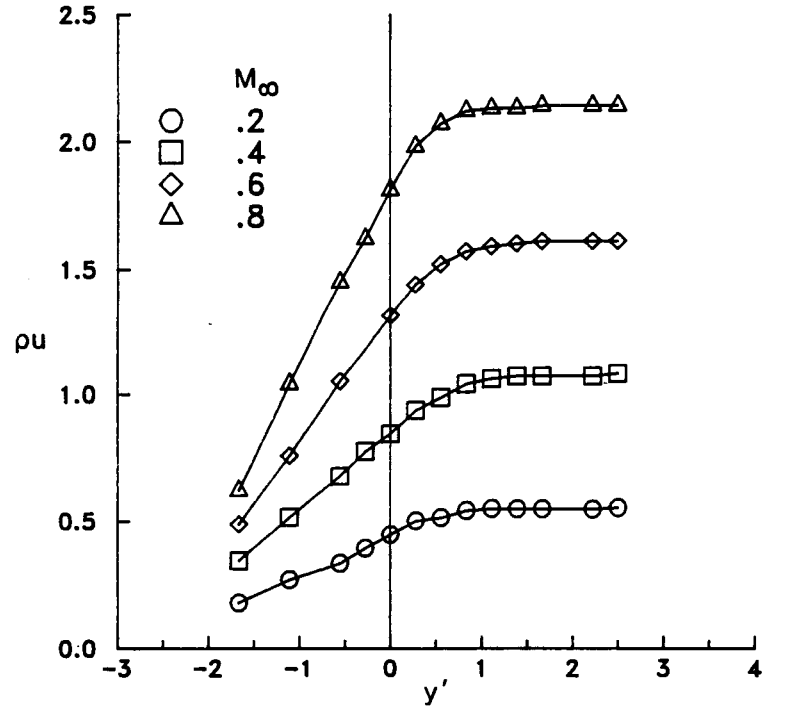

(b) Longitudinal mass flux.

Figure 54.- Effect of Mach number on the variation of tunnel-empty mass flux through the slot.

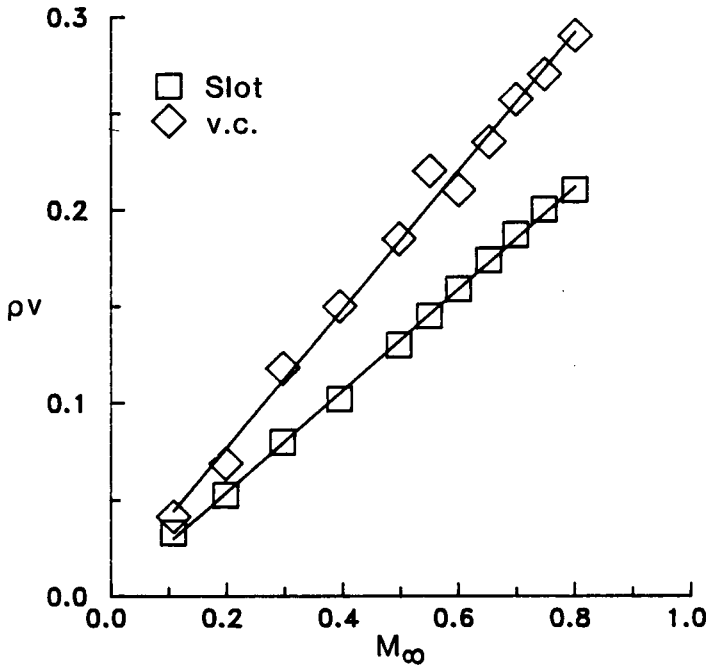

(a) Transverse mass flux.

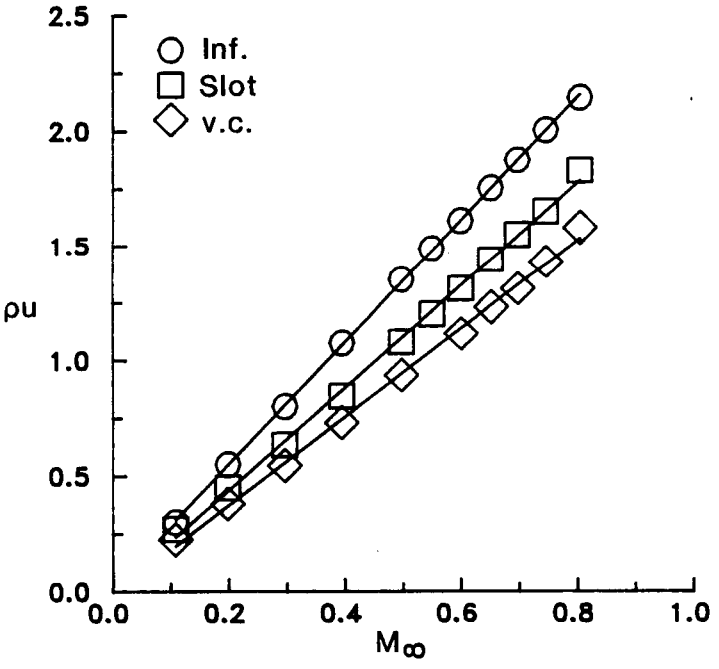

(b) Longitudinal mass flux.

Figure 55.- Tunnel-empty mass flux variation for the 15-1 wall.

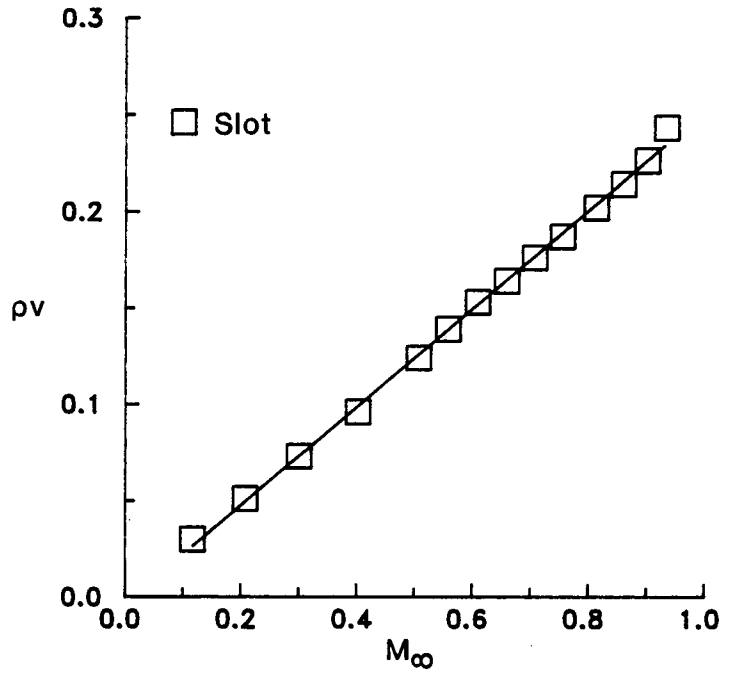

(a) Transverse mass flux.

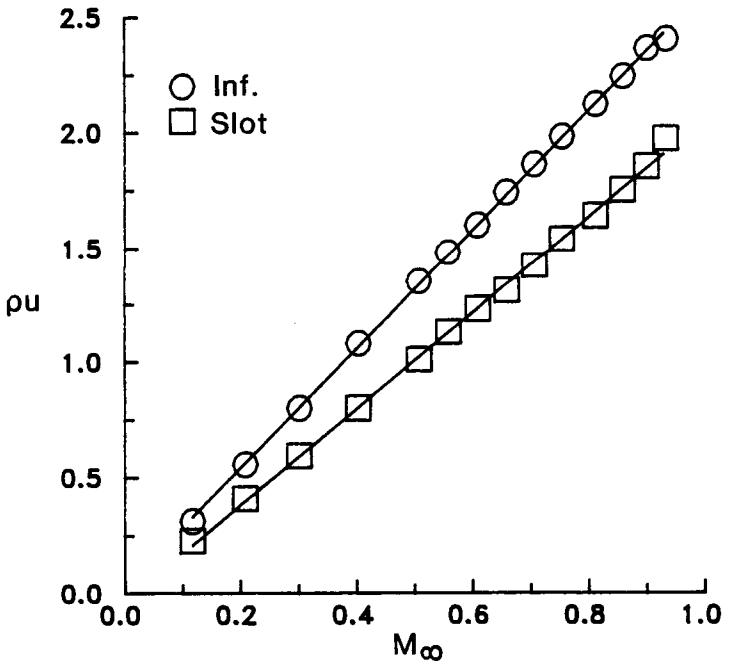

(b) Longitudinal mass flux.

Figure 56.- Tunnel-empty mass flux variation for the 15-2 wall.

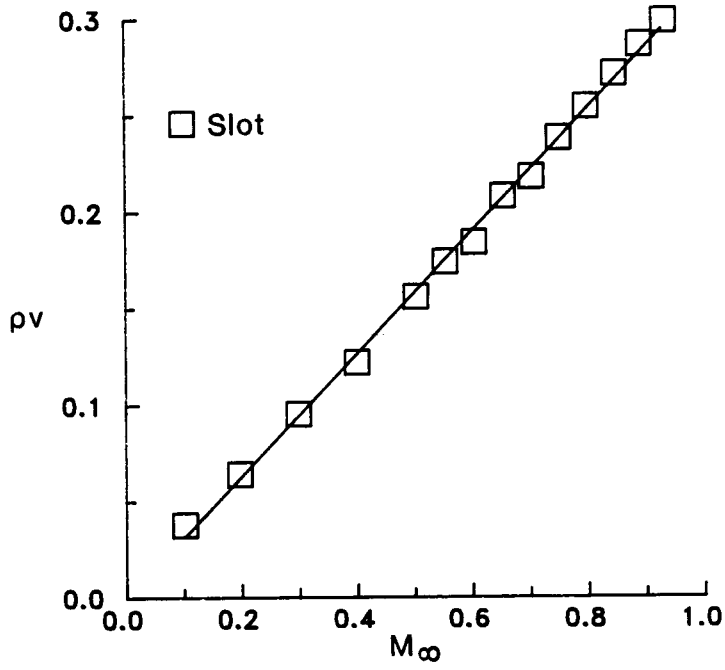

(a) Transverse mass flux.

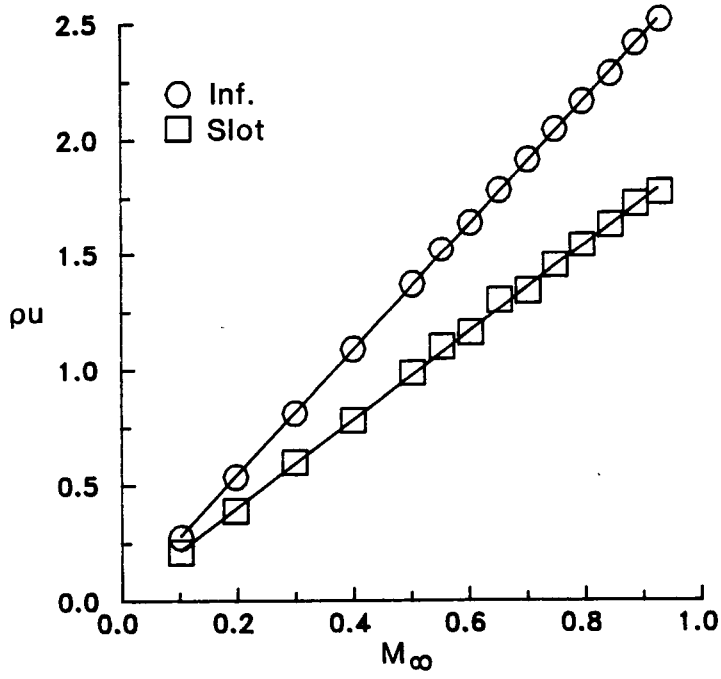

(b) Longitudinal mass flux.

Figure 57.- Tunnel-empty mass flux variation for the 15-4 wall.

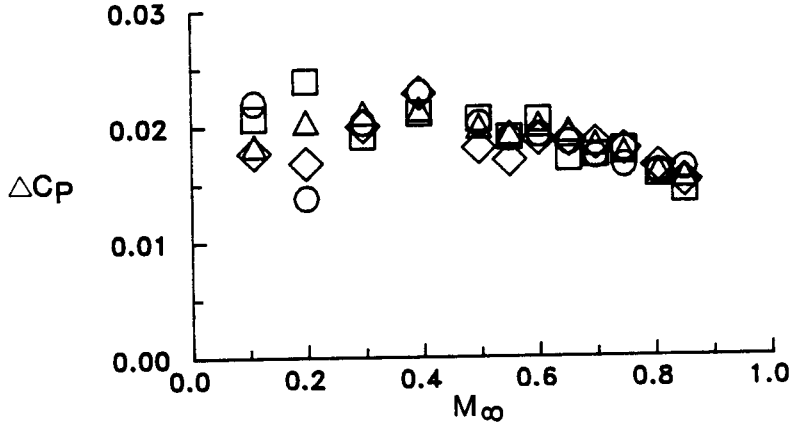

(a) 15-1 wall.

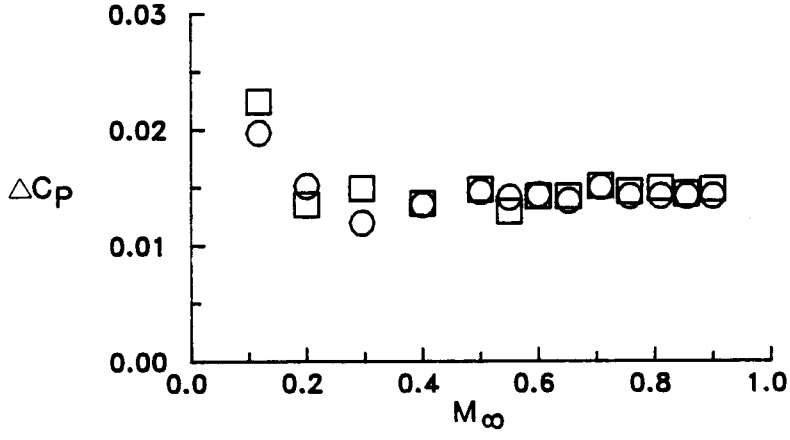

(b) 15-2 wall.

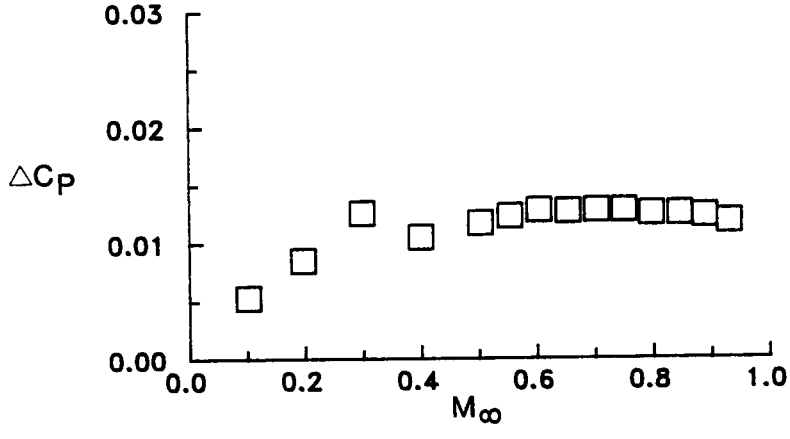

(c) 15-4 wall.

Figure 58.- Slotted-wall pressure drop at the probe station.

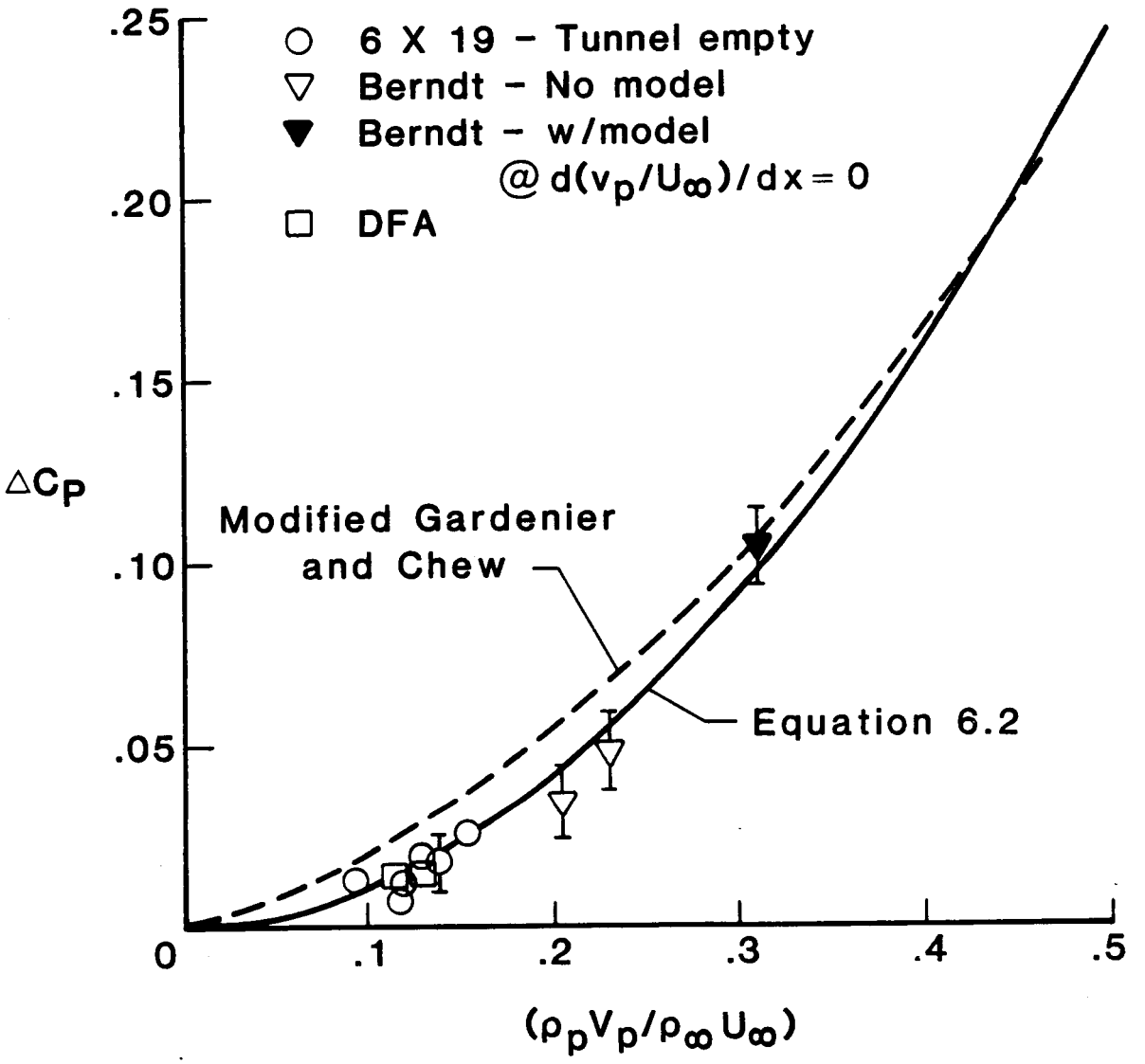

Figure 59.- Correlation of the tunnel-empty wall-pressure drop with slot flow angle.

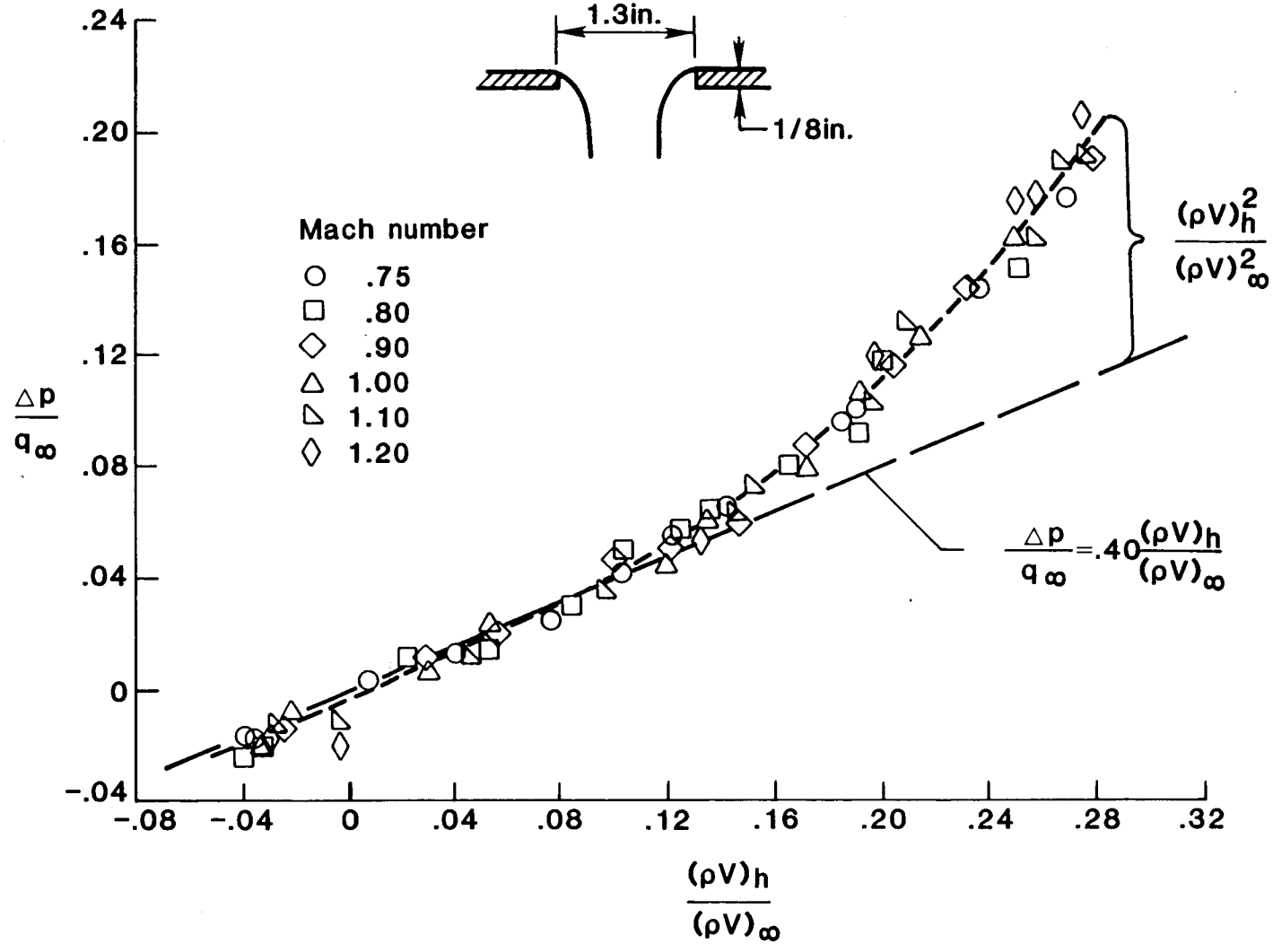

(a) Slotted-wall cross-flow characteristics for various Mach numbers.

Figure 60.- Gardenier and Chew data from ref. 28.

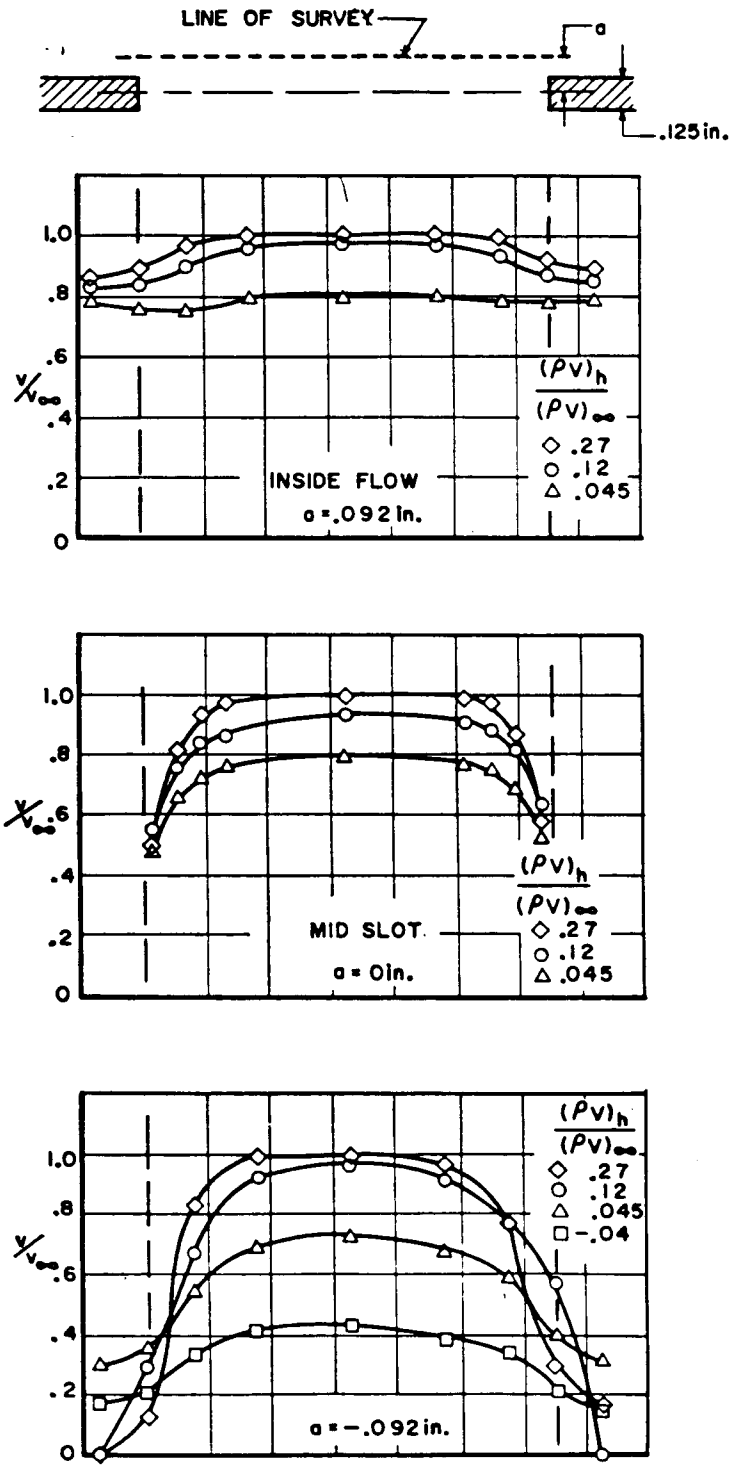

(b) Cross-flow characteristics of a single slot. $M_\infty = 0.75$.

Figure 60.- Concluded.

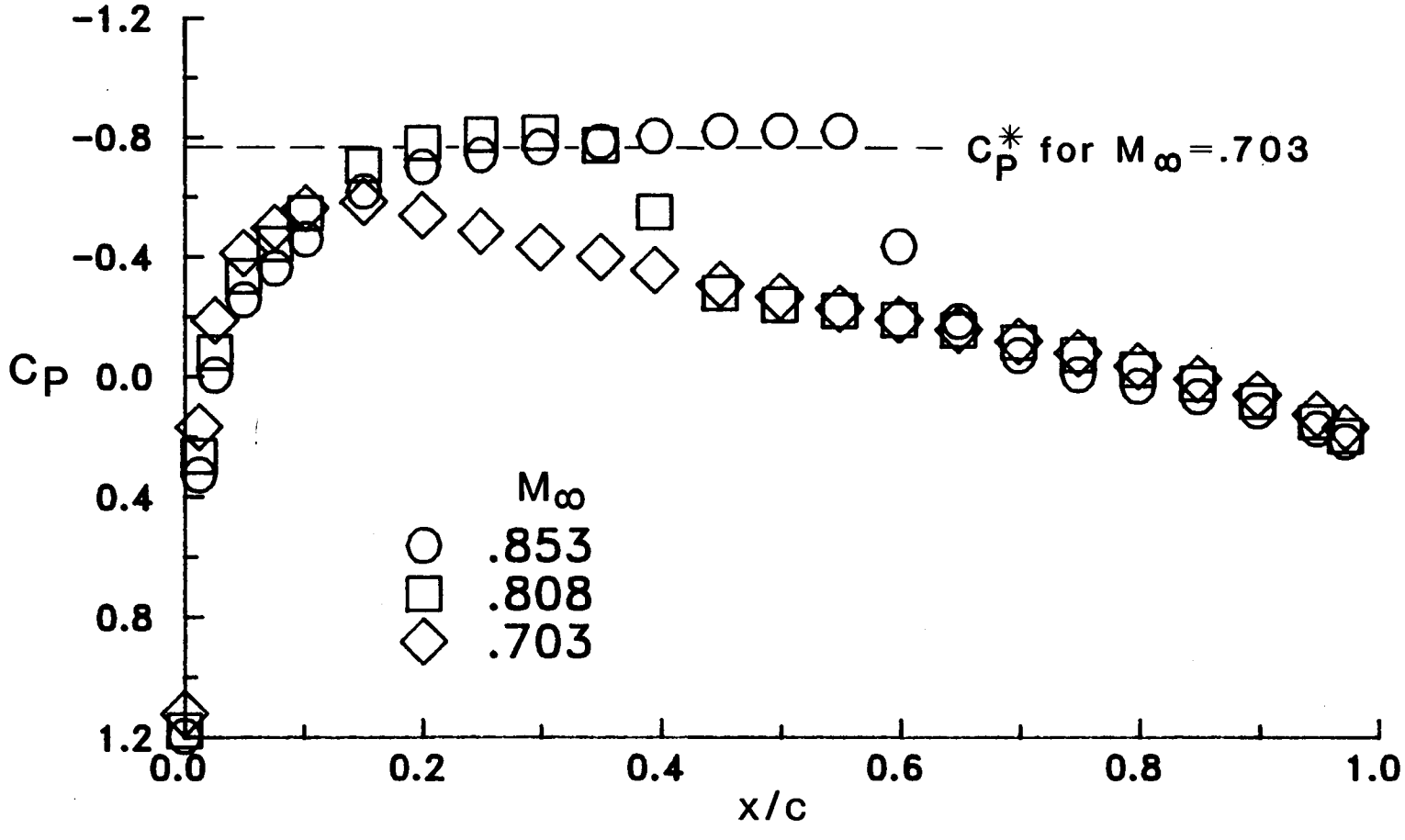

Figure 61.- Effect of Mach number on the typical upper-surface pressure distribution of an NACA 0012 airfoil. C_n= 0.0, 15-1 wall.

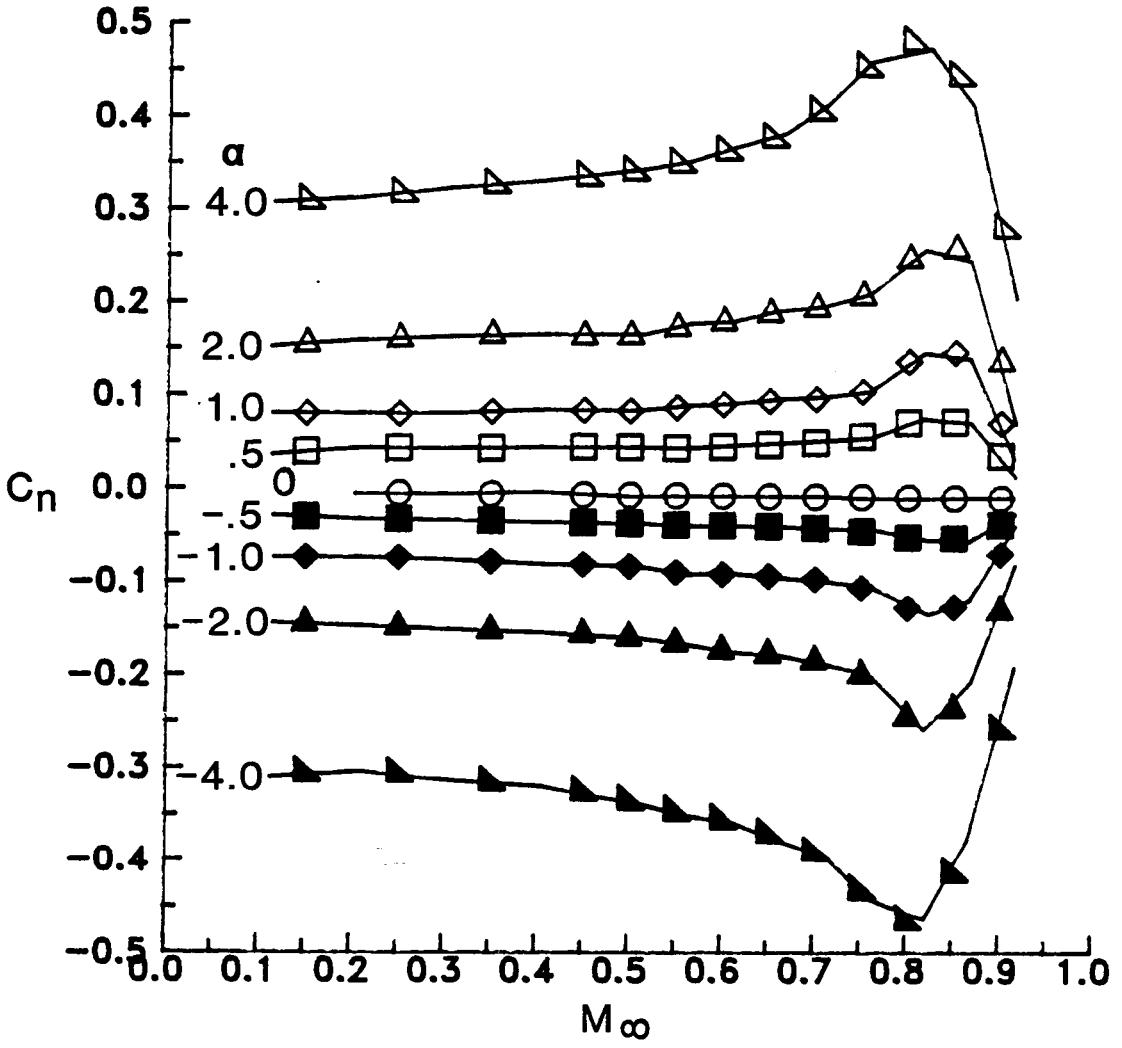

(a) Normal force.

Figure 62.- Typical NACA 0012 airfoil force measurements in the 6X19. 15-1 wall.

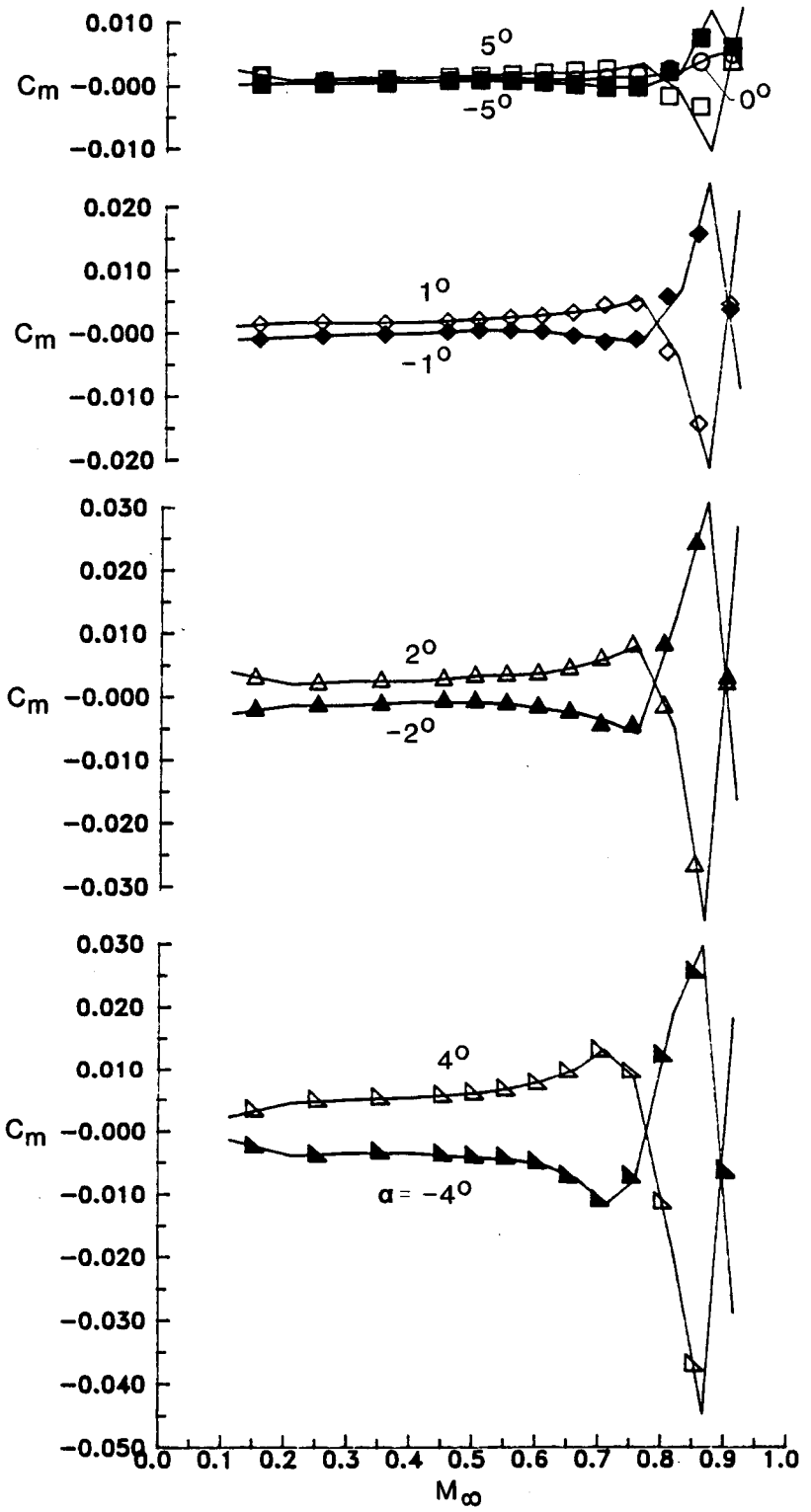

(b) Pitching moment.

Figure 62.- Concluded.

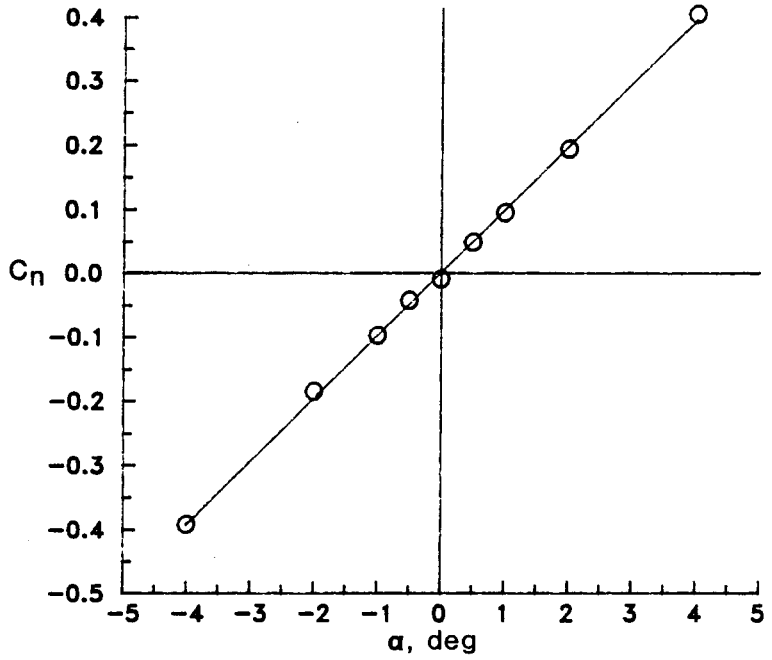

(a) Normal force.

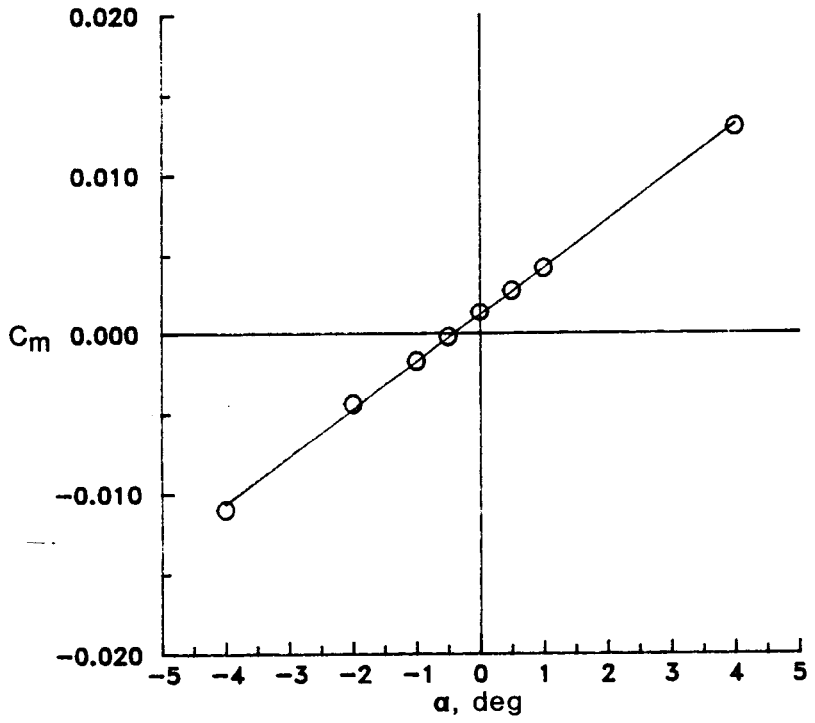

(b) Pitching moment.

Figure 63.- Variation of NACA 0012 airfoil force measurements with angle of attack in the 6X19. $M_\infty = 0.7$.

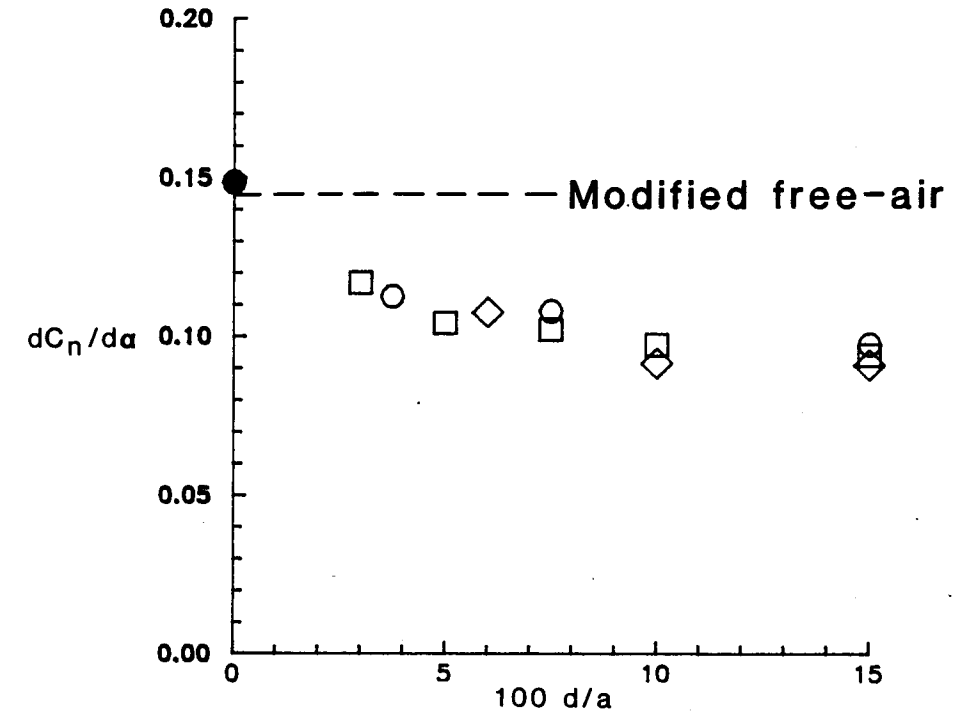

(a) Normal force.

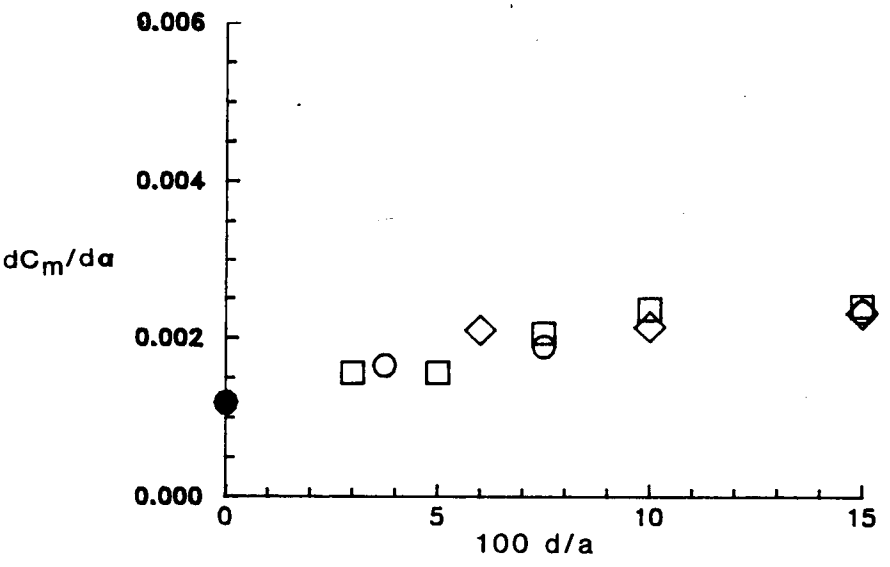

(b) Pitching moment.

Figure 64.- Variation of the airfoil force-curve slopes with wall openness.

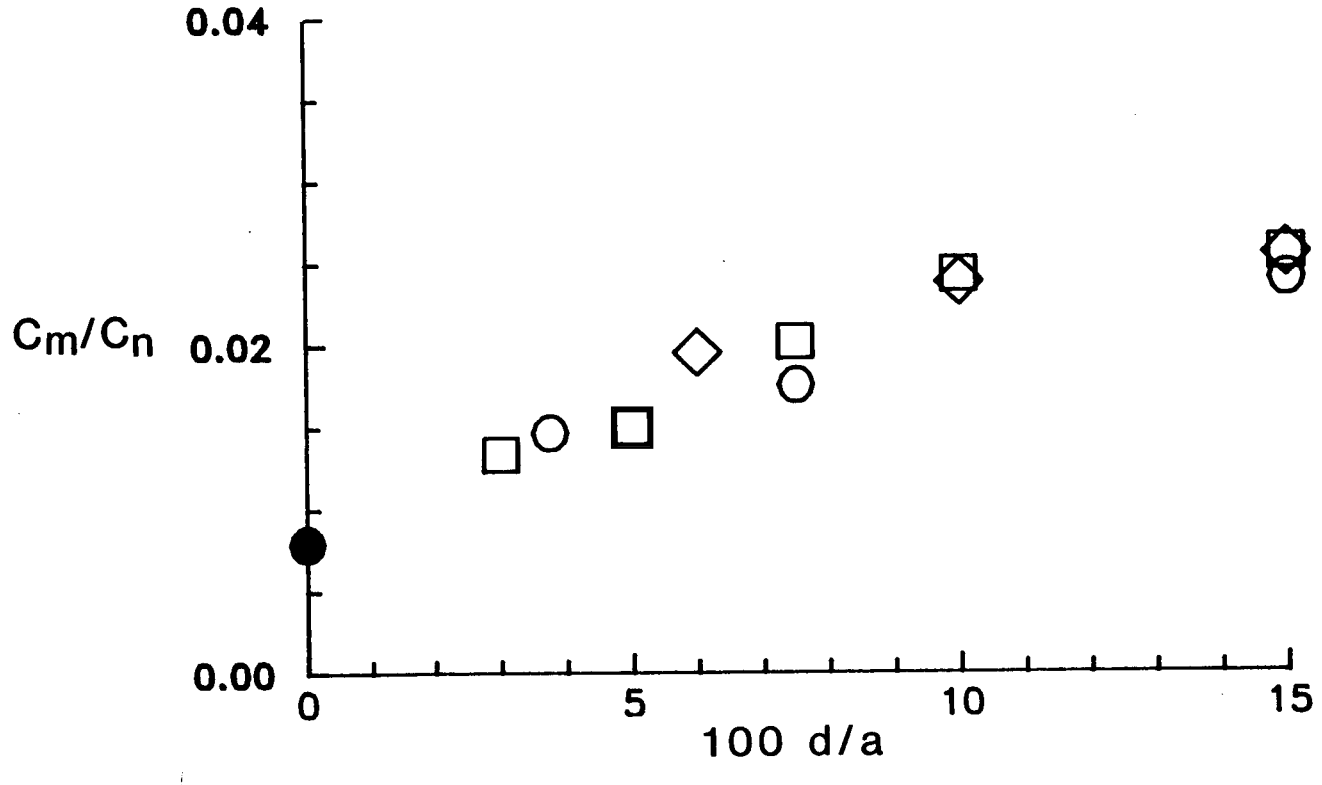

Figure 65.- Influence of wall openness ratio on the location of the airfoil aerodynamic center.

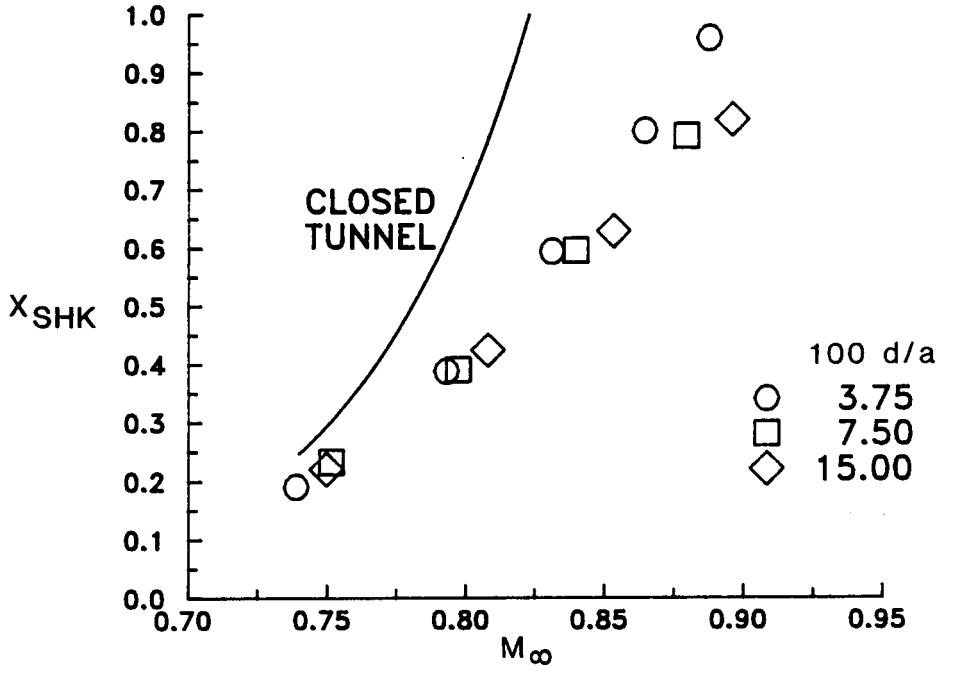

(a) One slot.

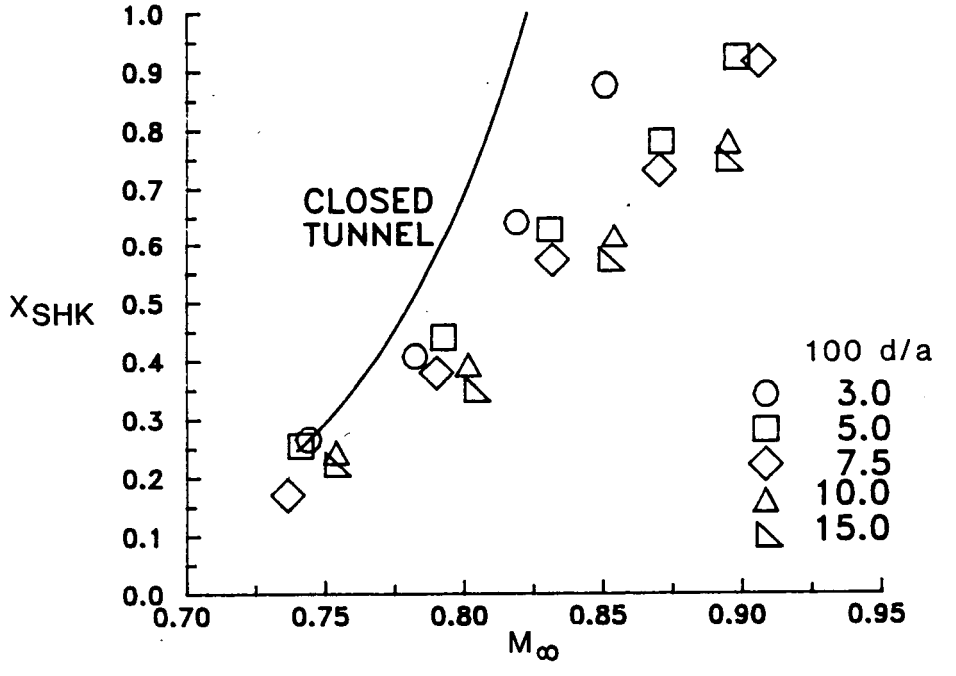

(b) Two slots.

Figure 66.- Variation of airfoil shock location with Mach number in the 6X19.

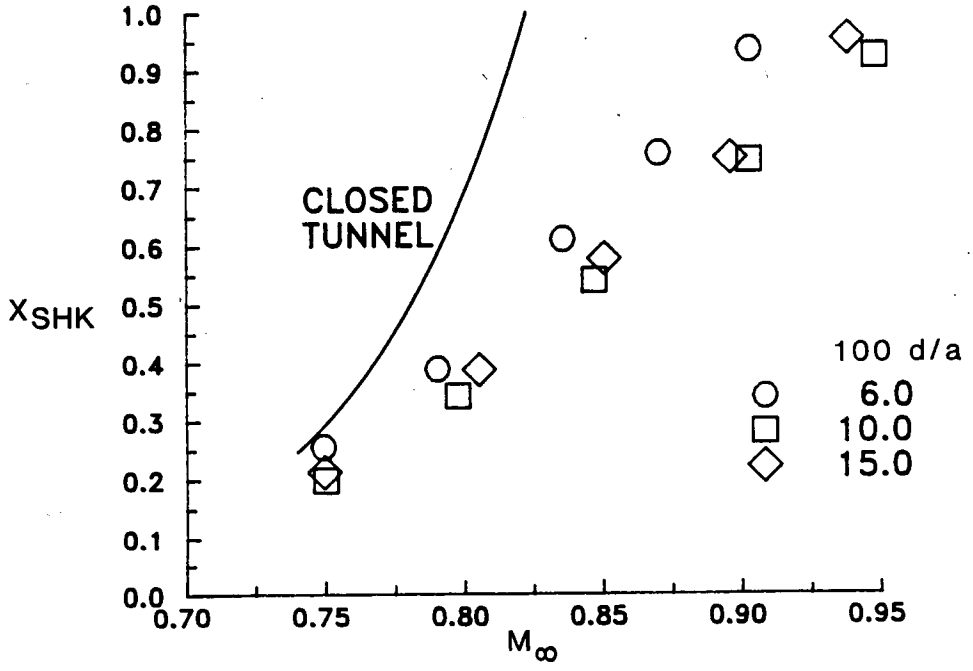

(c) Four slots.

Figure 66.- Concluded.

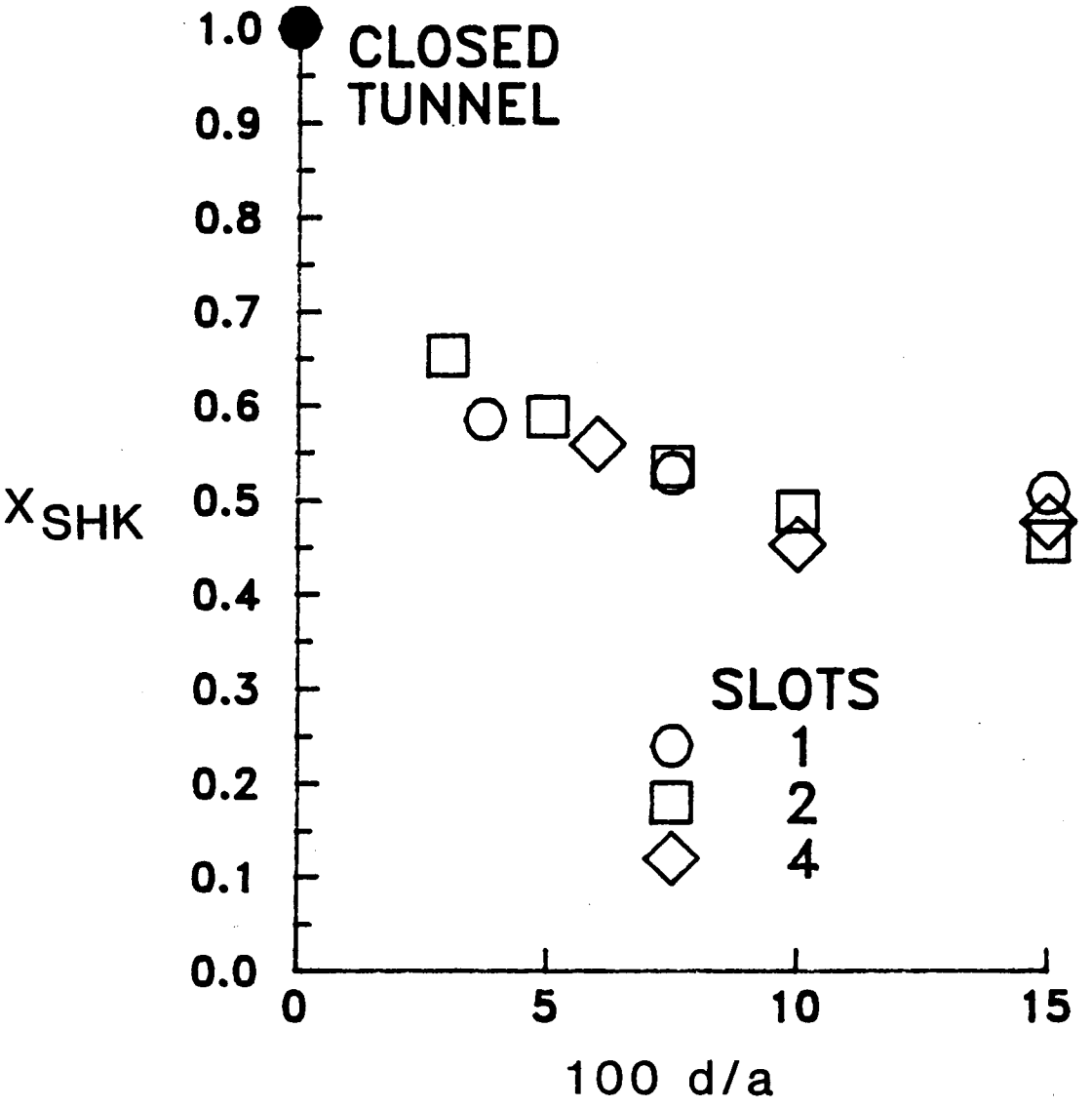

Figure 67.- Variation of airfoil shock location with wall openness ratio in the 6X19. $M_\infty = 0.8227$, $C_n = 0.0$.

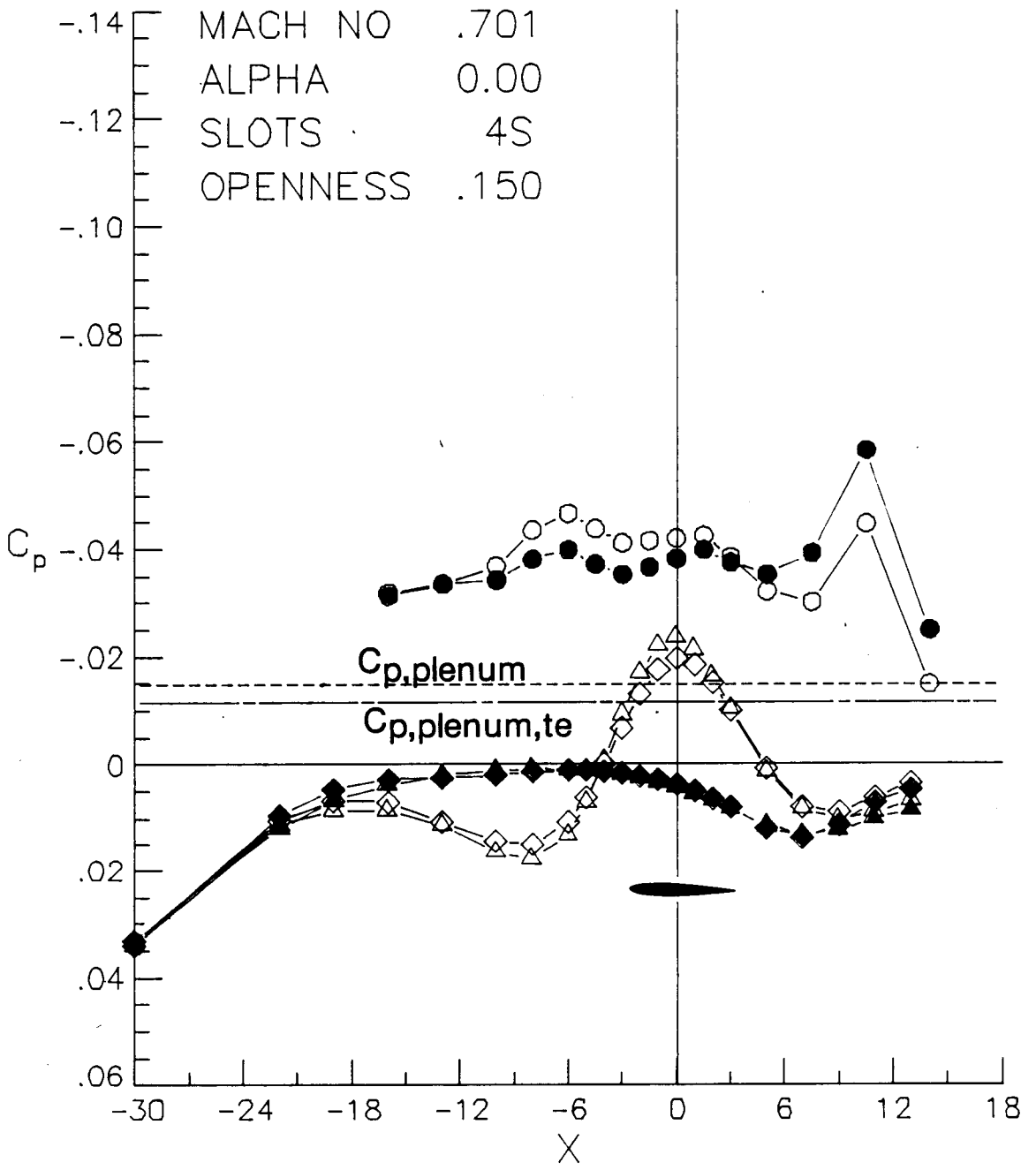

Figure 68.- Typical 6X19 wall-pressure measurements. $M_\infty = 0.7$, $\alpha = 0$, 15-4 wall.

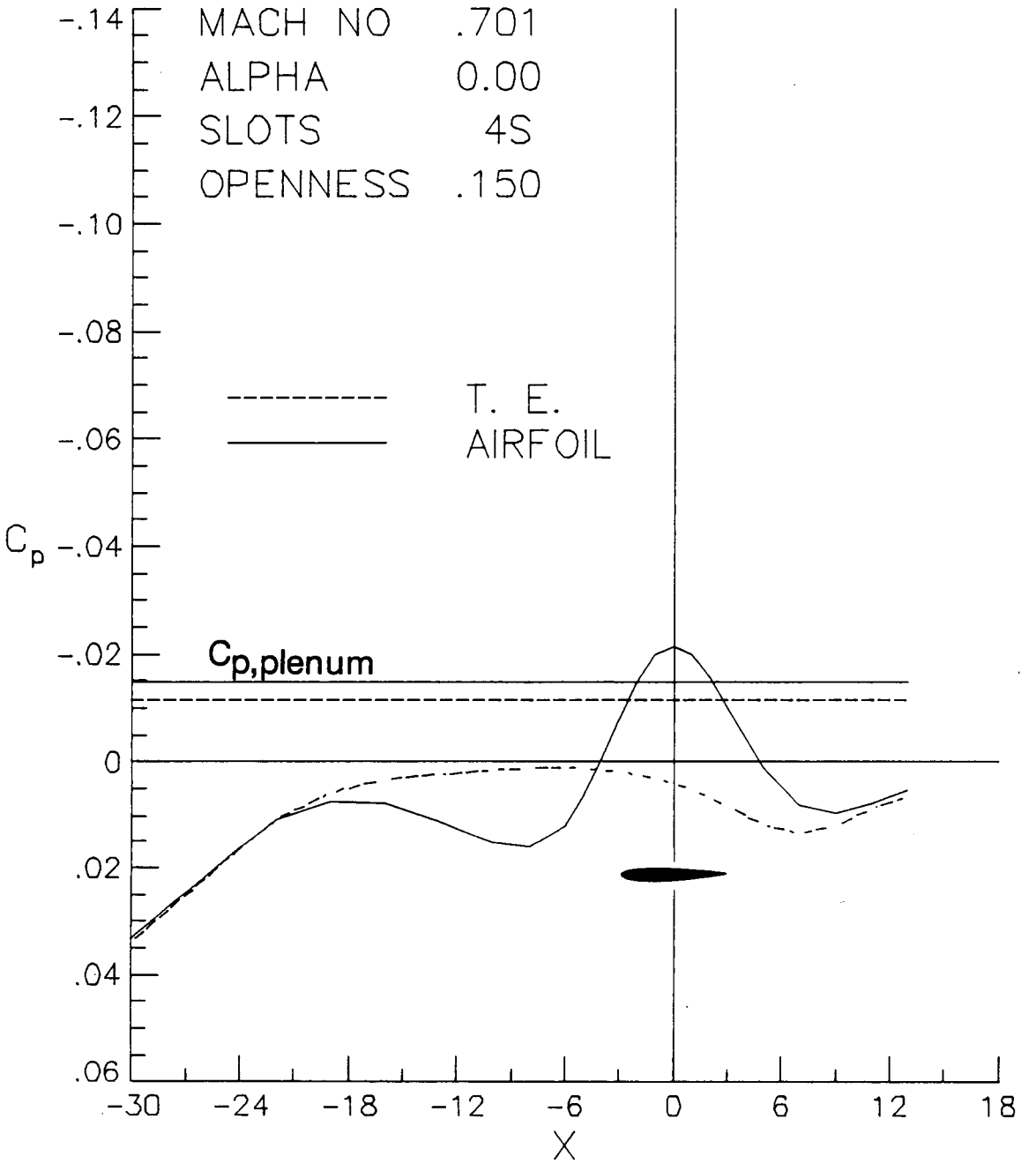

Figure 69.- Smoothed 6X19 wall-pressure measurements. $M_\infty = 0.7$, $\alpha = 0$, 15-4 wall.

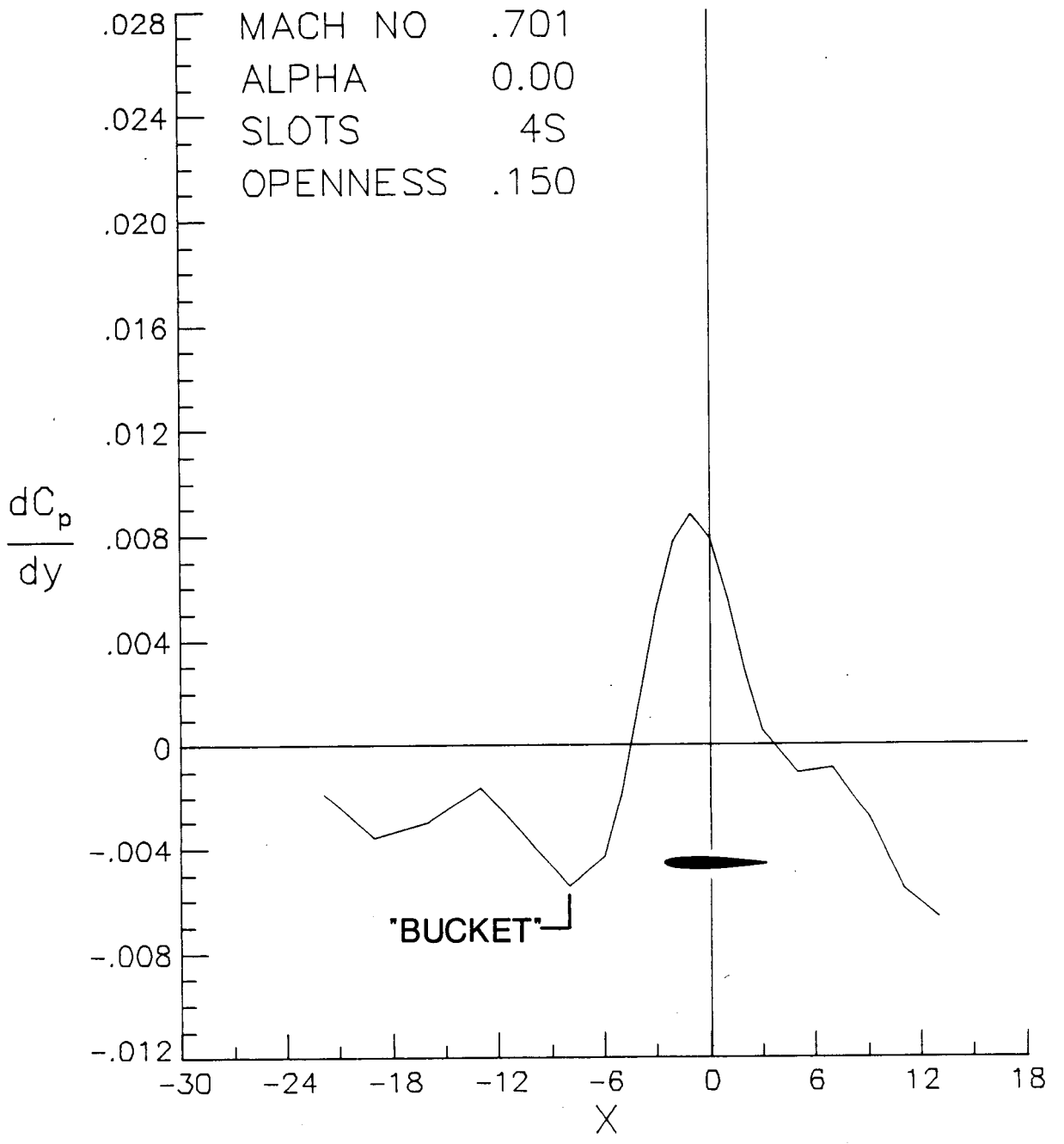

Figure 70.- Computed 6X19 normal pressure gradient. $M_\infty = 0.7$, $\alpha = 0$, 15-4 wall.

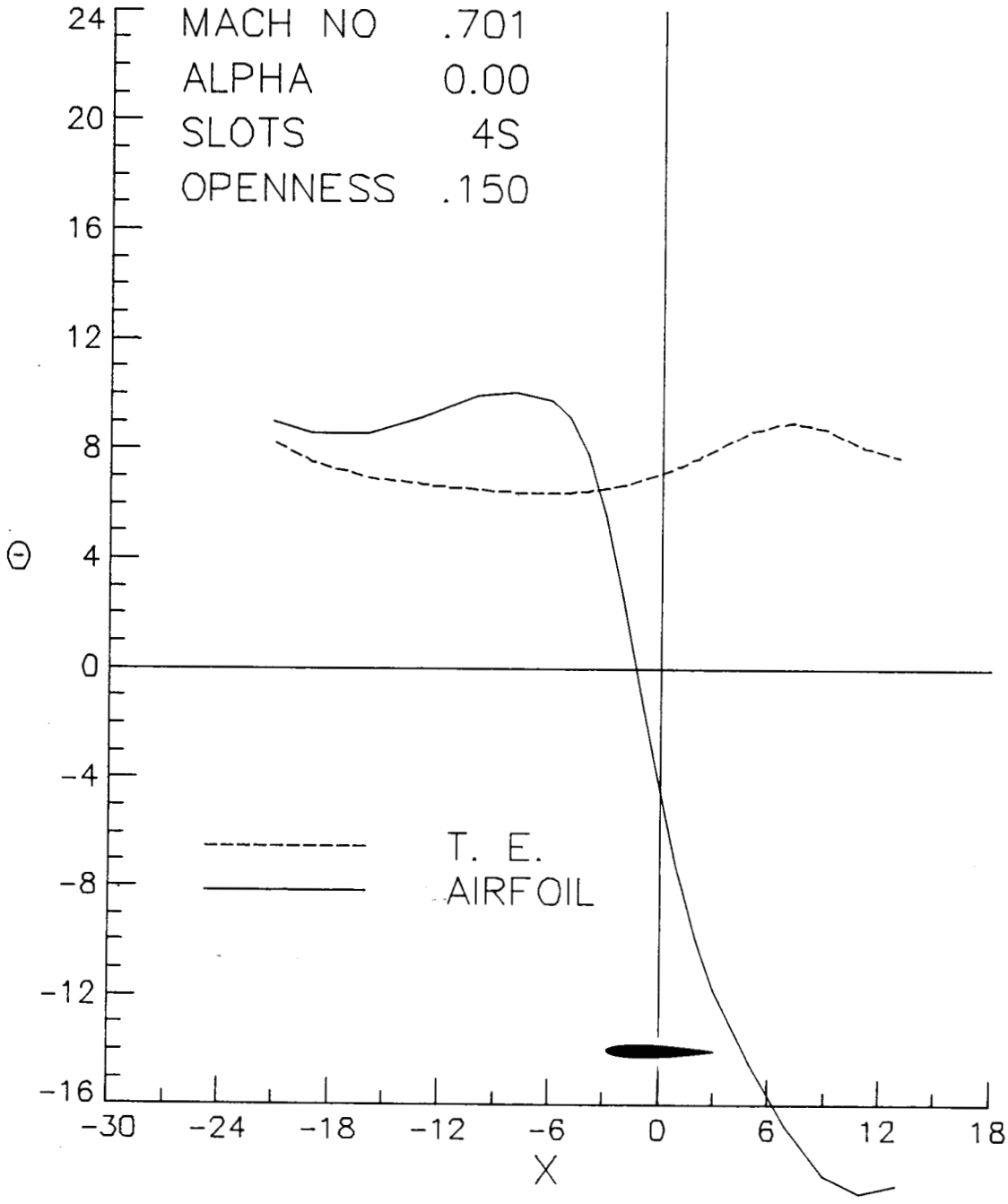

Figure 71.- Computed 6X19 slot flow angle. $M_\infty = 0.7$, $\alpha = 0$, 15-4 wall.

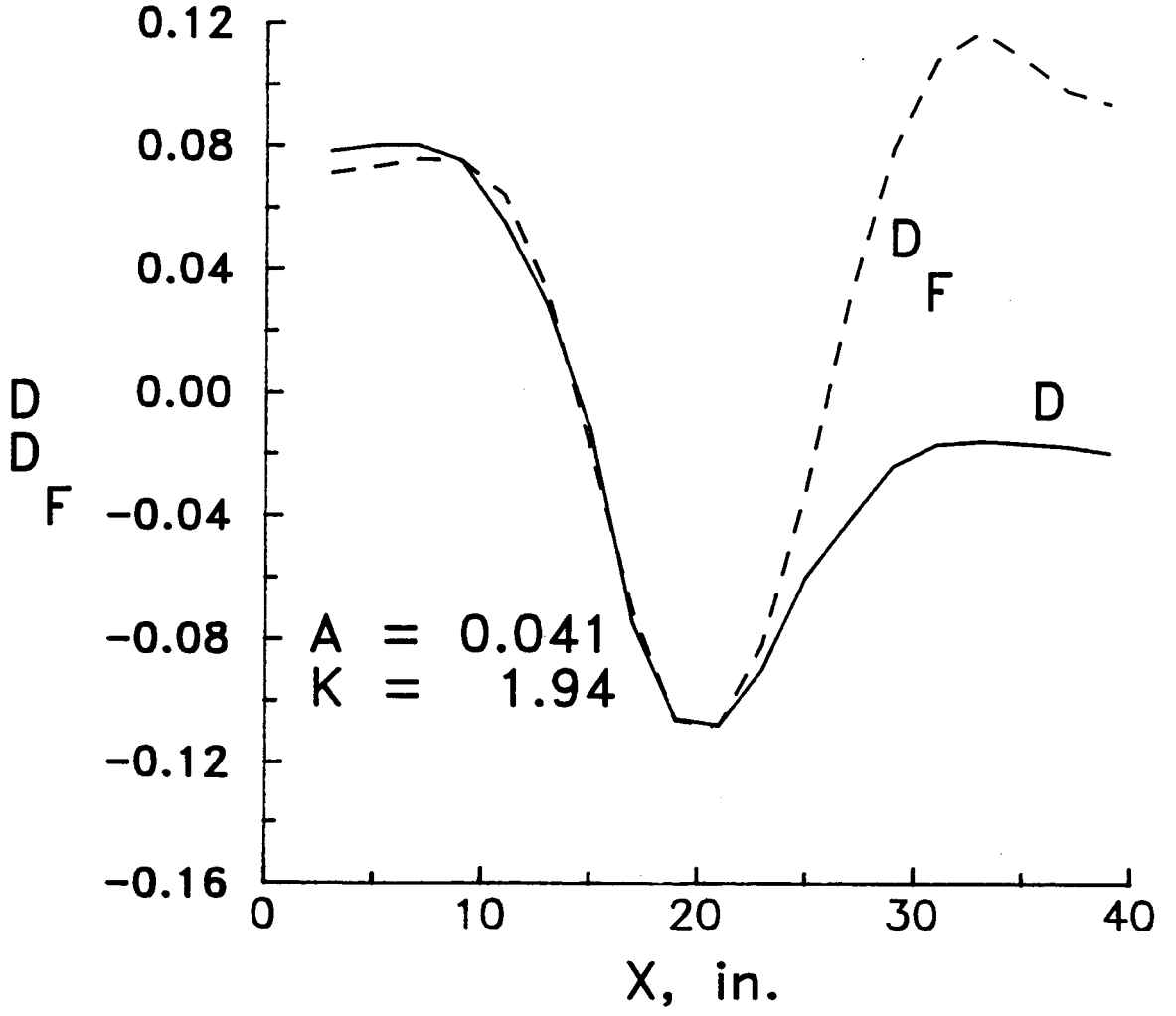

Figure 72.- Analysis of Chen and Mears' experimental pressure data using the Ideal form of the slotted-wall boundary condition.

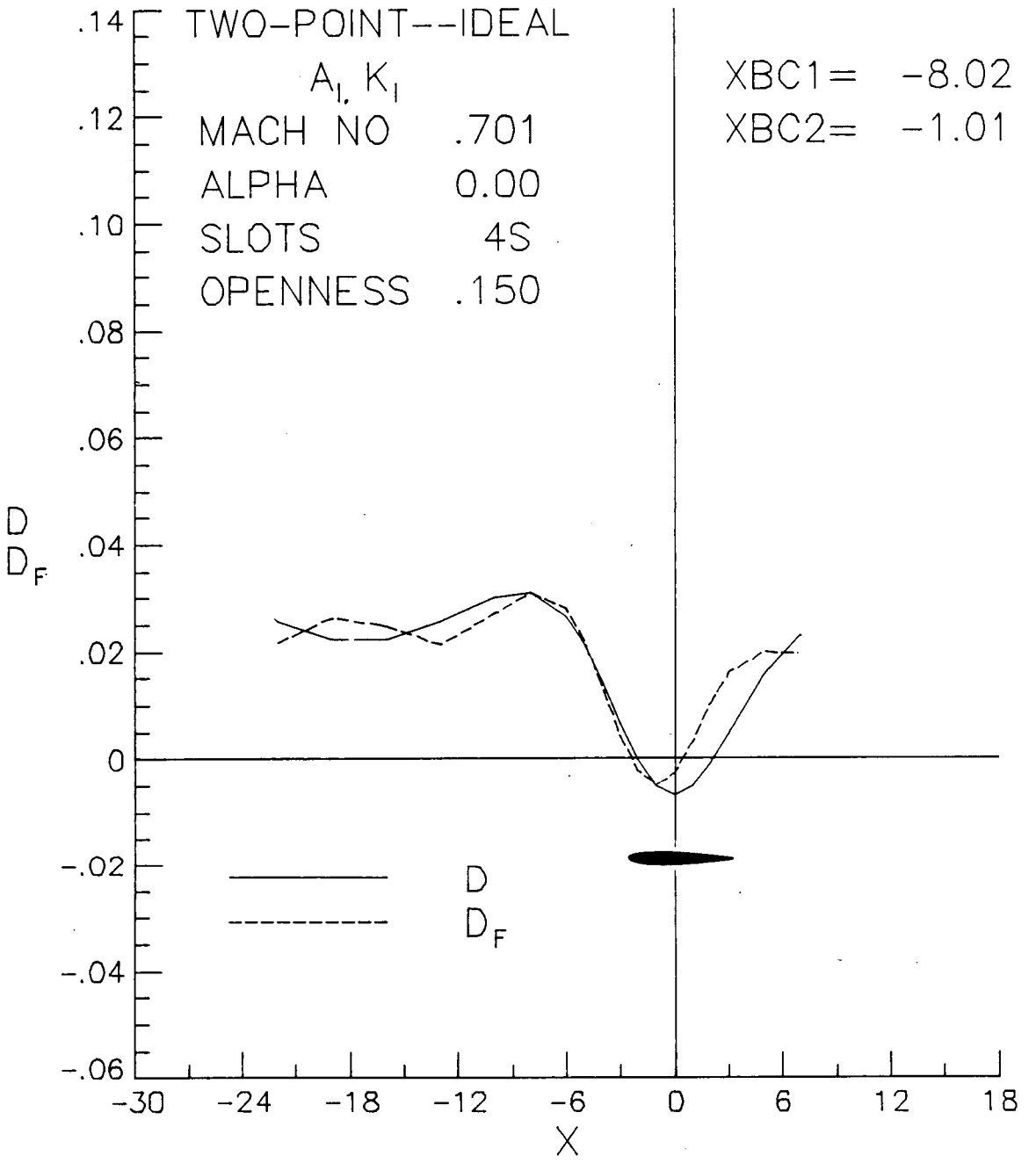

(a) 15-4 wall.

Figure 73.- Analysis of the 6- by 19-inch tunnel data using the Ideal form of the slotted-wall boundary condition. $M_\infty = 0.7$, $\alpha = 0$.

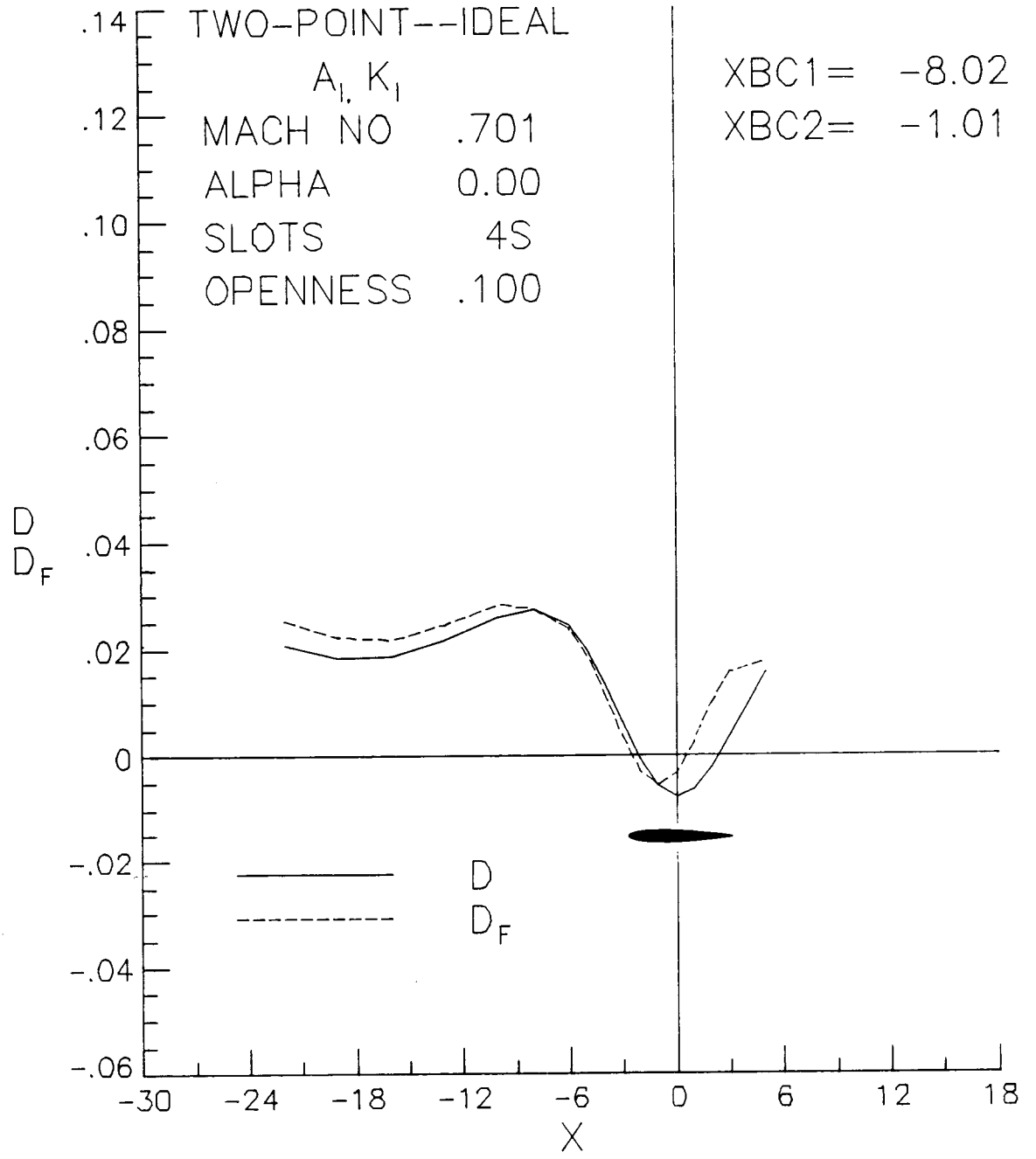

(b) 10-4 wall.

Figure 73.- Continued.

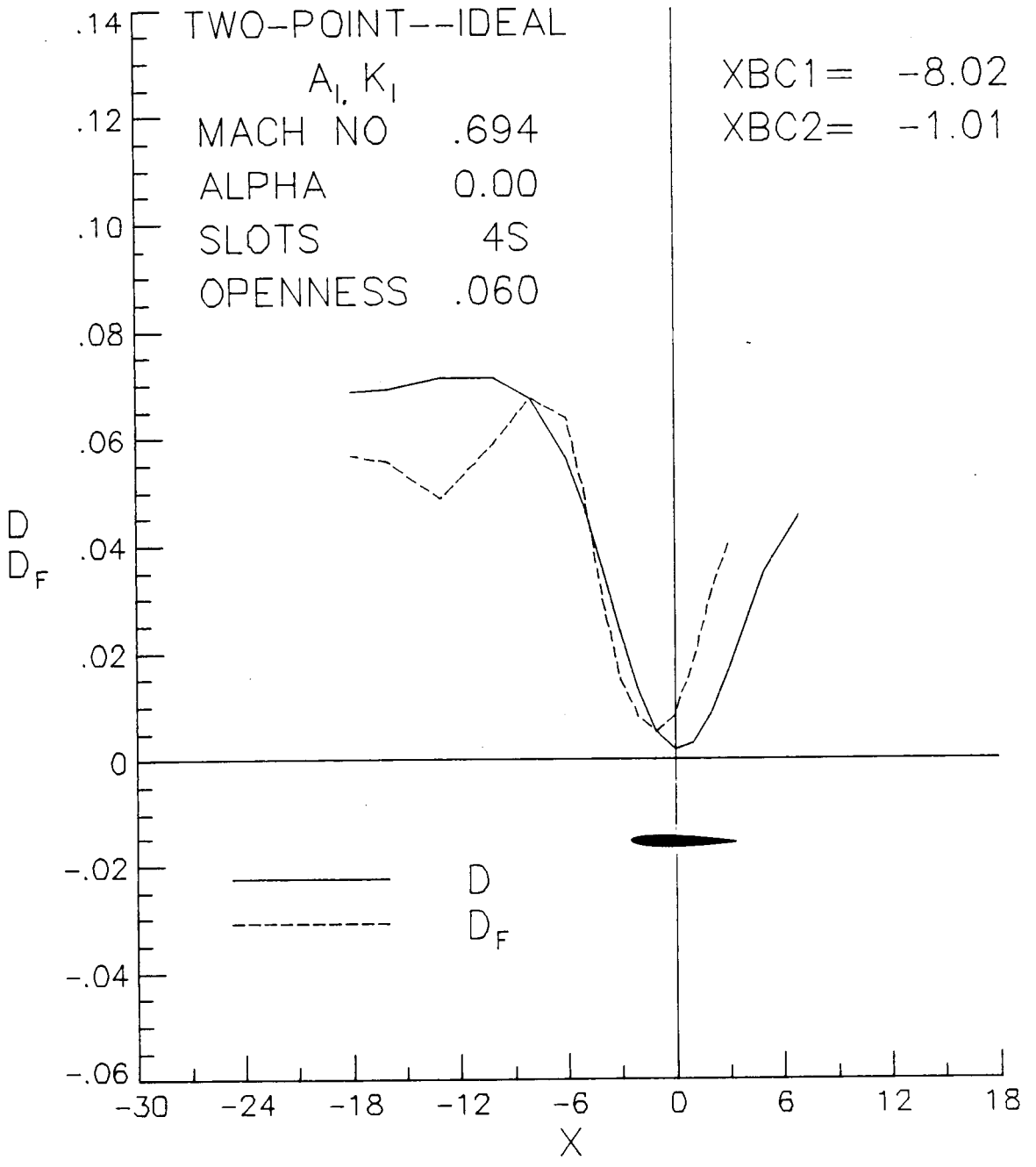

(c) 6-4 wall.

Figure 73.- Concluded.

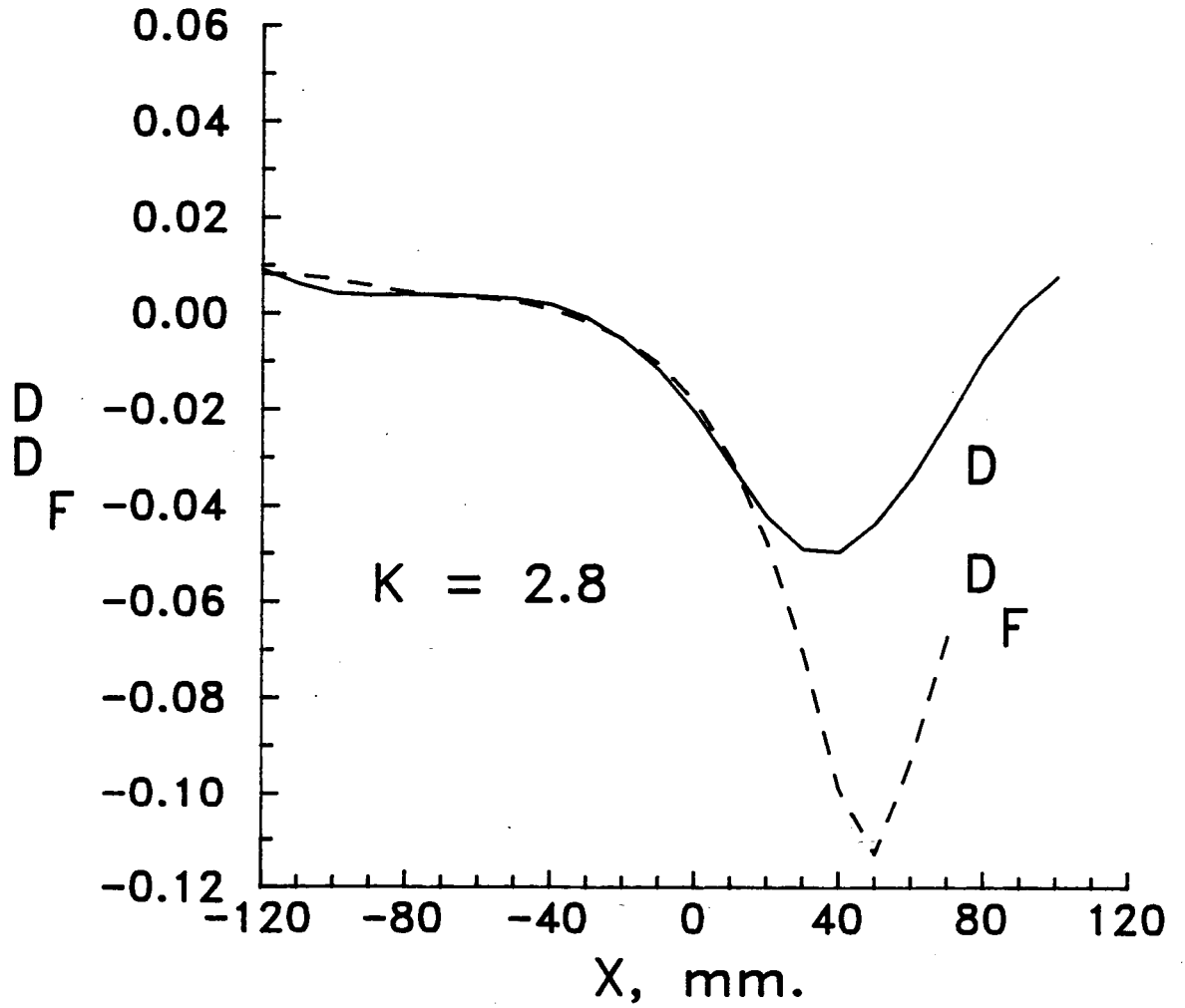

Figure 74.- Berndt's analysis of his experimental pressure data.

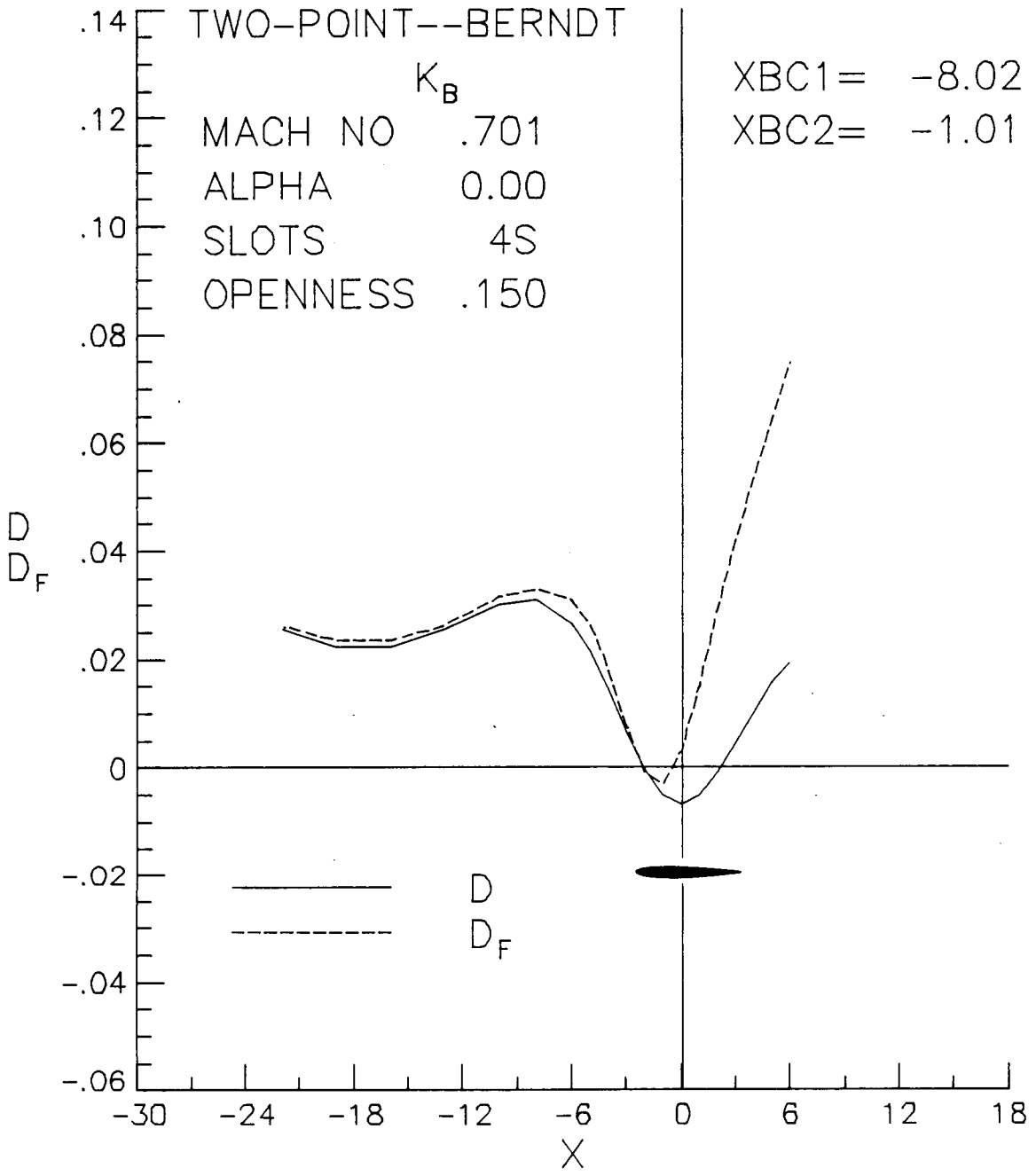

(a) 15-4 wall.

Figure 75.- Analysis of the 6- by 19-inch Tunnel data using Berndt's form of the slotted-wall boundary condition. $M_\infty = 0.7$, $\alpha = 0$.

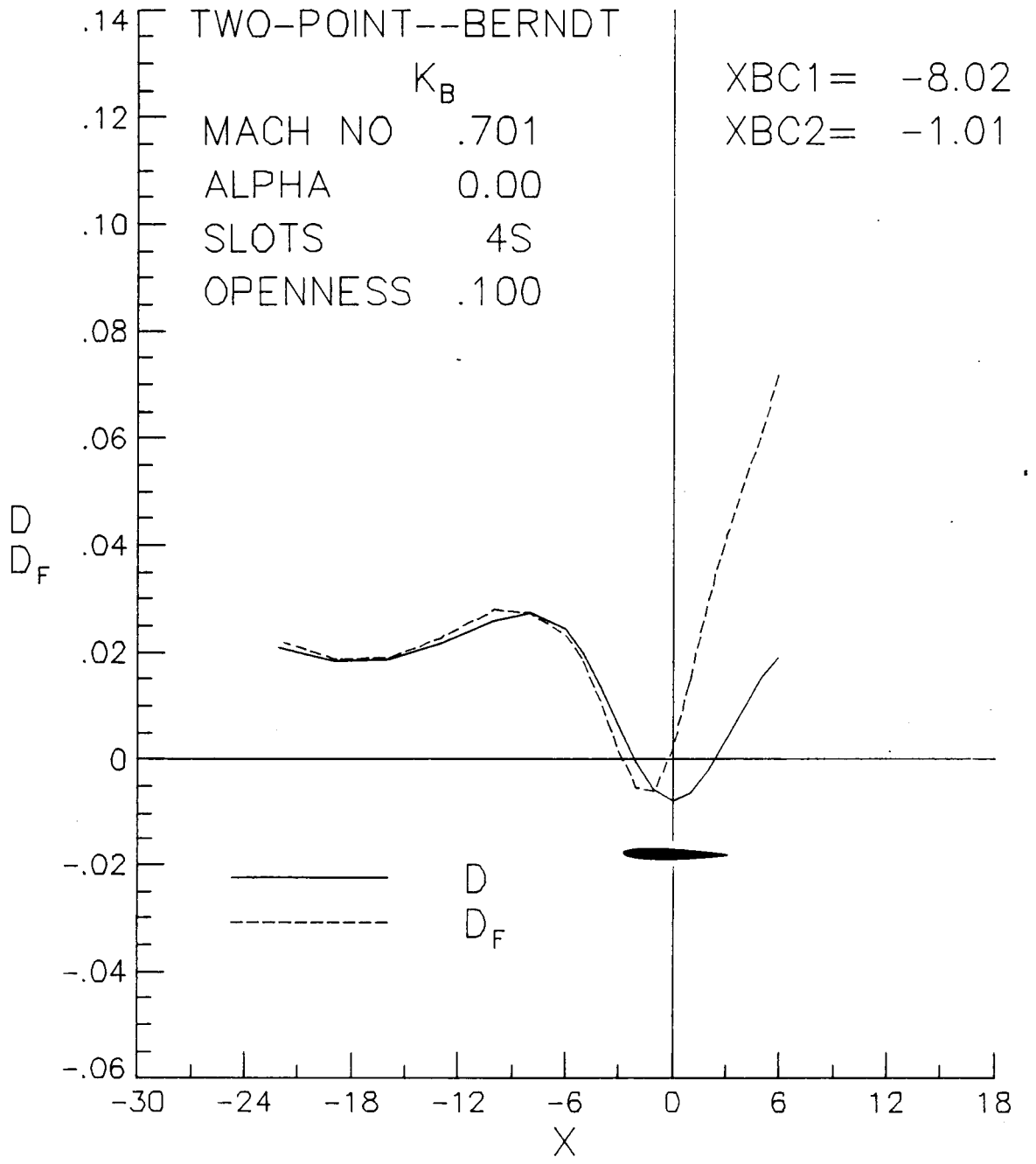

(b) 10-4 wall.

Figure 75.- Continued.

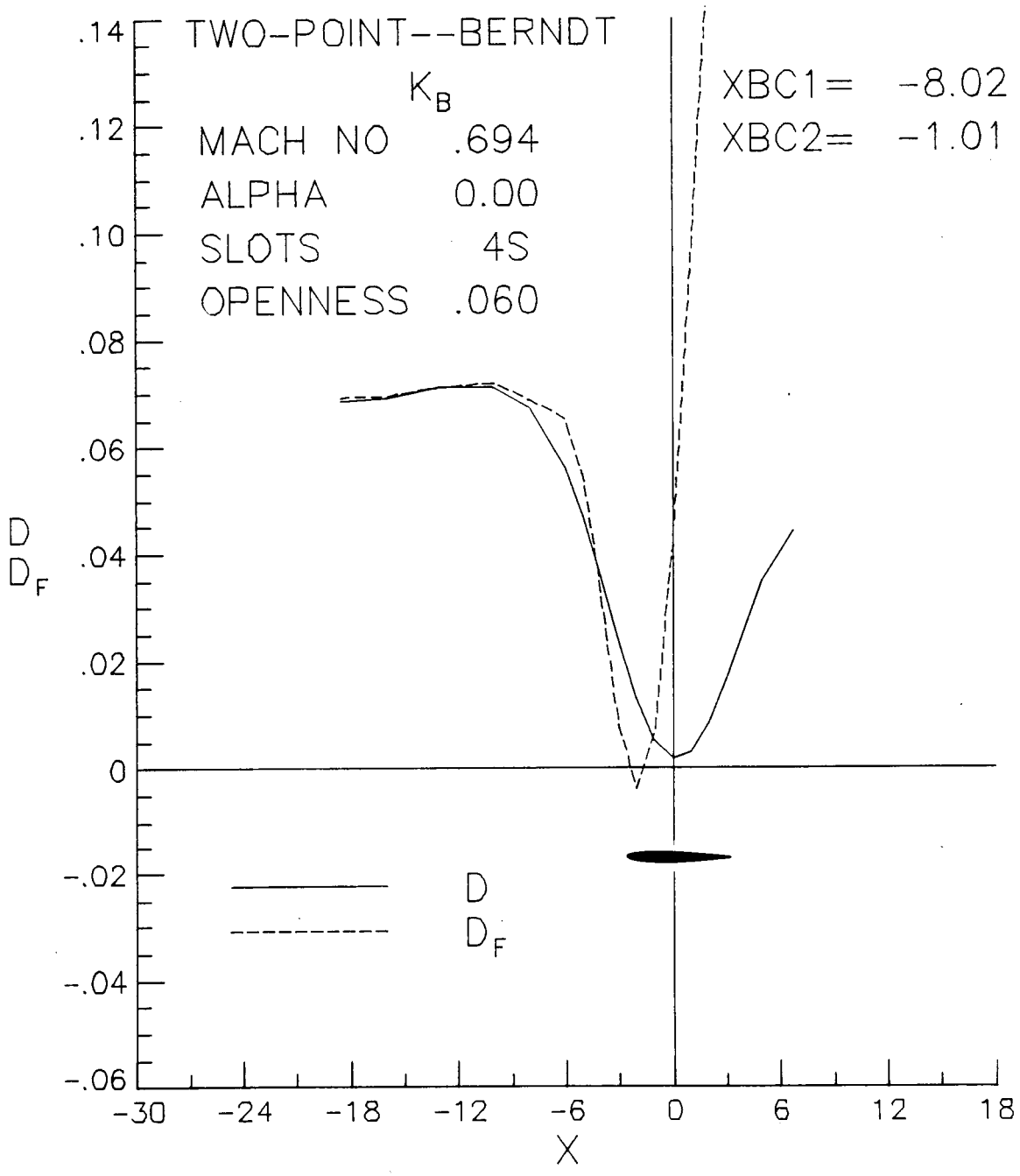

(c) 6-4 wall.

Figure 75.- Concluded.

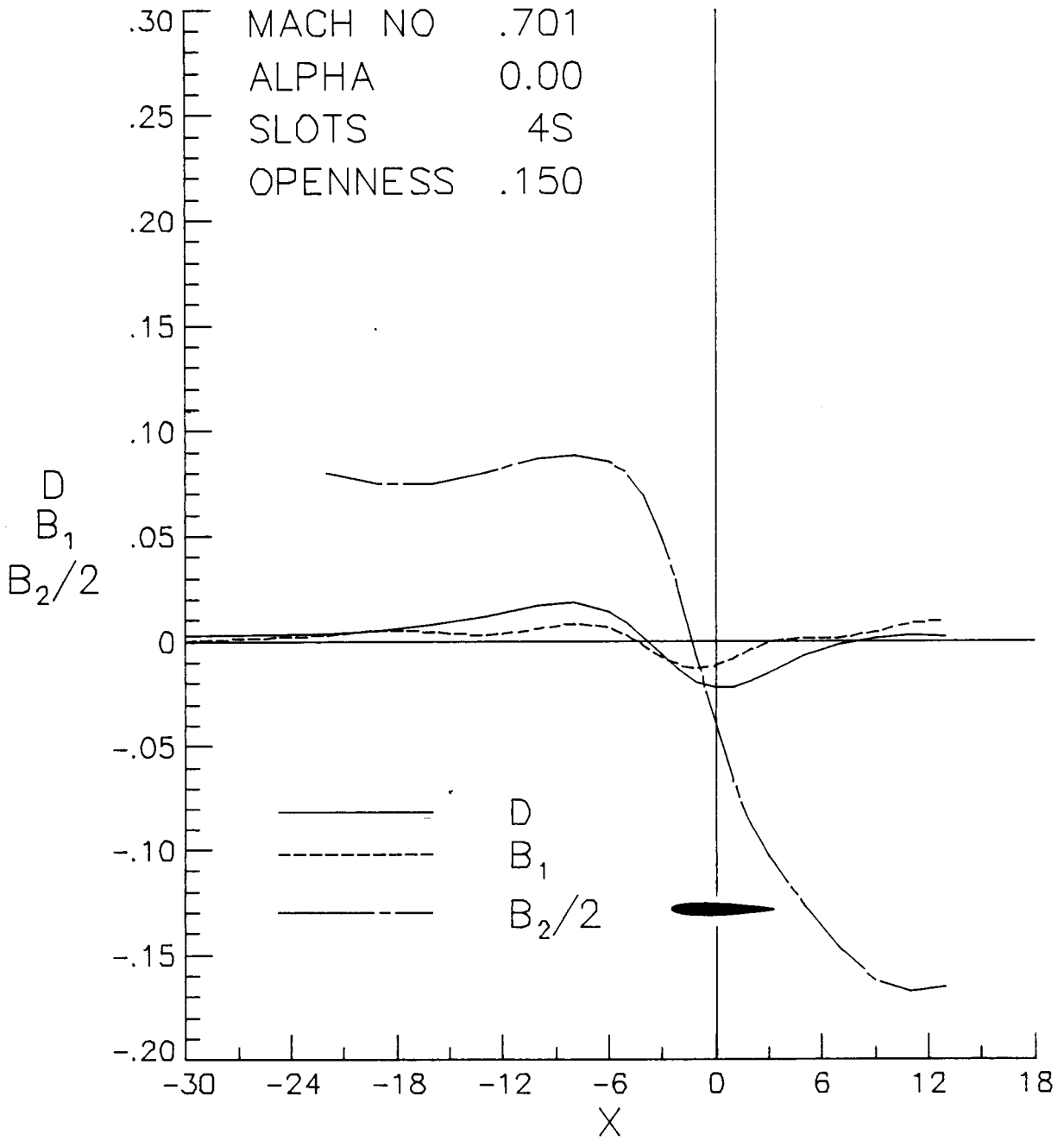

Figure 76.- Distribution of the terms in the present-method boundary condition. $M_\infty = 0.7$, $\alpha = 0$, 15-4 wall.

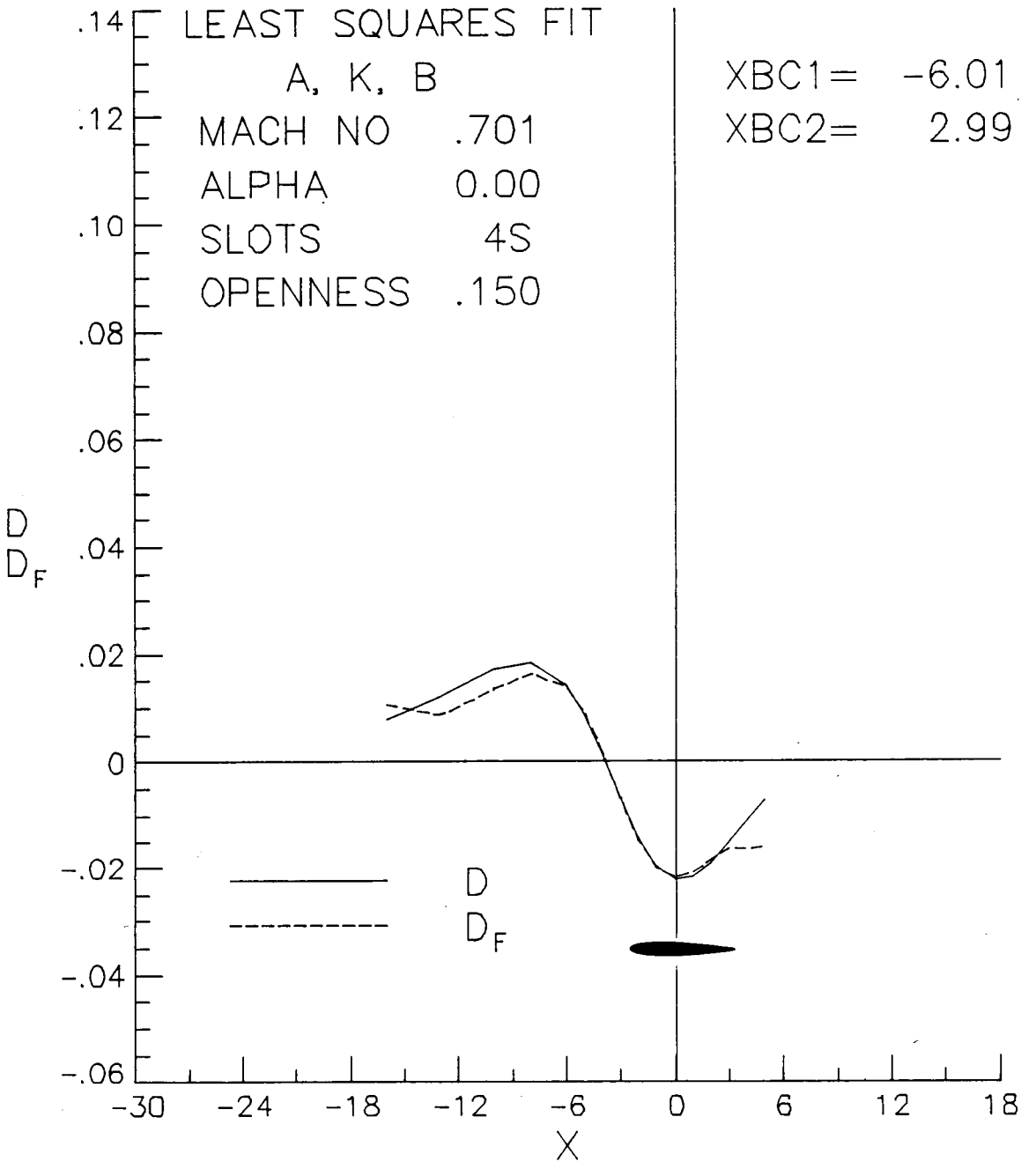

(a) 15-4 wall.

Figure 77.- Analysis of the 6- By 19-Inch Tunnel data using the present form of the slotted-wall boundary condition. $M_\infty = 0.7$, $\alpha = 0.0$.

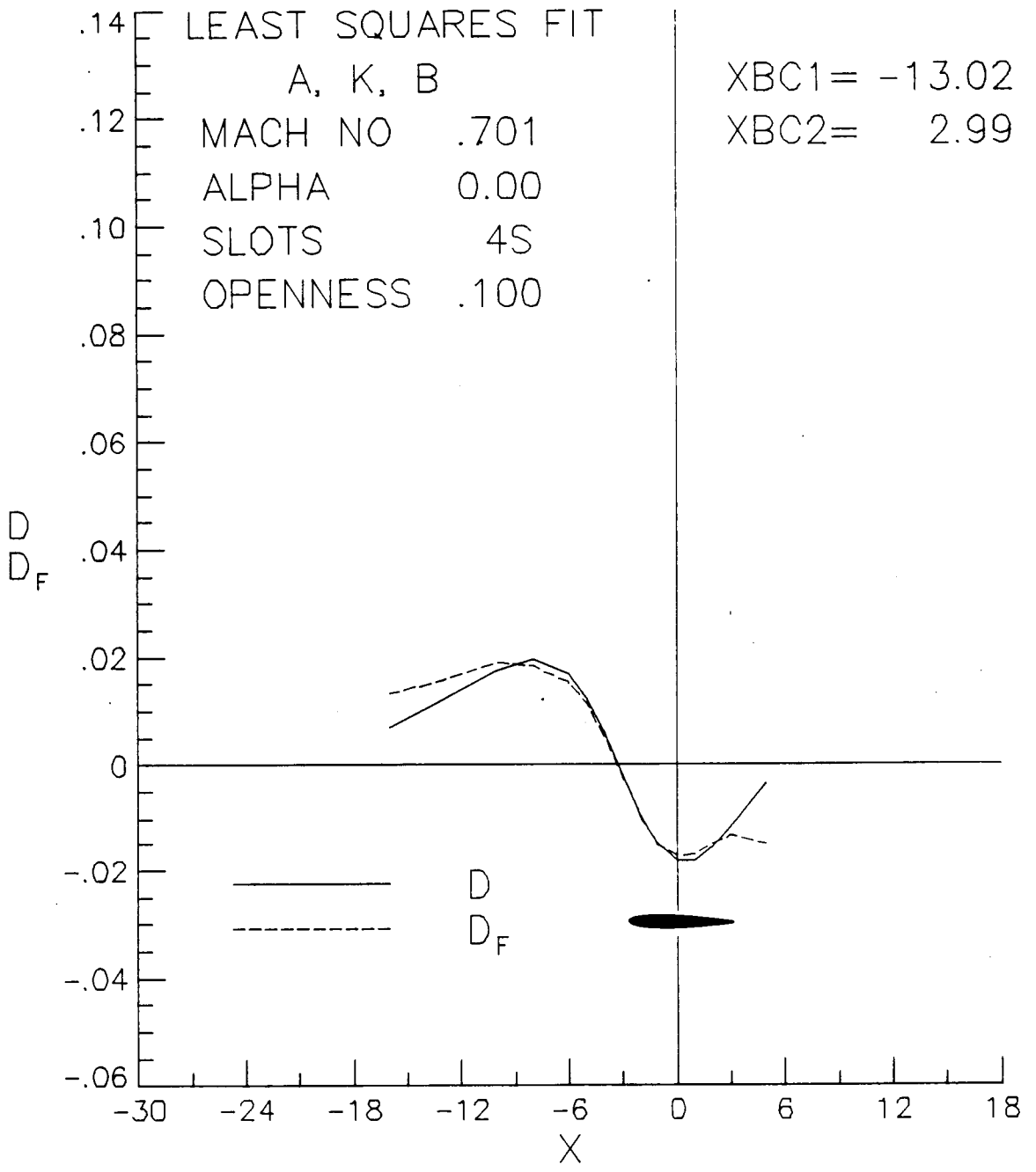

(b) 10-4 wall.

Figure 77.- Continued.

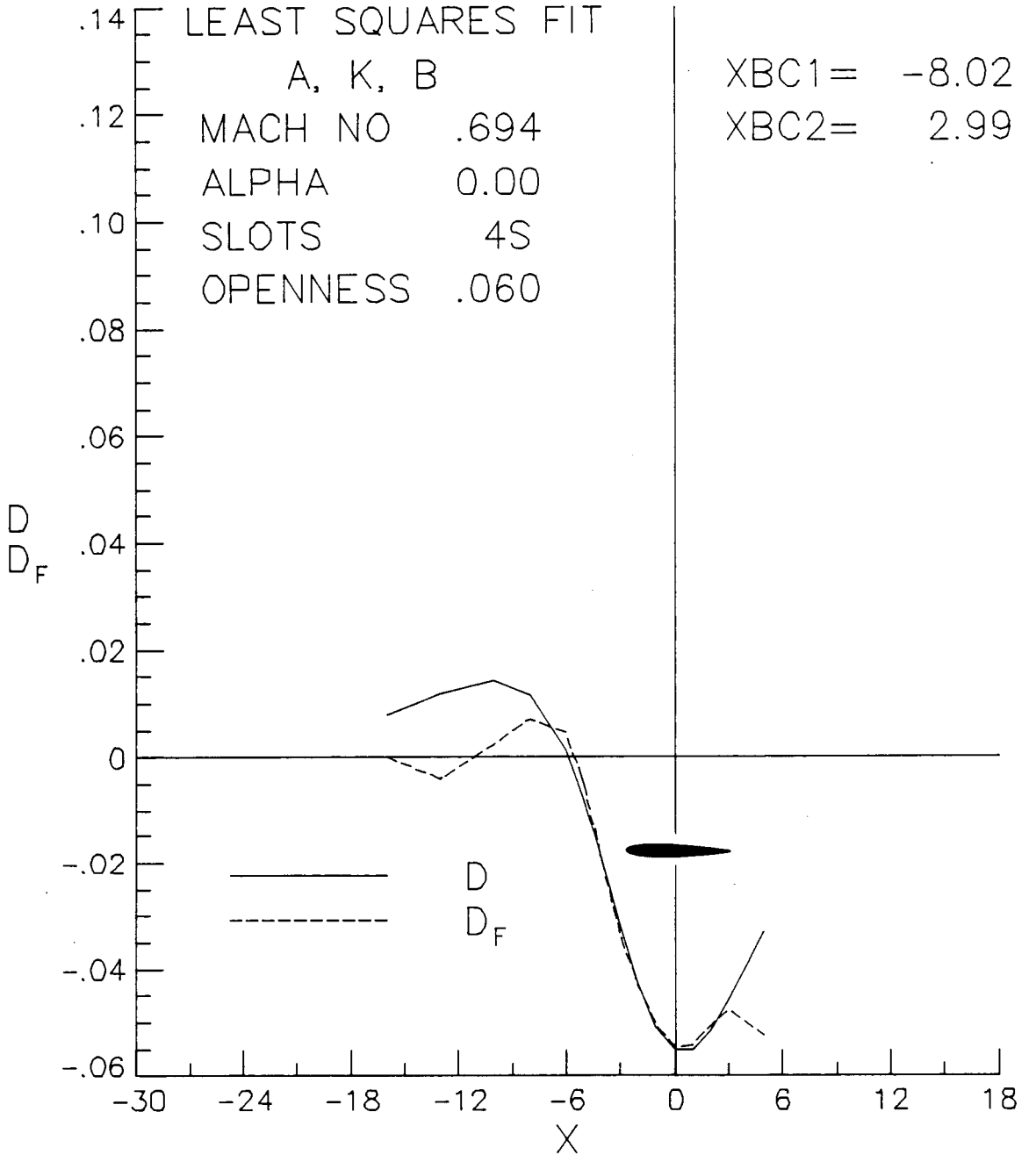

(c) 6-4 wall.

Figure 77.- Concluded.

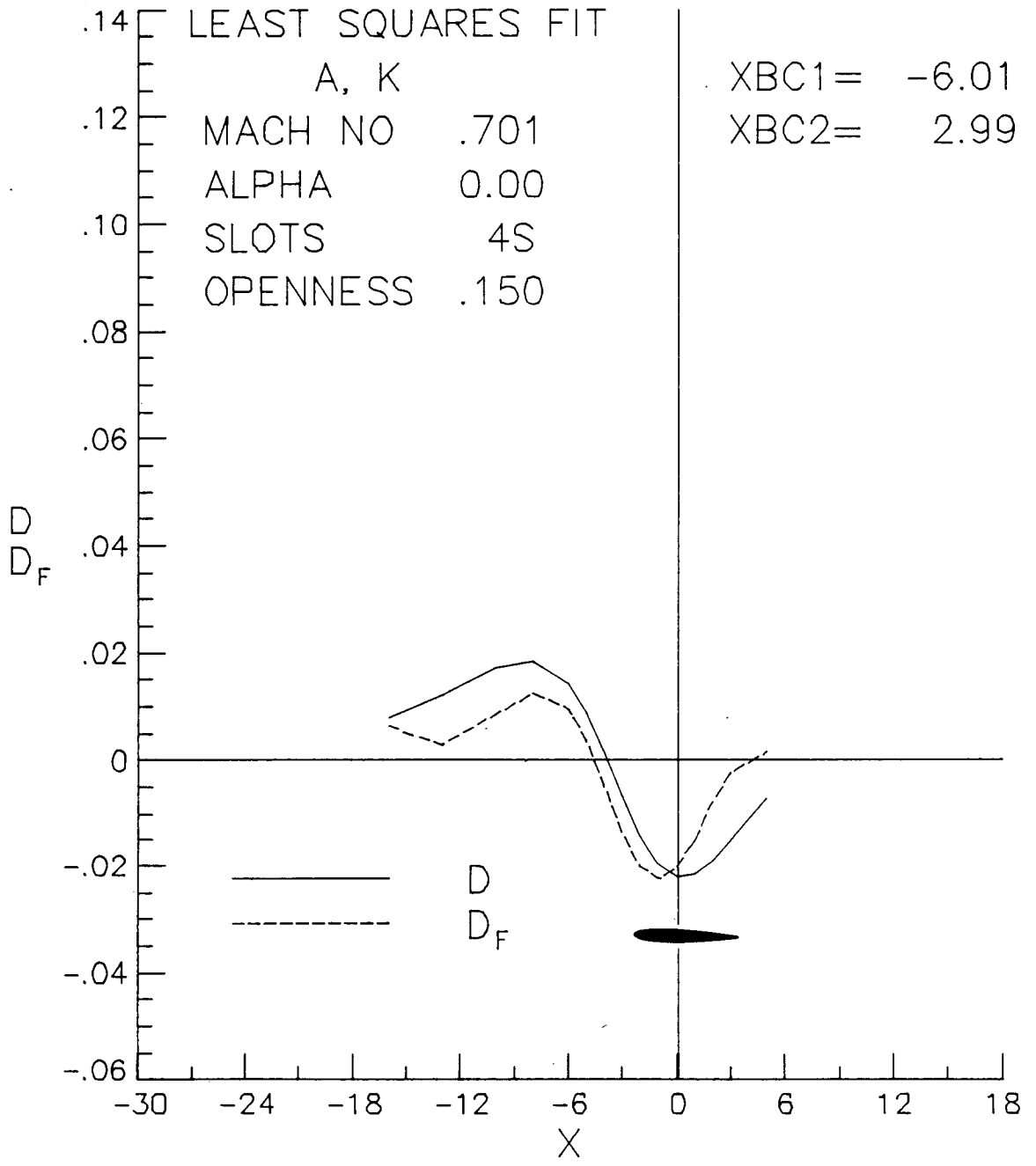

(a) 15-4 wall.

Figure 78.- The influence of dropping the B term on the analysis of the 6- by 19-Inch Tunnel data using the present form of the boundary condition. $M_\infty = 0.7$, $\alpha = 0$.

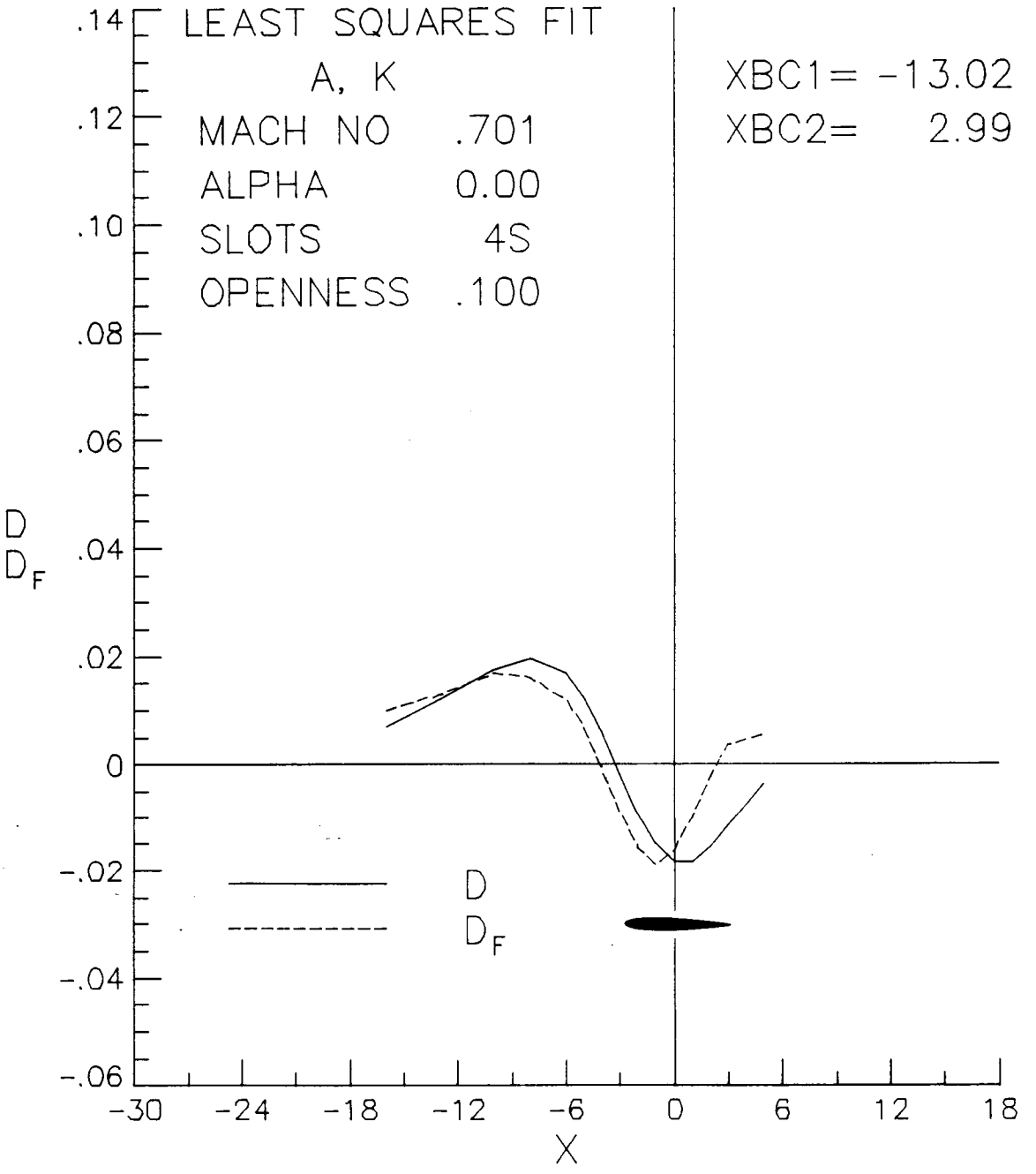

(b) 10-4 wall.

Figure 78.- Continued.

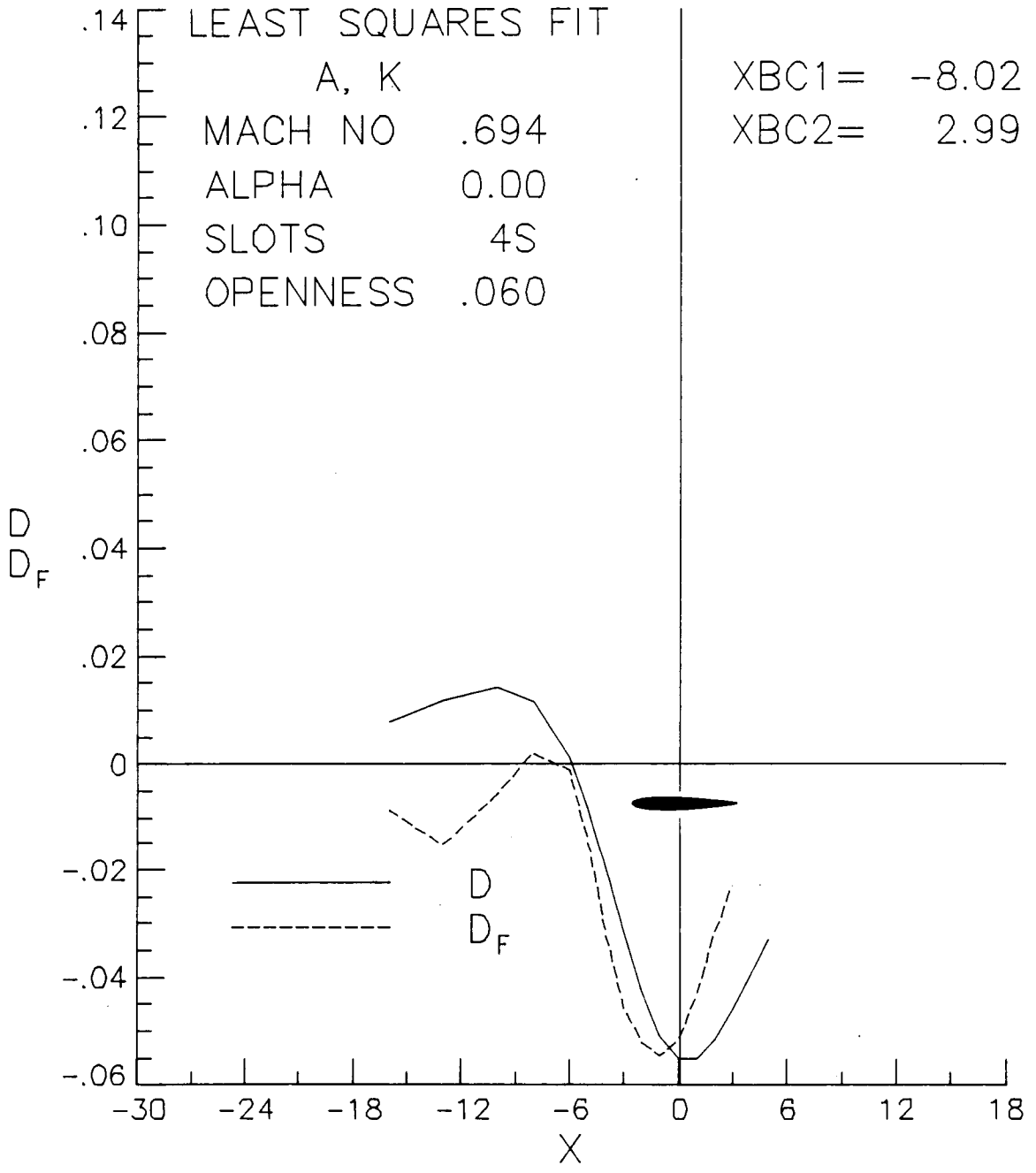

(c) 6-4 wall.

Figure 78.- Concluded.

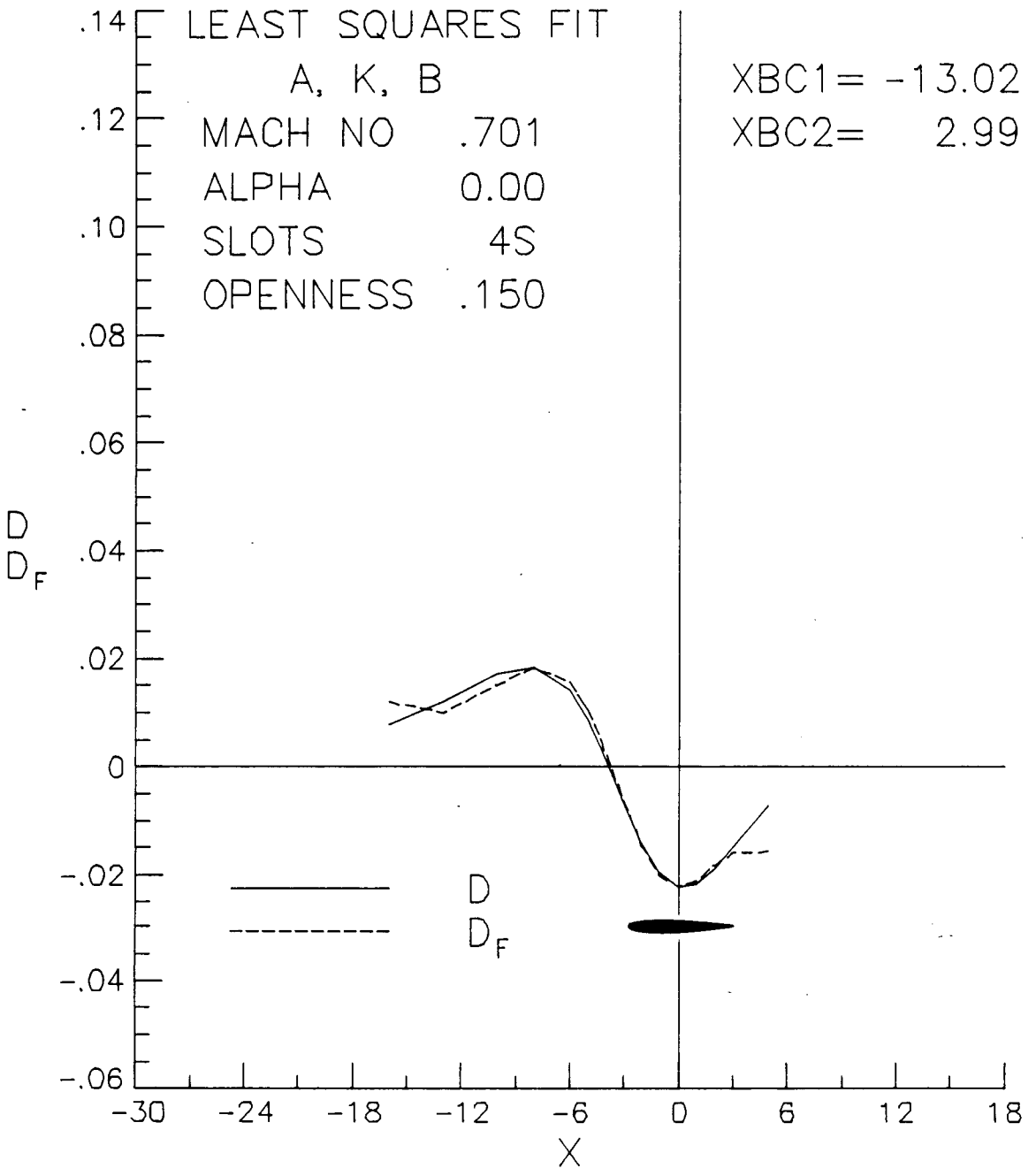

Figure 79.- The influence of the evaluation region on the correlation of the measured pressures with the computed pressures. $M_\infty = 0.7$, $\alpha = 0$.

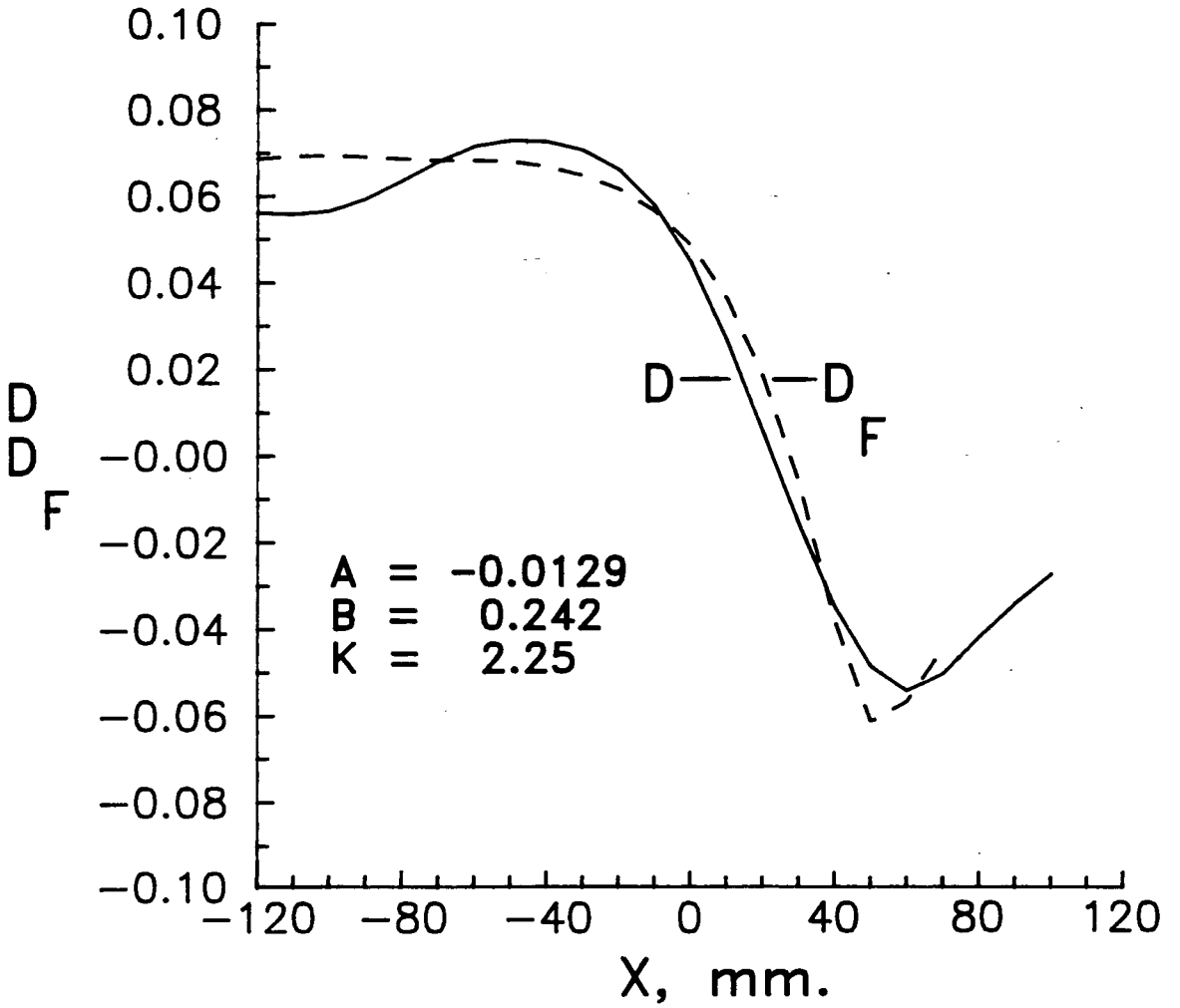

Figure 80.- Evaluation of Berndt's data using the present form of the slotted-wall boundary condition.

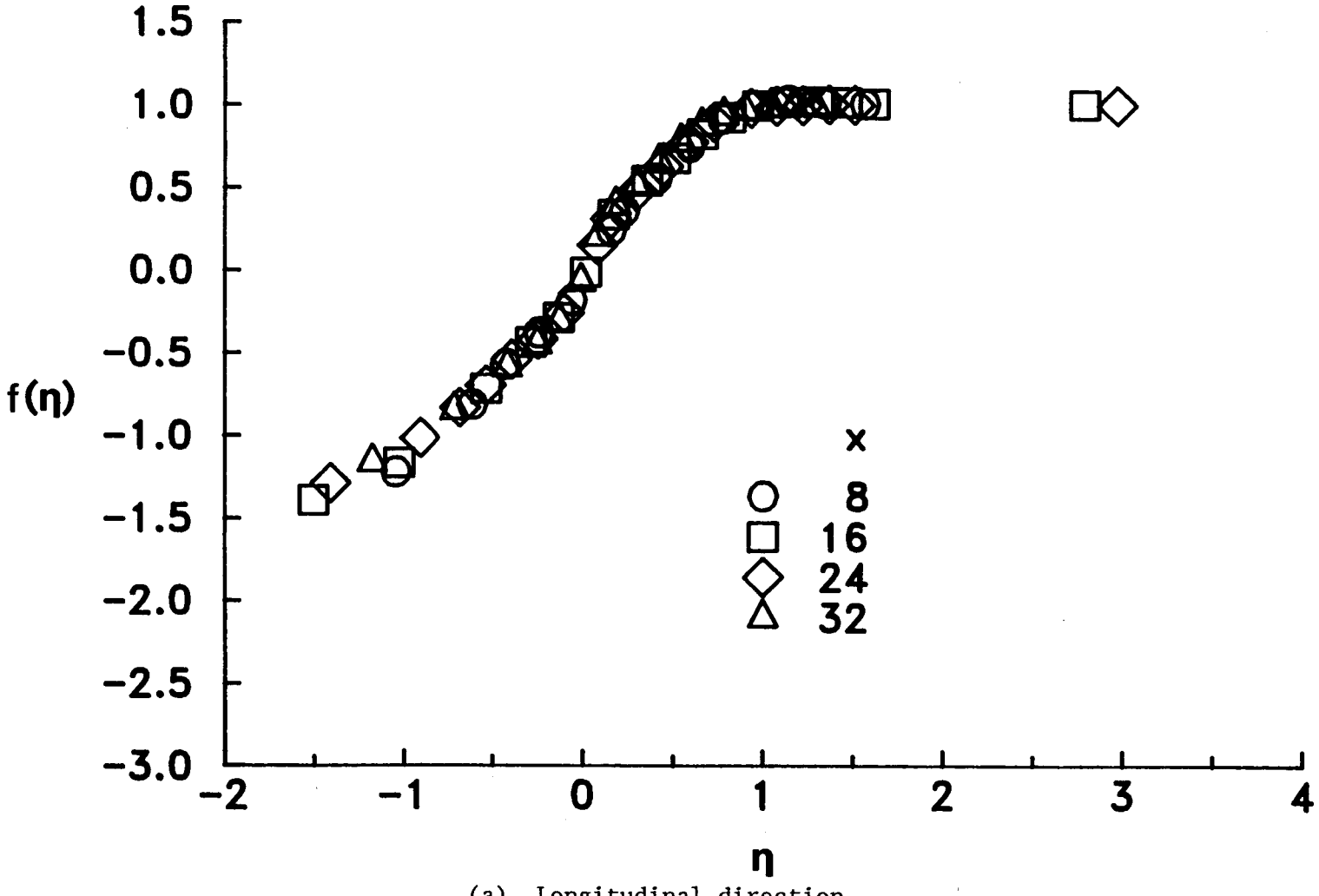

(a) Longitudinal direction.

Figure 81.- Demonstration of dynamic similarity in the slot region of the DFA. Tunnel empty, $M_\infty = 0.6$.

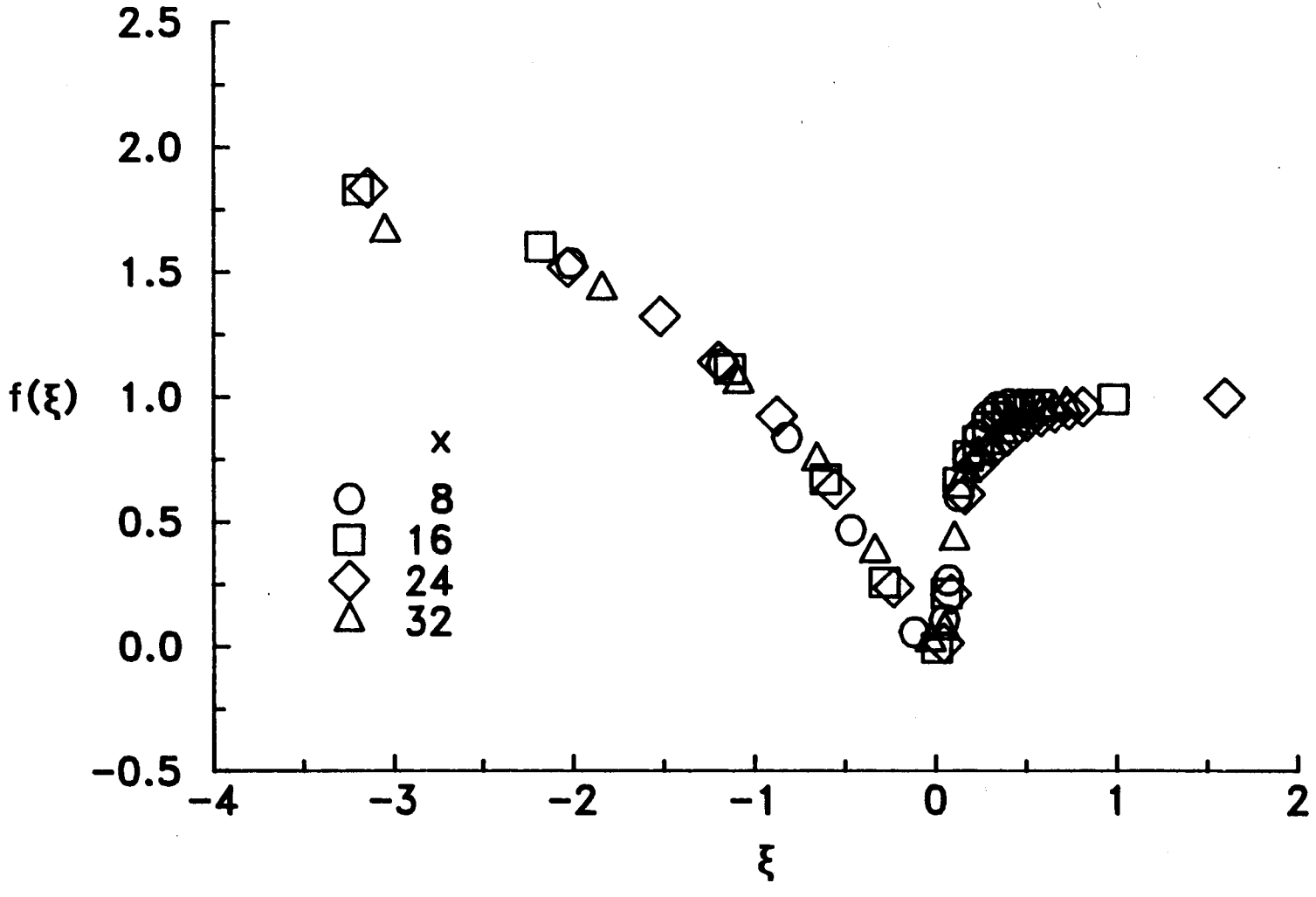

(b) Transverse direction.

Figure 81.- Concluded.

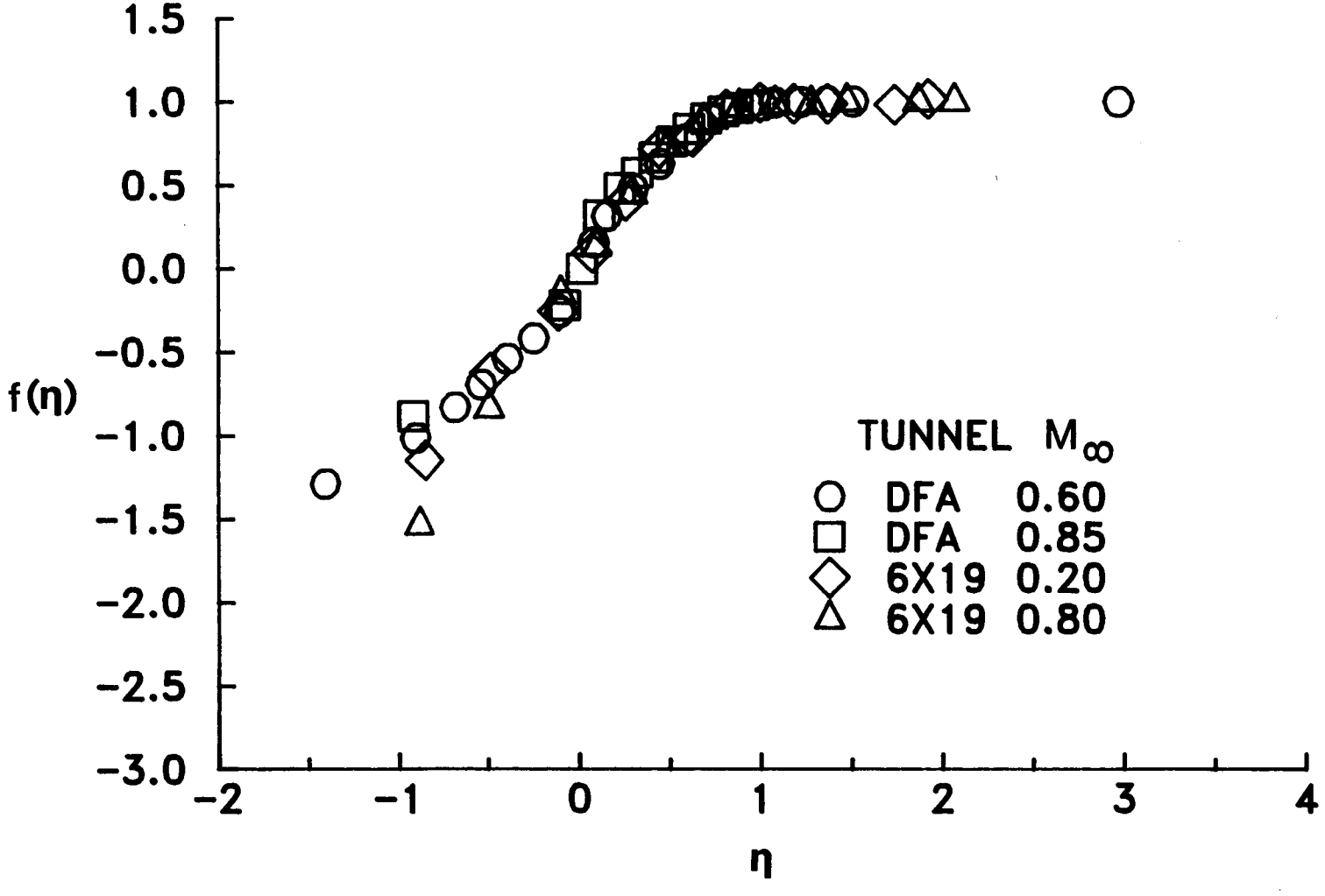

(a) Longitudinal direction.

Figure 82.- Effect of Mach number on the similarity parameters. Tunnel empty.

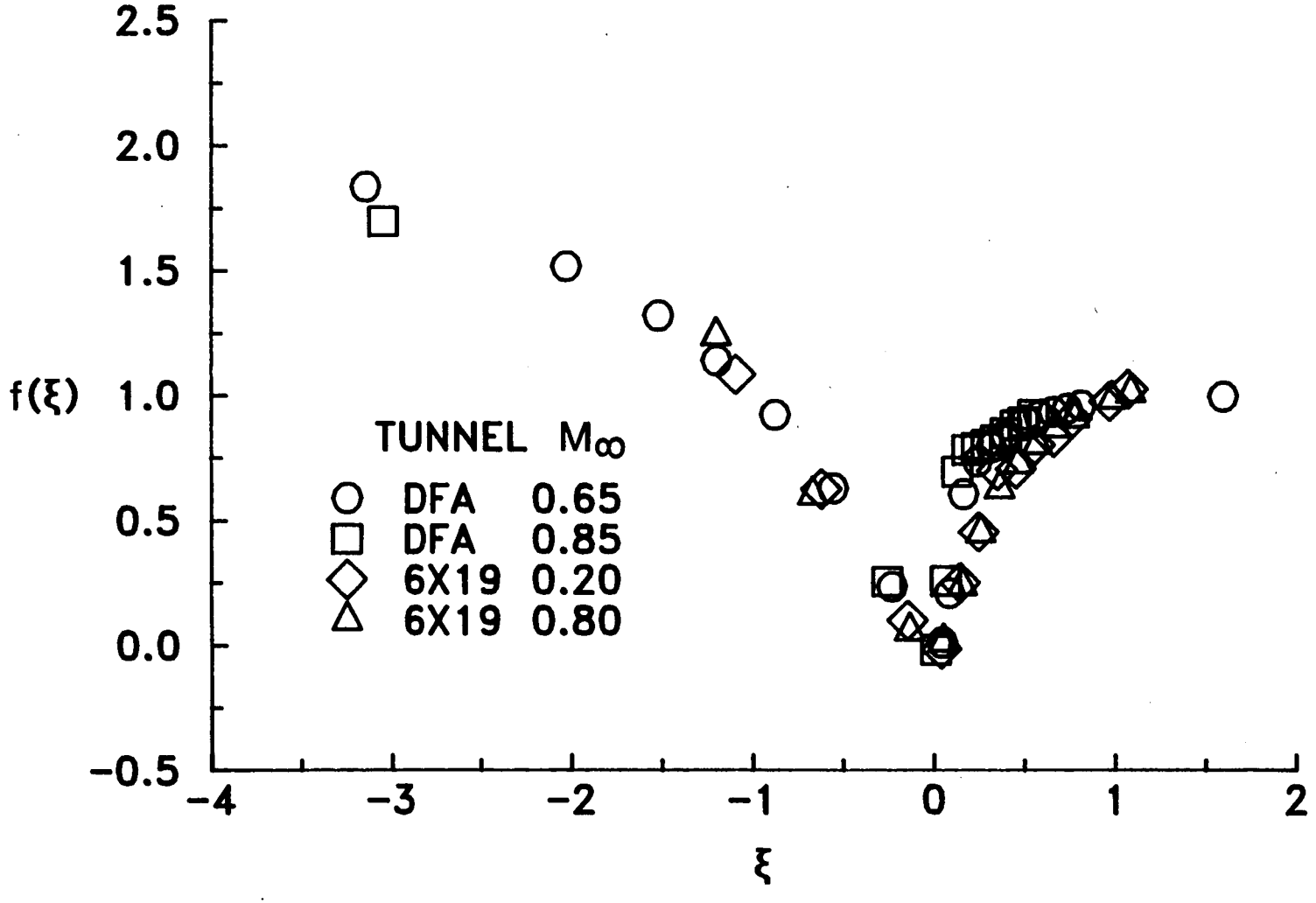

(b) Transverse direction.

Figure 82.- Concluded.

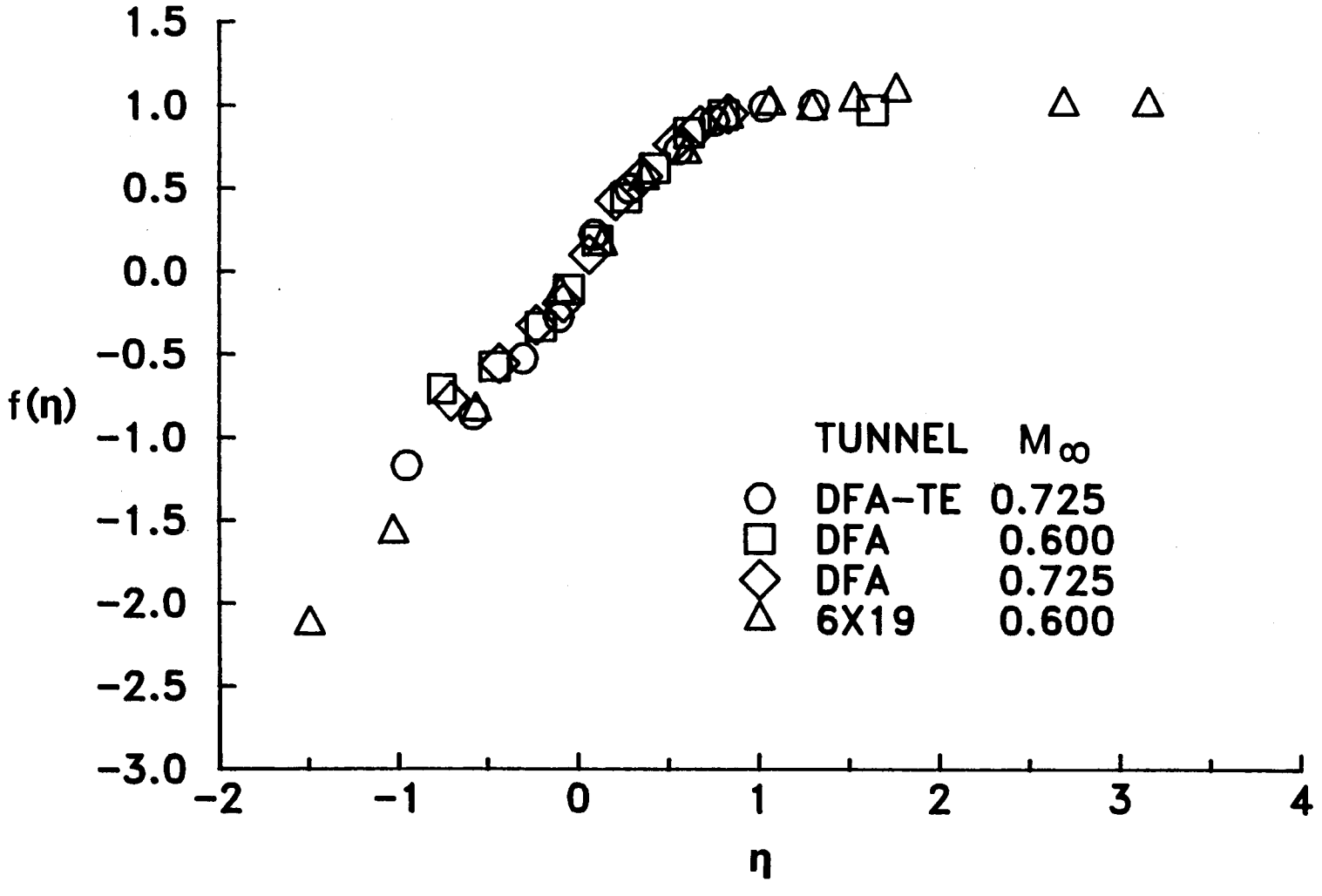

(a) Longitudinal direction.

Figure 83.- Effect of airfoil-induced streamwise curvature on the similarity parameters.

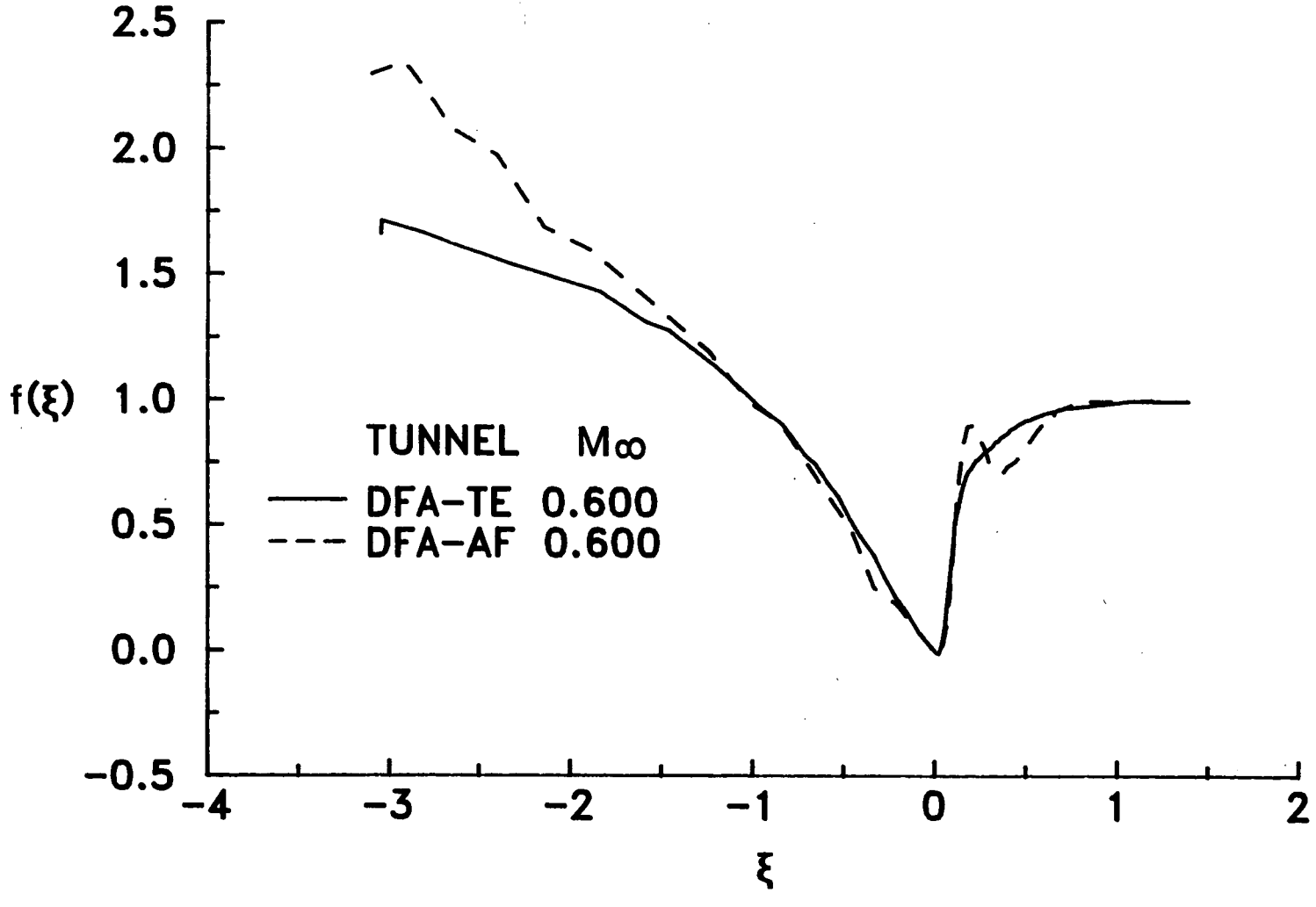

(b) Transverse direction, $M_\infty = 0.6$.

Figure 83.- Continued.

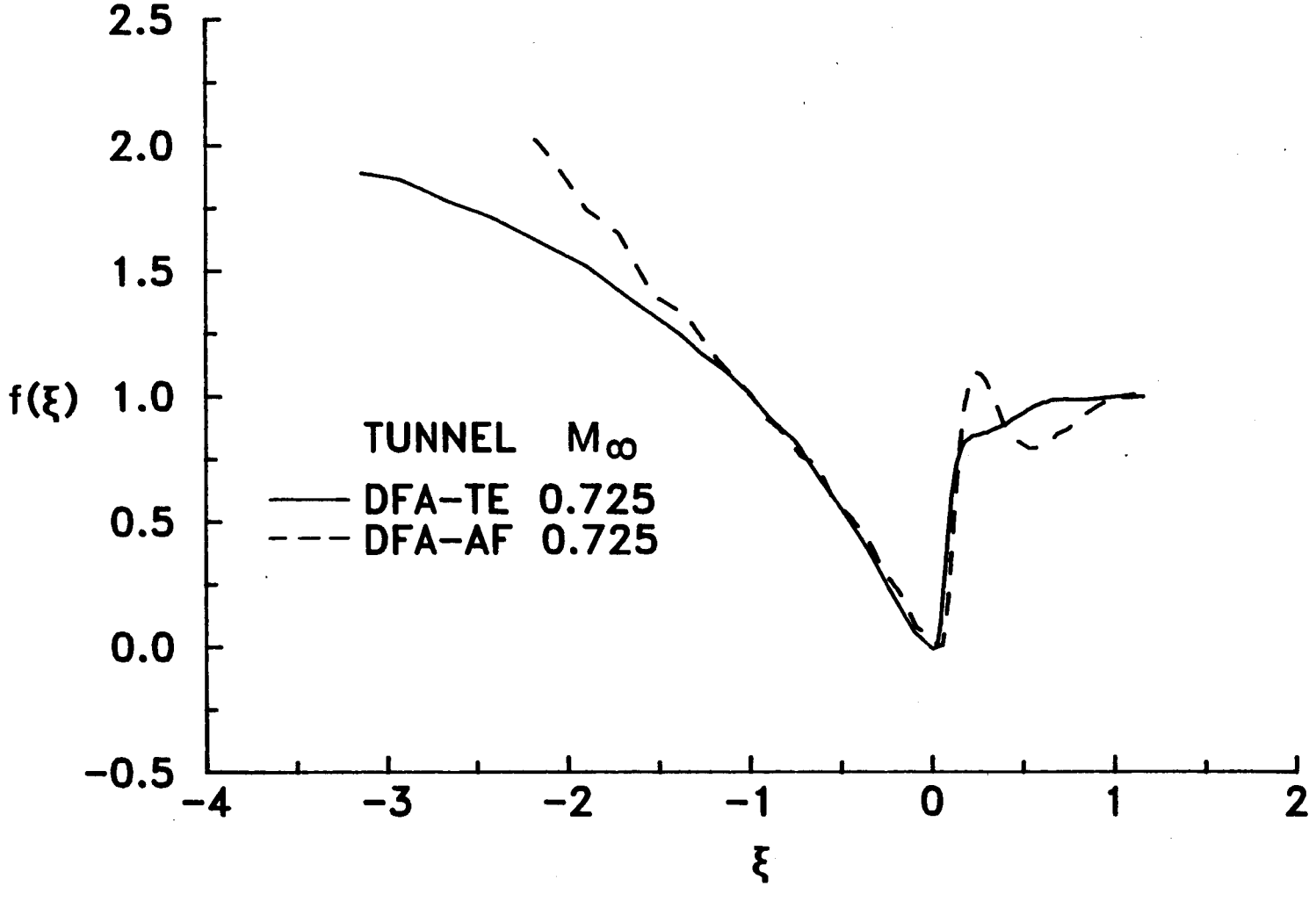

(c) Transverse direction, $M_\infty = 0.725$.

Figure 83.- Concluded.

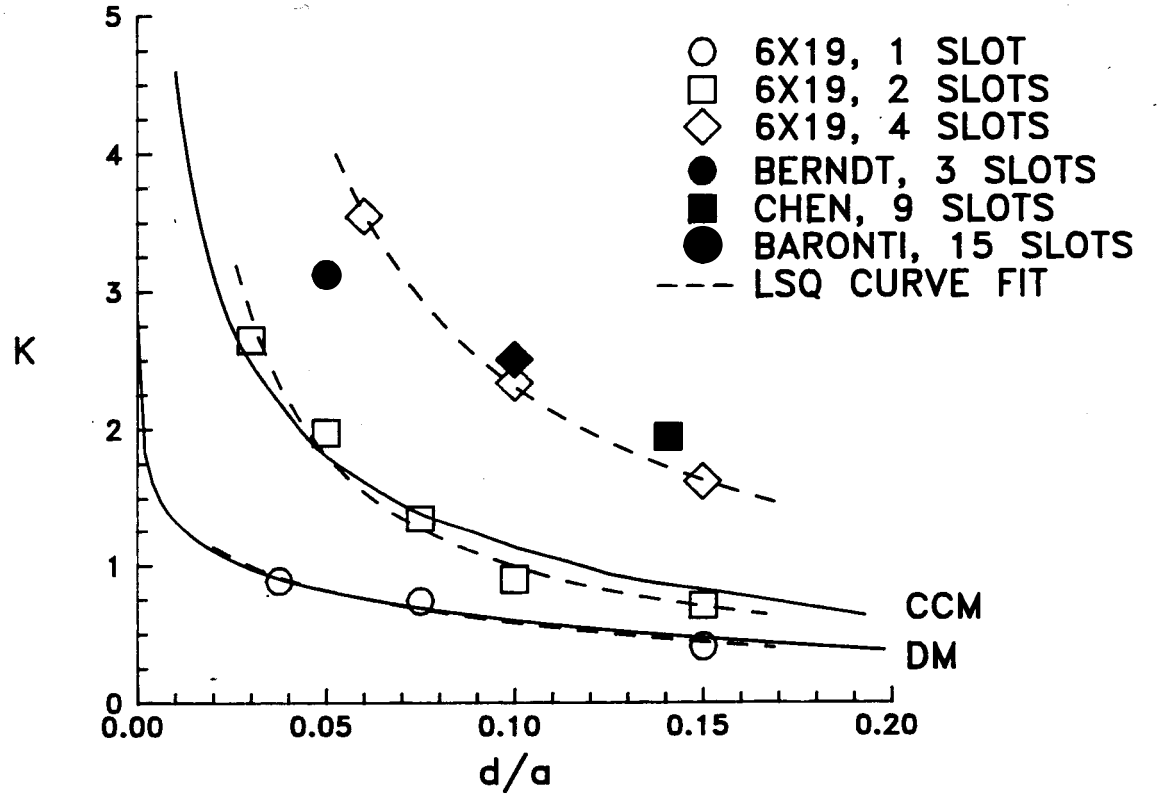

Figure 84.- Variation of the Ideal form of the slotted-wall coefficient K with openness ratio. $M_\infty = 0.7$, $\alpha = 0$.

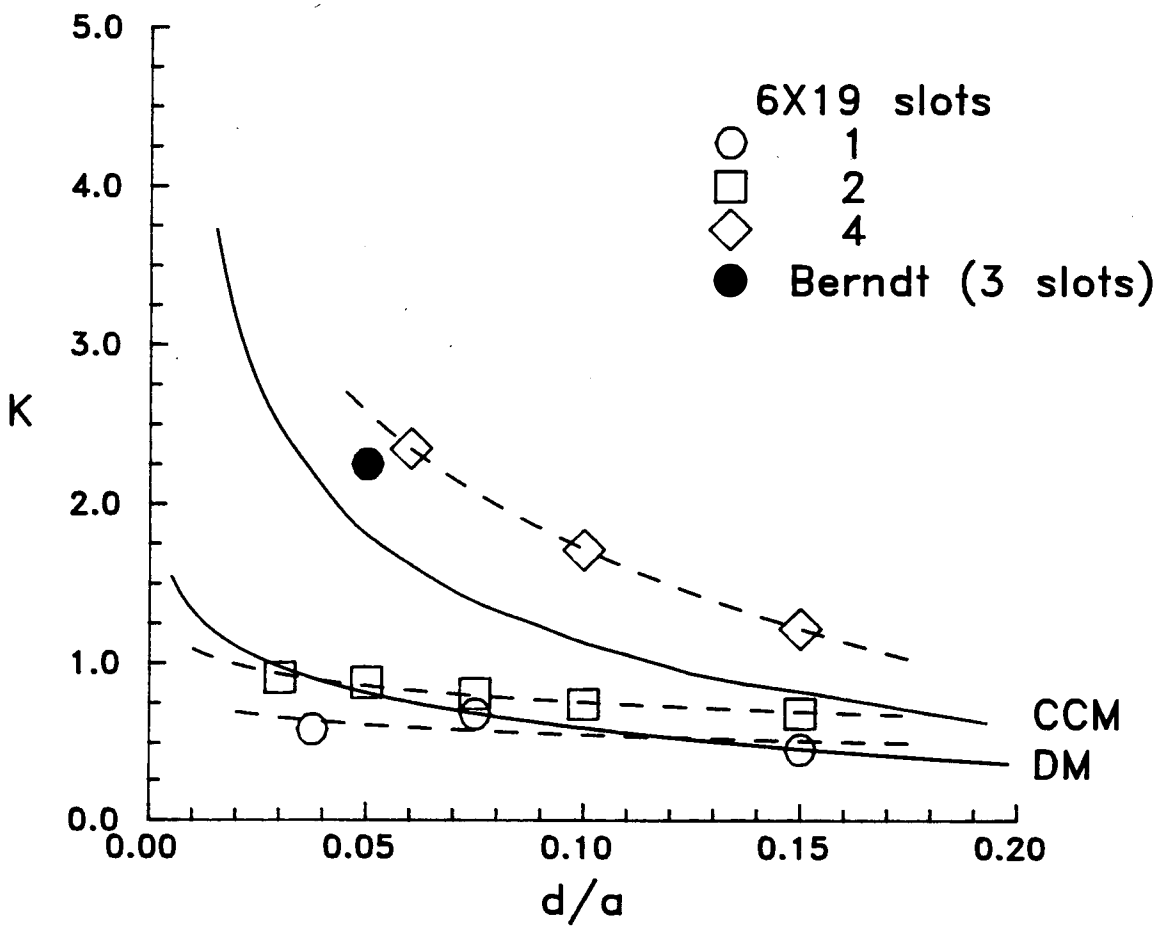

(a) K coefficient.

Figure 85.- Variation of the present-method boundary-condition coefficients with openness ratio. $M_\infty = 0.7$, $\alpha = 0$.

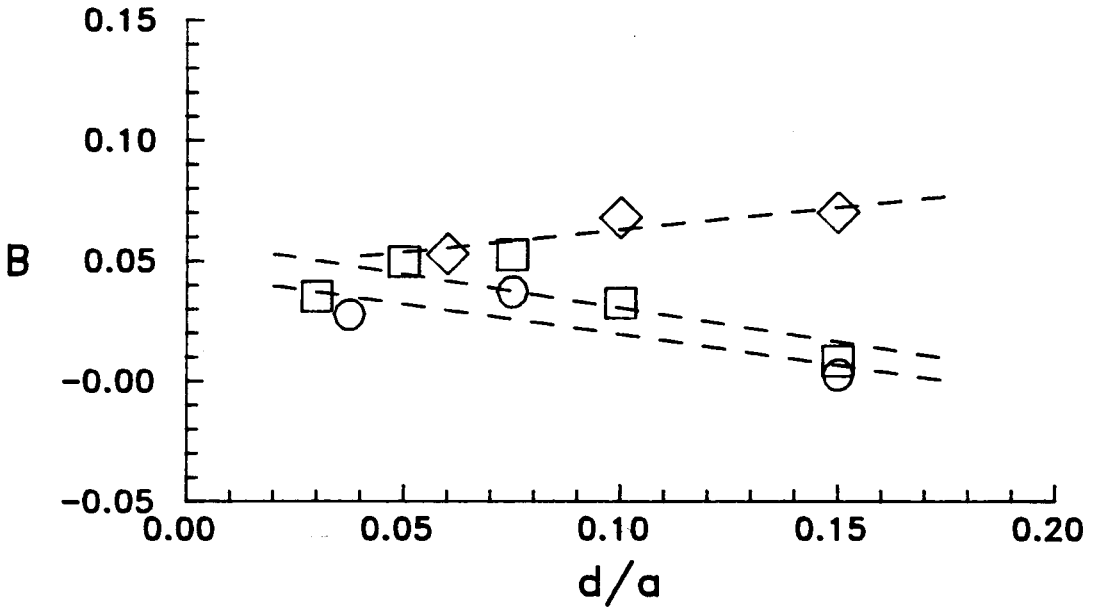

(b) B coefficient.

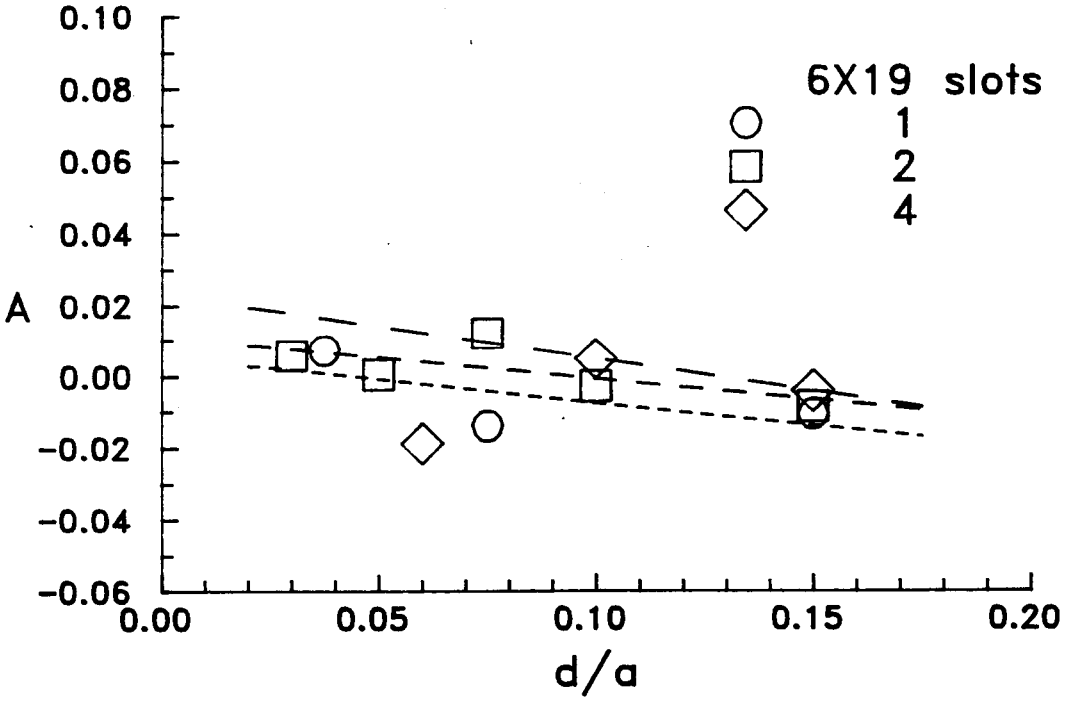

(c) A coefficient.

Figure 85.- Concluded.

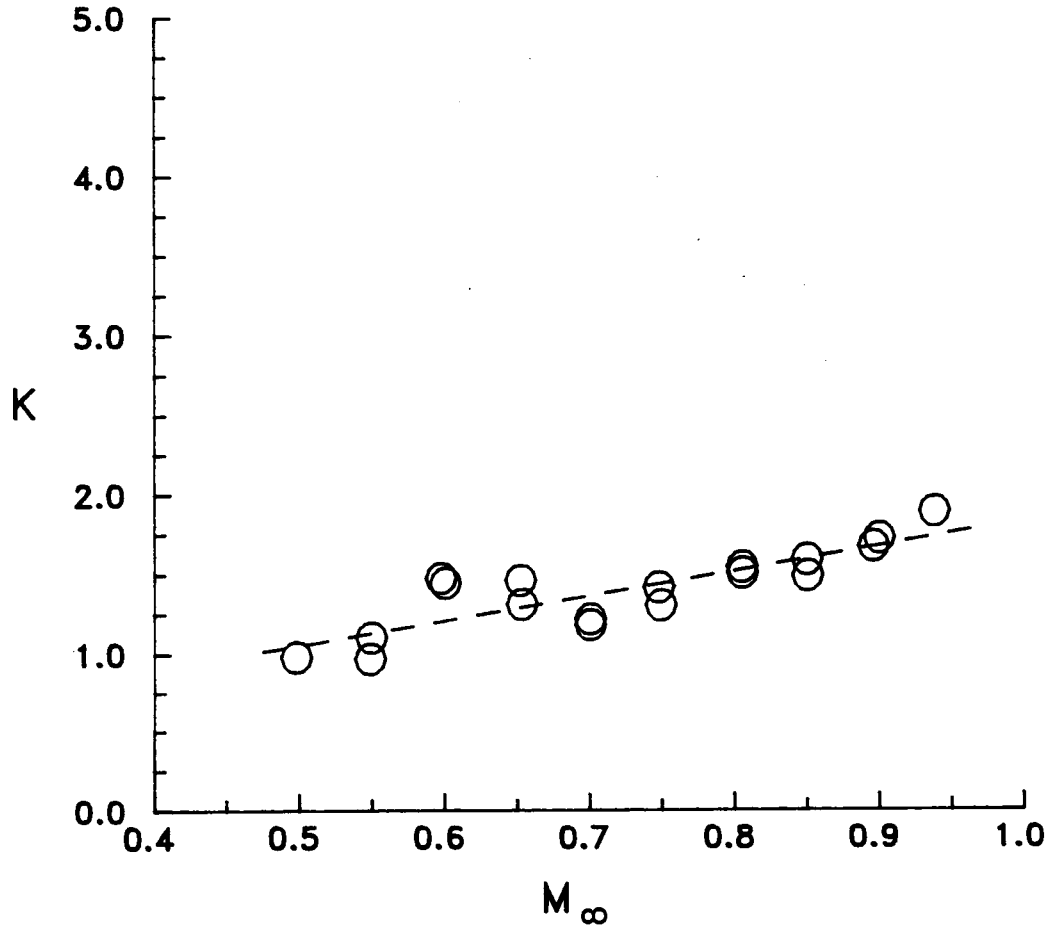

(a) K coefficient.

Figure 86.- Variation of the present-method boundary-condition coefficients with Mach number. 15-4 wall, $\alpha = 0$.

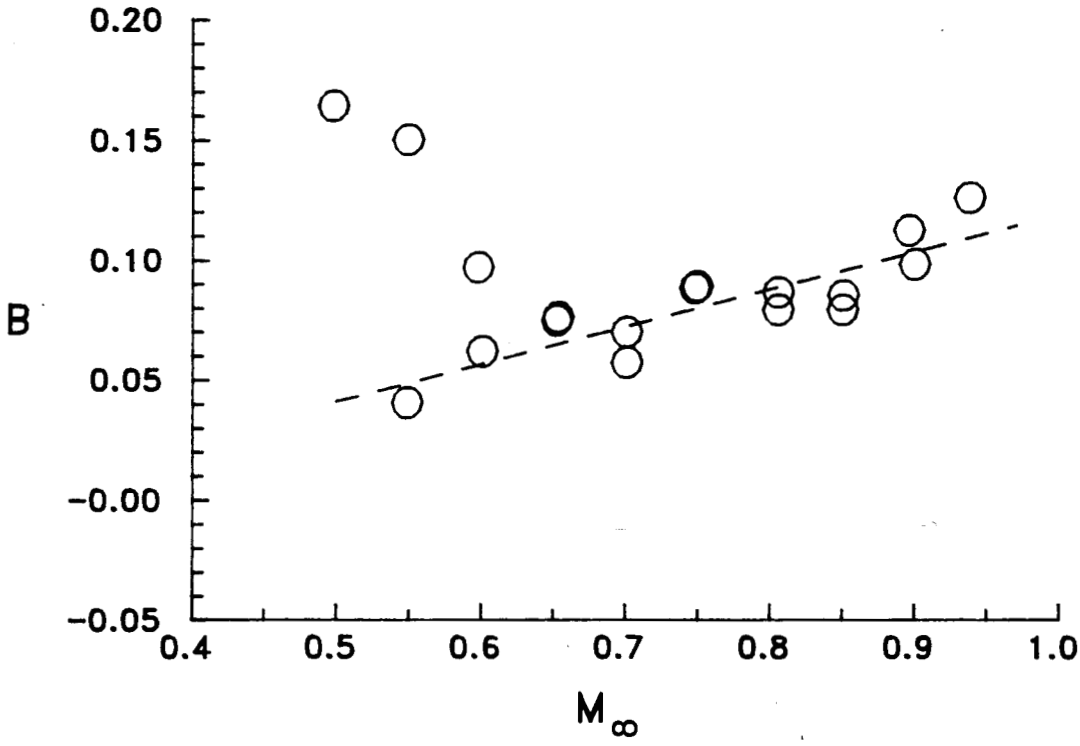

(b) B coefficient.

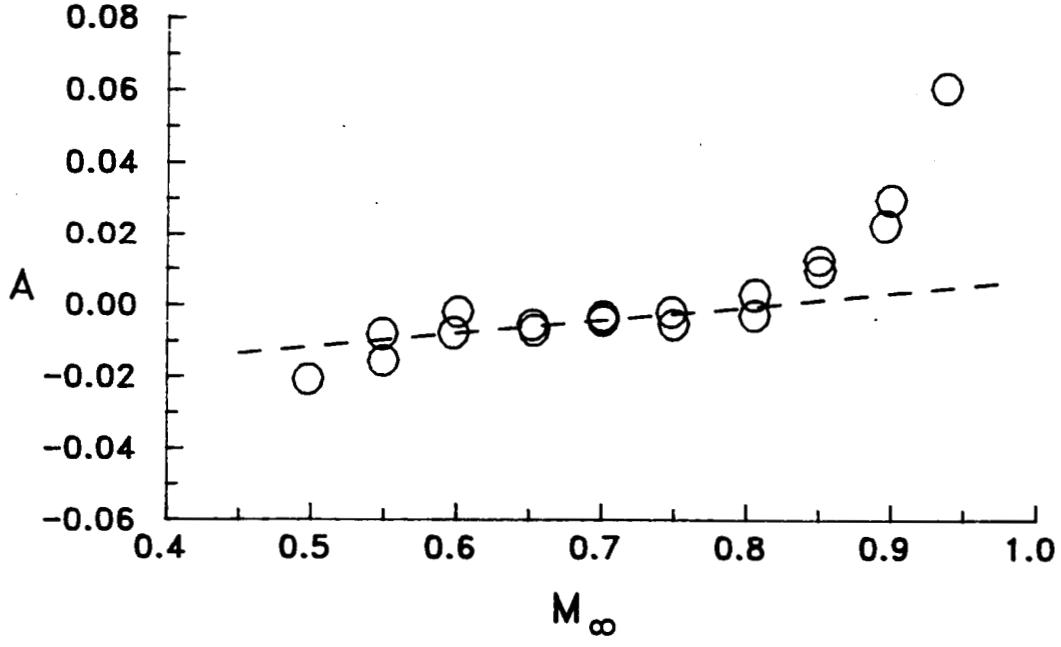

(c) A coefficient.

Figure 86.- Concluded.

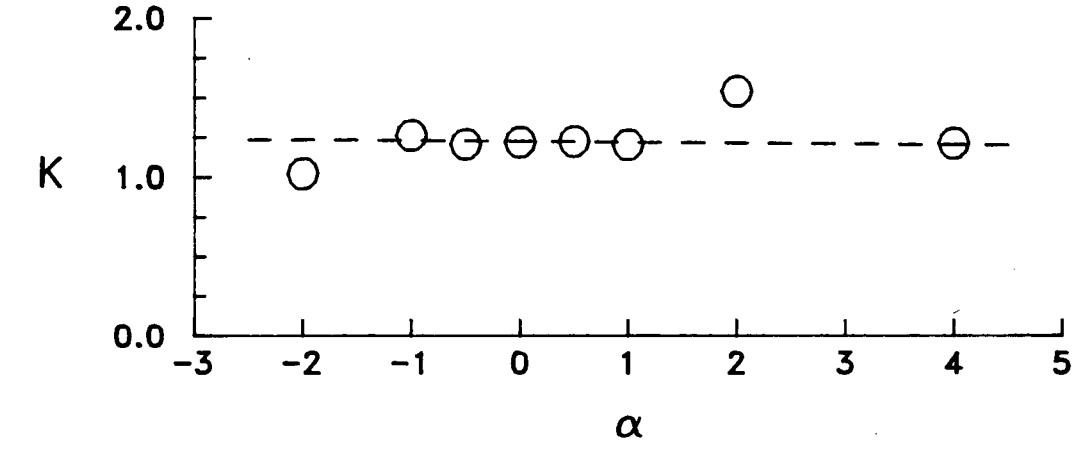

(a) K coefficient.

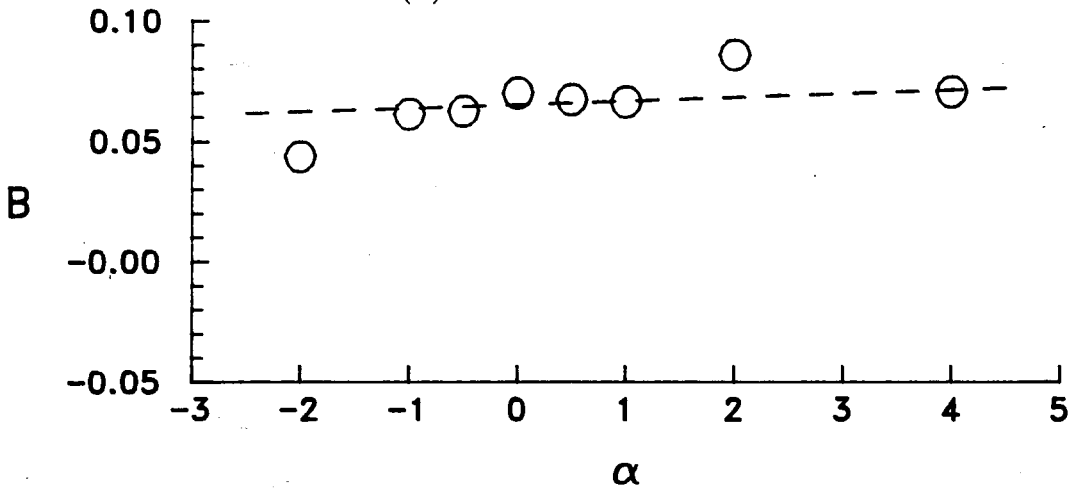

(b) B coefficient.

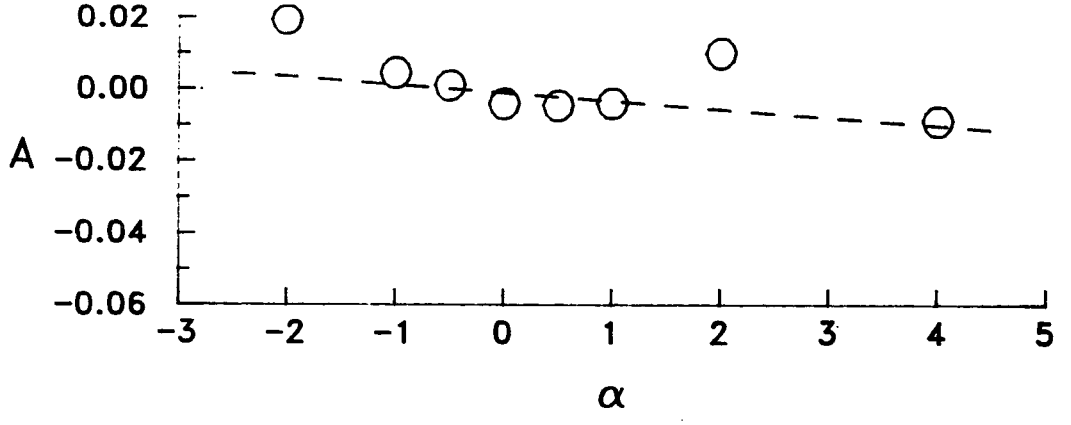

(c) A coefficient.

Figure 87.- Variation of the present-method boundary-condition coefficients with airfoil lift. 15-4 wall, $M_\infty = 0.7$.

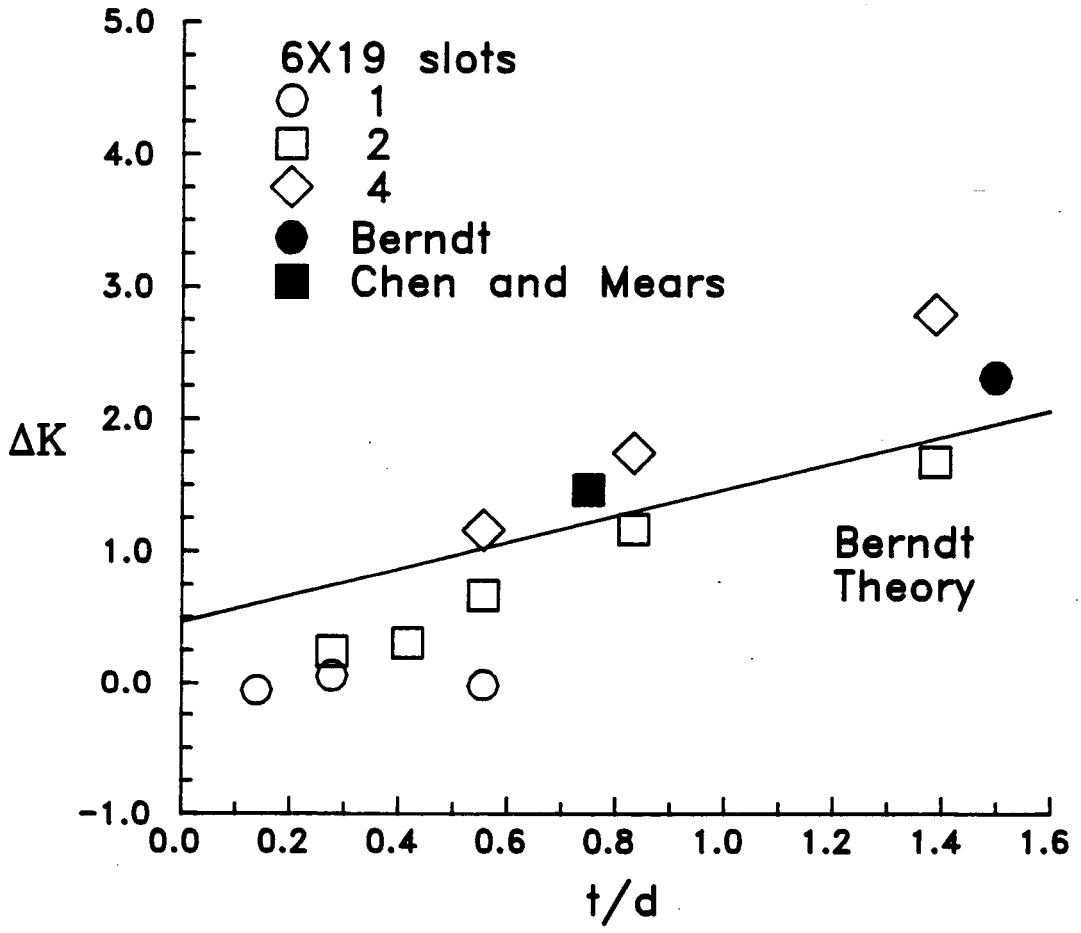

(a) Ideal-wall value of K.

Figure 88.- Influence of slot depth on the coefficient K. $M_\infty = 0.7$, $\alpha = 0$.

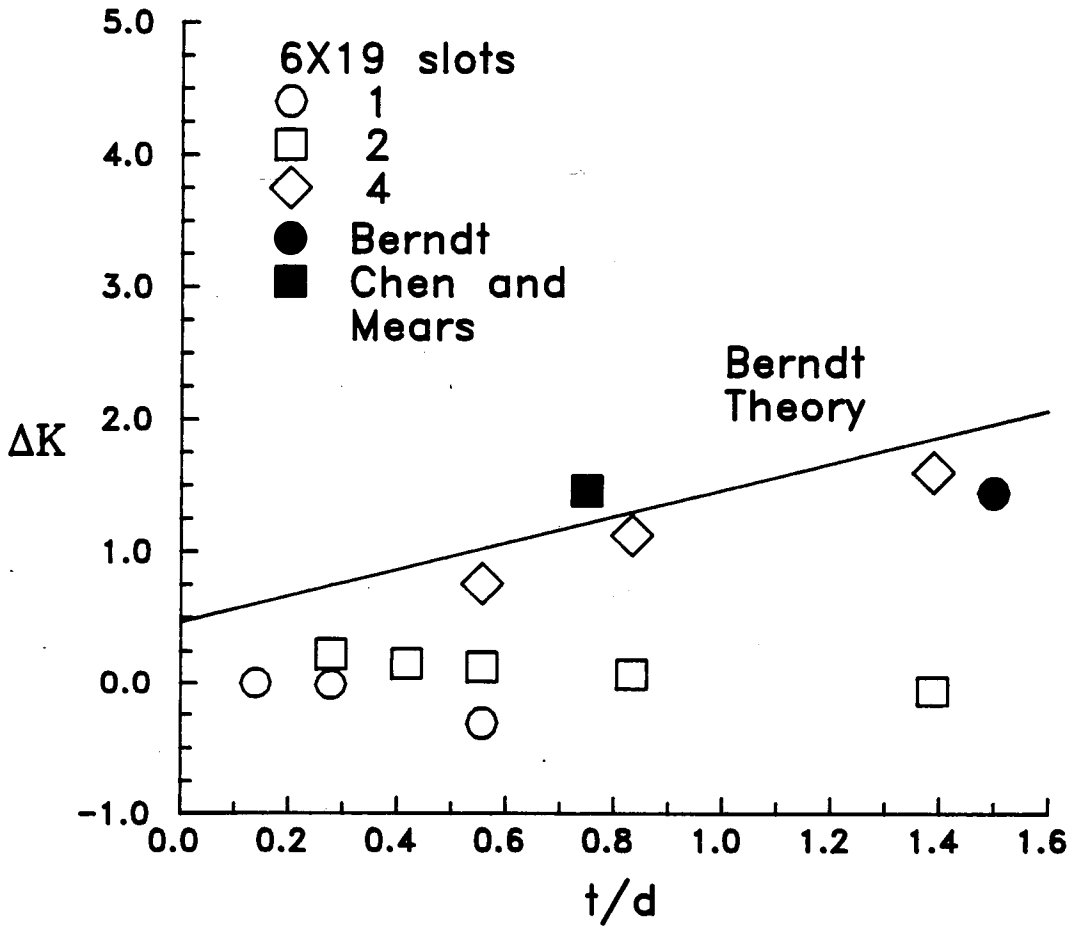

(b) Present-method value of K.

Figure 88.- Concluded.

APPENDIX A

CALIBRATION OF THREE-TUBE FLOW ANGULARITY PROBES

The probe-calibration data were obtained in the 6- by 19-inch Transonic Tunnel. The probe-support hardware was designed so that the tip of the probe maintained the same location with changes in pitch. These data were acquired at fixed angles while tunnel Mach number was varied. Examples of the data are shown in figures A1 for two different pitch angles. Data were acquired at both upright and inverted probe configurations. Since total pressure is the true independent variable (as opposed to Mach number), the differential pressures measured at each orifice along with the reference pressure were plotted and smoothed to remove any uncertainties due to experimental error. The Mach number was then determined from the total pressure and reference static pressure and the smoothed data were interpolated at predetermined values of Mach numbers for each run.

The next step was to reduce the data to a probe-variable format by applying the following equations:

$$p_1 = p_{ref} + dp_1 \tag{A1}$$

$$p_2 = p_{ref} + dp_2 \tag{A2}$$

$$p_3 = p_{ref} + dp_3 \tag{A3}$$

$$Q_p = dp_1 - \frac{dp_2 + dp_3}{2} \tag{A4}$$

$$C_{P32} = \frac{dp_2 - dp_3}{Q_p} \tag{A5}$$

$$\frac{Pbar}{p_1} = \frac{p_2 + p_3}{2p_1} \tag{A6}$$

$$BP = \frac{P_1}{P_t} \tag{A7}$$

The resulting value of C_{p32} (which is the parameter most sensitive to flow angle) was then plotted as a function of pitch angle for at a constant Mach number. The intersection of the upright and inverted probe data defined the angularity correction for the local tunnel flow. This resulting angle correction was removed from the mechanically-prescribed flow angle to determine the fluid flow angle.

The next step in the calibration procedure was to fit a spline through the data at fixed Mach number and interpolate the values on a predetermined grid of angles. This final step completes the calibration table and insures the existence of a cartesian grid of Mach number and pitch angle. Figures A2 show the variation of the probe data with respect to Mach number and figures A3 the corresponding variations with respect to flow angle.

Examination of the results presented in figures A2 and A3 suggest an appropriate table lookup scheme for obtaining the properties of an unknown flow field. Comparison of figures A2a and A3a show that $\frac{Pbar}{p_1}$ is predominately a function of Mach number while figures A2b and A3b show C_{P32} to be a function of flow angle. Further examination of A3b shows C_{P32} to be only weakly dependent on the intercept. Therefore, as a first guess, the measured value of the probe pressure coefficient may be used along with the first value of

the slope in the calibration table to obtain an estimate of the flow angle. With this estimate, a close approximation of the local Mach number may be quickly obtained by restricting the Mach number search to those angles nearest the first guess and comparing the measured Mach number with the calibration values. An iteration to the required accuracy is now required.

After the local Mach number and flow angle have been obtained the rest of the flow field properties can be determined. The value of BP is used to correct the pressure p_1 for probe misalignment with the oncoming flow and the local total pressure results. Knowing the local total pressure and Mach number gives the local static pressure. Assuming constant total temperature allows the speed of sound and, hence, the local velocity to be determined. This combined with the local flow angle will give the normal and tangential components of the local velocity.

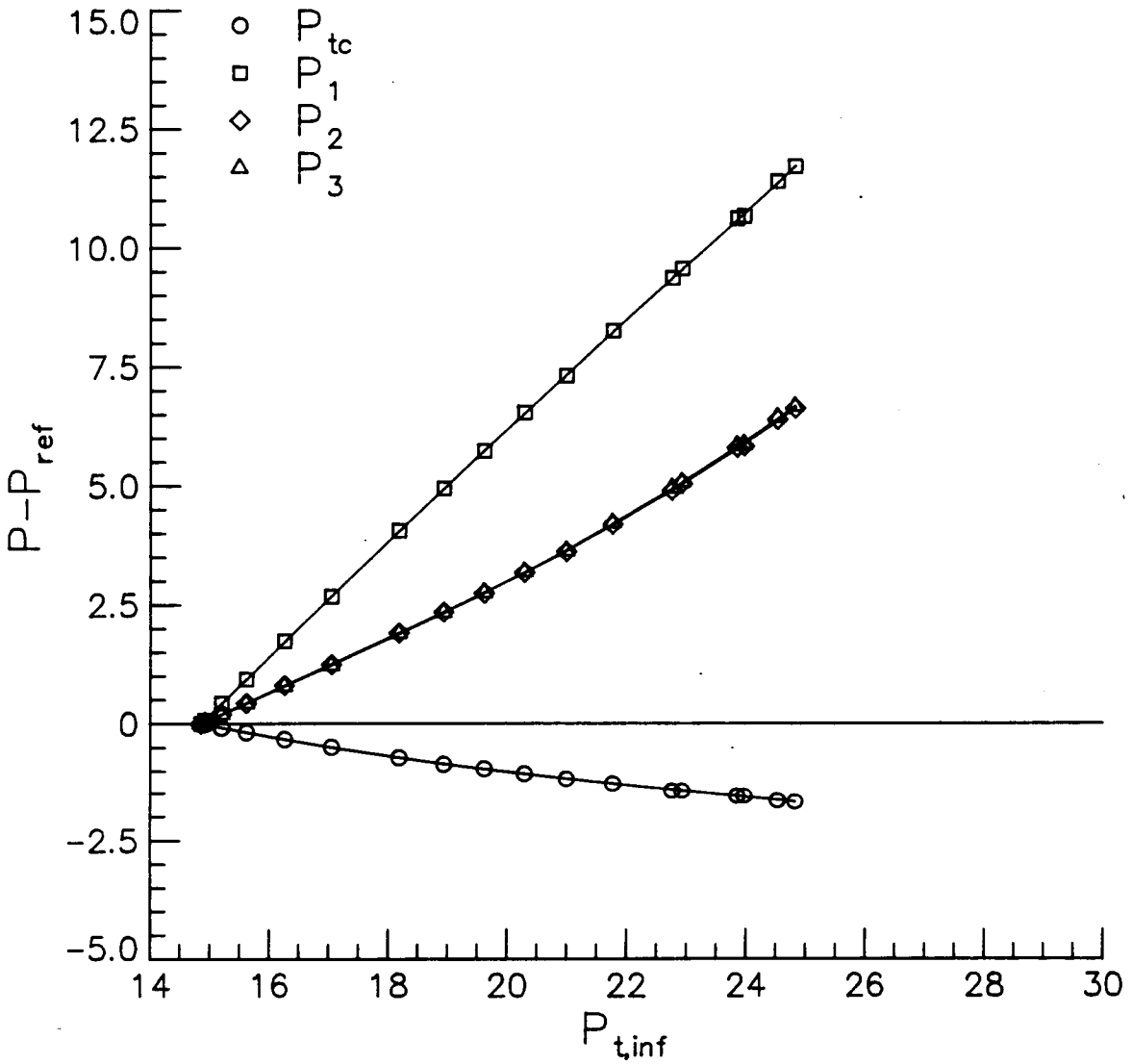

(a) $\alpha = 0.0$ deg.

Figure A1.- Sample probe-pressure data.

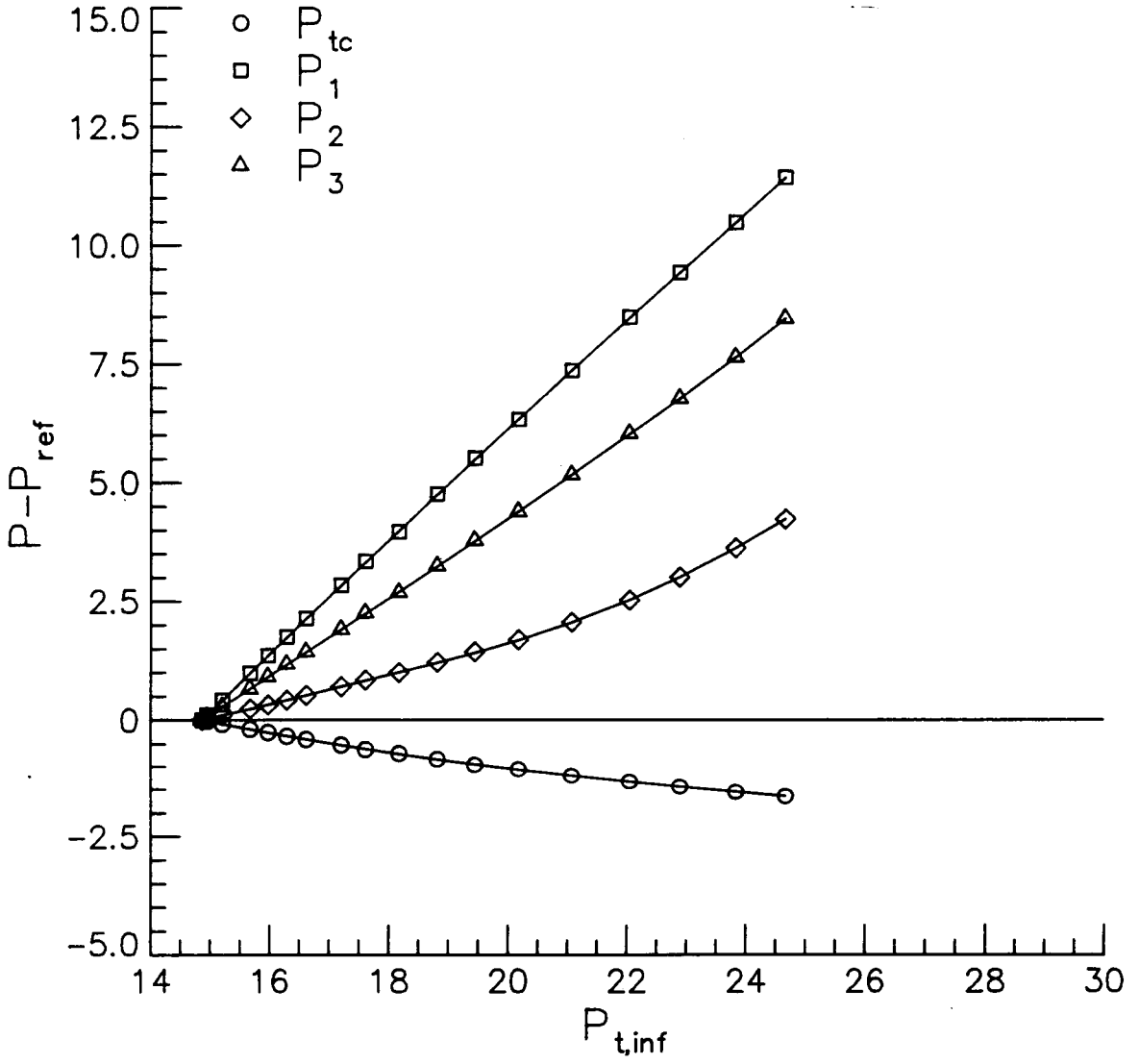

(b) α = 8.99 deg.

Figure A1.- Concluded.

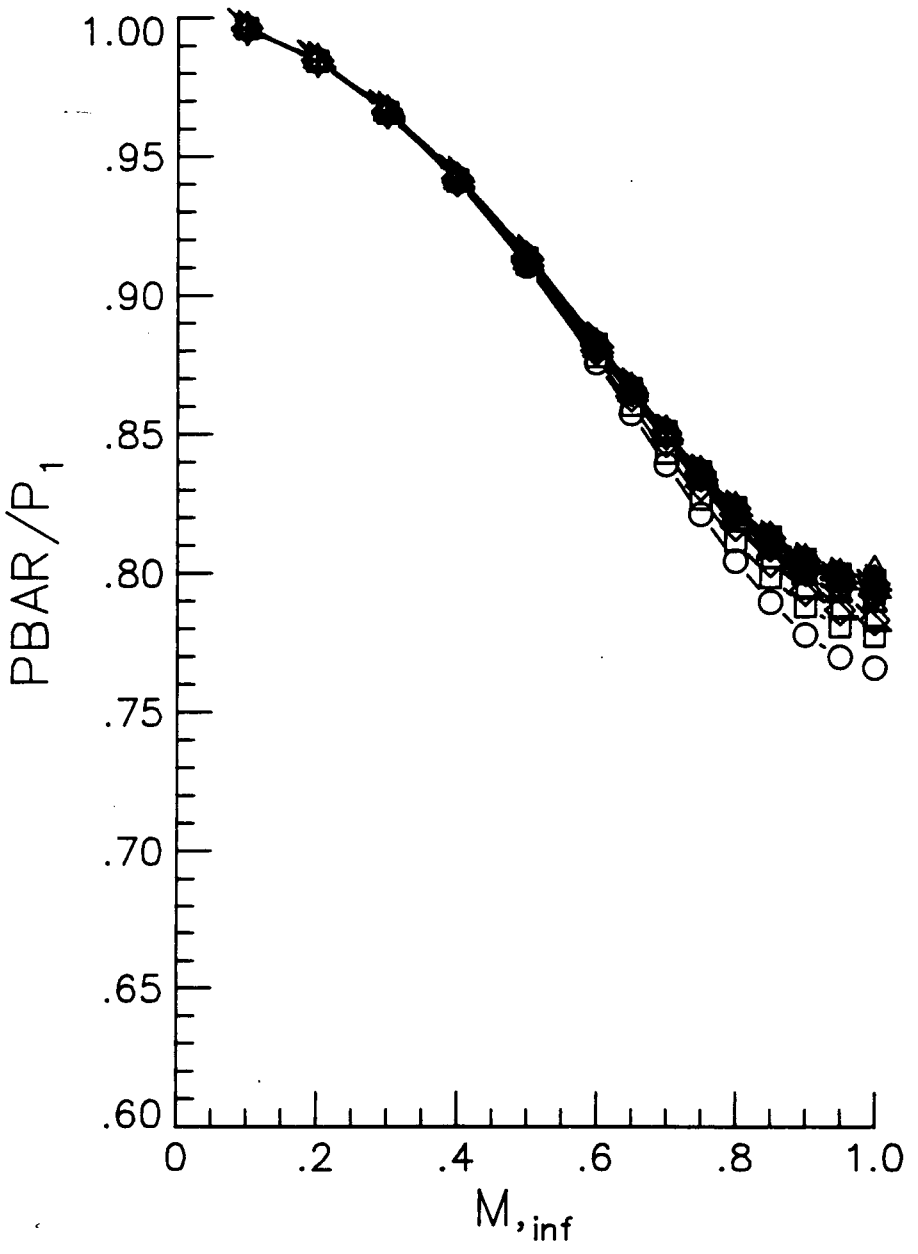

(a) Variation of Pbar/P_1.

Figure A2.- Variation of the probe variables with Mach number for different pitch angles.

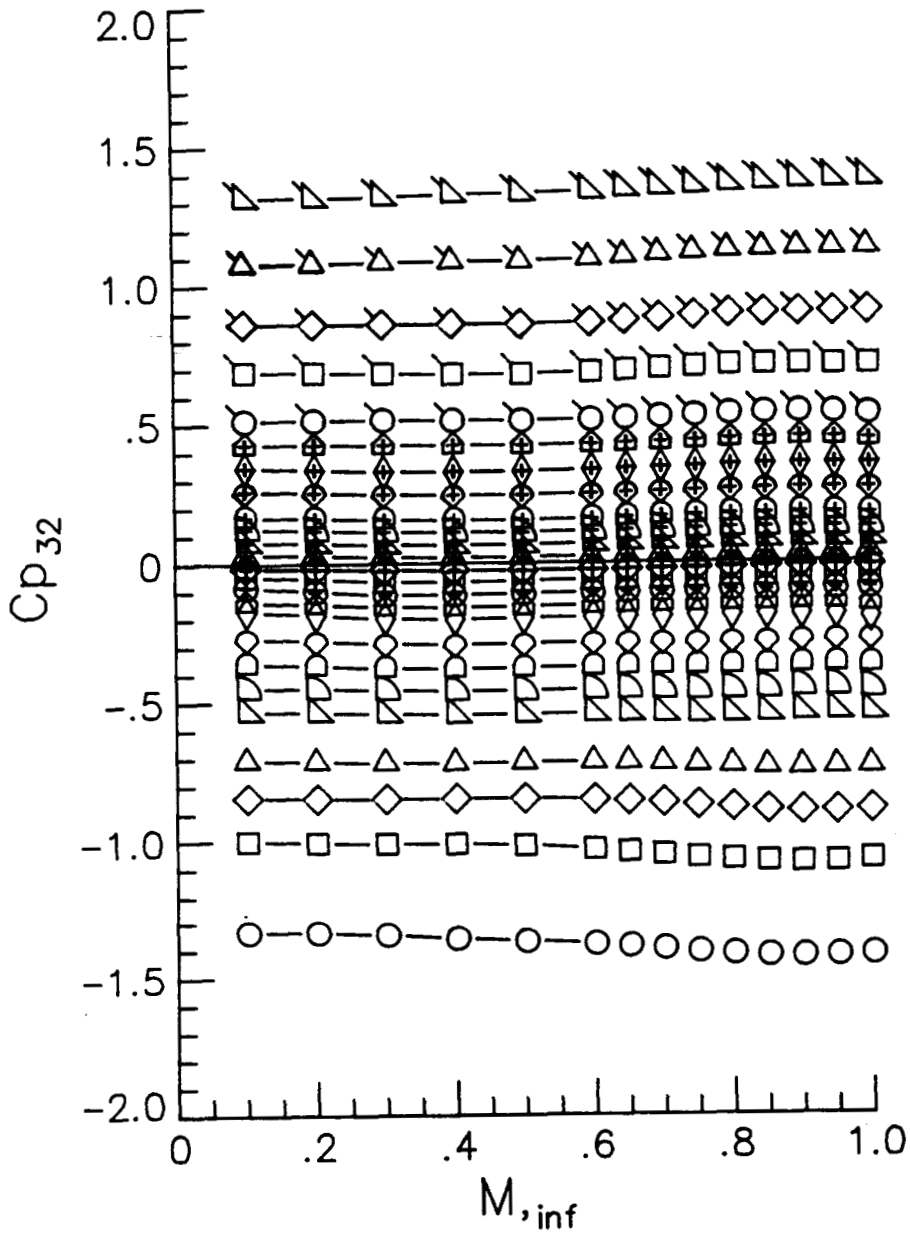

(b) Variation of C_{p32}.

Figure A2.- Continued.

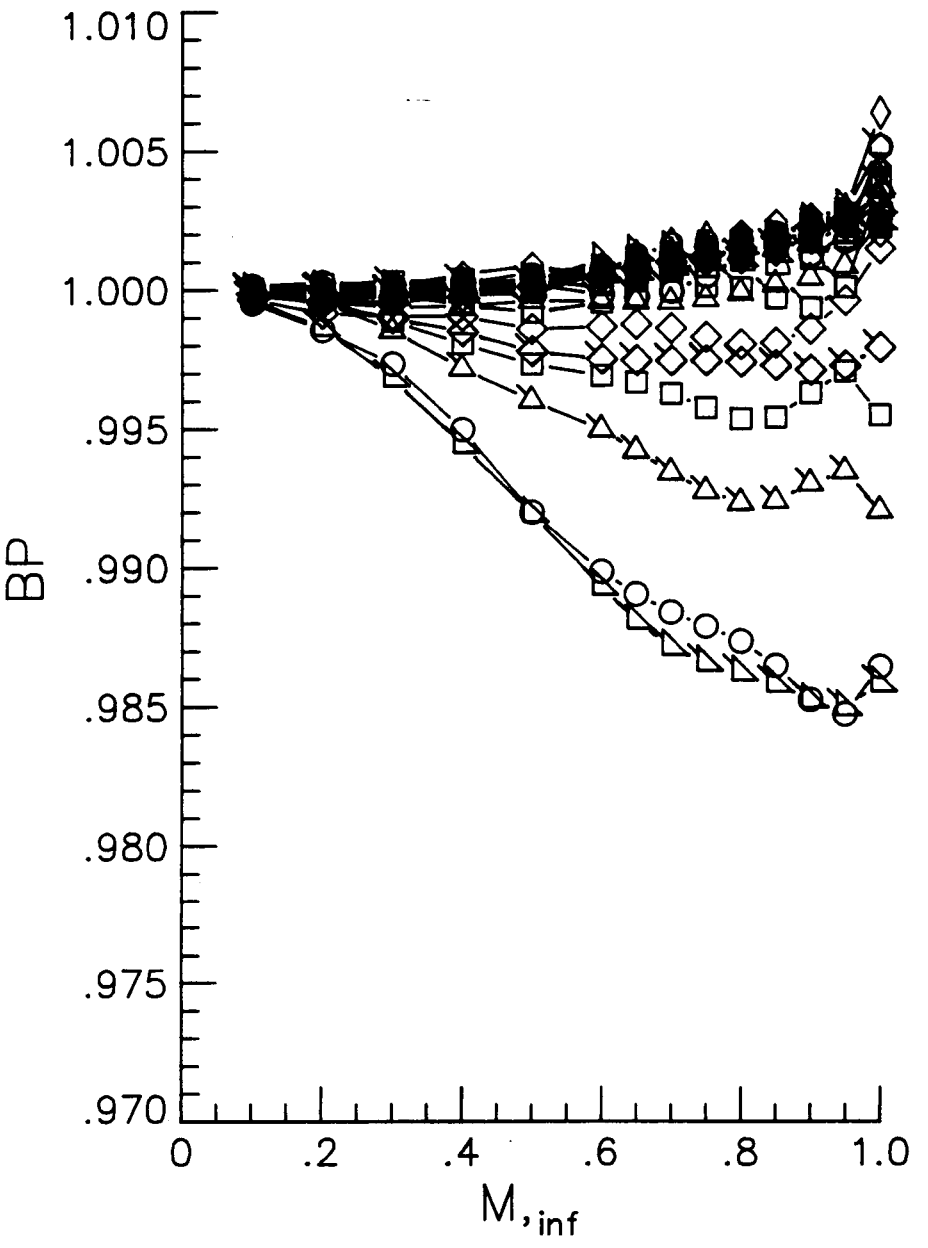

(c) Variation of BP.

Figure A2.- Concluded.

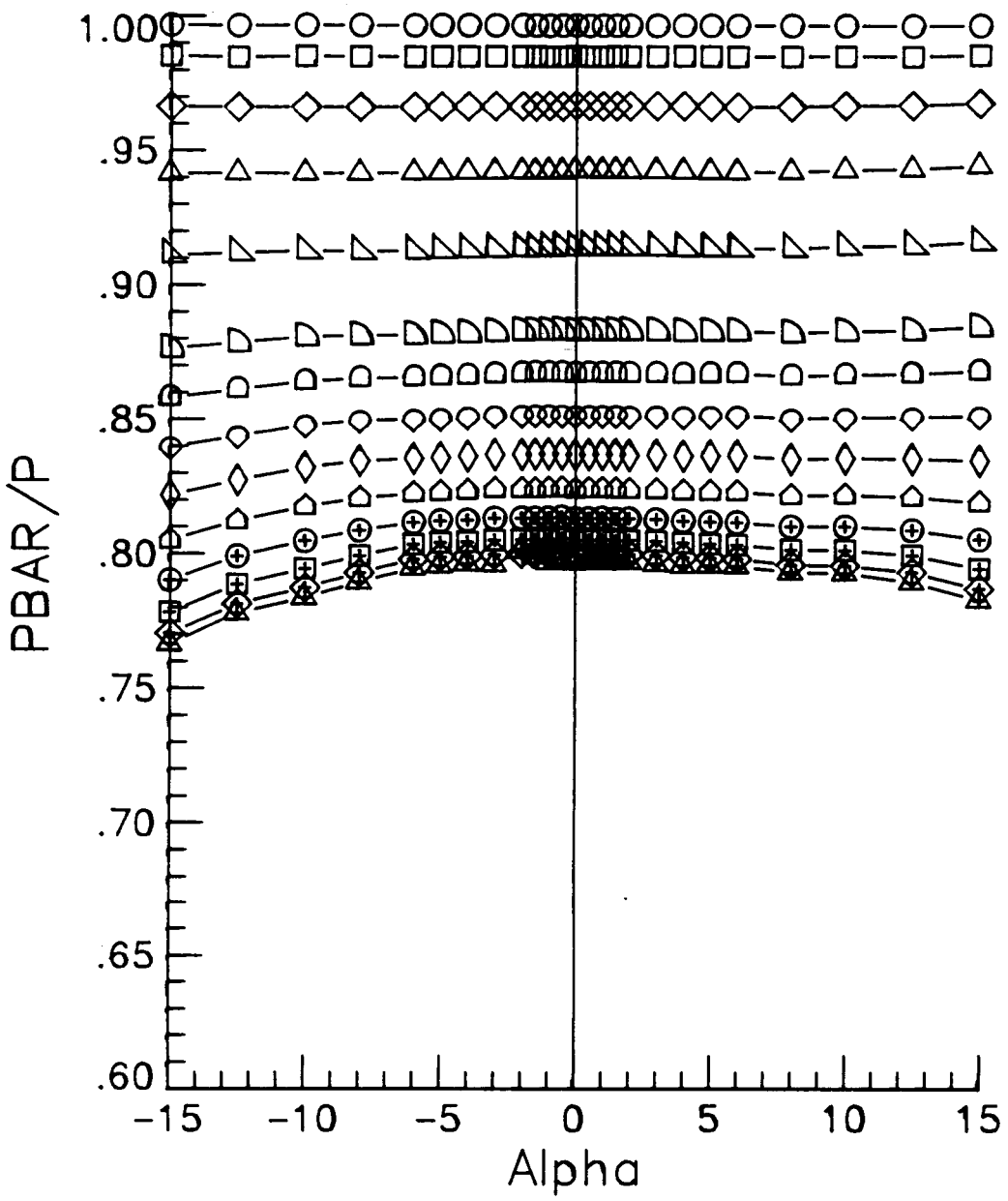

(a) Variation of Pbar/P_1.

Figure A3.- Variation of the probe variables with pitch angle for different Mach numbers.

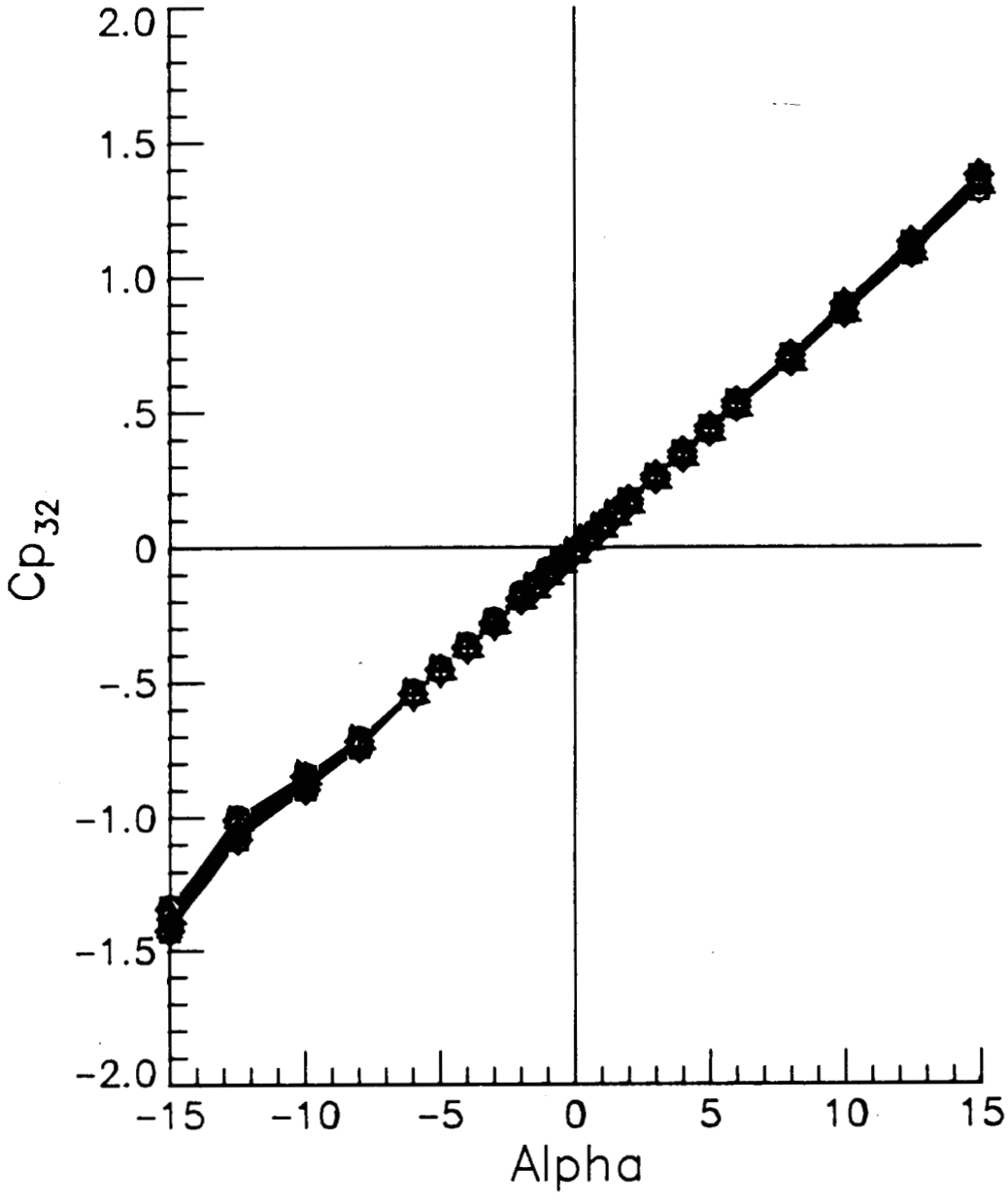

(b) Variation of C_{p32}.

Figure A3.- Continued.

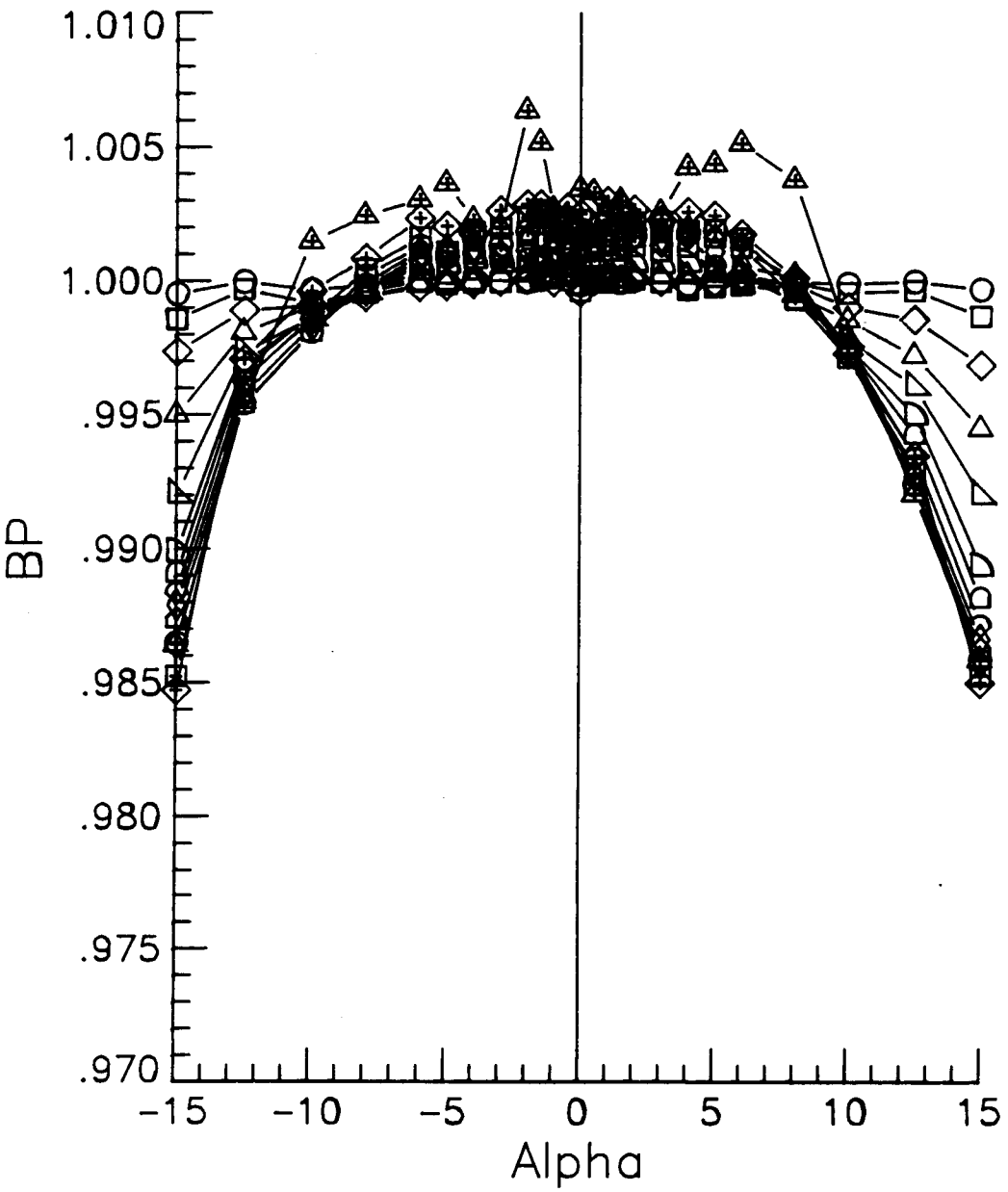

(c) Variation of BP.

Figure A3.- Concluded.

APPENDIX B

WALL INTERFERENCE CORRECTIONS

Generally, there are two categories of wall-interference corrections which can be applied to wind tunnel data: top- and bottom-wall corrections and sidewall corrections. The classic, inviscid corrections for the interference attributable to the top and bottom walls has been compiled in a concise and notation-consistent format by Pindzola and Lo (ref. 5). A more recent set of corrections for the interference due to the effective narrowing of the wind tunnel resulting from the growth of the sidewall boundary layer has been presented by Barnwell (ref. 31), Sewall (ref. 30), and Murthy (ref. 32). In this appendix, these corrections will be applied to solid-wall data obtained in the 6X19 for $M_\infty = 0.7$. A "modified-free-air" solution for the flow about the NACA 0012 airfoil will also be defined.

A. Corrections for the Sidewall Boundary Layer

Sewall (ref. 30) extended the subsonic, sidewall boundary-layer analysis of Barnwell (ref. 31) to transonic flows. In his analysis, he theoretically and experimentally demonstrated that the influence of the sidewall boundary layer in wind tunnels could be accounted for by using the concept of transonic similarity. His analysis yielded the following similarity variables and corrections.

$$\frac{\bar{\bar{M}}_\infty}{(1-\bar{\bar{M}}_\infty^2)^{3/4}} = \frac{M_\infty}{\bar{\bar{\beta}}^{3/2}} \tag{B1}$$

C-4

$$(\bar{\bar{C}}_P,\ \bar{\bar{C}}_n,\ \bar{\bar{C}}_m) = \frac{\bar{\bar{\beta}}}{\sqrt{1 - \bar{\bar{M}}_\infty^2}} (C_P,\ C_n,\ C_m) \tag{B2}$$

where $\bar{\bar{M}}_\infty$ is the free-stream test Mach number corrected to an "ideal" tunnel with no sidewall boundary layers, and $\bar{\bar{C}}_P$, $\bar{\bar{C}}_n$, and $\bar{\bar{C}}_m$ are the corrected pressure, normal-force, and pitching-moment coefficients, respectively. The $\bar{\bar{\beta}}$ factor is the traditional Prandtl compressibility factor modified by the addition of a term which accounts for the sidewall boundary layer displacement thickness, δ^*. Barnwell and Sewall defined it as

$$\bar{\bar{\beta}}^2 = 1 - M_\infty^2 + \frac{2\delta^*}{b}\left(2 + \frac{1}{H} - M_\infty^2\right) \tag{B3a}$$

where b is the width of the wind tunnel and H is the sidewall boundary-layer displacement thickness. Equation B3a was derived assuming a constant thickness boundary layer in the vicinity of the model.

Murthy (ref. 32) extended the analysis to include the effect of the model aspect ratio by using a wavy-sidewall boundary-layer assumption in the vicinity of the model. His formulation of $\bar{\bar{\beta}}^2$ is defined as

$$\bar{\bar{\beta}}^2 = 1 - M_\infty^2 + \frac{2\delta^*}{b}\left(2 + \frac{1}{H} - M_\infty^2\right)\frac{k_2}{\sinh k_2} \tag{B3b}$$

with

$$k_2 = \frac{\pi\sqrt{1 - M_\infty^2}\, b}{l} \tag{B4}$$

where b is the tunnel width and l is the reference "wavelength" of the boundary layer which is assumed to be a function of the airfoil chord length. Note that equation B3b reduces to equation B3a for k_2 approaching zero.

From reference 30, equations B1 and B3 can be expanded using the Taylor series to give

$$\bar{\bar{M}}_\infty = M_\infty + \Delta M \tag{B5a}$$

and,

$$\bar{\bar{\beta}}^2 = 1 - M_\infty^2 + \Delta\bar{\bar{\beta}} \tag{B5b}$$

where the change in the Prandtl factor is given by

$$\Delta\bar{\bar{\beta}} = \frac{2\delta^*}{b}\left(2 + \frac{1}{H} - M_\infty^2\right)\frac{k_2}{\sinh k_2} \tag{B6}$$

and the Mach number correction for the effect of the sidewall boundary layer is given by

$$\Delta M \approx \frac{-3M_\infty}{2(2 + M_\infty^2)}\,\Delta\bar{\bar{\beta}} \tag{B7b}$$

These corrections have been applied to the solid-wall data acquired in the 6X19 at a free-stream Mach number of 0.7. The shape factor and displacement thickness were determined from the information presented in

reference 30 as ≈1.5 and 0.0848 inches, respectively. The resulting sidewall corrections are

$$\Delta M = - 0.026 \frac{k_2}{\sinh k_2} \tag{B8a}$$

and

$$\Delta\bar{\bar{\beta}} = 0.062 \frac{k_2}{\sinh k_2} \tag{B8b}$$

Because of the lack of experimental data, Murthy (ref. 32) was unable to give a precise definition of the value of the parameter 1; however, the following table shows the influence of the variation of this parameter on the corrections for a free-stream Mach number of 0.7.

b/l	$k_2/\sinh k_2$	$\Delta\beta$	ΔM	$\bar{\bar{\beta}}$	$\bar{\bar{M}}_\infty$	$\bar{\bar{C}}_f/C_f$
0	1.00	0.062	-0.026	0.756	0.674	1.024
1	0.85	0.053	-0.022	0.750	0.678	1.020
1/2	0.48	0.030	-0.012	0.735	0.688	1.012

The subscript f corresponds to the appropriate subscript of equations B2. It can be seen from the table (for these conditions) that the greatest effect of the sidewall boundary layer is on the value of the free-stream Mach number. The results presented in chapters IV and VI of this paper indicate that major influence of the airfoil on the top and bottom wall pressure distributions and flow angles is contained within $-1.0 \leq x/c \leq 1.0$ which would correspond to $b/l = 1/2$ ($l \approx 2c$). It is assumed that the sidewall boundary layer will

respond accordingly; therefore, this value of b/l will be taken for the sidewall correction. The resulting corrections for the effect of the sidewall boundary layer for $M_\infty = 0.7$ give

$$\bar{\bar{M}}_\infty = 0.688 \tag{B9a}$$

$$\bar{\bar{\beta}} = 0.735 \tag{B9b}$$

and

$$(\bar{\bar{C}}_p,\ \bar{\bar{C}}_n,\ \bar{\bar{C}}_m) = 1.012\ (C_p,\ C_n,\ C_m) \tag{B9c}$$

B. Solid-Wall (Closed-Tunnel) Corrections

Pindzola and Lo (ref. 5) have compiled from the literature the general, classic, inviscid corrections for wind tunnels with various types of walls using a consistent notation. These corrections (for an unspecified wall type) are listed as follows. For blockage,

$$M_c = M\left[1 + \left(1 + \frac{\gamma - 1}{2} M^2\right)\epsilon_B\right] \tag{B10a}$$

$$Re_c = Re\left[1 + \left(1 + \frac{\gamma - 1}{2} M^2\right)\epsilon_B\right] \tag{B10b}$$

and,

$$C_{F,c} = C_F\left[1 - \left(2 - M^2\right)\epsilon_B\right] \tag{B10c}$$

where the subscript c denotes "corrected" and the subscript F is for any integrated force coefficient. The blockage parameter, ϵ_B, is the sum of the solid blockage due to the model and the wake blockage. That is

$$\epsilon_B = \epsilon_{SB} + \epsilon_{WB} \tag{B11}$$

For upwash, the correction is given by

$$\Delta\alpha_{upwash} = \frac{c\ C_L}{2h}\ \delta_0 \tag{B12}$$

where δ_0 is the lift-interference parameter which is dependent on the type of tunnel under consideration.

Corrections for streamline curvature are given as

$$\Delta\alpha_{sc} = \frac{c\ C_L}{4\beta h^2}\ \frac{\bar{c}}{4}\ \delta_1 \tag{B13a}$$

$$\Delta C_L = \frac{\Delta\alpha_{sc}}{\beta}\ \frac{\partial C_L}{\partial\alpha} \tag{B13b}$$

and

$$\Delta C_M = -\frac{\Delta C_L}{4} \tag{B13c}$$

where $\bar{c}$ is the average chord length for a wing ($\bar{c} = c$ for an airfoil). The term δ_1 is the streamline-curvature parameter which is dependent on the type of tunnel under consideration.

Blockage and lift interference parameters for a closed wind tunnel are given by

$$\epsilon_{SB} = 0.131 \frac{A}{\beta^3 h^2} \qquad \epsilon_{WB} = \frac{C_D c}{8\beta^2 h}$$

$$\delta_0 = 0 \qquad \delta_1 = 0.1309 \tag{B14}$$

where A is the cross-sectional area of the model and C_D is the drag coefficient.

Since these corrections have been developed for "ideal" wind tunnels with no sidewall boundary layer, they should be applied to those tunnel conditions which have previously been corrected for sidewall interference. Therefore, for the 6X19 previously corrected for sidewall interference, we have

$$\bar{\bar{M}}_\infty = 0.688 \qquad \bar{\bar{R}}e \approx 3 \times 10^6$$

$$\bar{\bar{C}}_n = 1.012\ C_n, \quad \frac{\partial \bar{\bar{C}}_n}{\partial \alpha} = 1.012 \frac{\partial C_n}{\partial \alpha} = 0.1503, \quad \bar{\bar{C}}_m = 1.012\ C_m$$

$$c = 6 \text{ in.}, \qquad h = 9.5 \text{ in.}, \qquad A = 4.32 \text{ in.}^2$$

$C_D \approx 0.01$, (approximate value obtained from ref. 44)

The value of $\bar{\bar{\beta}}$ corresponding to this Mach number is

$$\bar{\bar{\beta}} = 0.7257$$

These values give solid-wall blockage corrections of

$$\epsilon_{SB} = 0.0161, \quad \epsilon_{WB} = 0.0015, \quad \epsilon_{B} = 0.0176 \tag{B15a}$$

$$M_c = 1.0193\ \bar{\bar{M}}_\infty = 0.7013 \tag{B15b}$$

$$Re_c = 1.0193\ \bar{\bar{Re}} = 3.06 \times 10^6 \tag{B15c}$$

and,

$$C_{n,c} = 0.9731\ \bar{\bar{C}}_n = 0.9848\ C_n \tag{B15d}$$

The upwash correction to the pitch angle for closed tunnels, $\Delta\alpha_{upwash}$, is theoretically zero by equations B12 and B14c; however, corrections for the streamline curvature exist and are given by

$$\Delta\alpha_{sc} = 0.0045\ \bar{\bar{C}}_n = 0.0046\ C_n \tag{B15e}$$

$$\Delta C_n = 0.0009\ C_n \tag{B15f}$$

and,

$$\Delta C_m = -0.0002\ C_n \tag{B15g}$$

Several interesting observations can be made regarding the top- and bottom-wall corrections as compared with the sidewall corrections for these test conditions in this tunnel. First, the sidewall Mach-number correction is

approximately equal to that due to the top and bottom walls but in the opposite direction. Second, the sidewall force-coefficient correction roughly cancels the top- and bottom-wall correction. Finally, the top- and bottom-wall interference corrections for streamline curvature are negligible and the predominant correction is to the Mach number due to blockage. Therefore, under these test conditions, for this wind tunnel configuration, the interference corrections are negligible.

C. Modified Free-Air Solution

The two previous sections have detailed interference corrections which should be applied to solid-wall wind-tunnel data so that a realistic representation of free air can be obtained. Similar corrections must be made to the data obtained in open-jet and slotted- or porous-wall tunnels. However, for the slotted and porous walls, there is a large degree of uncertainty in the application of the corrections. It is the uncertainty existing in tunnels with slotted-wall boundaries which is being addressed in this paper.

For this study, the influence of top- and bottom-wall geometry changes on the wind-tunnel wall boundary condition are being considered. Because of this, applying interference corrections for the influence of these surfaces is inappropriate. The application of sidewall corrections is a different matter. It has been shown that these corrections have a large impact on the effective value of the tunnel Mach number. In order to make rational comparisons, a "modified, theoretical, free-air solution" which includes the effects of the sidewall was computed for the NACA 0012 airfoil using the method of reference 45. The computations were performed for a free-stream Mach number of 0.7 at a corrected Mach number of 0.688 and Reynolds number of 3×10^6 as determined by

the previously discussed sidewall boundary layer correction theory. Corrections for the normal force coefficient were made using using equation B9c resulting in a normal force curve slope of 0.1452 at zero lift and a corresponding pitching moment slope of 0.0059.

APPENDIX C

CALCULATION OF THE WALL COEFFICIENTS BY THE METHOD OF LINEAR LEAST SQUARES

The method of Linear Least Squares was used to determine the value of the unknown coefficients in equation 7.38. This is a standard statistical method which is simple, powerful, and, above all else, consistent in its application. The multiple correlation coefficient (R^2), which is a measure of the "goodness of fit", is a by-product of the analysis.

Prior to deriving the equations, the following definitions are taken from chapter VII for reference:

$$D = \left(C_{Pw} - C_{Pw,te}\right) - \left(C_{Ps} - C_{Ps,te}\right) \tag{C1a}$$

$$B_1 = -a\frac{\partial C_{Pw}}{\partial y} \tag{C1b}$$

and

$$B_2 = \theta_s \tag{C1c}$$

Equation 7.38 becomes

$$D = A + KB_1 + BB_2 \tag{C2}$$

By letting the unknown coefficients A, K, and B assume arbitrary values, the above equation is written as

$$D = D_F + e \tag{C3}$$

where the subscript "F" indicates the fitted value of D. The term e is the resulting local error between the left-hand-side which is known and the right-hand-side which contains the unknown coefficients. By summing the squares of this error at each of the data points, the expression

$$E^2 = \sum e^2 = \sum \left(D - D_F\right)^2 \tag{C4}$$

is obtained. It is noted, here, that all summations are over i=1 to i=n, the total number of data locations. The set of coefficients A, K, and B which best satisfy this equation are those which minimize E^2 and are obtained by solving the system of equations

$$\frac{\partial E^2}{\partial A} = \frac{\partial E^2}{\partial K} = \frac{\partial E^2}{\partial B} = 0 \tag{C5}$$

The solution of (C5) results in

$$A = \frac{1}{n}\left[\sum D - K\sum B_1 - B\sum B_2\right] \tag{C6a}$$

$$K = \frac{X_{22}Y_1 - X_{12}Y_2}{X_{11}X_{22} - X_{12}X_{21}} \tag{C6b}$$

and

$$B = \frac{X_{11}Y_2 - X_{12}Y_1}{X_{11}X_{22} - X_{12}X_{21}} \tag{C6c}$$

where

$$Y_1 = n\sum DB_1 - \sum D\sum B_1 \tag{C7a}$$

$$Y_2 = n\sum DB_2 - \sum D\sum B_2 \tag{C7b}$$

$$X_{11} = n\sum B_1^2 - \left(\sum B_1\right)^2 \tag{C7c}$$

$$X_{12} = n\sum B_1\sum B_2 - \sum D\sum B_2 \tag{C7d}$$

$$X_{21} = X_{12} \tag{C7e}$$

and

$$X_{22} = n\sum B_2^2 - \left(\sum B_2\right)^2 \tag{C7f}$$

The importance of the $B\theta_s$ term on the boundary condition was examined during the analysis. If B has a prescribed value (zero or otherwise), the system of equations which must be solved is

$$\frac{\partial E^2}{\partial A} = \frac{\partial E^2}{\partial K} = 0 \tag{C8}$$

A similar set of equations to those given by (C6) and (C7) can be derived.

A measure of the "goodness of fit" is given by the multiple correlation coefficient, R^2. This coefficient is a measure of how well the fitting

function, D_F, models the known functional variation of the measured data, D, and is obtained as follows. Consider the expression

$$\left(D - D_h\right) = \left(D_F - D_h\right) + \left(D - D_F\right) \tag{C9}$$

term 1 term 2 term 3

where D_h indicates the average of D. Term 1 is defined as the total variation in a particular measurement from the mean. The second term is the variation from the mean accounted for by the fitting function D_F and term 3 is the resulting error. If the data are squared and summed, it can be shown (see ref. 46) that

$$\sum\left(D - D_h\right)^2 = \sum\left(D_F - D_h\right)^2 + \sum\left(D - D_F\right)^2 \tag{C10}$$

term 1 term 2 term 3

where term 1 represents the total sum of the squares, term 2 represents the sum of the squares due to fitting the data, and term 3 represents the error sum of the squares. The multiple correlation coefficient is then defined as

$$R^2 = \frac{\sum\left(D_F - D_h\right)^2}{\sum\left(D - D_h\right)^2} = 1 - \frac{\sum\left(D - D_F\right)^2}{\sum\left(D - D_h\right)^2} \tag{C11}$$

It is seen from (C10) and (C11) that the R^2 measures how well the fitting function accounts for the total variation in the data. The closer R^2 is to 1,

the smaller the error and the better the fit. Typically, R^2 values should be greater than 0.9 for any meaningful correlation to occur.

VITA

The author was born in Erwin, [redacted] on [redacted]. He lived in Lillington, North Carolina and graduated from Lillington High School in June 1969.

In September 1969, he entered North Carolina State University where he received a Bachelor of Science in Aerospace Engineering in December 1973 and a Master of Science in Mechanical Engineering (fluids option) in December 1975. During this period, he was granted a National Science Foundation assistantship to conduct research on the steady-state freezing of moving fluids in pipes.

In August 1975, he was granted a research assistantship with the George Washington University/NASA Langley Research Center Joint Institute for the Advancement of Flight Sciences (JIAFS) to begin studies leading to the degree of Doctor of Sciences in Fluid Mechanics. The general subject of his research is in the area of wind-tunnel-wall interference.

He accepted employment with the National Aeronautics and Space Administration at the Langley Research Center in the Transonic Aerodynamics Branch in July 1977. The author continued the NASA supported work on his dissertation problem.

The author is married and lives with his wife, Kathy, and their two children, Jessica and Brooke, in Grafton, Virginia.